Author:
Ooi, (Didi) Sher

Title:
Origin and Early Diagenesis of Evaporites in a Coastal Sab-kha

Origin and Early Diagenesis of Evaporites in a Coastal Sabkha

Process-based Insights from Sedimentology, Hydrogeology and Geochemistry of Mesaieed, Qatar

by

Didi Ooi Sher Mey

A thesis submitted to the University of Bristol in accordance with the requirements for award of the degree of Doctor of Philosophy (PhD) in Faculty of Science

School of Earth Sciences
May 2018

Doctoral Thesis
68,951 words

Abstract

In most carbonate reservoirs in the Middle East and Cretaceous reservoirs, anhydrite is one of the major pore-occluding mineral phases that affects hydrocarbon reservoir quality. Whilst anhydrite is a commonly observed CaSO4 mineral in the subsurface, the most common CaSO4 mineral deposited in modern setting today is gypsum. Sabkha system is commonly used to understand the formation of this diagenetic evaporites with a focus on dolomitization, but little studies have focused on the distributions and drives for the formation of diagenetic gypsum. The classic sabkha model is currently based on Abu Dhabi, which is a windward carbonate sabkha setting.

This integrated study focuses on Mesaieed sabkha, a 75 km^2 leeward, prograding and a mixed siliciclastic-carbonate Holocene sabkha overlying an Eocene Dammam Formation. The sedimentology of four spatial sabkha zones within the sabkha was studied in detail, and this zonation is evident by geochemical and hydrodynamic observations. The sabkha geomorphology offers evidence of spit formation, marine flooding, meteoric input in the landward zone and hints of aeolian deposition during shamal events.

Gypsum precipitation is ubiquitous at the vadose zone and the phreatic zone in the upper and middle sabkha zone, and in the Dammam Formation underlying the middle and lower sabkha zones. Hydrogeology studies suggest that the vertical flow is about an order of magnitude larger than lateral flow, with the greatest evaporitic drawdown in the middle sabkha. Gypsum dissolution in the outcropping Dammam Formation updip is evident from the excess of calcium and sulphate in the continental waters, which provides the solutes downdip for the proximal and upper sabkha. Evaporation is a main driver of the hydrodynamic and consequently the geochemistry, which drives precipitation of poikilotopic and displacive gypsum within the sabkha, resulting in the enrichment of conservative ions and linear depletion in both aqueous calcium and sulphate ions. 1:1 magnesium depletion and calcium enrichment providing evidence of secondary dolomitization. Parts of the sabkha are not enriched by calcium but are depleted in magnesium, potassium, and the trace element silica and aluminium, suggest precipitation of K-clays.

This holistic sedimentology-hydrogeochemical workflow can be applied to improve accuracy of facies modeling, reservoir quality estimation and the assessment of the uncertainty for pre-drill value of information studies.

"The world is complex, dynamic, multi-dimensional; the paper is static, flat. How are we to represent the rich visual world of experience and measurement on mere flatland?"

- Edward Tufte, 1990

Acknowledgements

It is difficult to overstate my gratitude to my supervisor, Professor Fiona Frances Whitaker, whose colossal ambition and prodigious attention to detail drove me to push beyond my self-perceived limits and ability. I am thankful for her in taking a chance on me, right out of my three-year bachelor's degree. Fiona was instrumental in my development as a lateral-thinking scientist.

I am very grateful and humbled by my supervisor Dr. Jeremy Jameson for his exceptional patience in introducing me to the invaluable insights of the deserts in Qatar. His trait of always wanting to give, share and teach is truly remarkable. In addition, this project would have been challenging if it wasn't for Dr. Christian Strohmenger, my other supervisor, who made sure I strike a balance between research ambition and realistic expectations. With that, I gratefully acknowledge ExxonMobil Research Qatar for the generous funding of this research for my first 3 years.

While many mentors helped shape my intellect, no one was more influential than my former supervisor, Dr. Simon Gough. His sustained curiosity and creativity in exploration geology, coming from a metamorphic geoscience background, was inspiration for me to get out of my comfort zone and do a PhD research that is far from my strongest suite in school. In addition, I would like to thank Dr. Paul J. Moore for being pivotal in inculcating my appreciation for hydrogeology and aqueous geochemistry to greater heights. I have learned so much from PJ than I could ever learn in one year.

Fieldwork in Qatar was a vital part of my PhD and it wouldn't have been the same without my dad Osa Ooi. Your creative problem-solving in the field and 4WD skills taught me how to survive the desert in one piece and still bring back tonnes of data. My appreciation extends to Dr. Huw Pullin and Dr. Alia Jasim, for their unwavering support in the field.

Mohamed Fatima, Anthony Watts and Karl van Kessel from the New Doha Ports Project (NDPP) were extremely helpful in providing present and historical data from the Mesaieed site. I would also like to thank Qatar Petroleum for access to Dukhan sabkha and Mohamed Shamrukh from the Water Resources of the Ministry of Environment (MoE) for providing historical data of Qatar and on the Mesaieed site. James Duggan and Lee Nachtegaele were both crucial for teaching me GIS.

My assistants slash Master's students - Joshua Simmonds, Gemma Tong, James Teoh, thank you for allowing me to learn my mentoring skills in return for your great assistance in the lab and in the field.

Living in Bristol has been a memorable experience. I am indebted to Dr. Katherine Cooper for choosing me to be your right hand woman on your gargantuan Bahamas fieldwork and for training me to be a superhuman field geoscientist. Also, to the Carbonates research group (or did we decide on renaming it Water-Rock Interaction so that I'd feel more inclusive?) legacy members, including Miles Frazer, "Bree" Hemmings, Tatyana Gabellone for being great support buddies. And Hamish Robertson for being the awesome 'night owl' work buddy back in G31. Thank you to my external committee Dr. Heather Buss and Professor Rachel Flecker for supporting my wellbeing all while ensuring my progress.

I wouldn't be able to do this without the incredible support of the Ooi clan - my dad Osa, my mum Ann, brothers Dillen and Darren, for virtually accompanying me during my night-owl hours. I would like to also thank Kimberly Mah and James Teoh for your helpful editing and deciphering Da Vinci Code-like handwriting.

Mica the shiny biotite was probably the one that has kept me company for more than thousands of hours. I acknowledge your steadfastness in shocking me to full wakefulness with your random barks or for

dealing with my rants/self-talk during graveyard hours. Gomez, without you, adjusting to Houston for my write-up would be challenge. Siti Rohani Bahjam, for feeding this poor graduate student's bottomless pit of an appetite.

My sincerest thanks go out to Google, Dell, Microsoft and Dell- without their continuous technological innovation, this dense research would have been near impossible.

I would like to thank the unlikely army - Dawn Jobe, Yan Zaretskiy, Bob Martin, Yitian Xiao, Vikram Sen, Linda Cobb, Wesley Cobb, Evan Bianco, Matt Hall, Licheng Zhang, Chengzhan, Zhenzhen Zhong, Nicole Lu, Justin Gosses, and Brendan Hall. In the last 8 months, you have been my enabler, my great source of hope, the candle in the dark et cetera. Thank you for being leaders for the future in Data (Geo)science. I cannot understate my gratitude for keeping checking on me and maintaining my sanity from time to time. You have all propelled me, in your own unique ways, see this thesis to completion with a renewed excitement for the digital future.

Finally, to April Denise Coker. My rock. My everything. The combination of your discipline, intelligence, curiousity is such a rarity and it has defined the person I am today. I am humbled for your monumental patience and unconditional love which helped get through difficult times and temper my irritable mood swings. Thank you for making the choice to be by my side during times of both joyous and self-doubt, this thesis would not be where it is today without you! Here is to your new phase of life, one that includes more quality time together.

University of BRISTOL

Author's Declaration

I declare that the work in this dissertation was carried out in accordance with the requirements of the University's *Regulations and Code of Practice for Research Degree Programmes* and that it has not been submitted for any other academic award. Except where indicated by specific reference in the text, the work is the candidate's own work. Work done in collaboration with, or with the assistance of, others, is indicated as such. Any views expressed in the dissertation are those of the author.

SIGNED: [redacted] **DATE:** May 9th 2018

Table of Contents

UNIT CONVERSION, VERTICAL DATUM

Multiply	By	To obtain
cubic meter per day (m^3/d)	35.31	cubic foot per day
centimeter (cm)	0.394	inch
kilometer (km)	0.62137	mile
square kilometer (km^2)	0.3861	square mile
kilopascal (kPa)	0.14503	pound per square inch
liter (L)	0.26417	gallon
liter per second (L/s)	15.85	gallon per minute
meter (m)	3.2808	foot
meter per day (m/d)	3.2808	foot per day
meter squared per day (m^2/d)	10.76	foot squared per day
meter squared per day (m^2/d)	0.055916	gallon per minute per foot
meter squared per day (m^2/d)	80.52	gallon per day per foot
square meter (m^2)	10.76	square foot

Temperature: Temperature degrees between Fahrenheit and Celcius can be converted using Fahrenheit = 1.8 *Celcius + 32.

Sea-Level: Sea-level in the thesis is in reference to meter above datum based on code 6614 geodetic Qatar National Datum 1995 (QND95), which is derived from International 1924 ellipsoid and the Greenwich prime meridian. This is a transformation from WGS84, with coordinate operation code 1840 (see Mugnier, 2008 for more information)

List of Figures

List of Tables

1 Introduction

Author's note: This work is done in collaboration with ExxonMobil Upstream Research Center, specifically the Qatar Coastal Research Center. The data that are generated for this thesis is shown and some dataset (whole core photographs) are proprietary.

7,600 words

PREFACE

Denison et al (1998) said the work of determining the origin of a gypsum "presents a geological challenge" and defining the parent brine "can be controversial and difficult." This project will attempt to tackle the chimera focusing on diagenetic processes that modify sediments in arid climate coastal plains. The study area is a small area of coastal plain sabkha called Mesaieed, on the east coast of Qatar, which lies on the southern Arabian Gulf coastal margin.

This introductory chapter is written as a three-part series:

Part 1: Fundamentals

Section 1 provides the foundation with the sub-disciplines of applied Earth Sciences in terms of nomenclatures, definitions, and concepts. This includes the basic understanding of *hydrology, hydrogeology,* and *geochemistry* and terminologies such as *sabkha, evaporites,* and *carbonates*. This assumes the reader has a background of geology and geosciences. More comprehensive description of evaporites is provided in Warren (2016).

Part 2: Motivation and Outline

This section provides the framework of goals that this thesis accomplished. It includes the significance of Mesaieed sabkha as a leeward coastal setting and a mixed siliciclastic-carbonate system as the motivation behind the research, followed by the objectives and the methodological approach taken. The outline of the thesis is thus presented in a way that it fulfills the objectives.

Part 3: Literature Review

Section 3 provides a relevant, and broader, overview of the current understanding for the modern sabkha systems in the Arabian Gulf. Individual journal-style chapters contain their own background material and relevant literature review. Specifically, the context will focus on sabkha hydrogeochemistry (including prior knowledge on sabkha diagenesis), previous work on Qatar sabkhas, and sea-level history since the Holocene highstand.

PART 1: Fundamentals

1.1 Sabkha

Sabkha is an Arabic word used interchangeably, and inconsistently, with salina, salt flat, sebkha, salar, playa, evaporite pan and salt plain depending on the language that dominates the province. In the Arabian Gulf, it is used to describe any area of extensive and barren topographic lows that are periodically flooded from ephemeral marine, direct precipitation or from continental floodwaters originating from surrounding updip areas after a precipitation event (Warren, 2016). Solute sources may be of continental (athalassic) meteoric or marine-derived (thalassic) source. And thus, it can be divided into three types: continental sabkha, coastal (sea-margin) sabkha, or aeolian (interdunal) sabkha (Figure 1-2). Sabkhas are sediments with original composition comprising of either carbonate, siliciclastic or a mixture of both, that appear to have been diagenetically altered by secondary evaporites and associated carbonates (Jameson and Puls, in press). They are characterized by a low relief topography, with surface elevation being determined by the height of the capillary fringe. The diagenesis can be a result of brine and pedogenic processes.

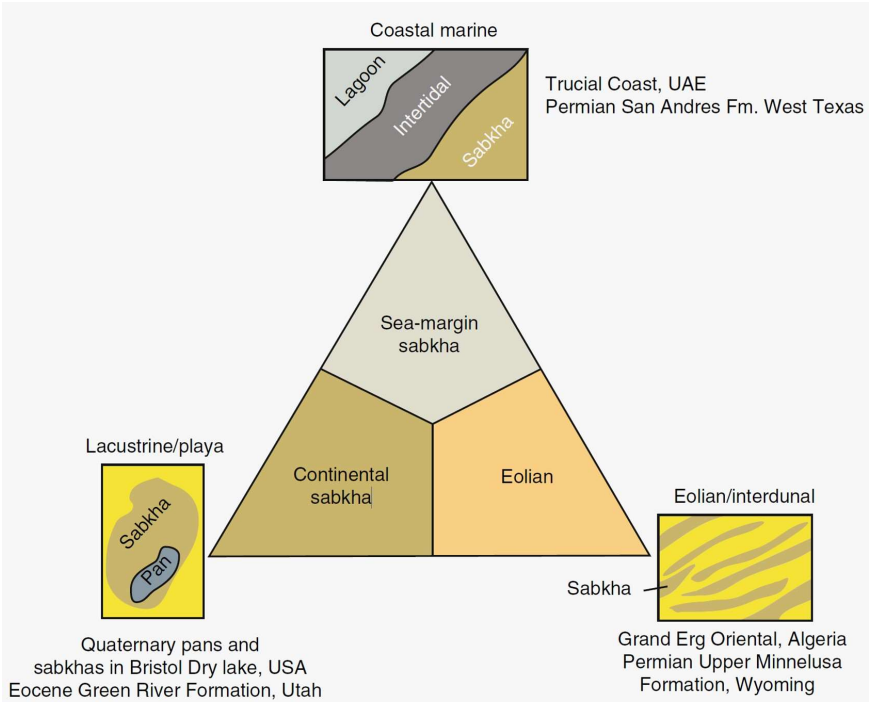

Figure 1-1. Sabkha classification based on depositional setting with Mesaieed, the sabkha of this study is part of the sea-margin sabkha (modified from Warren, 2016; Handford, 1981a).

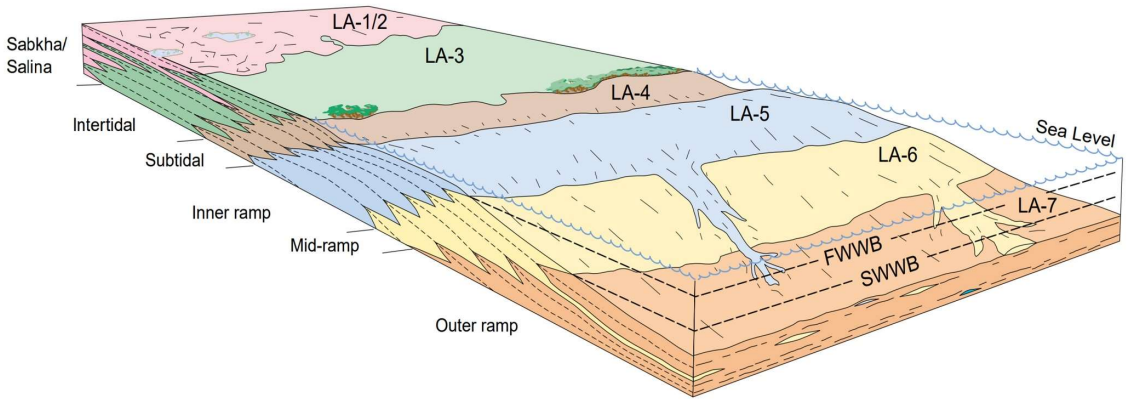

Figure 1-2. Position of coastal sabkha and continental sabkha, in pink, relative to an Arab intrashelf ramp. FWWB = fair-weather wave base and SWWB = storm weather wave base. (After Grotsch et al, 2003)

The most commonly observed evaporitic overprints at the near-surface sabkha environments are $CaSO_4$ precipitation in the form of gypsum (Warren, 2016), with minor associated anhydrite, and halite. Evaporation of the sabkha surface drives widespread displacive gypsum growth within vadose zone, which typically raises sediment that are then blown away (Figure 1-4).

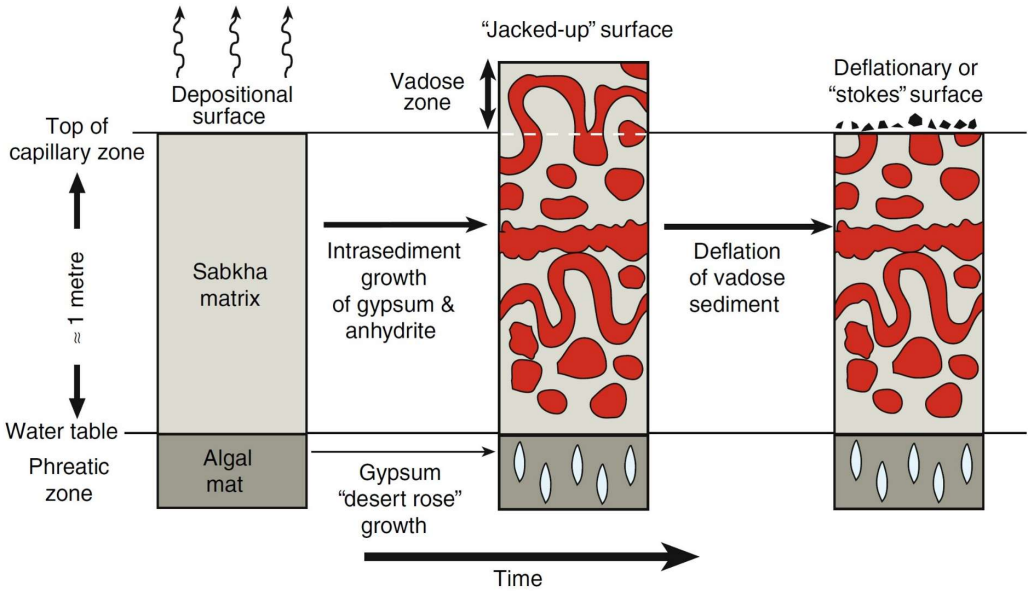

Figure 1-3. Effects of evaporation of a modern sabkha capillary zone which results in precipitation of pore-filling nodular and crystalline gypsum and anhydrite (Source: Warren, 1991; Warren 2016)

Development of extensive sabkha, comprising of primary coastal sediments and diagenetic evaporite and carbonate, is only possible in an arid and hot subtropical climate (Warren, 2016). Precipitation of evaporite minerals that occur within sabkhas are due to the rate of evaporation exceeding rainfall (Shearman, 1966). Many sabkha systems are transient, but their role as sources for subsurface evaporites may be significant (Warren and Kendall, 1985).

In summary, a sabkha is essentially a groundwater-driven evaporitic sedimentary system, that forms by syn- and postdepositional intra-sediment evaporite encrustation above and beneath a flat geomorphologic surface whose elevation is determined by the top of the capillary fringe, provided that evaporation exceeds precipitation (Warren and Kendall, 1985; Wood et al, 2005; Warren, 2016).

1.2 Evaporitic Diagenetic Processes

Evaporite minerals have a poor preservation potential and are chemically vulnerable to solution and replacement (Chandler, 1988). Carbonate minerals are equally chemically reactive (Moore and Wade, 2013), which means that both evaporite minerals and carbonate sediments may be diagenetically altered at any time after their formation.

Diagenesis involving these two minerals can cause significant modifications to the depositional texture, the pore network and the mineralogical composition (Warren, 2016). Thick repetitions of dolomite-anhydrite in the geological column is commonly observed in evaporitic carbonate reservoir rocks (Kendall and Alsharhan, 2011), and this makes evaporites uniquely associated with dolomite ($CaMg(CO_3)_2$), a poorly understood sedimentary carbonate.

Four main diagenetic processes that may occur during early diagenesis in a modern arid environment include – dolomitization, dissolution, cementation by secondary evaporites and stabilization. James and Choquette (1984) proposed the classification of diagenetic process to be divided into either mineral or water-controlled reactions. In our case, this means that dissolution is water-controlled, stabilization is mineral-controlled, while cementation can be considered to be both (Cooper, 2015).

I. Dolomitization

When there is a seawater source that is Mg-rich, the replacement dolomitization of a previously deposited calcium carbonate rock precipitates dolomite $CaMg(CO_3)_2$ (Babel and Schreiber, 2014) and frees up Ca^{2+} ions:

$$2CaCO_{3(s)} + Mg^{2+}_{(aq)} \rightleftharpoons CaMg(CO_3)_{2(s)}\ (\text{dolomite}) + Ca^{2+}_{(aq)} \quad (1.9)$$

When there are no processes that remove Ca^{2+}, dolomitization can be represented by other reactions driven by CO_3^- (Machel, 2004), which in turn does not free up Ca^{2+} ions:

$$Mg^{2+}_{(aq)} + Ca^{2+}_{(aq)} + 2CO_3^{2-}{}_{(aq)} \rightleftharpoons CaMg(CO_3)_{2(s)} \quad (1.10)$$

Reactions [1.9] and [1.10] can be combined as follows:

$$Mg^{2+}_{(aq)} + (2 - a)\ CO_3^{2-}{}_{(aq)} \rightleftharpoons CaMg(CO_3)_{2\ (s)} + (1 - a)\ Ca^{2+}_{(aq)} \quad (1.11)$$

This reaction is more realistic as it takes into account how much Ca^{2+} is removed from the system during dolomitization, which depends on parameter *a* (Machel, 2004). However, the fluid-flow mechanism does not work in isolation to allow dolomitization, it requires favourable thermodynamic and kinetic conditions (Whitaker et al., 2004).

II. Cementation

Cementation requires three conditions to be met: (1) a stable host sediment, (2) a constant supersaturated state within pore waters relative to the mineral, and (3) an adequate source supplying solute in solution (Taylor and Illing, 1969). Precipitation of minerals within pore spaces in the near-surface can be driven by evaporation (Warren, 2006) or through CO_2 degassing (Moore and Wade, 2013). Cementation can form confining layers which reduce permeability and occlude porosity of the aquifer, thus inhibiting fluid flow (Cooper, 2015).

III. Stabilization

The stabilisation of minerals is dependent on several factors, including temperature and pressure. $CaSO_4$ polymorphs may occur as hydrous gypsum, intermediate hemihydrate (bassanite) and the dehydrated phase anhydrite. Understanding the mechanisms of calcium sulphate (CaSO4) precipitation, remains largely unexplored (Van Driessche et al., 2012). Gypsum is commonly observed on the surface and near-surface (Warren, 2016). Anhydrite preferentially occurs in the burial regime, but it can also exist in highly arid and hot supratidal environments supplied with concentrated brines (Shearman, 1985). This ephemeral mineral is easily rehydrated after formation at atmospheric conditions.

$CaCO_3$ minerals may occur in three polymorphs: high Magnesium calcite (HMC), aragonite and low Magnesium calcite (LMC) (Moore, 1989). Dolomite can occur as either ordered or disordered dolomite (Reeder and Nakajima, 1982; Montes-Hernandez et al., 2014). These aspects of carbonate mineral polymorphs will not be explored in this thesis in-depth, as the thesis pertains to evaporite-forming processes from a field-scale perspective.

IV. Evaporite Dissolution

Halite has a high solubility (359 g/L in water at 25 °C), and hence, it is susceptible to dissolution upon contact with natural waters, which are commonly undersaturated with respect to halite.

$$NaCl_{(s)} \rightleftharpoons Na^{+}_{(aq)} + Cl^{-}_{(aq)} \quad (1.12)$$

Although gypsum, a retrograde mineral, has low solubility (~2.0-2.5 g/l in water at 20-25 °C), it is still susceptible to dissolution when in contact with waters at lower temperatures that are undersaturated with respect to gypsum.

$$CaSO_4.2H_2O_{(s)} \rightleftharpoons Ca_{(aq)} + SO_4^{2-}{}_{(aq)} + 2H_2O_{(l)} \quad (1.13)$$

PART 2: Motivation and Outline

1.3 Hydrocarbon Reservoir Quality

Sabkhas are important environments of deposition for several major Arabian Gulf oil and gas reservoir systems (Purkis et al., 2017). In Qatar, hydrocarbons are produced from geologic zones including the Upper Jurassic Arab (Dukhan Field) and Permo-Triassic Khuff (North Field) formations. These Middle Eastern reservoirs show similar depositional environments with evaporitic diagenetic overprint seen in a range of marine and sabkha environments in Qatar.

The most common evaporite mineral in these subsurface reservoirs is anhydrite ($CaSO_4$) (Figure 1-5). It occurs over a wide range of burial depths as pore-filling phases or nodules that replace mineral phases, occluding porosity and permeability, and thus, exerts an important control on the quality of the hydrocarbon reservoir (Sullivan et al., 1994; Machel, 2013).

It is believed that much of the anhydrite in the subsurface may be secondary, and likely precipitated from pore fluids saturated with calcium and sulphate ions (Kendall and Walters, 1978). In many ancient rock studies, anhydrite is common in non-evaporitic facies, such marine carbonates. This observation implies that there has been a late introduction of $CaSO_4$-rich pore fluids and kinetics suitable for local precipitation of $CaSO_4$, possibly during burial. Such remobilised evaporite can severely reduce reservoir quality, as documented in the Jurassic Arab, Permian Khuff and Zechstein formations (Figure 1-8). Controls of anhydrites origin and evolution as a pore-filling cement is poorly understood.

Gypsum ($CaSO_4.2H_2O$), a hydrated precursor to anhydrite, is a much more commonly observed $CaSO_4$ mineral within modern outcrops today compared to anhydrite. Anhydrite is limited to extremely arid land-locked environments, often associated with halite (Warren, 2016). Studies of arid carbonate rarely differentiate between anhydrite as a diagenetic dewatered product from gypsum and as secondary evaporite such as primary anhydrite. Modern analogues help us develop a better understanding of early diagenetic $CaSO_4$ to reconcile the potential source and origin of diagenetic evaporites formed during early post-deposition diagenesis.

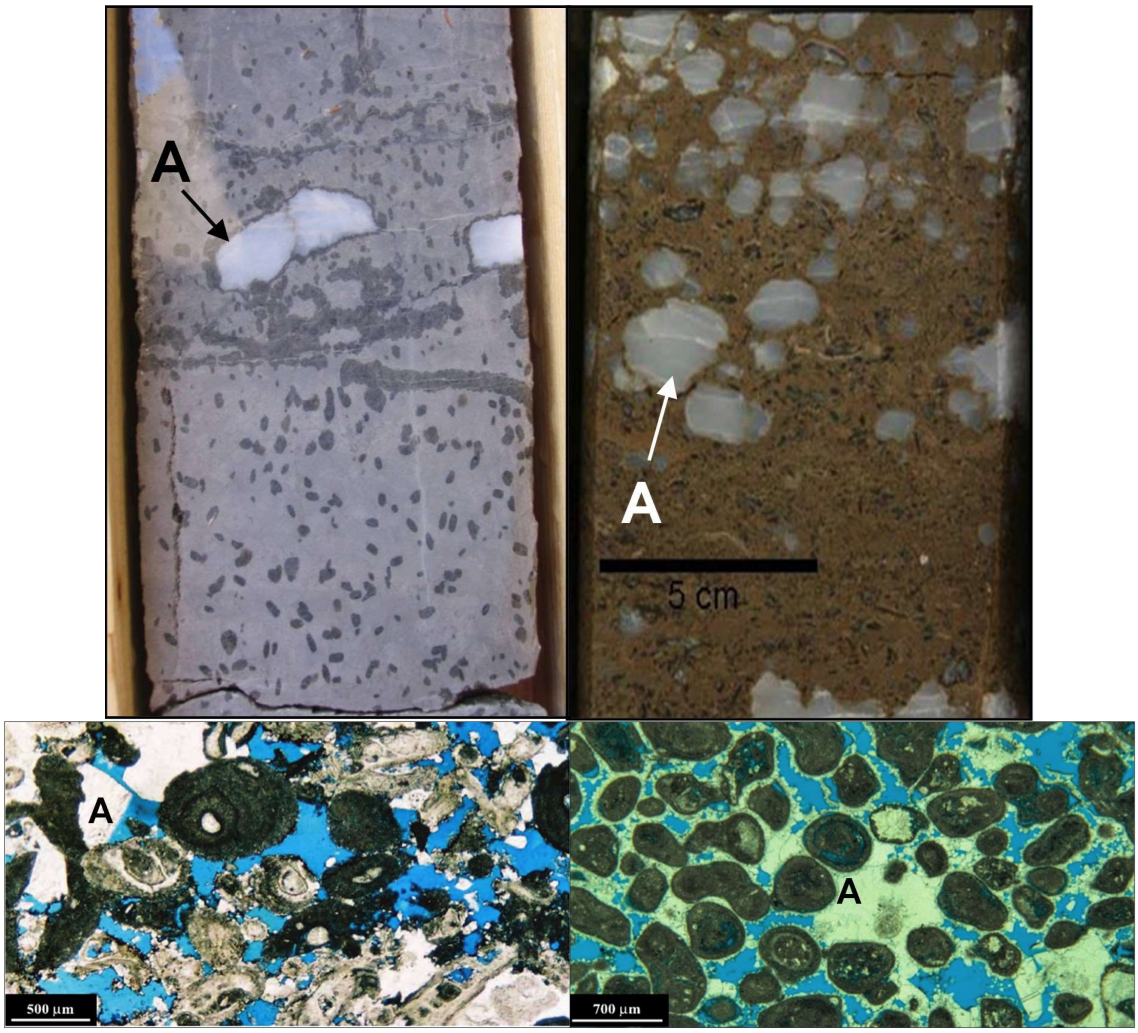

Figure 1-4. Subsurface examples of (1) thin section and (2) cores of carbonate with anhydrite cement (A), are shown here to occlude open marine facies in the Jurassic Arab formation. (Source: Jameson and Puls, 2013)

Holocene sabkhas are analogous to arid carbonate hydrocarbon reservoirs (Kendall and Alsharhan, 2011). The low-angle carbonate ramp of the Arabian Gulf, with supratidal evaporitic sabkhas updip and complex depositional and diagenetic facies within the intertidal to subtidal, has been studied as an analog to many of the Gulf's reservoirs of Mesozoic age. In the Arabian Gulf, many hydrocarbon reservoirs are currently in the middle of the production phase and this has driven a need for a more precise hydrocarbon reservoir characterization. The need to revise earlier reservoir analogues drives the renewal of interest in studying the modern sabkha (Lokier, 2013).

Since the 1960's, research has been heavily focused in the southeastern Arabian Gulf, particularly the United Arab Emirates (UAE), especially Abu Dhabi. Interest in the coastal sabkhas was initially focused on their geomorphology and depositional environments (Kendall and Skipwith, 1969; Evans et al., 1969), primary and diagenetic mineralogy characterization (Curtis et al., 1963; Evans et al., 1964), and microbial mat (Kendall and Skipwith, 1968; Kinsman and Park, 1976). Subsequent work has extended to consider sabkha

hydrogeology (McKenzie et al., 1980; Sanford and Wood, 2001), aqueous geochemistry (Wood et al., 2002, 2005), and depositional processes (Strohmenger et al., 2010; Strohmenger and Jameson, 2015). Various polygonal features in the sabkha have also been studied in detail (Lokier and Stueber, 2008, 2009; Lokier, 2012). Recent overview studies and new insights include review papers on Abu Dhabi sabkhas (Alsharhan and Kendall, 2003; Strohmenger et al., 2010; Kirkham, 2011; Riegl et al., 2010; Warren, 2016).

Hence, it is of no surprise that Abu Dhabi sabkhas are one of the most often studied arid system in the world (Warren and Kendall, 1985), giving rise to the 'classic sabkha model'. Most of the sabkhas found worldwide, however, do not share the same attributes with the Abu Dhabi sabkhas (Handford, 1981, Warren, 2016). When observing satellite imagery, the Abu Dhabi coastline is also a windward facing, barrier island-protected, coastline whilst Mesaieed is on the leeward side of Qatar with no protection on the south-east. This creates a need for understanding the variations among sabkha systems.

Extensive literature on Abu Dhabi sabkhas and sedimentology has created an impression that coastal sabkhas are diagenetic evaporites hosted in carbonate matrices (Warren, 2016). Therefore, this is extensively used as a modern analogue to understand ancient arid hydrocarbon reservoirs, many of which, however, are hosted in siliciclastic sediments. This can be exemplified by the Permian Zechstein sandstone, Permian Rotliegend sandstone (Rossel, 1982) and Guadalupian lagoon of the Permian Central Basin Platform in West Texas and New Mexico.

Despite the abundance of recent gypsum precipitates in sabkha environments, and more localised anhydrite and halite, a very large proportion of studies are focused on dolomitization (McKenzie et al., 1981; Patterson and Kinsman, 1982; Bontognali et al., 2012) rather than early evaporite diagenesis. In addition, most previous studies were based on surface observations and are limited to the reach of a shovel. Previous studies often study the Holocene sabkha as one unit, disregarding the relationship between the landward parts of the sabkha with continental waters, and the relationship to the coastward parts of the sabkha with seawater. In addition, there is little understanding of the Neogene carbonates underlying the Holocene sabkha and how the brines may interact in these two hydrogeologically-connected aquifers. Permeabilities of sabkhas, up-dip of the sabkha and the underlying system have also received little attention even though they provide important baffles or conduits in fluid flow.

Studies on siliciclastic sabkhas are relatively rare. Quartz is less reactive than polymorphs of carbonate minerals and, hence, different reactions are expected. This thesis provided an opportunity to incorporate high-resolution depth-related data. Mesaieed sabkha thus provides a unique opportunity to fully capture a coastal sabkha system that is predominantly siliciclastic, and leeward facing, relative to the wind.

1.3.1 Impact for Hydrocarbon Exploration

Within the upstream oil and gas industry, combined use of sequence stratigraphy and geophysics is not sufficient to adequately predict the distribution of early diagenesis and how the processes impacts the pore system. This work presents models of processes that might be employed on the scale of a high-resolution geologic model (Figure 1-6). The research impacts provide direct application to aid conditioning of subsurface geologic models of arid mixed siliciclastic-carbonate formations, by improving:

1. syndepositional diagenetic concepts and models for arid ramp systems that are impacted by early diagenesis, such as gypsum cements and associated mineralogy
2. prediction of reservoir quality trends and diagenetic geobodies, such as 3-dimensional rock property distribution – which serves as input properties to static reservoir model

Knowing the geometry, distribution and extent of gypsum cements will provide a more robust geologic model, which ultimately improves in-field well placement, field development, and secondary and tertiary recovery strategies.

Modern sabkha environments in Qatar provide a unique and unparalleled opportunity for characterization and interpretation of early diagenetic processes that have substantial impacts on reservoir quality in in an arid mixed siliclastic-carbonate depositional system (Figure 1-10).

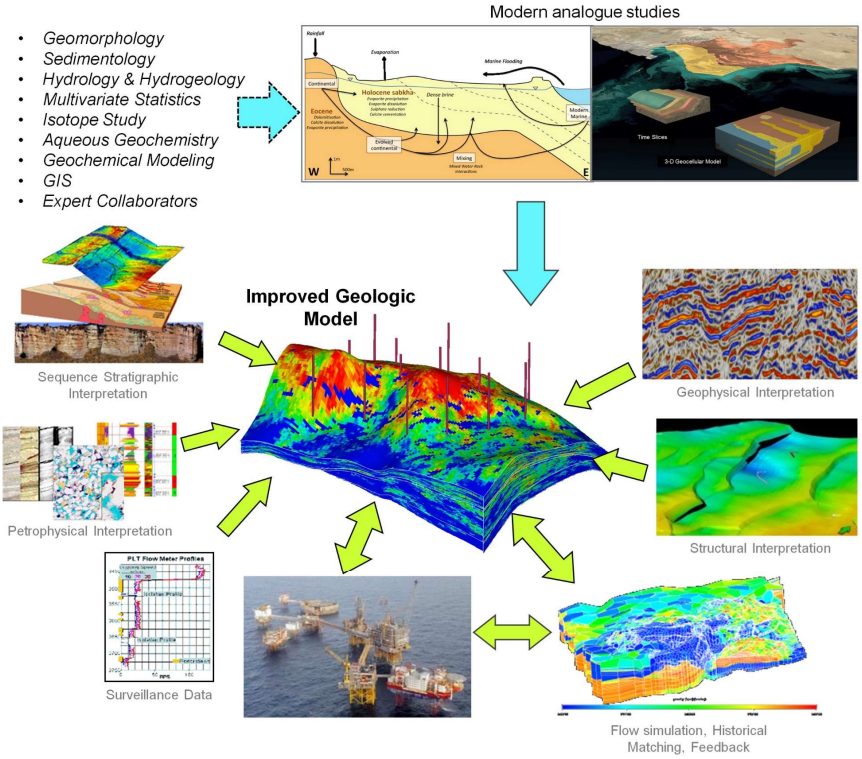

Figure 1-5. The components involved in the exploration and production workflow for petroluem geoscientist, petrophysicist and petroleum reservoir engineers in the mining and oil and gas industry.

1.4 Wider Research Impacts

Mars

Sabkhas have been noted as good Earth analogues to Martian paleo-environments (Ori and Marinangeli, 2002; McKay et al., 2016). The perception of Mars as a cold, dry and dead planet is no longer true. Photogeologic surveys of channels cutting through stratigraphically young rocks, paleoshorelines, and crater lakes provide evidence of possibly still active hydrology (Komatsu et al, 2007; Dohm et al, 2008). High albedo zones are interpreted as evaporitic deposits, supported by detection of sulphate minerals in abundance from both the orbit and at the surface (Ori and Marinangeli, 2002; Wray et al, 2009). Evaporite veins were found to be rich in calcium and sulphur with ratios consistent with relatively pure hydrated calcium sulphate, gypsum (Figure 1-7).

At Olympia Undae, the largest field of sand dunes, high concentrations of gypsum minerals were detected in the eastern region, with a preference for precipitation at the crests of the dune (Roach et al., 2007). With ground missions still ongoing, a more conclusive study of a suspected sabkha at the Columbus crater in Terra Sirenum (Ori, 2010; Wray et al, 2009) could link to a large-scale active hydrological regime in the subsurface.

Understanding and anticipating the nature of sabkhas and associated diagenesis may provide an in-depth understanding of the provenance of evaporites. This study can help constrain the processes leading to the confirmation of presence of water, and thus, contribute a solid framework on what is expected during the Mars exploration in the next decade.

Figure 1-6 Evaporite veins encountered by NASA's Mars Evploration Rover Opportunity in 2011 with width of 1-2 cm and length of about 0.5 m long. It is found to be rich in calcium and sulphur with ratios of a relatively pure hydrated calcium sulphate, gypsum. (Source: NASA Photo Journal, 2013).

Geotechnical Challenge

Sabkhas prevail along most of the southern Arabian Gulf coastline, a location highly valued by developers for urbanization and residential settlement as well as development of ports and other industrial facilities (see publications by Al-Amoudi, 1994, 1995; Al-Homidy, 2017). Unfortunately, they present a fundamental geotechnical challenge due to their poor mechanical properties coupled with aggressive geochemical characteristics and high variability in both lateral and vertical extents (Dhowian et al, 1987). Engineering hazards of interest include heaving from salt crystallization - recrystallization, subsidence from dissolution of intrasediment salts, and flooding risk due to low infiltration capacity (Shehata & Amin, 1997; Shanin, 2009). In an event of gypsum dehydration as it transitions to anhydrite during continued hyperaridity, about 38% of the sabkha volume will decrease, whilst anhydrite rehydration corresponds to a 60% increase (Bjorlykke, 2015). Such dramatic change from the introduction of fluid reflects on the damaging effects sabkha can have on foundations.

1.5 Objectives

The overarching goal of this thesis is to refine our understanding of the early diagenesis of a mixed siliciclastic-carbonate leeward coastal sabkha system to establish the origin of gypsum and associated minerals. These models are derived from the study of depositional history, hydrogeology, and aqueous geochemistry of Mesaieed sabkha in Qatar. By understanding the syndepositional diagenesis of a coastal sabkha system, like Mesaieed, it will be possible to develop a better-constrained process-based early diagenesis models for the development of Holocene sabkhas of the Arabian Gulf. These arid coastal systems are commonly used as analogues for many hydrocarbon reservoirs of the Middle East, thus, an understanding of their formation is crucial to the interpretation of ancient subsurface systems and the development of accurate geologic models.

Specifically, the goal of the thesis is to develop insights into the origin of diagenetic evaporites, particularly calcium sulphate minerals within a modern arid mixed siliciclastic-carbonate system, and its subsequent flow pathway and brine evolution. The study encompasses sequence stratigraphy, geomorphology, primary sedimentology and mineralogy, diagenetic overprint, and permeability distribution in both the sabkha and the Dammam Formation sequences. This provides a holistic process-based framework to understanding the hydrogeological and geochemical evolution of the sabkha system.

Reconstructing early diagenesis of a sabkha system relies on being able to answer the following four key questions:

1. What is the geomorphology and distribution of primary sediments and secondary evaporites in a leeward coastal sabkha in Mesaieed?

2. What are the sources of fluids and flow pathways by which fluids are exchanged between marine waters, the updip aquifers, and the sabkha and the underlying aquifer?

3. What are the sources of solutes for diagenetic evaporite mineralisation, and the subsequent evolution of the brine?

4. In what way are hydrogeology and aqueous geochemistry able to provide insights into evaporite diagenesis, and what are their limitations?

1.6 Methodology

The sabkha system is a highly dynamic system, hence studying the early diagenesis to understand the origin of the evaporites requires a cross-disciplinary methodology. It entails analysis of the pore network and products, followed by progressive evolution of intrasedimentary brine, and the resulting sequence of water-rock interaction. The study will use coupled field characterization and quantitative process-based studies, which have not been previously undertaken for Qatar sabkhas. This interdisciplinary study integrates an understanding of sedimentology, diagenesis, hydrogeology, and aqueous geochemistry to address the gaps in our understanding of sabkhas.

The study can be divided into product- and process-based approaches. Such a combined approach will help consolidate our understanding of processes in modern evaporitic systems and offer new insights on the origin of diagenetic distribution of formations.

Product-based approach

To understand the depositional sequence, characterizing the depositional products of the system in the geologic record is the first and most commonly used approach. This traditional approach involves a multi-scale petrographic study to identify and classify the porosity and permeability network, for example using macroscopic description of core and microscopic study of the thin-sections. Pore classification, involving rock fabric and petrophysical characteristics, aid the interpretation of diagenetic stages and the associated hydrological setting (Lucia, 1995; Flugel, 2013). The associated diagenetic processes, fluid composition, pressure, and temperature are often inferred from such a study to capture the whole paragenetic sequence. Other associated techniques include characterising elemental composition of products, cathodoluminescence microscopy, trace element analysis, isotopic analysis, and/or fluid inclusions (Goldstein, 1986; Paquette and Reeder, 1995; Fairchild et al., 2000; Vuillemin et al., 2011)

This approach has its limitations, as paragenetic and diagenetic sequences occur in stages and are variable over time. Often, the assumption made in this methodology is that the solute system is geochemically closed (Wood et al., 2005). This means that the minerals are assumed to represent the initial pore water solute at the time of deposition. This can be circumvented by understanding the system from its input sources, from the stratigraphy underlying and the stratigraphy surrounding it. This

method can be more robust by incorporating multiple sampling to account for temporal effects like changes in seasons.

Process-based approach

While hydrogeochemical studies in modern environments have been substantial, they are not often used to infer water-rock interaction and diagenetic processes. Rather, these techniques are typically used for the classification of hydrozones and characterizing variations in aqueous geochemical and contaminants, often from an environmental context.

In the last decade, an increasing number of geoscientists have used process-based techniques (including hydrogeochemical studies) to quantify the diagenetic processes that are occurring in dynamic surface systems (Wood et al., 2002; Whitaker and Smart, 2007a; Martin and Moore, 2008; Moore et al., 2010; Gulley et al., 2014; Cooper, 2015). This approach involves first, constraining both the surface and groundwater flow pathways (both vertical and horizontal), potential source (as input flow) and potential outputs, followed by an aqueous geochemical characterization of the waters along the pathways. Often, the geochemical characterization involves chemical modelling with regards to thermodynamics.

A substantial product-based approach usually precedes this method. Comparison with a product-based study will help constrain the diagenesis of the system. Often, the process-based approach is time-consuming and costly, which is why only a handful of workers have been taking this approach.

1.7 Thesis Structure

The thesis is presented in an alternative format in the form of a hybrid thesis-journal style, with the intention that the chapters are interdependent. Thus, each chapter consists of an introduction, literature review, methodology, results, discussions and conclusions. As these three chapters address similar overarching themes, some repetition across chapters is unavoidable.

A thesis offers a format to expand at length on detailed insights that are often excluded from an academic paper. As such, the typical format where each chapter in this thesis equals one academic paper is not appropriate.

Data tables and results are presented in Electronic Appendix (p 295).

The following paragraphs detail the outline of this thesis:

Chapter 2: Geomorphology, Sedimentology, Diagenetic Overprint and Permeability of Mesaieed

The thesis will begin with the field and subsurface characterization of the sabkha and Dammam formation, followed by an analysis of sediment and bedrock permeability. This chapter presents existing data and historic data combined with collected data to generate spatial maps, cross-sections, a distribution map of sabkha sub-environments and gypsum. The chapter contributes to the understanding of geomorphology, sedimentology of the sabkha and underlying dolomite bedrock, its environments of deposition, diagenetic overprints by gypsum and permeability.

Chapter 3: A Hydrological and Hydrogeological Perspective on Early Diagenesis in the Coastal Sabkha of Mesaieed

The physical hydrology and hydrogeology of the Mesaieed coastal sabkha in south-eastern Qatar are examined in this chapter. This contributes to the understanding of the physical factors i.e. aquifer properties, end-members of waters in the sabkha, mixing zones and fluid flow pathways. The study is based on coupling groundwater head, and salinity distribution both spatially and vertically. Chapter 3 allows for the building of a hydrological conceptual model which is a stepping stone to the understanding of aqueous geochemical pathway contribution to the major solutes for evaporite precipitation. This will be linked to the aqueous geochemistry in a subsequent chapter to aid in understanding the distribution and nature of diagenesis.

Chapter 4: Geochemistry in the Coastal Sabkha of Mesaieed

Chapter 4 presents chemical factors that are responsible for providing sources of solutes and solute ratio compositions for precipitation and/or dissolution of evaporites, and the associated dolomite and clay. This chapter provides insight on solutes bounded by thermodynamic laws and the subsequent evolution of brine.

Chapter 5: Summary of Early Diagenesis in Mesaieed Sabkha

Chapter 5 summarizes the principal findings of chapters 2 to 4.

PART 3: Literature Review

1.8 Arabian Gulf: Geography and Climate Setting

The Arabian Gulf connects to the Indian Ocan by the Strait of Hormuz in the southeast. It is a partially restricted shallow basin, that trends northwest-southeast. The bathymetric axis of the Arabian Gulf is a natural separation between the Iranian Fold Belt and the Arabian Foreland (Purser and Seibold, 1973). Mesozoic collision between Arabia and Asia formed the Arabian Gulf and Zagros Mountains. The depth of the sea is shallow, approximately 30 m deep, with increasing depth from the northwest to the southeast (Purser, 1973; Purser and Seibold, 1973). The Arabian Gulf is of geological interest, because it is the only present-day analogue of an inland sea wherein extensive carbonate ramps are forming (Warren, 2016). The Arabian Gulf forms part of a low-angle carbonate ramp depositional system, whereby active sabkha system forms the supratidal portion of the ramp (Lokier, 2012).

The state of Qatar, which lies on the eastern coast of the Arabian Gulf, is situated between 23° 17' north and 51° 32' west. The small peninsula is a distinctive geomorphologic feature on a near-linear Gulf coastline, which is likely to have caused atypical trends in seawater currents and in sedimentation patterns along the southern margin (Warren, 2016). Structurally, Qatar appears as an elliptical North–South anticlinal arch. Qatar's coastal profile is largely flat, with a low relief between 2-10 m (based on Google Earth Pro DEM), while the highest point is only 100 m above sea level (asl) in the centre of the state. The surface geology consists mostly of the Eocene-aged Dammam Formation, which is a limestone with localised dolomitisation, with occasional some chert and marl.

The general climate of peninsula can be described as extremely arid during the summer months and mild during the winter, with a Köppen climate classification *BWh*. Rainfalls are extremely rare, scanty and are often localised, occurring as short bursts of heavy rainstorms. Air temperatures show a mean of 28.3 °C (Table 1), with maximum temperatures up to 59.1 °C. Humidity reaches dewpoint in the summer and rarely in the winter. The seawater circulation in the Gulf is counter-clockwise and the salinities are slightly elevated compared to global seawater, up to 40 ‰ in local coastal waters. The tidal regime in the Gulf is microtidal, which means tidal range does not reach > 2 m.

Table 1. Overview of the climate parameters in Qatar, as recoded at the Doha International Airport from March 1999 to January 2014 in 3-h resolution (after Matzarakis and Frohlich, 2014).

Parameter	Min	1st quantile	Mean	Median	3rd quantile	Max
Air temperature (°C)	1.4	22.0	28.3	29.0	34.0	59.1
Relative humidity (%)	4.7	38.2	54.3	56.2	71.0	100.0
Vapor pressure (hPa)	1.4	13.8	20.4	18.74	25.75	50.16
Wind velocity (m/s)	0.0	2.6	4.9	4.6	6.5	44.5

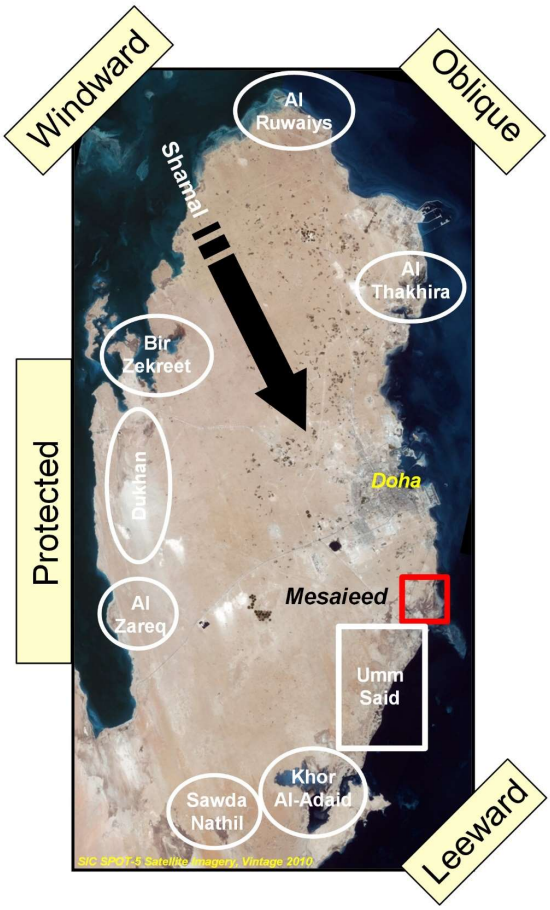

Figure 1-7. Types of coastline in Qatar relative to the shamal wind. White boxes highlight the sabkhas in Qatar, while the red box highlighting Mesaieed sabkha, which is the study area of interest. (Source: Strohmenger and Jameson, 2014)

Holocene sabkhas fringe much of the coast of the Qatar Peninsular, onlapping the Dammam Formation (Jameson and Puls, in press). The coastal sabkhas in Qatar are divided into four coastlines relative to the shamal winds: oblique, protected, windward and leeward (Jameson et al., 2009) (Figure 1-8). The diversity of coastal profiles observed around the Qatar peninsula reflects the importance of interactions between the prevailing shamal wind providing sediment supply (see Appendix, Figure A-1) and the elevation profile in creating different facies, and physiographic areas of sabkhas (Jameson et al., 2009).

The prevailing wind in this region is the northwesterly Shamal. As a small peninsula, Qatar's immediate aeolian sources are limited, but its proximity to extensive dust and sand source regions of the Arabian Gulf especially in Saudi Arabia and Iraq means that Qatar is plague with intense seasonal dust storms (Figure 1-9). This highlights the power of wind to transport relatively large grains over thousands of kilometres. On deposition, these grains may provide the nuclei for precipitation of evaporite and carbonate minerals.

Mesaieed coastal sabkha, shown as a red box on Figure 1-8, is situated on the eastern coastline of Qatar on a leeward coastline zone with respect to the shamal (Jameson and Strohmenger, 2015). It is located at the country's northernmost barchan dunes, which consists of both siliciclastic and carbonate sediments. Previous works on the physical sedimentology of the area were focused only on the greater Umm Said which is the greater 440±8 km² portion just south of Mesaieed (Groot, 1973; Al-Youssef, 2003).

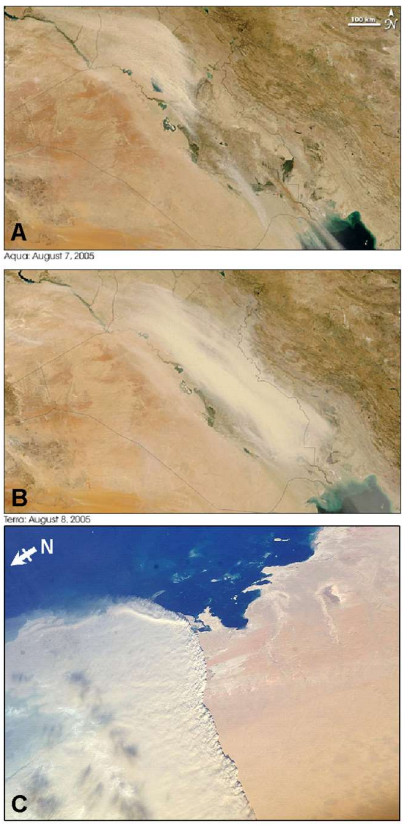

Figure 1-8. Massive sandstorm sweeping over Iraq (**A** and **B**) in 2005 and over the Arabian Gulf into Qatar and (**C**) toward Saudi Arabia and the southwestern United Arab Emirates in February 15, 2004 (modified from NASA Earth Observatory).

Rapid urbanisation of Qatar has led to the massive expansion of both industrial and commercial development at a scale rarely observed elsewhere, leading to modification of coastal sabkha environments. In response to a similar coastal sabkha loss in the neighbouring UAE, whereby only 35 % of the Abu Dhabi natural coastline remains today (Lokier, 2013), the Qatari government applied for UNESCO-recognized protection for conservation of Khor Al-Adaid (UNESCO, 2008), an inland sea some 60 km south of Doha. However, this does not stop Umm Said to undergo more infrastructure development than ever before – from only 30±2 km² in 1984 to 180±5 km² in 2016 (Figure 1-10). This thesis is an extensive characterization of the sabkha system prior to the construction of Hamad Port,

or previously known as New Doha Ports (NDP), where little of the sabkha remain. The thesis is a document of the coastal sabkha Mesaieed prior to New Doha Ports (NDP) construction.

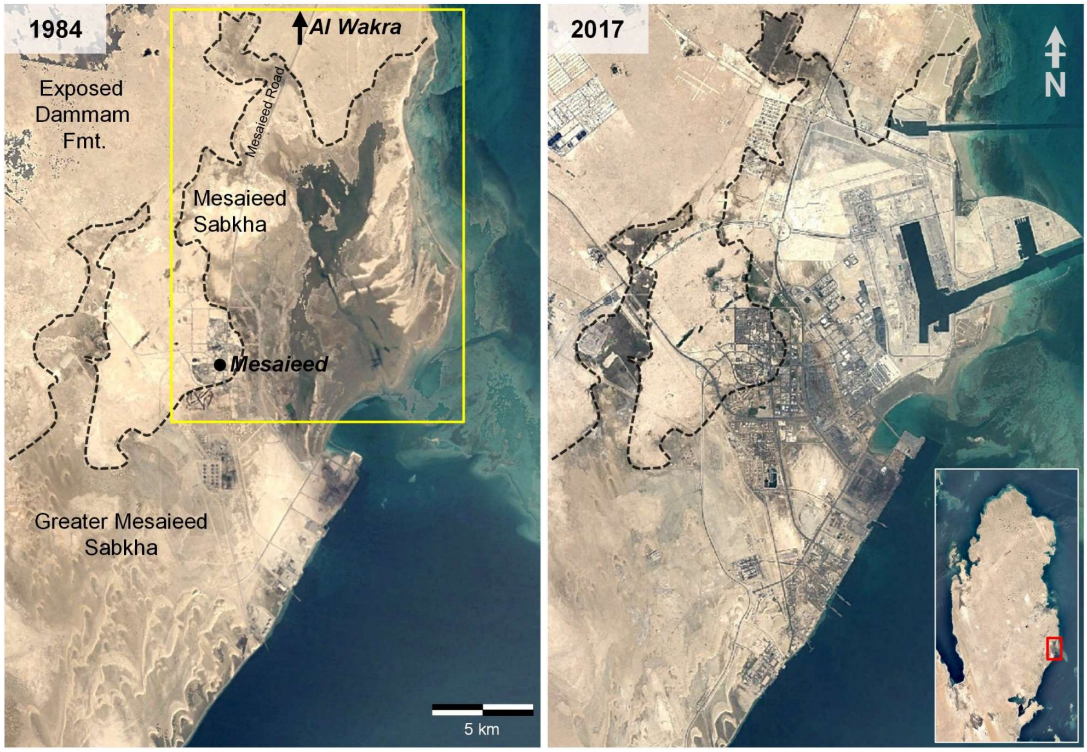

Figure 1-9. Paired Landsat images of Mesaieed coastal sabkha (inset showing relative location in Qatar), with clear destruction of sabkha environments in a 33-year period since December 1984 (left) to January 2017 (right). Yellow box denotes study area of the chapter while dashed black lines shows the limit of bedrock of Eocene-age Dammam formation updip of the sabkha. Recent urban developments have obscured the former sabkha.

1.9 Sea-level History and Holocene Highstand

The shallow depth of the Arabian Gulf has made it highly sensitive to periods of exposure and flooding over its Quaternary history, driven by fluctuating sea-level (Strohmenger and Jameson, 2015). The Pleistocene was a time of high humidity and a wet climate, from 80 ka (thousand years ago) (Rosenberg et al., 2012, 2013) to 18 ka (Goodall, 1995; Weijermars, 1999).

Since the last glacial maximum (between 26.5 and 19 ka), marine regression reached its lowest, between 120 m and 130 m below present-day sea level (Lambeck et al., 1996; Clark et al., 2009), leaving the Arabian Gulf sea floor exposed and aeolian processes to dominate (Lokier et al., 2015). The recent sediments are a product of Holocene marine transgression, which entered the Arabian Gulf seafloor and established a seaway by circa 12.5 ka. The post-glacial event marked a hyper arid climate and peaked at the highest level at >1 m above sea level just after 5290-4570 cal yr BP (Lokier et al., 2015). During the mid-Holocene transgression period, shamal winds have blown most of the sand trapped on the Qatar peninsula, transporting it towards the southeast, as observed in Mesaieed, Umm Said and Khor Al-Adaid (Strohmenger and Jameson, 2015).

The sea-level fell to its present-day levels by 1440-1170 cal yr BP (Lokier et al., 2015). The rapid fall in relative sea-level thereafter led to periods of exposure whereby the shamal wind causes deflation and erosion of the Holocene highstands. The sea-level fall resulted in a forced regression of the coastal sediments, which is a downstepping geometry, and consequently, a rapid progradation of the sabkha facies (Lokier et al., 2015). The leeward side of Qatar allowed coastal areas like Mesaieed sabkha to grow in a relative short span of time. Satellite images of Mesaieed and field observations found Holocene beach deposits at approximately 2 m above current local sea-level.

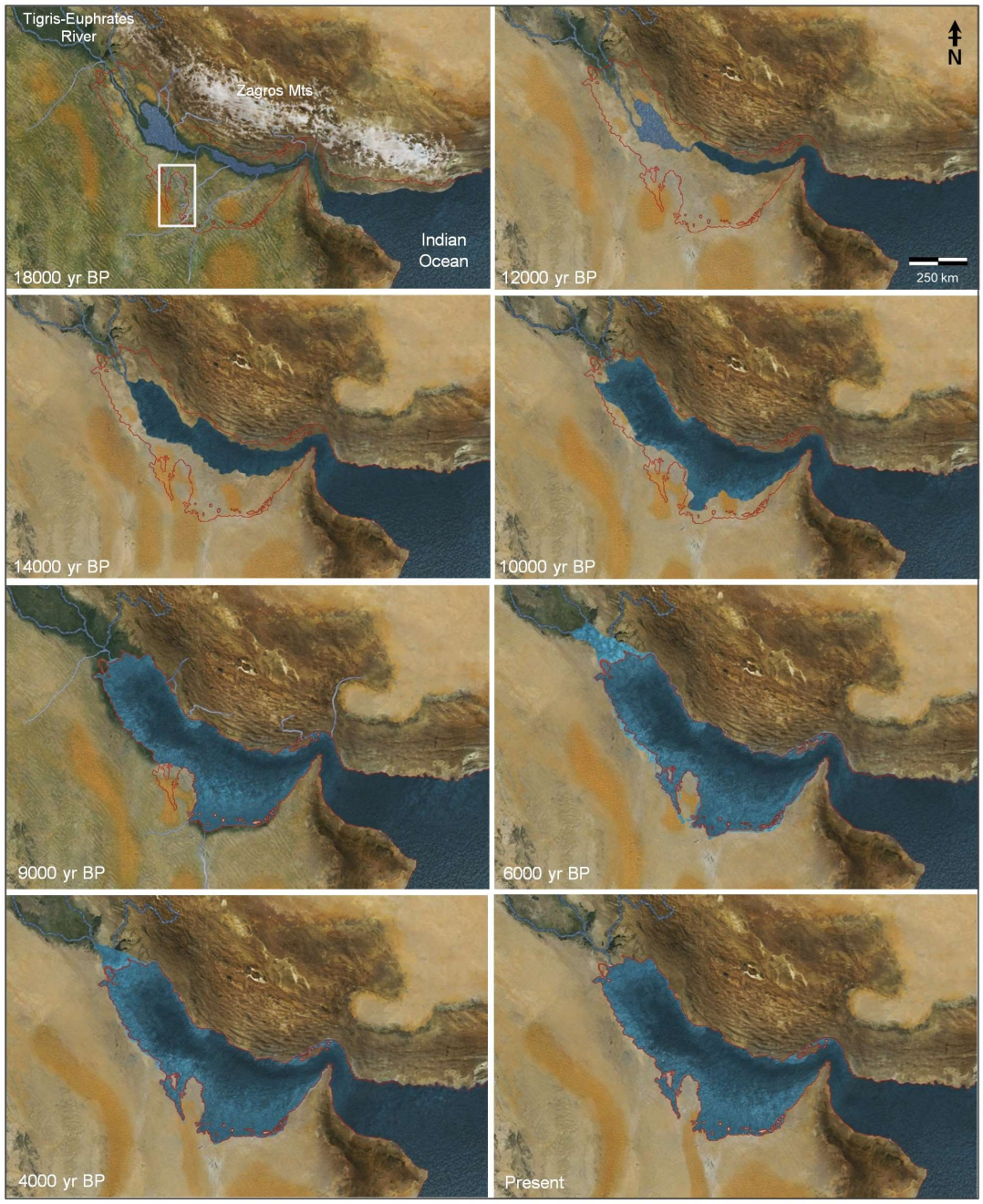

Figure 1-10. Overview of sea-level history in the Arabian Gulf from 18,000 yr BP to present day with Qatar peninsula (white box). (Screenshots 18,000 yr BP, 14,000 yr BP, 9,000 yr BP and 6,000 yr edited from Strohmenger and Jameson, 2015; Other timeline screenshots were provided by Jameson and Strohmenger, altered after Lambeck, 1996)

1.10 Overview of Previous Work on Sabkhas in Qatar

Qatar's coastline was studied initially by Shinn (1973), as part of a regional survey team led by Bruce Purser who focused along the coast of the United Arab Emirates (at that time known as the Trucial Coast. Shinn (2011) later revisited the peninsula to study the sedimentology of Al Thakira (or known as Ras Umm Said), a carbonate sabkha in the north (Figure 1-8). Jameson has conducted nationwide surface geology mapping of Qatar combining gypsum distribution mapping, field sedimentology, sequence stratigraphy, and GIS studies (Jameson and Puls, in press). Authigenic dolomite was documented in a supratidal coastal sabkha (Wells, 1962) while Groot (1973) studied the Mg/Ca geochemistry of the sabkha brines at Umm Said (Figure 1-8). Groot recognized that there is an evaporation-driven reflux system within the sabkha system close to the coastline but found no relationship to dolomitization. Further studies were undertaken on dolomite formation in Bir Zekreet (Figure 1-8), northwest of Qatar (Illing et al, 1965); high Mg-calcite as primary precipitate and as aragonite replacement cementing layers of the coastal sabkhas (Taylor and Illing, 1969); changes in chemistry to explain penecontemporaneous dolomitization in Faishakh sabkha, just north of Bir Zekreet (Illing and Taylor, 1993).

Anhydrites were studied on Dukhan sabkha (Figure 1-8) by Perthuisot (1977), who suggested an oxidizing environment to explain the possibility of anhydrite precipitation when the reaction is beyond equilibrium conditions, considering gypsum-anhydrite transformation is endothermic. Edwards et al (2010) conducted Raman spectroscopic analysis on the Dukhan sabkha as an analogue to astrobiological elements in future Mars exploration missions. That study focused on biogeological molecules under extreme environments. A study on geochemistry and porewater gradients below the surface of the microbial mat was preliminary conducted at Umm Alhool sabkha, located north of Mesaieed sabkha (Al-Raei et al, 2012).

Eccleston et al (1981, 1987) undertook a nationwide hydrogeology study jointly funded by FAO and Qatar government focusing on the water resources in the Umm Er Radhuma and Rus aquifers within the Dammam Formation bedrock (also see Lloyd et al, 1987). A study on the northern Qatar aquifer was conducted to determine the feasibility of artificial recharge (Kimrey, 1985; Streetly & Kotoub, 1998). The Ministry of Environment (2008) conducted a follow-up study of a similar scale to understand the hydrogeology and geochemistry of the deeper aquifers in Qatar. The PhD work of Al-Youssef (2003) on the Umm Said sabkha, the greater southern extension of the Mesaieed, and field research by Jameson and Strohmenger, provided the regional foundation for this research. Their work was mainly focused on the mineralogy and geochemical characteristics of the sediments. This provided opportunities for more in-depth analysis of relationships between different solutes and the water-rock-interaction, to arrive at a more critical interpretation of the results.

1.11 Sabkha Hydrology

Hydrological studies of the Arabian Gulf sabkhas began in an area close to Abu Dhabi (Hsu and Siegenthaler, 1969; Hsu and Schneider, 1973; McKenzie et al., 1980; Patterson and Kinsman, 1977, 1981), before a broader study along the coast of Abu Dhabi was undertaken (Sanford and Wood, 1991, 2001; Wood et al., 2002; 2003; 2005). The initial studies of coastal sabkhas focused only on the top 1 m below the surface of the sabkha (Evans et al., 1969, Kinsman, 1969), but the potential importance of hydrologic and chemical interaction with underlying and updip formations has been ignored. Previous studies have disagreed on the dominant source of fluids and solutes for the Holocene coastal sabkha in Abu Dhabi. These studies proposed three major and conflicting conceptual models (Figure 1-12) to explain coastal sabkha settings: 1) the seawater flooding, 2) the evaporative pumping, and 3) the ascending brine models.

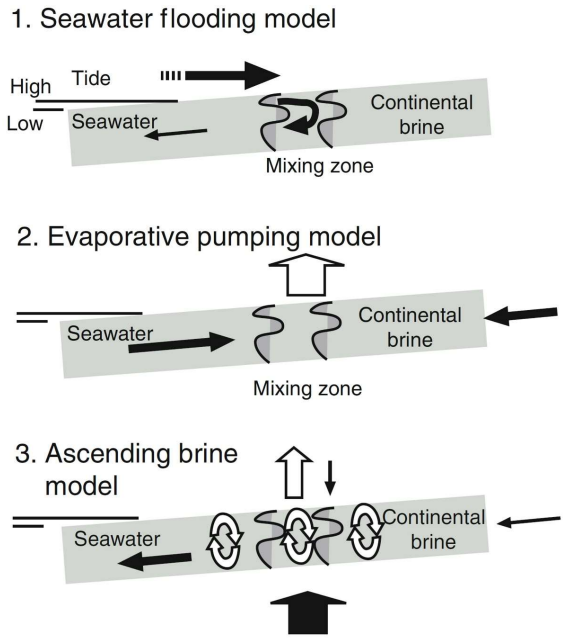

Figure 1-11. Schematic of various models for sources of fluids and solutes (1) seawater-flooding model, (2) evaporative-pumping model, (3) ascending brine model. Relative mass fluxes of solute are represented by the size of the arrows. Open arrows represent loss of water via vapour, solid arrows represent solute sourcing the sabkha. (modified from Wood et al., 2002; Warren, 2016)

The **seawater flooding model** (Figure 1-12-1) proposes that marine flooding from the Arabian Gulf is the dominant source of fluids and solutes to the coastal sabkha (Butler, 1969; Evans et al., 1969; Kinsman, 1969). This model suggests the main recharge is sourced from ponded marine waters driven by high tides and strong onshore shamal winds. These waters then evaporate, flow onto the Holocene sabkha, and laterally flow outward to the ocean. This ignores the effect of the hydraulic gradient generated regionally by recharge from Al-Hajar mountains in north western Oman.

The **evaporative pumping model** (Figure 1-12-2) suggests that strong evaporation of water, either from pore waters or from standing open water bodies, resulting in a change in hydraulic gradient which subsequently induces lateral inflow from continental and marine water sources into the sabkha system (Hsu and Siegenthaler, 1969; Hsu and Schneider, 1973; McKenzie et al., 1980). This model is also applicable to continental sabkhas with limited or no contact with the marine system. In the case of endorheic basins (Handford, 1982) such as Chott El Gharsa in Tunisia (Watson, 1985), continental groundwater will be the only source of solutes. Another example of this includes the Bristol Dry Lake, located in California. However, evaporation-induced cycling of water may not be enough to draw sufficient volumes of water, considering the low permeability of sabkhas.

The **ascending brine model** (ABM) is the most recent model (Figure 1-13), proposing that the underlying Tertiary brines is the major source of solutes, while direct precipitation on the surface sediment is the major source of fluids. This was examined in Abu Dhabi (Sanford and Wood, 2001; Wood et al., 2005; van Dam et al., 2009; Wood, 2011, Kraemer et al., 2014) and in one study in Sabkha Al-Khiran (Al-Hurban and Gharib, 2004). The model suggests that strong evaporation at the sabkha surface creates an increase in hydraulic gradient which pulls brines upward from underlying aquifers. This supplies solutes that will ultimately precipitate within the capillary zone of the sabkha. The process alternates with the dissolution of halite at the surface resulting from precipitation, which forms denser saline waters and then sinks into the underlying aquifer. This cycling of brines can potentially form a conducive environment for reflux (Patterson & Kinsman, 1982; Whitaker et al., 2015).

From the ABM model, it is theorized that major solutes are concentrated by evaporative processes and will, thus, flow back downwards within the aquifer system **by density-driven free convection**. Large-scale convection is possible, depending on the Rayleigh number for the area (Simms and Garven, 2004). This additional mechanism for fast subvertical mixing of sabkha groundwater brines was investigated using numerical simulations and geophysical observations by Van Dam et al. (2009, 2014). During the initial stages of evaporation, brines concentrate at the capillary zone alongside evaporite precipitation. High solubility evaporites, such as halite, are subjected to dissolution during rare events of high precipitation. Such events result in many high concentration "finger-like" plumes to develop from the top surface and descend downwards within the sabkha system (Figure 1-13). The rate of brine descent is numerically simulated by Simmons et al (2001) and Van Dam (2014) as relatively rapid, initially at around 0.2 m/day which decreases to 0.02 m/day after one year. The slowing of descent could be due to mechanical dispersion, fluid entrainment, molecular diffusion that reduce the density of the fingering plumes (Xie et al., 2011). Wood and Böhlke (2016) used isotopically fractionated nitrate to further propose this model and reiterated that density-driven free convection model within the Abu Dhabi sabkha only occurs following rare but strong precipitation events.

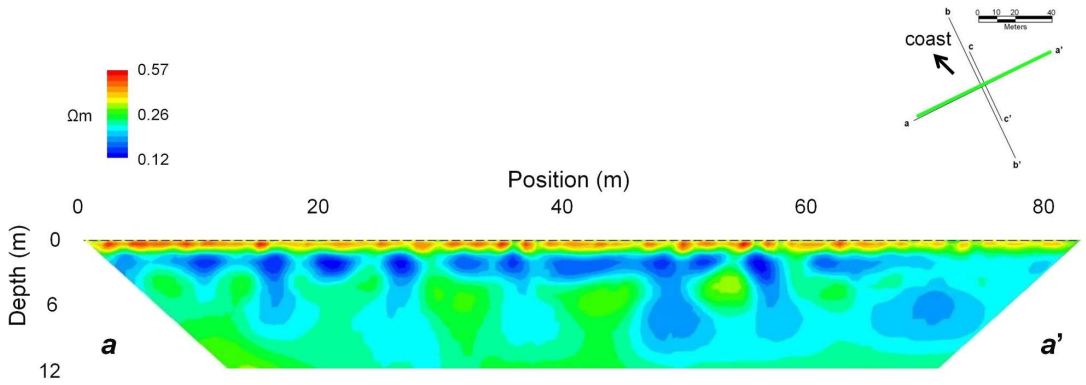

Figure 1-12. Free convection profile of Abu Dhabi sabkha one month after 100mm precipitation. Capillary zone at 0.7 m shows the highest resistivity due to evaporites precipitation. Low resistivity layers are encountered at about 2 m below water table, indicating high salinity from evaporite mineral dissolution from recharge. Below that depth saline finger plumes are seen refluxing into lower salinity groundwater. (modified from Van Dam et al, 2014)

1.12 Sabkha Geochemistry

Most geochemical studies of sabkha systems have been almost exclusively in Abu Dhabi, with some studies are undertaken in on Southern Kuwait sabkhas (Gunatilaka and Mwango, 1987; Gunatilaka, 1990; Robinson and Gunatilaka, 1991). The geochemistry of sabkha pore waters and sediments has been studied in an attempt to to understand dolomitization (Hsü and Siegenthaler, 1969; Butler, 1969; Groot, 1973; McKenzie et al, 1980; Illing and Taylor, 1993), but only rarely have studies focused on evaporite precipitation. Gunatilaka (1990, 1991) for the Sabkha Al-Khiran in Kuwait.

Aqueous geochemistry studies of sabkha systems typically present a generalized characterisation of the entire sabkha (e.g. Wood et al., 2001; Kendall and Alsharhan, 2011), but sabkha system is hypothesized by this research to contain more complexity that is crucial to understand.

Many workers consider seawater to be the dominant source of solutes, either via seawater flooding of the sabkha surface (Kinsman, 1969; Butler, 1969; Patterson and Kinsman, 1977) or via evaporative-pumping of saline groundwaters (Hsü and Siegenthaler, 1969; Hsü and Schneider, 1973; Müller et al., 1990). None of these conceptual models were constrained by the quantitative data characteristics of the hydrogeologic system allowing fluid and thus solute fluxes to be budgeted (Wood et al, 2002; Warren, 2016). Previous workers who studied the aqueous geochemistry of sabkhas did not consider the geochemical nature of the input waters and trace ions to capture the processes occurring within the sabkhas system. A notable exception is Wood et al. (2001, 2003) in which he found that solutes in Abu Dhabi is found were sourced by >95% from ascending brines from the underlying formation and that the system is vertically mixed.

Older studies suggest that no solutes are sourced from the continental updip groundwater (Patterson and Kinsman, 1977; McKenzie et al., 1980; Hardie, 1987), or that they are an insignificant input

to the system (Wood et al., 2001). Wood et al (2001), however, did not undertake the sampling of the exposed Dammam aquifer up-dip of the sabkha to understand the hydrology and solute behaviour in relation to the sabkha system.

Sabkha studies also often present just the molar concentration of the major ions (Groot, 1973; Illing and Taylor, 1993; Al-Youssef, 2003; Basyoni and Aref, 2016) and only occasionally used isotopes in their interpretation (McKenzie et al., 1980; Wood et al., 2002). Integrating molality and molar activity, phase diagram and thermodynamic potential in modern sabkha setting were very never previously undertaken to provide a greater depth of understanding on the aqueous geochemistry.

The geochemistry of the coastal sabkhas in Qatar has been studied in the northwest (Illing and Taylor, 1993), Sabkha Faishakh and in Umm Said, south of Mesaieed (Groot, 1973; Al-Youssef, 2003), which provides a broad hydrogeochemical characterization. Groot (1973) inferred that the sabkha brines are stagnant, and it was based on how high the salinity is. Both workers offer contradicting conclusions on the movement of solutes: Al-Youssef (2003) inferred that the proportion of Na and Cl increases landward and that there is a seaward discharge through the Holocene (assuming the Dammam was impermeable), while Groot (1973) hypothesised that recharge into the sabkha comes from the seawater.

Groot (1973) geochemical study was focused on dolomitization which highlights that a loss of Mg ions was due to recent dolomite precipitation that is unrelated to reflux of the system. In addition, data of 5 wells and 5 pits in Groot (1973) inferred that the sabkha is "saturated, or almost saturated with halite" using chloride concentration, rather than actual thermodynamic calculation to quantify the potential of precipitation relative to halite. Al-Youssef (2014) mentioned that high concentrations of Ca and SO_4 ions may facilitate the formation of gypsum and attributed the main source of these two ions to gypsum dissolution with a secondary source from carbonate. This conclusion was made without establishing geochemical mass balance thermodynamic calculations nor with an attempt to compare with the input waters to quantify these processes.

2 Sedimentology and Diagenetic Overprint of Mesaieed Sabkha

Author Contributions: Core data within the proximal sabkha, upper sabkha and middle sabkha and hand-dug pits, XRD analyses, GIS analyses within the proximal and upper sabkha were carried out by the author with assistance from Jeremy Jameson, Christian Strohmenger and James Duggan. Co-author Jeremy Jameson critically reviewed and provided direction during the progress of this study. Uncalibrated ^{14}C data and XRD data of the middle and lower sabkha were provided by Jeremy Jameson. Cores of the Dammam Formation underlying the middle and lower were provided by NDPP to the author for analysis. Fiona Whitaker and April Denise Coker reviewed the manuscript and suggested improvements. Didi Ooi Sher is the lead author of this chapter and is responsible for the data mining, analysis and interpretation, subject to the above caveats. All figures were created solely by the author unless otherwise specified.

20,434 words

2.1 Introduction

Holocene coastal sabkhas in the Arabian Gulf have been extensively studied, particularly in Abu Dhabi (e.g. Butler, 1970; Bush, 1973; Evans et al., 1979; Strohmenger et al., 2010). A few sabkhas in Qatar were also previously characterized (Shinn, 1973; Jameson et al., 2009). Studies on sabkha characterization are mostly limited to the near surface (<1 m). These sabkhas are however mostly carbonate dominated and on the windward side, with Abu Dhabi sabkhas being the prime example (Figure 2-1b). Little study has been completed in detail on the leeward arid coastlines that are mixed siliciclastic-carbonate, with the exception of a prominent one being the western sabkhas of Barr al Hikman in Oman (Figure 2-1c), which in itself was limited to a reconnaissance-type study (Mettraux et al., 2011). Mettraux et al. (2011) is the only study of the four sabkhas in the peninsula and hence is limited to only within 20-30 cm below the surface.

Figure 2-1. Satellite image of the southern Arabian Gulf region, highlighting the sabkhas mentioned in the text (as red boxes): a - Mesaieed; b - Ras Umm Said (Al Thakira) sabkha; c – Dukhan; d – Abu Dhabi; e - Barr Al Hikman. Detailed map showing the location of Mesaieed sabkbha, highlighting the leeward location of the coastal sabkha relative to the outcropping Eocene-aged Dammam Formation.

Since the last Holocene highstand, the drop in sea-level has caused a forced regression and thus, progradation in coastal sediments up to present day (Lokier et al., 2015). The subsequent major climatic shift in the Arabian Gulf from wet Pleistocene to arid Holocene has allowed the formation of sabkha systems with varying degrees of evaporites (Jameson and Puls, in press).

The regional stratigraphy of the Qatar subsurface consists of Lower Eocene Umm er Rhaduma Formation, Upper Eocene Rus Formation, and Upper Eocene Dammam Formation (Figure 2-2). In a few areas on the southwest of Qatar, Miocene Hofuf and Miocene Dam formations are seen overlying the Dammam Formation. In the coastal areas and local depressions, however, the Dammam Formation is overlain uncomformably by Holocene sabkha sediments (Llyod et al., 1987) with minor marine carbonate at the wedge (Figure 2-2).

The exposed geological succession of Qatar is made up of Cenozoic limestones, often dolomitised (Jameson and Puls, in press) with Quarternary and recent deposits draping the coastal areas. Qatar was an in the interior platform of the Arabian Peninsula in which a marine regression at the end of the Eocene marked a widespread unconformity, causing the absence of the Upper Eocene and Oligocene stratigraphy, leaving the Middle Eocene Dammam Formation as the dominant exposure of the peninsula (Al-Saad, 2005).

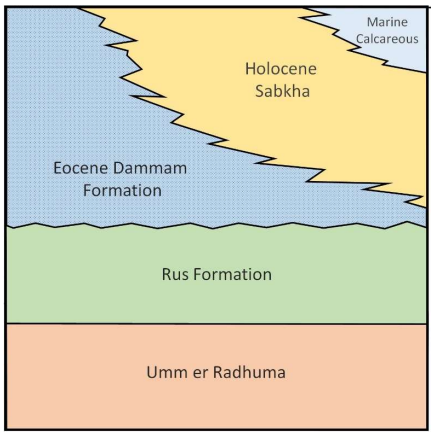

Figure 2-2. Summarized Holocene and Cenozoic stratigraphic column of the coastal geology of southeastern Qatar.

Mesaieed sabkha, some 20 km south of Doha (Figure 2-1), presents a unique opportunity, with its spectacular set of sedimentology features, to understand the synergies between surface processes, diagenetic processes and sea-level changes in a leeward coastal sabkha systems. Mesaieed is located at the north of Umm Said, the greater 450 km² southern extension of southeastern Qatari coastline. Regional-scale sabkha architecture in the country has been studied in Umm Said (Ragab, 1991; Al-Youssef, 2003; Strohmenger and Jameson, 2015; Jameson and Puls, in press), Dukhan (Al-Youssef, 2003) and Ras Umm Said (or also known as Al Thakira) (Shinn, 2010).

Previous work in Umm Said focused more on the physical sedimentology (Groot, 1973, Al-Youssef, 2003, 2014). Al-Youssef, as part of her PhD, extensively characterized the various types of gypsum crystal habits and the mineralogy within the vadose zone. However, the study did not take into account the spatial relationship and vertical distribution of the gypsum within the phreatic zone and in

the Dammam formation. A semi-qualitative study on the back-barrier evolution in Mesaieed were previously undertaken by Jameson (2009) while general geomorphology of the sabkha area focused on semi-quantifying gypsum cementation as a proxy for geologic model conditioning (Strohmenger and Jameson, 2015; Jameson and Puls, in press).

The nature and the distribution of permeability (or hydraulic conductivity) within the sabkha system is seldom studied within a geoscience context. Sanford and Wood (2001) performed a study on the permeability of the sabkha sediments in Abu Dhabi, but it is limited to 6 data points. Insights into permeability can be derived from the geotechnical engineering reports and in literature such as those of Al-Amoudi (1992, 1994, 1995). Studies of the Mesaieed sabkha were initiated in anticipation of the construction of the New Doha Port (NDP), or sometimes called the Hamad Port, the largest of its kind in the Middle East covering 26 km^2 (Finn, 2017). This study characterizes the sabkha prior to the construction of the NDP, which began its excavation in 2012. This chapter includes unpublished datasets from the Ministry of Environment and Phase 2 datasets from New Doha Ports Development. Only half of the original sabkha remains (Chapter 1), and thus this study presents the last dataset as an extension of previous work (Jameson and Puls, in press; Strohmenger and Jameson (2015).

Here I present a detailed study of the whole sabkha system which includes the Dammam Formation both in the updip and in the underlying succession of the sabkha sediments, the proximal sabkha, and the multi-scale permeability which were not previously undertaken for Mesaieed sabkha. The chapter aims to document the internal surface dynamic processes in Mesaieed, primary sedimentology, diagenetic overprint, and semi-quantitative model of sabkha progradation, and serves as an example of a mixed siliciclastic-carbonate sabkha.

2.1.1 Chapter Objectives

The goal of this chapter is to understand the geomorphology, primary sedimentology and secondary diagenesis of the leeward and mixed siliclastic-carbonate coastal sabkha system. This includes a holistic understanding of the different sabkha zones

2.2 Study Area

The Mesaieed sabkha, east of Qatar, is located between the towns of Al-Wakra and Umm Said. The Mesaieed sabkha has an overall width of 6-10 km and it fills topographic lows in the Dammam formation towards the coast. Seasonal tides were observed to drive marine flooding landward of Umm Said (Groot, 1973; Al-Youssef, 2003).

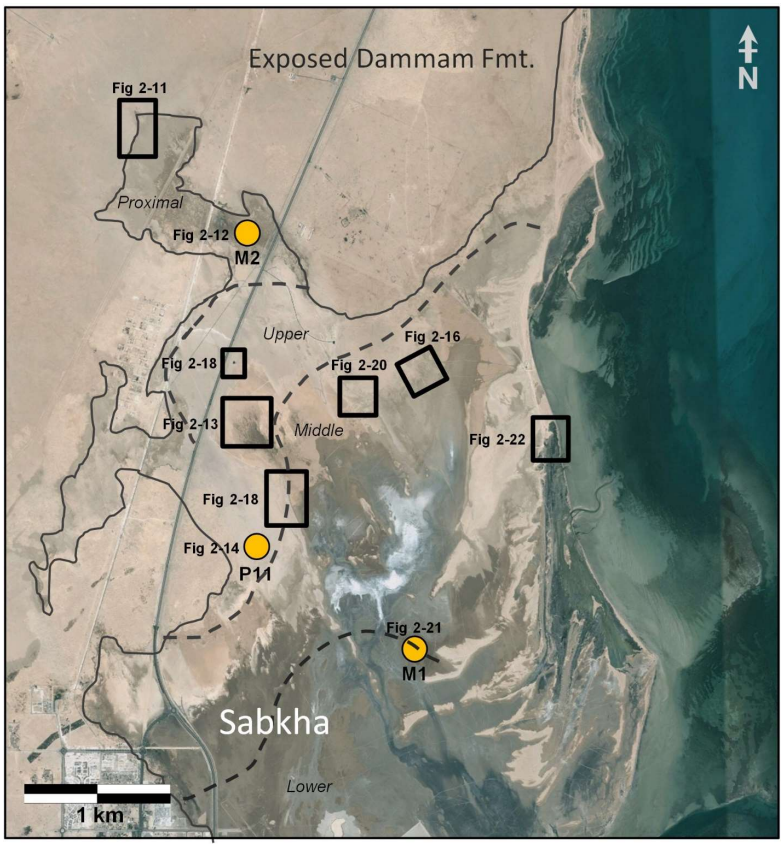

Figure 2-3. Google image of study area Mesaieed with the sabkha geospatial zones. Solid black line indicating the boundary between the exposed Dammam Formation and sabkha. Black rectangular boxes indicate areas where subsequent figures are referred to. Yellow data points indicate wells for this chapter for geomorphology features and permeability.

The updip of the Mesaieed sabkha is the Dammam Formation bedrock, located approximately 10 m above sea level and reaching a height of 13 m asl (above sea level). It is the immediate host for groundwater for the overlying Holocene sabkha. The bedrock is comprised of Eocene-aged Dammam

formation, a carbonate with local dolomitisation, that has been subaerially exposed in the past 30 million years (Ross, 2009). This exposure resulted in a range of geomorphologic features from physical and chemical weathering, including karsts, eroded Dammam rubbles and low-lying depressions. The bedrock surface is covered with subtle drainage channels that form wadis discharging onto the sabkha. Some vegetation was observed in these drainage channels after rainfall events. To the southeast of the exposed bedrock, Holocene-aged sediments onlap on what is believed to be a paleo-drainage system incised within the Dammam Formation (Figure 2-3B) (Strohmenger and Jameson, 2015). These drainages are believed to be carved during the Pleistocene period, which is believed to be humid and wet (Eccleston et al., 1981; Weijermars, 1999). For the scope of this study, the Dammam Formation underlying the sabkha sequence is also described.

In satellite imagery, the Holocene sabkha can clearly be distinguished from outcropping Dammam Formation (Figure 2-3). Using the Munsell® Color Chart, the sabkha appears to be distinctively dark brown, with shades ranging from pale reddish brown (when dry and arid for years without rainfall) to grayish red or moderate brown (when saturated especially after a rainfall). The Dammam Formation is light brown, between the shades of pale yellowish orange and moderate orange pink. Other important features are ponding of water especially after marine flooding, which displays as a dusky blue green colour, and ephemeral salt which is yellowish grey to white.

2.3 Field and Analytical Methodology

Field campaigns in Mesaieed were conducted during the months of October 2012, February 2013, June 2013, and November 2013 to document physical features of Mesaieed via hand dug pits, shallow cored samples and outcrops. Cores of the sabkha were studied during July and August 2013, where they were described and sampled for mineralogy measurements using XRD. Studies of Dammam core samples at the New Doha Port Authority site and permeability testing of Mesaieed wells were conducted between January and February of 2014. Figure 2-3 summarizes the sites and formation in which data was collected.

2.3.1 Elevation datum

The vertical datum of the wells, which is the surface elevation relative to mean sea level (abbreviated in the thesis as asl), were surveyed by Gulf Lab, Dar-Handasah and AECOM. Additional dataset from unpublished New Doha Ports (NDP) 2008 and 2010 geotechnical reports were included. The vertical datum for sabkha pits were validated using high-precision GPS which were calibrated with primary GNSS geodetic control stations located in Mesaieed (Figure 2-4) with assistance from James Duggan.

Figure 2-4. One of two primary geodetic control network station in Mesaieed, G5, located to the northwest of the Mesaieed study site.

These data points were employed to create the top Holocene surface. Data from well control were used to delineate the top Dammam Formation underlying the sabkha, with additional dataset made available from New Doha Ports Project's unpublished reports, and ExxonMobil's 2010 Geographical Information Services (GIS) project. The ExxonMobil GIS project was based on a CGIS DEM terrain dataset (Duggan, 2014), which was in compliance with government guidelines as listed in the Qatar Survey Manual and subsequently serve as a topographic base map. Surface elevation for historic data that had no elevation survey, such as Al-Youssef's sabkha pits, were queried off the digital elevation model (DEM) derivative output using Extract Values to Points tool on ArcGIS 10.3. Root mean square error (RMSE) accuracy for this data was 1.7 cm (Duggan, 2014).

2.3.2 Geomorphology Identification Using GIS

Geomorphology identification were carried out using a combination of colour hues observed on the satellite images. Observation is calibrated with field observations as ground truths. The imagery study was undertaken using GIS software (Google Earth Pro and ArcGIS 10.4). The distribution and first-pass morphology of sedimentary bodies were studied using satellite imagery from the Centre for GIS, Qatar. Although marine flooding and dust storms cannot be studied from satellite imagery alone, time-lapse of historical images can be combined with meteorological data over the same period to understand these events. Historic images of over 32 years were obtained from the Time-lapse tool within Google Earth, which appeared to be generally dated in the month of December. The weather on the day the satellite images were taken were cross-checked with local meteorological data obtained from NDP.

2.3.3 Mineralogy Studies

Field observations, core description and petrographic observations using binocular and transmitted light microscope were undertaken to understand the morphology and facies, both depositional and diagenetic. Core recovery of Mesaieed sabkha sediment was done in December 2012 and February 2013, Dammam cores from below the middle and lower sabkha was recovered by NDP between 2009

and 2012 and were made available to this study. Middle sabkha pits mineralogy and photomicrographs from Jameson and Strohmenger (2014) were included to the dataset. Core descriptions of Mesaieed sabkha sediments and Dammam Formation was done during July 2013 at ExxonMobil Research Qatar Lab and February 2014 at NDP site.

93 samples were collected for optical analysis of x-ray diffraction (XRD) analyses. XRD on sabkha sediments were initially carried out at the Interface Analysis Centre, University of Bristol and then at Gulf Labs, Qatar in a 30:70 ratio. XRD of three Dammam Formation samples were done by NDP and Gulf Labs.Philips X'pert Pro Diffractometer with a Cu-K α (1.54056 Å) X-ray radiation source was used for XRD analyses. Samples were prepared by grinding 0.2 g of the sample into a fine powder before being sonicated with 1 mL of pure ethanol for 2 to 3 minutes. The resultant liquid was pipetted onto a HCl-sterilized 1 mm thick amorphous silica glass microscopic slide before being placed on a deep-well slide holder. The radiation source was operated at 40 kV generator voltage and 30 mA tube current. Results were recorded over the 10 - 70 or 10 - 90 °2θ range, using a step size of 0.02 °2θ with a dwell time of 2 s per step. The XRD data were analysed using PanAnalytical Data Viewer and Philips X'pert Graphics and Identity softwares. Peak angles are quoted to the nearest 0.5 °2θ. While XRD is useful to identify mineralogy that is present, it only provides semi-quantitative information due to the possibility of underrepresentation of gypsum cementation that may occur during sampling. Hence, the combination of XRD and the use of optical analysis (in the field and using petrographic microscope) were more reliable in quantifying the mineralogy. Petrographic analysis and photomicrographs were conducted using a Nikon ECLIPSE LV100D-U microscope at the University of Bristol and Zeiss microscopes at the ExxonMobil Upstream Research Lab in 2015. The percentage of gypsum compared to the whole mineralogy was assessed using core observation, XRD and pits observation.

2.3.4 ^{14}C Dating

Radiocarbon carbon-14 (^{14}C) dating was performed on 43 samples using Accelerator Mass Spectrometry (AMS) on carbonate sediments in the form of bulk sediment and as carbonate shells. Samples were pre-treated with acid wash or etch. Analysis was done by Beta Analytic in Miami, Florida. Data were sampled and tested by ExxonMobil and provided to this study for analysis. Use of calibrated ^{14}C is necessary as the relationship between ^{14}C and calendar age is not linear, and uncalibrated ^{14}C dating is assumed to have a normal distribution of errors (Blaauw, 2010). Hence results were calibrated into calendar years before present (BP) using CALIB (version 7.0.0) calibration program (Stuiver and Reimer, 1993), using a marine calibration curve (MARINE13) (Reimer et al., 2009; Heaton et al., 2009) and a regional reservoir age correction (ΔR) of 180 ± 53 years collected to the east of Qatar (Hughen et al., 2004) (Figure 2-5). Radiocarbon age results are reported as calibrated age in yr BP (years before

present) with a 2σ interval range and a local marine radiocarbon calibration offset. ^{14}C data from Jameson and Puls (in press) was used to supplement this study after calibration.

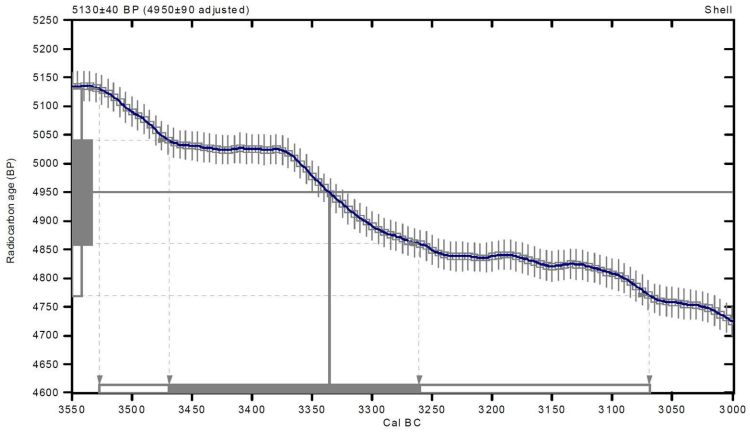

Figure 2-5. Example of a calibration curve for ^{14}C.

2.3.5 Geocellular Progradation Model

A preliminary 3D property model was created with ^{14}C age dates and a geomorphologic map with erosional surfaces to highlight the progradation of the sabkha system at the end of my two-part internship at ExxonMobil in August 2015 under the guidance of Christine Ianello-Bachtel and was further refined in December 2017. A geomorphologic map with added erosional surfaces was provided by Jameson. Top and bottom Holocene elevation surfaces were created using natural neighbour interpolation in ArcGIS 10.3 (Esri, 2015). The bottom sabkha succession in Mesaieed also represents the top of the Dammam formation top stratigraphy. A general DEM map was previously interpolated nationwide by Duggan (2014) but this had a 1 m resolution. This terrain model was further resolved using Z data points from borehole surveys and stratigraphic review of well reports. This allowed the DEM to have a 10 cm Z resolution when cross-checked against well reports. This DEM dataset was imported into Petrel™ version 2017 using the ARCGIS PetrelDatalink plugin and forms the deterministic skeletal input for the model. Adjustment to well tops data employed a convergent method, which is a Taylor series projection that acts as the basic gridder, and Briggs biharmonic was used (minimum curvature) to smooth the surface (Schlumberger, 2017).

The subset Holocene surfaces were resolved using calibrated ^{14}C age dated data, core interpretations and historic well reports. The modelled region used well controls outside the area of interest to increase the accuracy of model interpolation, especially the surface distribution at the metre-scale. The surfaces were then cropped using Dammam-sabkha boundary vectors extrapolated on Google Earth Pro and area of interest (AOI) polygons. These combined inputs resulted in a grid of the 12.9 km long, 13.8 km wide and 31.2 m thick 3D Holocene geocellular model with a 10 cm Z resolution.

2.3.6 Permeability

Hydraulic conductivity K indicates the ease with which a fluid passes through a porous medium, while k describes the ability of a porous medium to allow another fluid to pass through. Due to high density values encountered in Mesaieed brine (up to 1.2 kg m^{-3}), the conversion between hydraulic conductivity and permeability hinges on the nature of the fluid density which complicates simple conversion. Results from both the pumping test and slug test (see below) yield hydraulic conductivity (K), in which was converted to permeability (k) using;

$$K = \frac{k\rho g}{\mu_{23}}$$

whereby K is hydraulic conductivity (m/s), k is intrinsic permeability (m^2 or Darcy), ϱ represents density of groundwater brine, g is gravitational acceleration, and μ is dynamic viscosity (Pa.s or kg/s.m). Unit of results are quoted in Darcy as D.

Permeability of Holocene sediments was evaluated using both field-scale methods. In Mesaieed, slug tests and pumping tests were performed on wells (n = 29). Existing pumping tests data from NDPP were included and analysed (n = 27). Results will discuss the field-scale permeability of the sabkha and Dammam strata in all sabkha zones. A compare-and-contrast from two field-scale testing methods (slug versus pumping) were undertaken for the Dammam formation. Limitations to field-scale permeability tests is that diagenetic overprint may not be accurately represented proportionally, especially in slug and pumping tests. Field-scale tests are only able to capture the averaged vertical heterogeneity up to the height of the screen and fluid flow may still occur around the diagenetic overprint down hydraulic gradients through uncemented aeolian sand grains.

The following discusses the two field-scale permeability measurement methods:

1. Slug Test

[Scale = 10^0-10^1 m] Slug test (or bailing test), formalised by Ferris and Knowles (1954) enables the cost- and time-efficient acquisition of hydraulic conductivity in-situ without sediment disturbance (Figure 2-6). It uses a slug of a known volume, which is equivalent to adding a known volume of fluid, to rapidly displace the water level in a borehole with a known pre-test water level. The slug is a high-pressure PVC cylinder pipe filled with sand as ballast and capped at each end. The slug is removed rapidly (and theoretically instantaneously) using a self-built tripod setup (Figure 2-7B) allowing the water level to return to its equilibrium conditions. Responses from slug testing in recovery to initial water level can be either overdamped or underdamped (Figure 2-7A).

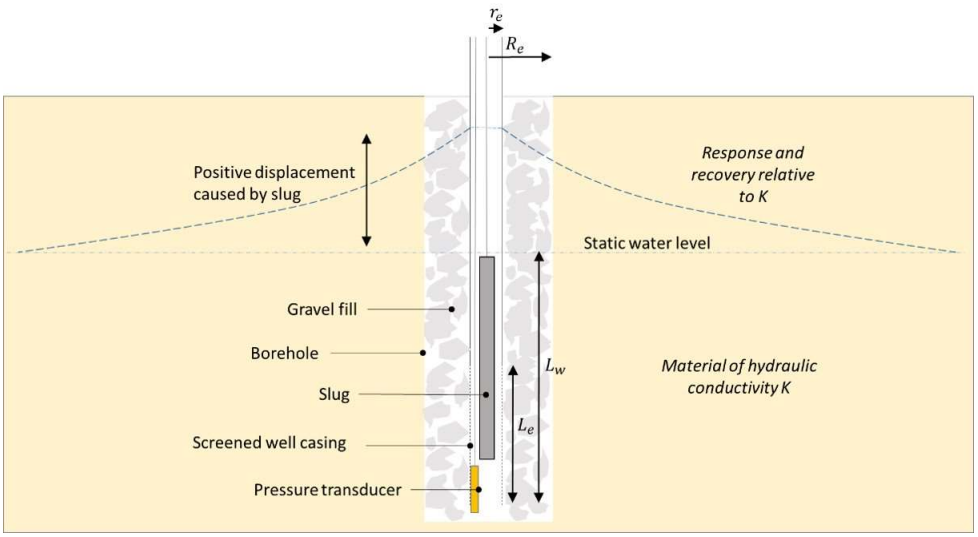

Figure 2-6. Methodology of slug test. The fluctuation of water level (± 0.05 m) in response to displacement of a predetermined volume of water is monitored by pre-programmed time interval submersible pressure logger (transducer) which is placed in the borehole well below the length of the submerged slug beneath the water level. Slug of the largest diameter and length that fits the wells on site (150, 80 and 50 mm in diameter) is selected to provide the largest volume of displacement for a measurable change in water level.

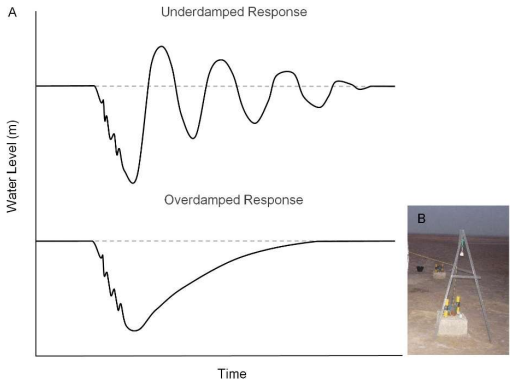

Figure 2-7. (A) Comparison of underdamped and overdamped water level response curves obtained following the slug removal during a slug test. (B) Setup frame above groundwater monitoring well for the deployment of slug.

Underdamped response (Figure 2-7A) from the slug test is determined by the inertial fluctuations of water levels between negative and positive recoveries at a frequency and amplitude. Underdamped response is a function of the hydraulic properties of the aquifer and is commonly observed in greater hydraulic conductivity aquifers and/or in wells with water columns (Nielsen, 2005). Many methods for analysis of underdamped responses are valid only for fully penetrating wells (Kamp, 1976; Kipp, 1985), which is not the case for wells tested during this study are partially penetrating. This necessitates using a modified version of the Bouwer and Rice (1976) model that incorporates a damping parameter (C_D) and a time parameter (t_d), both of which are dimensionless.

An overdamped response (Figure 2-7A) is a result of exponential reduction in the rate of recovery to initial water levels which typically occurs in aquifers or aquitards with low to moderate hydraulic

conductivity. These are then analysed using the Bouwer and Rice method (1976). Whilst wells are drilled to a specific diameter, the well casing is often supported by packing material, which are gravel-sized chippings from the Upper Damman Formation (with 40% porosity). This necessitates an adjusted radius to take into consideration the effects of the packing material (Bouwer, 1989):

$$r_{radius} = [(1 - n)r^2 + nR^2]^{0.5}$$

whereby n is the porosity of the packing material, r is the radius of the casing of the drilled diameter and R is the radius of the well casing. The five wells drilled in the sabkha succession and Dammam formation as part of the project, and the wells drilled by the NDP and MoE, all had a well radius (for the region) of 6 inches (15.24 cm). For wells drilled into the Dammam, the well casing is supported by Dammam Formation gravel pack.

2. Pumping Test

[Scale = 10^1-10^2 m] A pumping test (Figure 2-8) is often used to understand how much groundwater can be extracted from a well based on its long-term yield and well efficiency. Hydraulic conductivity K is estimated based on the response at the water level to the abstraction of groundwater at a known rate. Reduction in head in the aquifer causes an outward reduction of head forming a cone of depression, when the pumping test is stopped the groundwater recovers to its static equilibrium (Figure 2-8). The drawdown and recovery responses are monitored by transducers as a function of time. There are two types of pumping tests; step drawdown (variable discharge) and constant discharge tests. The former is normally used to measure well performance and efficiency whilst the latter is used to estimate aquifer characteristics and identify the nature of the aquifer and its boundaries (Hiscock, 2009). This study used a raw dataset from the 2 phases of New Doha Ports Development (NDPP) generation 1 (G1) and generation 2 (G2). Single-well pumping tests for the upper part of the Damman Formation have been carried out by NDPP G1 (well names beginning with A and B, 2008) using a variable head permeability test (step drawdown). This study performed a constant discharge test of 30 minutes duration followed by a recovery test of 30 minutes. The datasets were analysed using the non-equilibrium method Hantush-Jacob (1955) (Halford and Kuniansky, 2002).

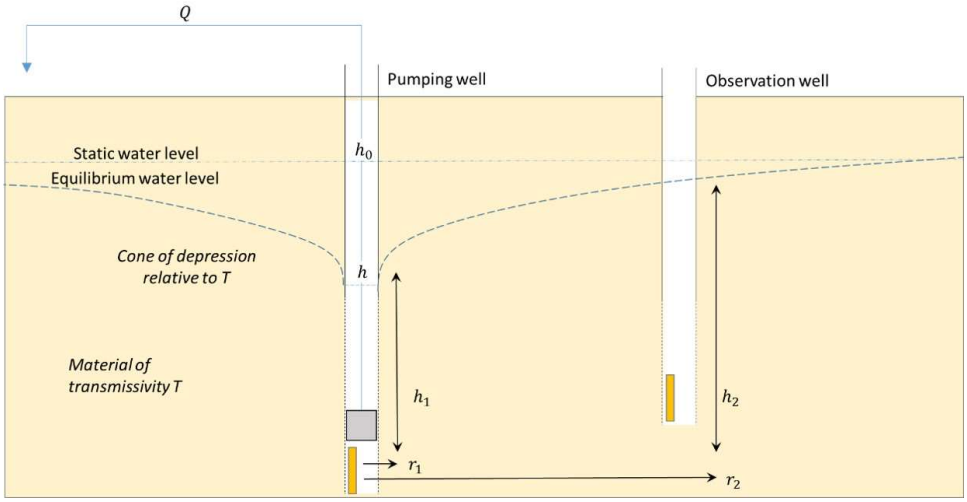

Figure 2-8. Methodology of pumping test for large-scale permeability determination. Groundwater is pumped out of a well at a known rate sufficient to cause measurable drawdown, creating a localised hydraulic gradient and inflow of groundwater into the well from surrounding aquifer.

Lost Circulation Zones

Data recording incidence of lost circulation zones (LCZ) encountered during NDP 1 were used to understand very high permeability zones (VHPZ) within Dammam Formation. Lost circulation is a result of drilling fluid or mud escaping from a borehole into large subsurface voids within a formation which was intersected during drilling, these are especially common in highly fractured limestones and karst aquifers (Davidson et al, 2000). Unfortunately, only a crude core description is made available to us and whole core photos is not available to compare alongside the data. LCZs can be classified as total loss circulation (TLC) or partial loss circulation (PLC) zones, with the former indicating no drilling fluid or mud return at the surface (100 % loss) while the latter can occur if the output flow rate of the drilling fluid or mud is less than an input flow rate. In such scenarios, it is difficult to estimate permeability using slug test or pumping test. The permeability dataset uses the depth range over which the well is screened, whereas LCZ are based on the depth at which VHPZ are initially encountered. This makes LCZ data unique to permeability data that were collected from the field post-well installation. Drilling data of the Dammam Formation from NDP on the first occurrences of LCZ (n = 110) were analysed. Sites range from locations up to 1 km offshore of the coastline, and from the middle and lower sabkha from boreholes that penetrate through the Holocene sabkha and into the upper 10 - 20 m of the Dammam Formation underlying the sabkha.

2.4 Geomorphology

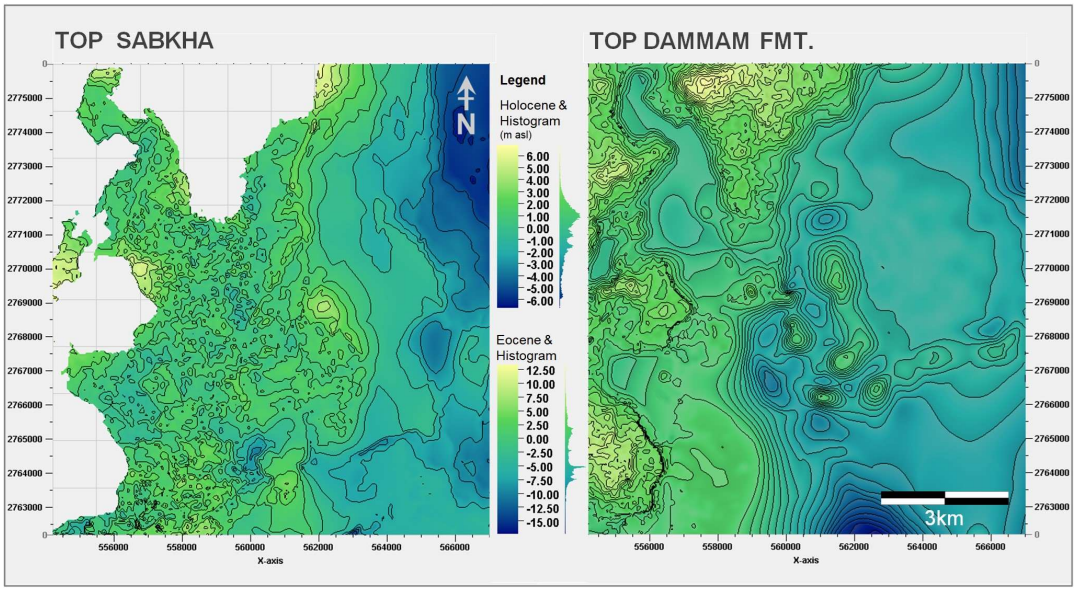

Figure 2-9. Surface elevation map of Holocene sabkha and structure map of Top Dammam Formation. Contours of (**A**) surface elevation of the sabkha sediments and Dammam Formation with contour interval of 1 m, based on ^{14}C age horizons. Legends for both surfaces include the histogram of the elevation surfaces (in m asl) which highlights most of the sabkha being 1 m above present-day sea level. The spits were excluded in the top sabkha.

The sabkha is relatively flat with a gentle dip direction towards the present-day coast, having slope gradients close to 1:1000 - 1:5000 (Figure 2-9). The Dammam formation's paleo-surface shows a relatively more pronounce surface topography with about a 2-3m drop from the upper sabkha to the middle sabkha, with a high dip angle towards the ocean in the south-southeast direction.

The sabkha elevations were above sea level (abbreviated as asl) datum, with an average elevation of 1.12 ± 0.54 m asl (n = 115). The upper sabkha zone had an average elevation of 1.13 ± 0.55 m asl (n = 13), the middle sabkha at 0.76 ± 0.45 m asl (n = 26), and the lower sabkha at 1.23 ± 0.58 m asl (n = 34). The study area has a surface area of 75 km^2 (proximal sabkha = 5 km^2, upper sabkha = 15 km^2, middle sabkha = 30 km^2, lower sabkha = 25 km^2), Taking account of the surface area multiplied by the thickness of the sabkha sequence, the gross volume of the sabkha is roughly 700 m^3.

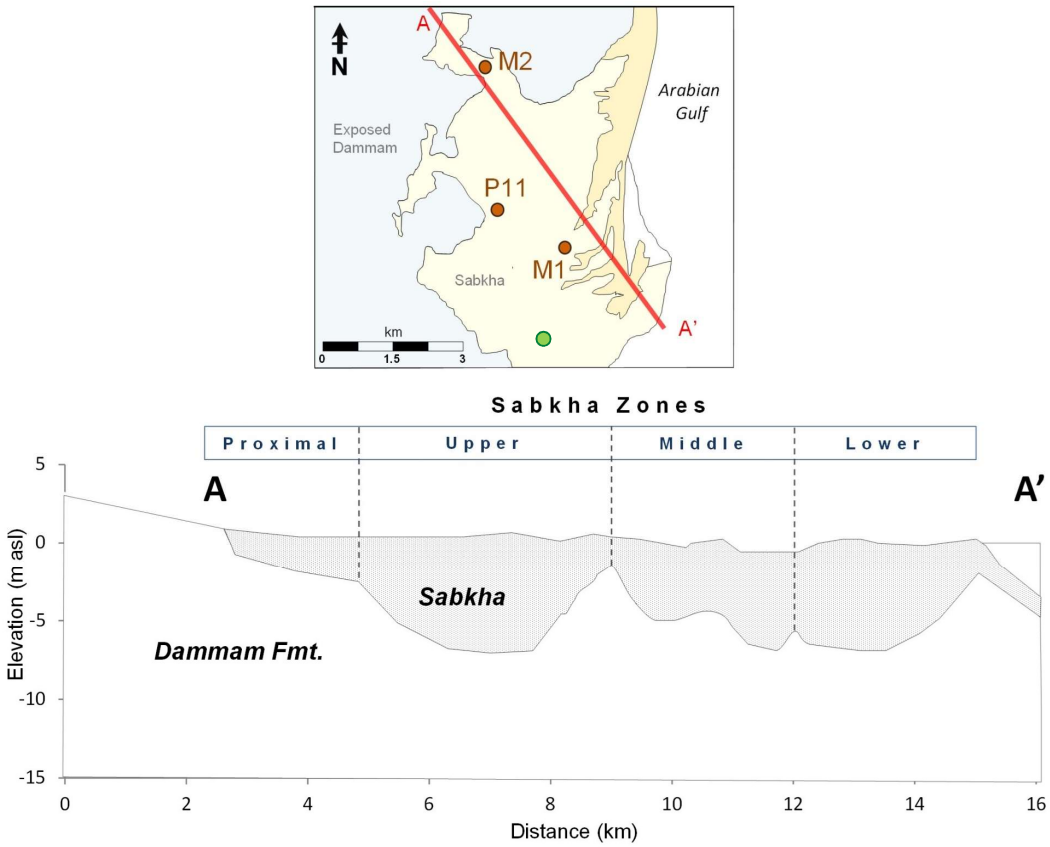

Figure 2-10. Map highlights the location of the cores that are presented in subsequent sections: M2 (proximal sabkha), P11 (upper sabkha), M1 (lower sabkha). A – A' line on the map denotes the cross-section through Mesaieed sabkha with the geographic zones, it does not highlight the thickening section of the Holocene sabkha towards the coast that is further south. Green dot highlights the location of maximum Holocene thickness (~15 m) that is not shown on the cross-section transect.

A cross-section across (Figure 2-10) A-A' derived from top sabkha sediment and Dammam Formation maps in Figure 2-9 shows an increase of Holocene thickness from the updip bedrock towards the middle and lower sabkha with a subsequent decrease in the offshore direction. Sabkha deposits were 3-5 m thick in the upper and middle sabkha, with thickness of ~10 m from lower middle sabkha towards the coast, reaching a maximum of 15 m (Figure 2-10, 25.01318° N 51.58801° E) where they infill the deepest part of the relict Pleistocene fluvial system incised into the Dammam Formation bedrock during lowstands (Duggan, 2015).

2.4.1 Proximal Sabkha

This 2-4 m thick sabkha, located on the southwest side of the outcropping Dammam Formation updip, fills an irregular bowl-shaped depression that sits about 1.0-1.5 m above the sea level. The proximal sabkha is partially isolated from the majority of the sabkha by a narrow neck of outcropping Dammam Formation headland of about 3 km wide. Vegetation is extremely limited to only within the drainage channels of the proximal sabkha (Figure 2-11A) and within 500 m from the exposed Dammam

formation. These areas were observed to be receiving meteoric runoff from the exposed outcropping Dammam Formation updip of the sabkha. A few xenophyte shrubs occur in low-lying areas (Figure 2-11B), likely with sufficient soil moisture, particularly during the wet season. Halophytes were observed in stabilizing the sabkha sediments in the form of nebkhas.

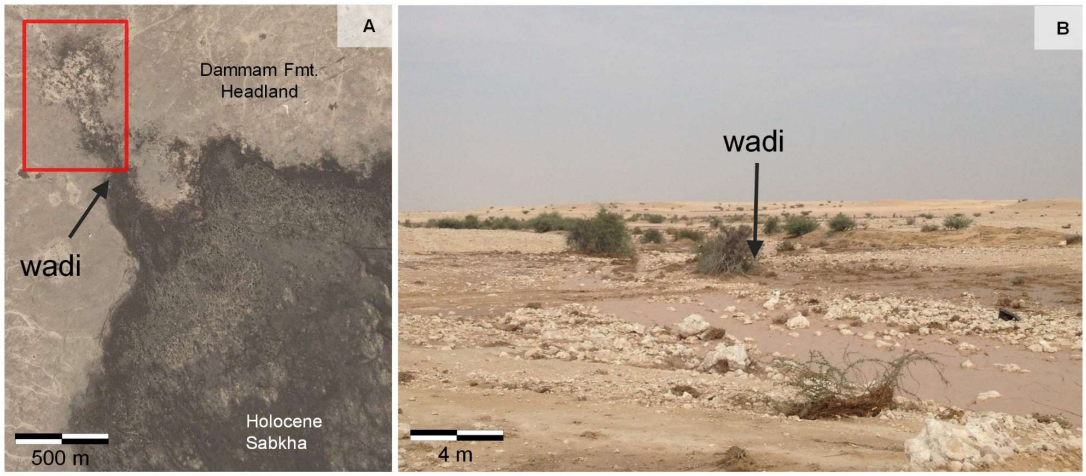

Figure 2-11. Location of xenophyte vegetation (B) in the upper edge of the proximal sabkha (A). Xenophytes are preserved as nebkhas and are abundant within an ephemeral drainage channels (wadi) that cuts through the exposed Dammam formation headland into the proximal sabkha. During precipitation events in the winter, this was observed to provide pathway for groundwater discharge from outcropping Dammam Formation bedrock.

Cores from the proximal sabkha show depositional and diagenetic textures, with weak laminae of well-sorted, fine to medium grain siliciclastics with a variable amount of calcite sand and gypsum crust of about 20 to 30 cm thick (Figure 2.12). Figure 2-12 shows that intervals from the subsurface Dammam formation to the sabkha surface consists of: Dammam pebbly gravel; sandy packstone with low-angle diffused parallel laminations with decreasing abundance of packestone in abundance upward; medium-grained quartz sand with fragmented mixed gastropod shells, parallel laminae and some thin gypsum mush layers; and laminated euhedral clear gypsum crust. Faint wavy bedded is seen at the bottom half of the core with bioturbated sediment.

Prismatic and lenticular gypsum is the major evaporite and is limited to the top 25 cm of the sabkha. At the base of the sabkha there appears to be reworked clasts of limestone, likely of the Dammam Formation. XRD analyses highlighted that on average, excluding the Dammam clasts at the base (rubble zone), the proximal sabkha consists of about 70 % siliciclastic sand with 15 % calcite sand, 10% gypsum and <5% minor dolomite sand. Pedogenic textures such as trace fossils belonging to roots disturb the pre-existing sedimentation laminae. ^{14}C age date of bulk sediment in the proximal sabkha at about 1.7 m below the surface is 7510-7803 yr BP.

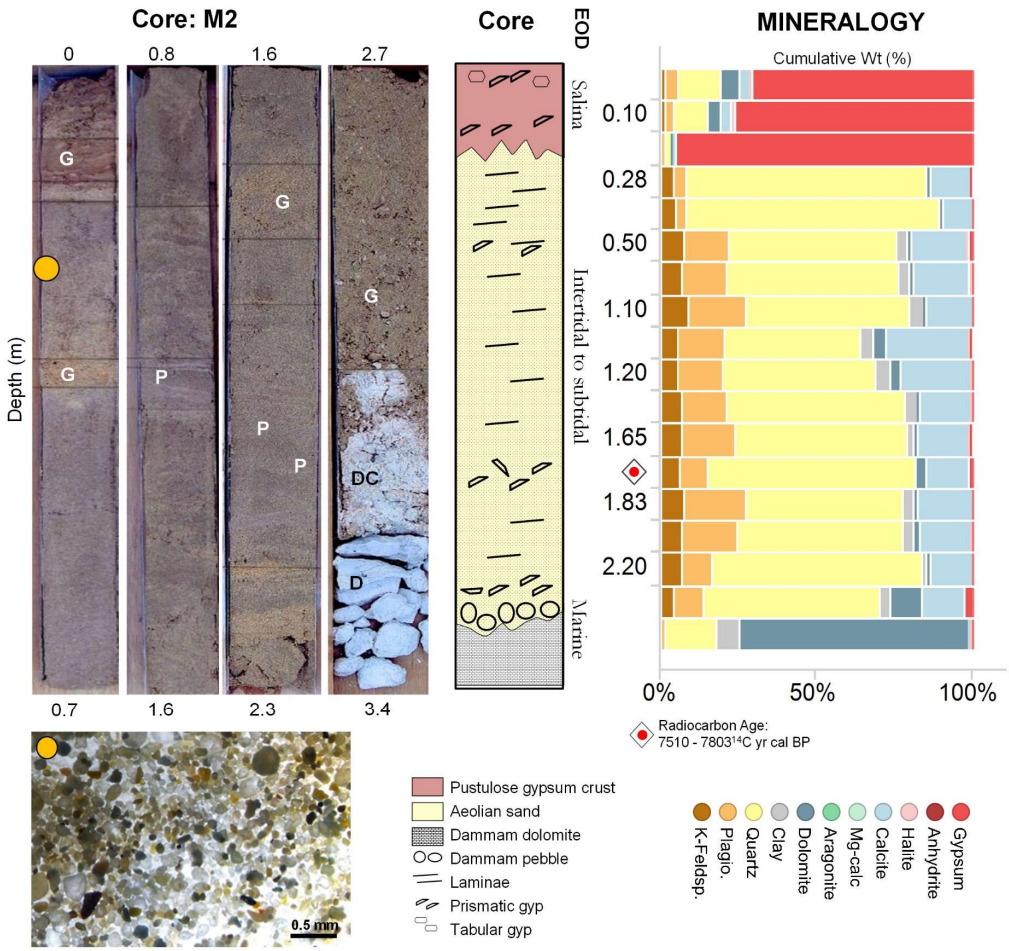

Figure 2-12. Representative core of the proximal sabkha (M2). Left to right: whole core photographs, diagrammatic observation of core with environment of deposition (EOD), mineralogical composition (XRD) of proximal sabkha with associated age dates of the gypsum. Labels on whole core photographs are gypsum precipitation (G), planar laminations (P), Dammam conglomerate (DC) and Dammam formation (D). Depths of core (in m) are labelled above and below each core photo. Associated photomicrograph shows typical proximal sabkha sediment which are high maturity aeolian siliciclastic deposition, consisting of clear quartz sand grains, dark peloids and minor altered carbonate grains with weak, clear gypsum cements.

2.4.2 Upper Sabkha

The supratidal portion of the sabkha zone lying about 5 km from the coast, has an area of about 12 km^2, with thickness ranges between 3-4 m and an elevation about 1-2 m asl. The southeast boundary was bounded by a belt of discontinuous Pleistocene beach ridges (Figure 2-15). The upper sabkha zone lacks vegetation and is extremely flat. It is surrounded by outcropping Dammam Formation on both sides with wadi channels observed in the proximal sabkha. The surface was covered with buckled crusts and erosional remnants.

At the top 15 cm of the sabkha, prismatic gypsum appear to show upward deformation into irregular folds (Figure 2-13C). The light brown colored, 5-30 cm thick, irregular semi-polygonal structure appears to blister or heave above the sabkha surface. The crystal fabric shows milimeter to centimetre

scale prismatic crystal, is poorly laminated. Each of the pustulose crust has a void of about 5 to 10 cm in between (Figure 2-13D), with a downward direction twinned gypsum. Based on the gypsum mineral's fish-tail and twin habit, the mineral growth at the bottom of the crust appears to be upward and clear while the gypsum mineral growth on laterally displaced top have downward direction and seems semi-dehydrated, like a detached buckle. This lateral displacement leads to an upward compressional feature, which appears as buckled pustulose gypsum crust. The 10 to 15 cm thin sediment are well-cemented by anhedral gypsum and micritic mud (Figure 2-13E).

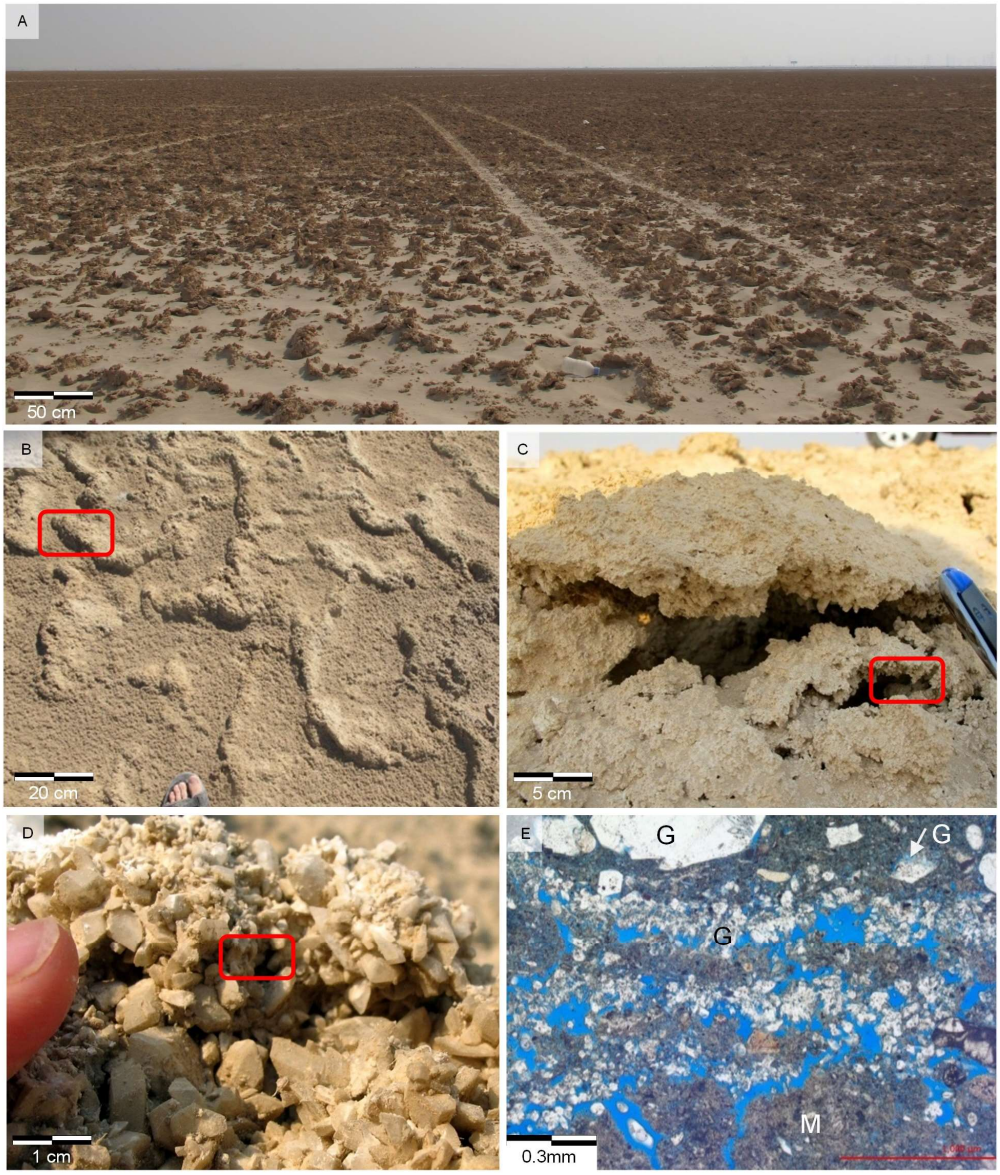

Figure 2-13. Upper sabkha zone showing (A) depression filled by pustulose gypsum crusts with recent aeolian sand blown over it; (B) the plan view of the pustulose gypsum after a rain event showing the compressionally buckled structures with the red box highlighting the photo in (C) which shows the side view of a 'buckle' well cemented by gypsum and mud sediment with dissolution voids of some 5 to 15 cm thick infilled with (D) bottomward growing tabular gypsum. (E) Thin section of the gypsum crust taken from the red box highlighted in (D) showing tabular gypsum crust with mud in PPL (plane polarised light).

The core study (Figure 2-14) shows poorly-sorted medium-grained siliciclastic sand (45%) with minor amounts of dolomite (8%) and calcite (5%) sand grains. Siliciclastics consist of mainly quartz with minor plagioclase and K-feldspar. Cementation of the sabkha sediments in this sabkha zone by poikilotopic gypsum (30 to 45%) and minor halite (3%) is pervasive from the surface to the bottom Holocene. Sand grains with crystal size range of 20 to 100 µm have been observed under microscopy to a thin coating of either carbonate or gypsum.

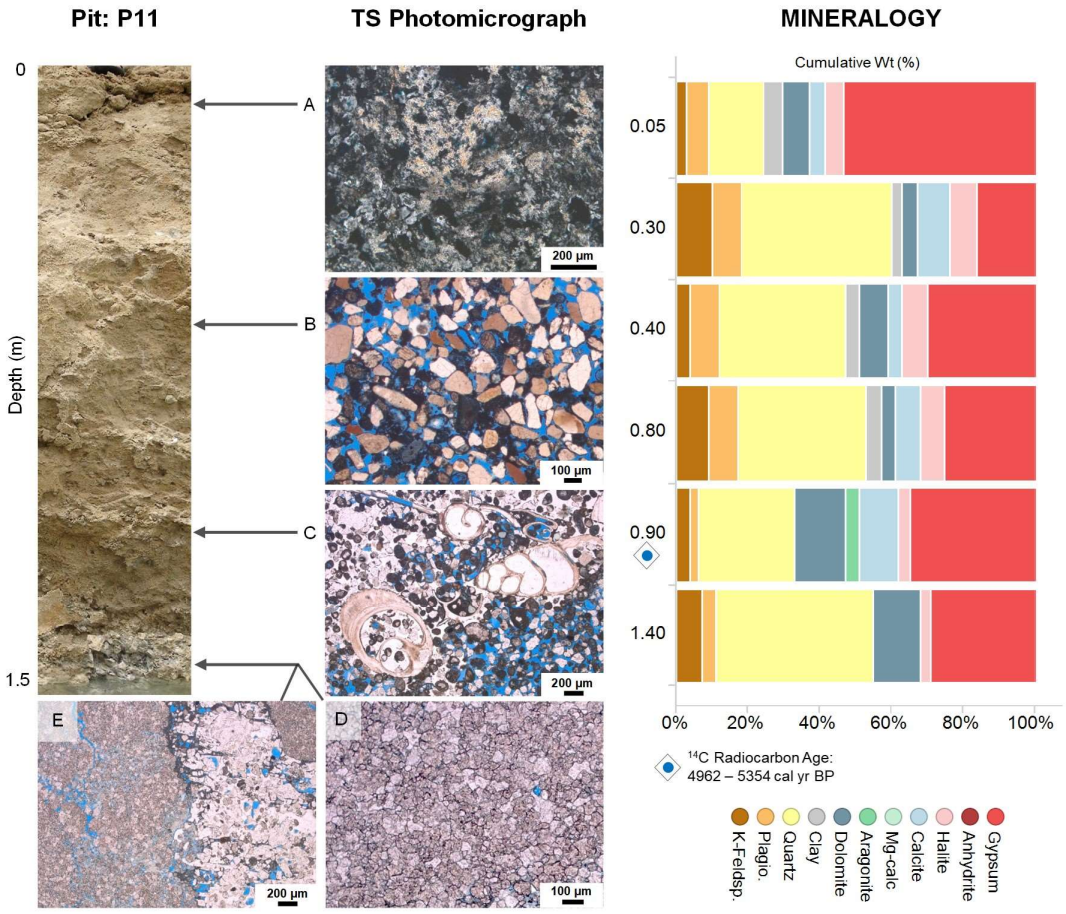

Figure 2-14. A representative shallow pit of the upper sabkha zone (P11) with associated thin section in PPL of (A) gypsum pustulose crust; (B) unconsolidated fine-grained polymodal siliciclastic distribution (subangular to rounded quartz, plagioclase and feldspar) highlighting different maturity (possibly different aeolian sources) with fine gypsum grains and carbonate mud; (C) patchy non-isopachous gypsum replacement both poikilotopic and intraparticle; (D and E) Dammam Formation rubble with gypsum cementation at the base of Holocene. Mineralogy plot with depth show a high presence (~35 %) of gypsum as compared to proximal and middle sabkha. (Source of TS photomicrographs A, C, D and E: Jameson)

Holocene Erosional Remnants

Localised gypsum-cemented structures are commonly observed in this upper sabkha zone (Figure 2-15), often within 500 m of the limits of the outcropping Dammam formation updip of the sabkha and typically exhibit two forms: (1) localised dome-like gypsiferous heave structures and (2) laterally continuous erosional remnants of laminated gypsum (Figure 2-15-2).

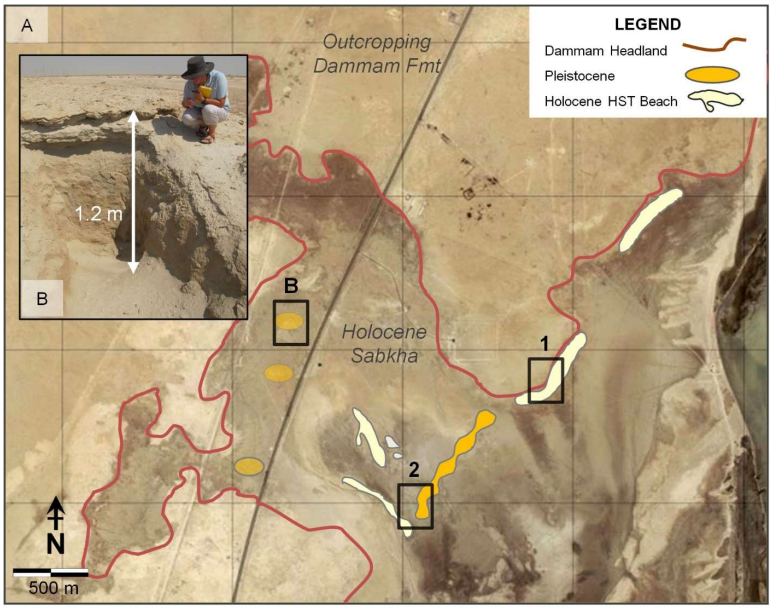

Figure 2-15. Upper sabkha zone showing areal cluster of distribution of erosional remnants with photo (A) showing a gypsum heave structure. Black boxes numbered 1 and 2 highlights the areal polygons where paleo-channels (Figure 2-16) and exposed Pleistocene (Figure 2-17) are observed, respectively. (Satellite imagery sourced from CGIS and ExxonMobil).

Dome-like gypsiferous heave structures were near-rounded structures (Figure 2-15B) of about 1.5-2 m in diameter and 1 to 1.8 m above the present day sabkha's flat surface. The heave features range between 30-120 cm in thickness above the surrounding sabkha surface. The heaves were heavily cemented by gypsum and its top 10-20 cm is nearly 100 % gypsum crust. They appear to be erosional remnants of earlier highstands (Figure 2-15A). Beneath the gypsum crust was a layer of laminated, gypsum-cemented sand. Gypsum cementation was observed to be decreasing downward from nearly 80% of mineralogy proportions to zero towards the present day ground surface. A thin, residual layer of fragemented shells, particularly cerithid gastropods, were present between the gypsum and the clastic sand. Dated cerithids have a ^{14}C age date of 6200 yr BP which indicates that the erosional remnant is a relict beach of the Holocene Highstand.

The laterally continuous erosional remnant (Figure 2.16), when observed in the satellite imagery, appear to tail off the outcropping Dammam formation in a meandering trend (Figure 2-16A). The erosional remnant, about 400 to 600 m in length, 0.5 to 1 m in height and 2 to 3 m in width, is cemented by a gypsum crust (Figure 2-16B) which helped the erosional remnant resist weathering over time. This indicates inverted topography paleo-drainage channels (Figure 2-16). The paleo-channels can indicate

the minimum extent of erosion that has taken place in the upper sabkha zone, which in this case is about 1 m. Over time, sand dunes remobilisation, aeolian sand deposition or marine carbonate sands will

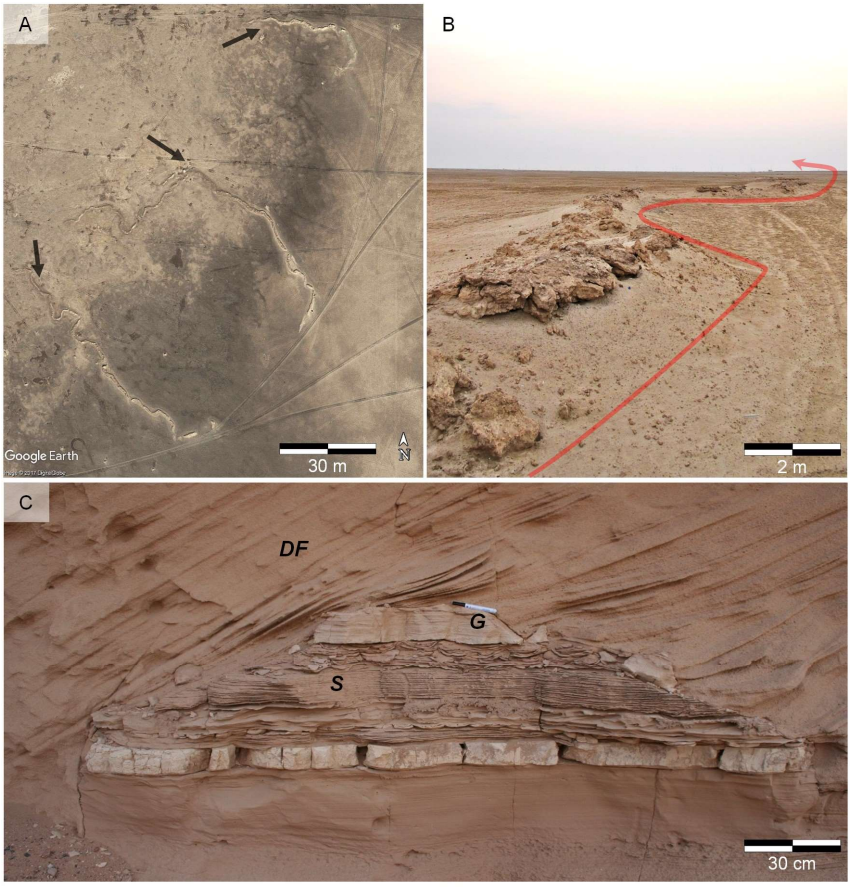

Figure 2-16. Holocene erosional remnants: (**A**) an overview of the meandering paleo-drainage with down-flow direction to the southeast; (**B**) close-up view of inverted topography, indurated gypsum crust allows it to resist aeolian and/or subaqueous erosion; (**C**) an analogous and older Quaternary outcrop in Wadi Sidri, Sinai Peninsula (Egypt) of an ancient preserved sheet flood with a gypsum cemented base and top allowing it to resist aeolian ablation over time, before being buried by a mobile dune. DF shows dune foreset (*Photography 3 source: Ian Sharp*)

Pleistocene Exposure

Pleistocene outcrops in Mesaieed were present as carbonate beach ridges up to 5 m in height. They consisted of well-lithified but discontinuous outcrop belts inland of the present coast and separate the upper and middle sabkha. The outcrop was never more than 100 m in length (Figure 2-17A). Cross-bedding was observed on most outcrops and the grains are well-sorted medium to fine grained, well-rounded, consisting of mostly ooids with broken shells including bivalves (Figure 2-17B). Photomicro-graphs (Figure 2-17B and 2-17C) show grainstone with well-developed oomoldic porosity which is indicative of extensive meteoric diagenesis. There is an isopachous granular rims of calcite crystals.

These beach ridges have Uranium series age range between 125 and 345 ka uncalibrated BP (Jameson, 2014).

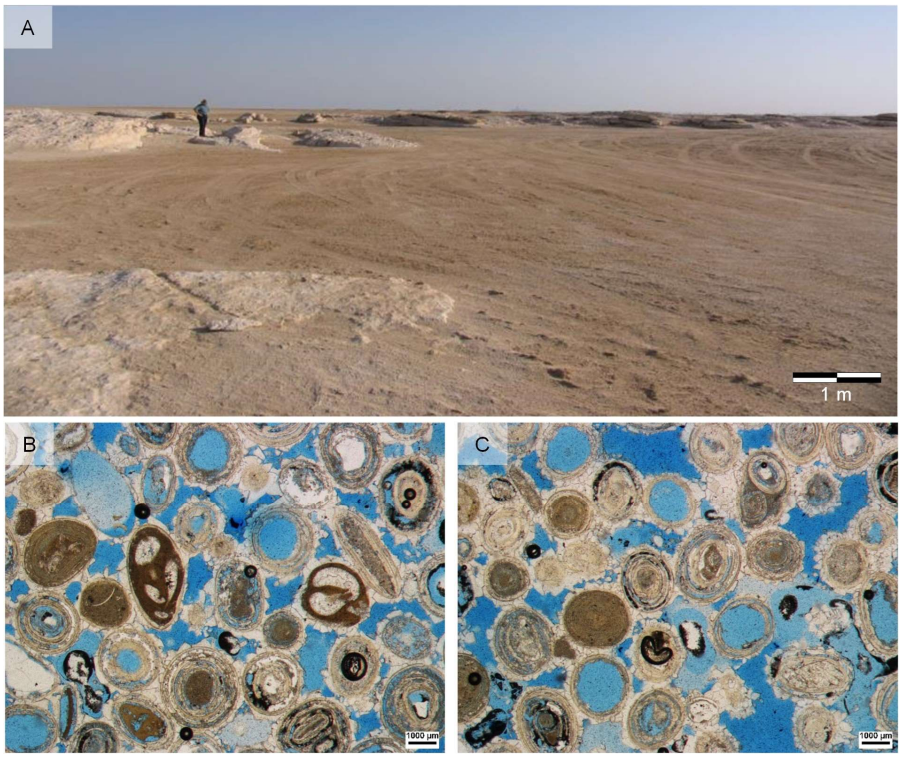

Figure 2-17. **(A)** Belt of exposed Pleistocene beach ridges located in between upper and middle sabkha, with person in photo as scale. Scale bar for this photo represents the foreground. **(B)** and **(C)** are photomicrographs of the beach ridge sediments (Mdd8) showing ooid grainstone with well-developed oomoldic porosity and isopachous rims of calcite crystals. The epoxy infills the interporosity as blue colour. Lithification of the Pleistocene is distinguishable from the Damman formation and sabkha sediments by euhedral calcite rim cementation.

Flow-through Pond

Situated just few hundreds of metres to the east of Al Wakra Main St road in the upper sabkha, is a flow-through pond with perennial, standing water sourced by bedrock discharge (Figure 2-18). A flow-through pond is defined as perennially inundated water body with continuous inflow by groundwater discharge (Rains, 2011). The pond is lined with thick gypsum deposits. (Figure 2-18A, 2-18B). The pond has been present prior to 1947 based on aerial photographs and may be associated with local collapse (Jameson, verbal comm.). The flow-through pond has a depth of about 4 – 5 m and diameter of 9 m (minor axis) and 30 m (major axis). Pond water is greenish (Figure 2-19) with about 1 m visibility near the surface suggesting microbial activity. The pond indicates perennial groundwater discharge into the sabkha.

The flow-through pond is lined with clear fish-tail or prismatic gypsum growths at the sides, an indication of a recent precipitate (Figure 2-20C). Gypsum is also seen cementing recent garbage which indicates that evaporite precipitation has been prevailing up to present-day (<50 years). The distribution

of gypsum sizes varies across the pond with larger gypsum size on the southeast side (up to 9 cm across) as compared to the northwest side of the pond (up to 5 cm).

Figure 2-18. Google Earth image (**A**) showing the dimensions of the main pond in **(B)** and the isolated pond. (**C**) Gypsum cementing rubbish, an important example of rapid rates of precipitation. Scale bar for images A and B represents the foreground. Length of pen in photograph C is 14 cm.

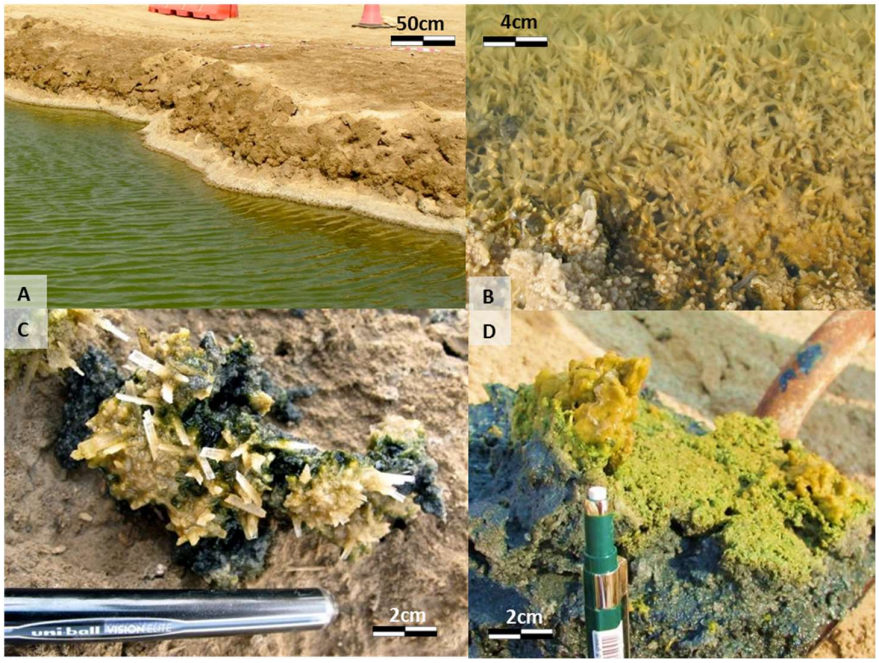

Figure 2-19. Features of flowthrough pond; (**A)** Gypsum crystals forming on the banks, note the variable water level of about 20-30 cm. (**B)** Shallow tail crystal habit of the bipyramidal gypsum. At the time the photograph was taken (13:00) it was 12cm below the top of the gypsum precipitation. (**C)** Stromatolites and anoxic mud are present under the gypsum crystal growth. (**D)** In the isolated pond the gypsum is observed to be growing in an orange layer mush. These microbial facies here have purple sulphur bacteria, fish droppings, about 1mm layer of sulphide and 5mm of green layer.

2.4.3 Middle Sabkha

The 17 km^2 middle sabkha surface is about 0 to 1 m above sea level (average of 0.46 m ± 0.45 asl) while the thickness of the sediments is about 5 to 10 m, with thickness increasing coastward. The supratidal - intertidal portion of the sabkha is separated from the upper sabkha by a Pleistocene outcrop belt (Figure 2-17), and is part of the back barrier behind the first and second generation of the cheniers.

Lithified Pleistocene beach ridges with gypsum-cemented erosional remnants were observed but are less common and smaller in dimension. This depocenter has a lower elevation than the rest of the sabkha zones.

The middle sabkha was the portion of the coastal plain that was intermittently flooded by tidal and wind-driven currents (Figure 2-28). It extended from the beach ridges on the seaward side to supratidal with gypsum flats on the landward side. A paleo water table can be observed in the core at the transition of tan to light grey at 1.30 m bs (Figure 2-21A). The upper 3.4 m interval is generally a mixed carbonate shelly quartz with foraminifera, ostracods and peloids, which is a typical lagoonal assemblage. A sharp erosional surface at 3.45 m bs, indicating a break in deposition. The environment of deposition throughout the Holocene below 3.50 m is interpreted as intertidal to subtidal.

Low-angled cross laminae were commonly observed within sabkha pits in the middle sabkha. This is interpreted as two-way flow, which may be from the deposition of thin veneer sand from updip of the sabkha in the northwest with the shamal wind, and the tidal flooding coming in from the southwest. An ephemeral salt flat is observed on this portion of the sabkha with halite being the dominant mineralogy of the salt flat. Large gypsum crystals within the sediment is commonly observed in pits within 0.5 to 1.0 m below the surface (Figure 2-20). These poikilotopic crystals, which consists of sand grains in the middle with increasing translucent at the edges, are often pervasive and can be up to 30 cm in length.

Figure 2-20. Photograph above shows a cross-section pit through the deflated middle sabkha, highlighting the cross-bedding, shallow water table (with capillary zone of 0.5 to 1.0 m thick) and gypsum cementation of the beds. Pronounced euhedral gypsum cementation above (seen in **A**) and below (seen in **B**) the water table within unconsolidated sand in the middle sabkha (M9), an indicative of subaqueous settings. Displacive gypsum cementation ranges from 5-30 cm in length.

A representative core (Figure 2-21) of about 7.3 m length was taken about 2 km from the coast. This showed parallel laminated clastic sands except for between 3.4 m to 4.0 m which are mostly carbonate shells with carbonate mud (85%). The overall mineralogy of the sabkha in this region indicates a decrease in siliciclastic content and increase in carbonate content with depth (20% to >60%), with weak cementation by gypsum, calcite and halite throughout the whole core (Figure 2-21B). Carbonate shells, both fragmented and complete, observed are mostly foraminifera and ostracods. This includes Certhiidae gastropods, *Veneridea Dosinia* and *Marcia Flammea.* Micritic and calcitic grain coatings are observed on most of the grains, especially from 4.5 m bs with depth.

Core study show that the Holocene sabkha sediments has less diagenetic overprint than in the upper sabkha, with scattered distribution from the surface to base. Diagenetic minerals comprise of mostly gypsum, with minor halite throughout the core. Gypsum is observed mostly as gypsum roses, poikilotopic crystals and massive cements within the sediments. Evaporite mineral cementation is mostly noticeable at the top 20 cm and the bottom 1 m near the base of the Holocene. The bottom 30 cm of the core consist of mostly Dammam Formation pebbles with a quartz sand matrix.

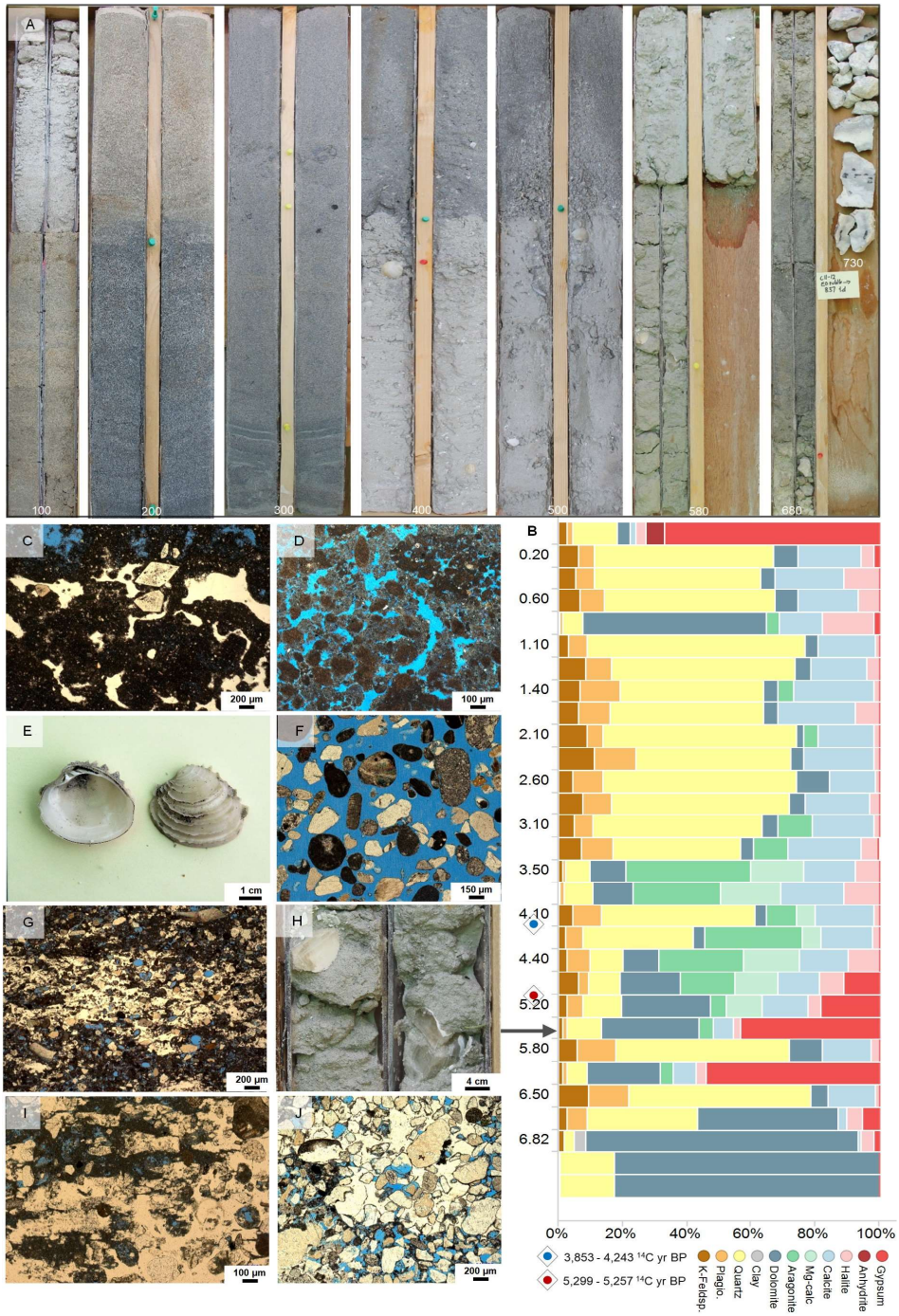

Figure 2-21. (A) A representative core of the middle sabkha M1 (elevation of 0.60 m) showing a typical lagoonal assemblage of foraminifera, ostracods and peloids with low angle laminae, (B) XRD profile for core, thin section of (C) poikilotopic halite infilling micritic carbonate mud with few euhedral gypsum 1.0 m below ground surface, (D) micrite mud composed of mostly calcite 0.20 m below ground surface, (E) *Veneridea Dosinia* at 3.80 m bs, (F) polymodal distribution of aeolian calcite grains and gypsum assemblage at 2.60 m bs, (G) mixed quartz and skeletal sand with calcitic micrite cemented by gypsum at 4.65 m bs, (H) large gypsum euhedral crystals in micritic mud at 5.53 m bs, (I) massive gypsum cementation engulfing dolomite and calcite grains hosted in micritic mud 5.50 m bs, (J) partially dissolved and displaced calcite grains with interparticle poikilotopic gypsum at 6.68 m below ground surface.

2.4.4 Lower Sabkha

The 16 km² sabkha has an elevation of about 1.23±0.58 m asl, and its thickness range from 5 to a maximum of 15 m where the deepest of the relict Pleistocene drainage system is infilled. The distal portion of the sabkha is a transition zone between intertidal to subtidal. The sabkha sediments is deposited in a northeast trend behind the spits until the southernmost spit, in which the coastal sedimentation veers eastward (Figure 2-30). Coastward of the sabkha, particularly behind the youngest generation of spit, lies a shallow lagoon with mangrove, burrowed mud flats, tidal inlets and microbial mats (Figure 2-22) which is frequently flooded via tidal inlets on a daily basis.

The lower sabkha sediment surface today is dominantly a carbonate mud, up to 50%. On the west of the spits are the back-barrier sediments, which is a mixture of medium to coarse grain. A trench through the back barrier side of the lower sabkha shows that it ranges upward from grey subtidal carbonate mud, light tan coloured intertidal sediment which is capped by thin layer (10-15 cm) of microbial mats.

XRD study of a representative core in the lower sabkha indicates a more carbonate-rich sediment (~50%) than of siliciclastic, which is about 35%. Siliciclastics in the core are mostly quartz while the carbonate mineralogy consists of aragonite and dolomite in nearly equal proportions. The large amounts of dolomite may be detrital, derived from the outcropping Dammam formation.

Spit-Back Barrier Systems

Following from the observation of the sabkha in the upper, middle and lower sabkha, the back-barrier sediments behind the spits make up the north-south coastline. Processes that form these barrier beaches and subsequent erosion were discussed by Jameson and Strohmenger (2013). This model will be explored in Mesaieed in detail, specifically to correlate with field and mineralogy observations of the sabkha. Each hook-shaped spit is roughly 2-3 m in height and 0.5 to 3 km long, often elongating southwards parallel to the present-day longshore currents before refracting landwards a continuous NE-SW lineation. The spits composed of coarse grained shelly sand, dominated by gastropods and bivalves. They were separated by lagoon and tidal flat deposits with mangroves and occasionally microbial mats.

The youngest spit is oriented N-S and the back-barrier comprises of a lagoonal system, with microbial mat on the west and mangroves on the north (Figure 2-22a). There are two tidal inlets identified that allows seawater to reach the restricted lagoon.

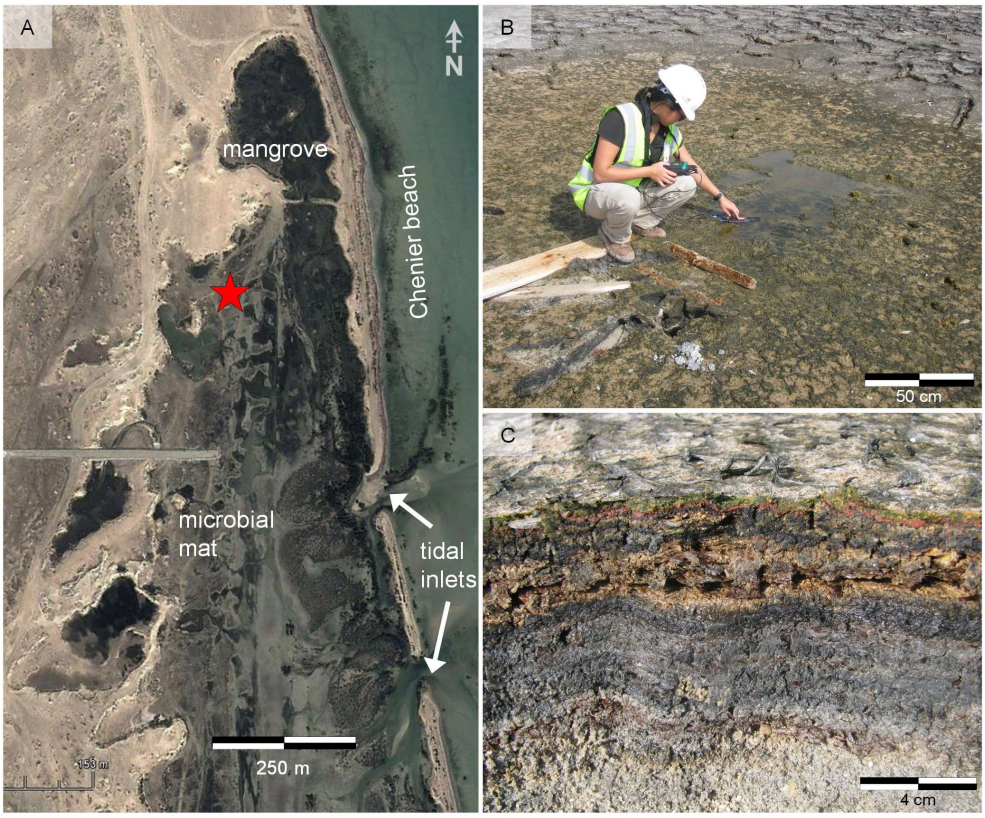

Figure 2-22. (A) Protected region located behind the youngest spit. It consists of shallow intertidal lagoons, burrowed mud flats, tidal channels, microbial mats and stromatolites. **Red star** showing location where photographs (B) and (C) were taken. (B) Evaporated seawater pooled in depressions within microbial mat communities from tidal flooding; (C) complex communities of microbes organized in layers.

2.5 Mineralogy and Diagenetic Products

2.5.1 Aoelian Deposits

Aeolian sand sourced from updip of the proximal sabkha is believed to provide sediment and therefore catch sampling was done using a sail fabric with the assistance of NDP in 2014. Together with the data provided by Jameson, sourced from Doha, XRD analysis (n=2) show that the dust sediment consists of mostly calcite (31-35%), dolomite (25-27%), quartz (23-28%), plagioclase (6-10%) and K-feldspar (3-4%). Gypsum and halite content in aeolian dust are negligible (<2%).

2.5.2 Holocene Mineralogy

To highlight the spatial distribution of sabkha mineralogy, mineralogy content was estimated from a combination of XRD data of each sabkha core or pit with visual petrography estimation (Table 2). Figure 2-23 summarizes the combined XRD and optical analyses mineralogy of the Holocene sediment, averaged at each well. Figure 2-24 highlights pie charts showing average mineralogy composition for each sabkha zone.

The dominant siliciclastic mineral in the whole sabkha is quartz (38%), with minor plagioclase (6%) and K-feldspar (4%). Carbonate minerals consist of calcite (15%) and dolomite (12%), with minor aragonite (5%). Other mineral observed includes clay (< 8%), in which is mostly palygorskite, $Mg_{1.5}Al_{0.5}Si_4O_{10}(OH)4(H_2O)$, with minor chlorite, $(Mg,Fe)_3(Si,Al)_4O_{10}(OH)_2 \cdot (Mg,Fe)_3(OH)_6$, and illite, $K,H_3O(Al, Mg,Fe)_2 (Si, Al)_4 O_{10} [(OH_2),H_2O]$.

The distribution of sabkha mineralogy varies spatially. Siliciclastic sand is the primary sedimentology of the proximal, upper and middle sabkha (up to 61 % of total mineralogy in the proximal sabkha). The proportion of siliciclastic decreases towards the coast (down to 33% in the lower sabkha) while carbonate sands become more common (up to 52 % of total mineralogy in the lower sabkha). Aragonite content increases up to 22% towards the coast.

2.5.1 Gypsum Mineral Habits and Spatial Distribution

The focus of gypsum distribution in this thesis will be on diagenetic gypsum (also known secondary gypsum), which consist of gypsum cements. This does not include reworked gypsum from earlier erosional remnants or aeolian-supplied gypsum grains, primary gypsum formed from evaporation of open water bodies. The vertical distribution of gypsum cementation habits within the sabkha sediments were usually found above or at ±30 cm of the present-day water table. The main diagenetic processes observed through the petrographic analysis and field observation of the sabkha system (including the Dammam formation) are various forms of evaporite precipitation with minor carbonate cementation. Gypsum is the most commonly observed evaporite in the Mesaieed sabkha (Figure 2-23, 2-24), with

average of 15.1% of the bulk sediment (consisting of up to 48%). Minor evaporites include halite (5%) and negligible anhydrite (0.3%).

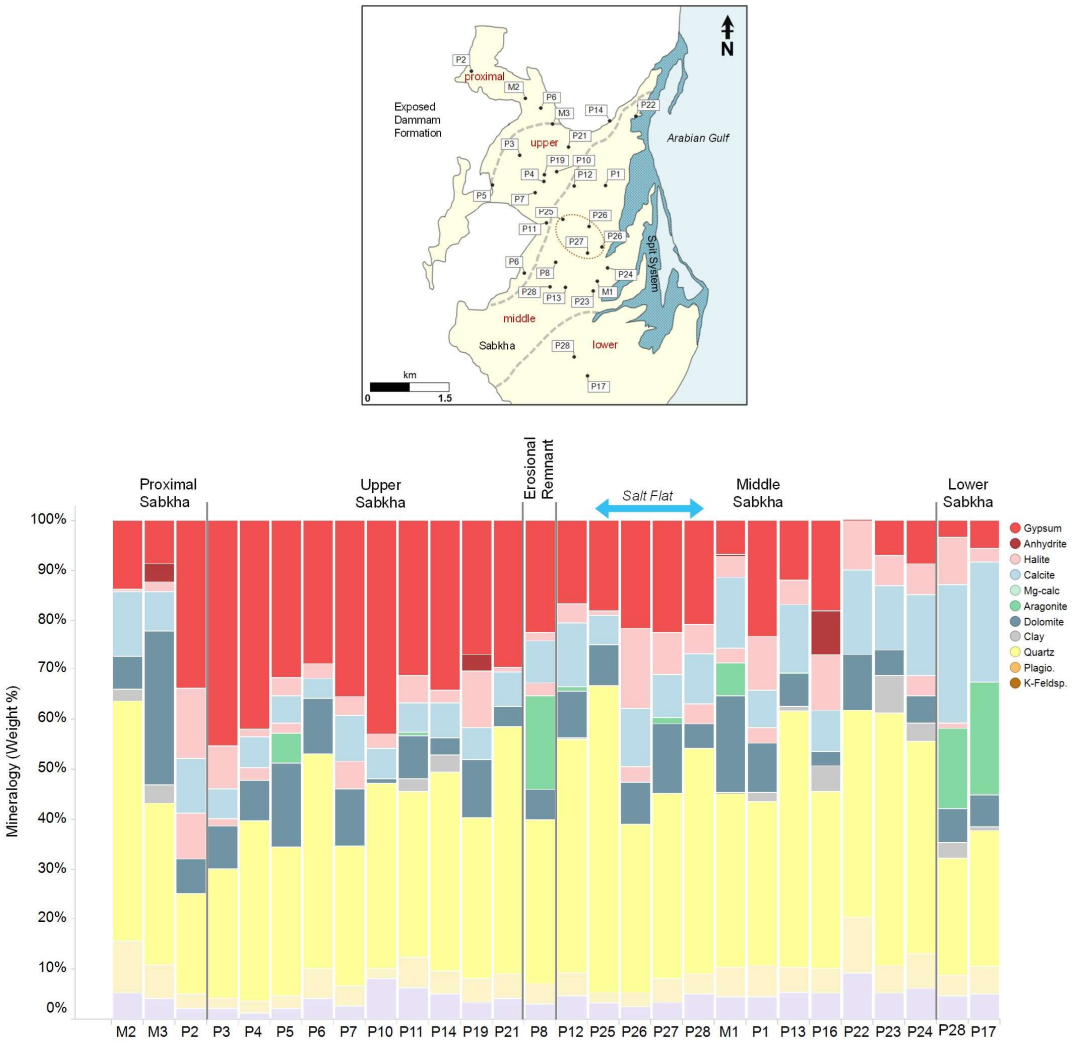

Figure 2-23. (**A**) Map of sabkha sites that were studied using XRD and optical analyses. Grey dashed lines highlight sabkha zonation boundaries, and dotted brown lines indicate where the ephemeral salt flat is located. (**B**) 100 % stacked bar chart showing average sabkha mineralogical profile per site in map above, arranged by spatial zones denoted in red on the map: proximal, upper, middle, and lower sabkha. Sites of the sabkha with ephemeral salt flat in the middle sabkha is highlighted with blue arrow.

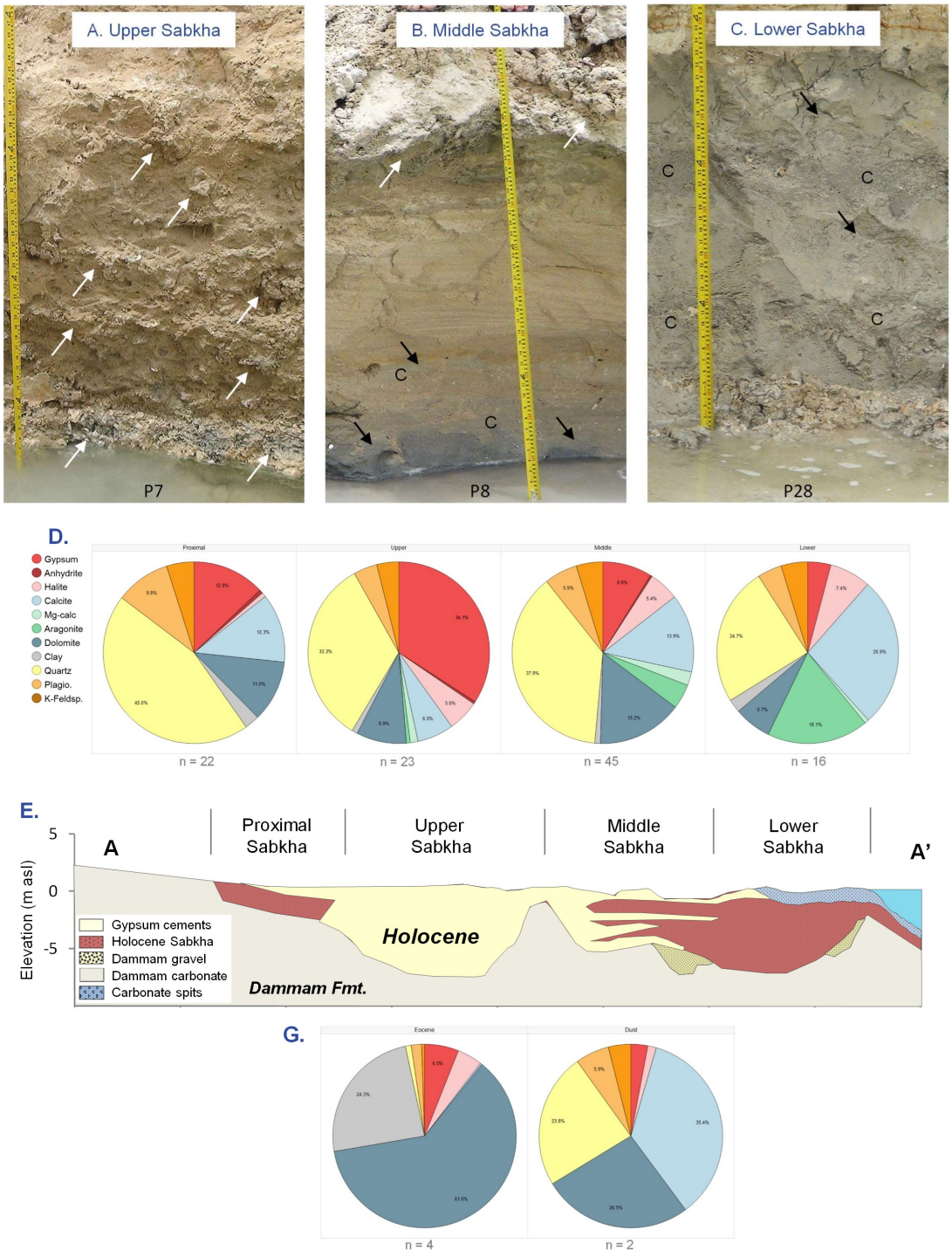

Figure 2-24. **Top**: Representative sabkha pits photographs per sabkha zones, highlighting the extent of gypsum cemented areas that resisted erosion (in white arrows). It also shows the increase of grey coloured mud (in black arrows) coastward from the upper sabkha to the lower sabkha, which comprises of carbonate with occasional layers of whole shell to shell fragments (abbreviated as C). **Below**: Pie charts of Average mineralogy per sabkha spatial zone in the form of pie charts using data shown in Figure 2-23 above a cross-section of Mesaieed shows the primary depositional sedimentology and diagenetic overprint by gypsum on the A – A' line from Figure 2-23. XRD data of Dammam Formation and dust samples were included below the cross-section.

Gypsum content is observed to be the highest in the upper sabkha zone with decreasing gypsum content into the lower sabkha and proximal sabkha. The ephemeral salt flat within the upper sabkha marks the gradual transition from about 40 % gypsum to about 25 % gypsum (Figure 2-24). The layers of gypsum crust which covers most of the Mesaieed sabkha surface comprise of approximately 90 % gypsum.

Gypsum in the proximal sabkha zone is limited to the top 10 cm as a pustulose crust with minor gypsum between the present-day water table to ground surface (Figure 2-12). Extensive gypsum precipitation is observed to be the prominent diagenetic alteration of the upper sabkha, followed by the middle sabkha. Upper sabkha consists of thick poikilotopic gypsum and cementation from surface of the sabkha formation to the base (or top of the Dammam formation) (Figure 2-24A). Gypsum cementation in the middle sabkha is limited to the near-surface and modern water table with minor intermittent gypsum cementation up to 22% throughout the sabkha succession (Figure 2-24B), possibly reflecting a paleo-water table. The pronounced and pervasive cementation of poikilotopic gypsum results in stabilisation of the upper sabkha resulting in greater elevation in the upper sabkha by about 1 m compared to the middle sabkha. The gypsum surface crust is largely absent in the lower sabkha with less than 10% of areal coverage, (Figure 2-24C) coincident with the seaward limit of evaporitic brines and in localised depressions.

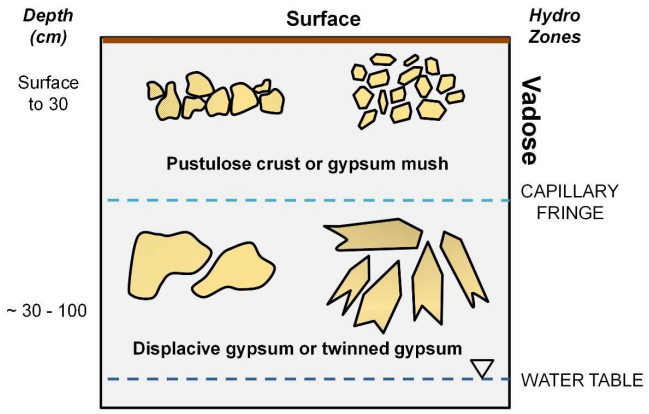

Figure 2-25. General habits of gypsum precipitation relative to depth and position of water table in Mesaieed.

Gypsum habits are shown in Figure 2-25. The gypsum distribution are typically in the form of laminar or pustulose crusts at the top 10 cm. The gypsum observed near-subsurface (top 30 cm) is usually displacive, anhedral and contains mud or sand-grade sediments within them. In the subsurface, gypsum cementation habits varies from twinned crystals above the water table to poikilotopic cements and/or rosettes at or below the modern and paleo-water table. Gypsum crystals tends to have mud content within it and increasingly clear on the edges, which may indicate a replacive growth engulfing the original host sediment. In subaqueous environment especially in open standing water like the

flowthrough pond (Figure 2-18), the gypsum observed tend to be clear, with a fish tail habit. Gypsum occurs as a cement in both siliciclastic and carbonate sands. The pattern of cementation does not appear to follow bedding and often it cross-cuts the sedimentation beds.

2.5.2 Dammam Formation

Twenty NDP cores and three cores from this study found that the top of the Dammam reached to a typical depth of 20-25 m and maximum depths of 50 m beneath the present-day surface. Overlying the Dammam formation marks 0.2-1.0 m thickness of conglomerates that looks the same as the Dammam formation (Figure 2-12, 2-21), with siliciclastic sand infilling in between which looks the same as the overlying sabkha sediment. The sand infill within the conglomerate is dated to be 8000-9000 cal BP. This is interpreted as a basal lag, and it is often cemented by gypsum and possibly calcite/dolomite.

The bedrock is composed of off-white to light grey dolomitized limestone with occasional infill of coarsely crystalline dolomite ranging between 2-8 cm thick, and gypsum cements (Figure 2-27). The facies range from mudstone, wackestone to packstone in the deeper sections and argillaceous dolomitic wackestone-packstone in the upper part (Figure 2-26). Layers of tan, palygorskite clay and clay infillings brecciated zones are common especially in the top 8 – 12 m of the core, with thickness of the infill ranging 10 - 30 cm thick. Numerous irregular joints and dissolution-induced vuggy cavities of 1 to 20 cm in diameter are observed in the upper 10 m (Figure 2-27, labelled V). The weathering trend becomes less visible with depth (Figure 2-26). Small irregular fractures are common, and many have been cemented by gypsum and clay. Open fractures are frequently observed with sub-horizontal orientation of up to 25 cm in width and extend laterally.

The main diagenetic processes appear to be micritization, recrystallization and compaction. These dissolution voids and fractures are filled with either clear gypsum, greenish clay, and carbonate mud (Figure 2-26). The filling order is variable, where it is observed as either greenish clay precipitation surrounded by gypsum or vice versa. The clay and mud are indurated. Many open vugs show traces of fossils such as bivalve and gastropod, indicating dissolution. Different gypsum precipitation patterns are observed (Figure 2-27, labelled G), for example clear euhedral gypsum precipitation in vugs, gypsum lenses, nodular translucent gypsum cementing veins, and gypsum precipitation infilling horizontal fractures.

Below 10 m from the top of the Dammam, the rock is massive, off-white dolomite with fewer vugs and fractures. XRD of three samples for the top 10 m Dammam cores shows that the mineralogy is mostly dolomite (62%), followed by clay (24%), and minor gypsum (6%). Calcite is insignificant (<1 %).

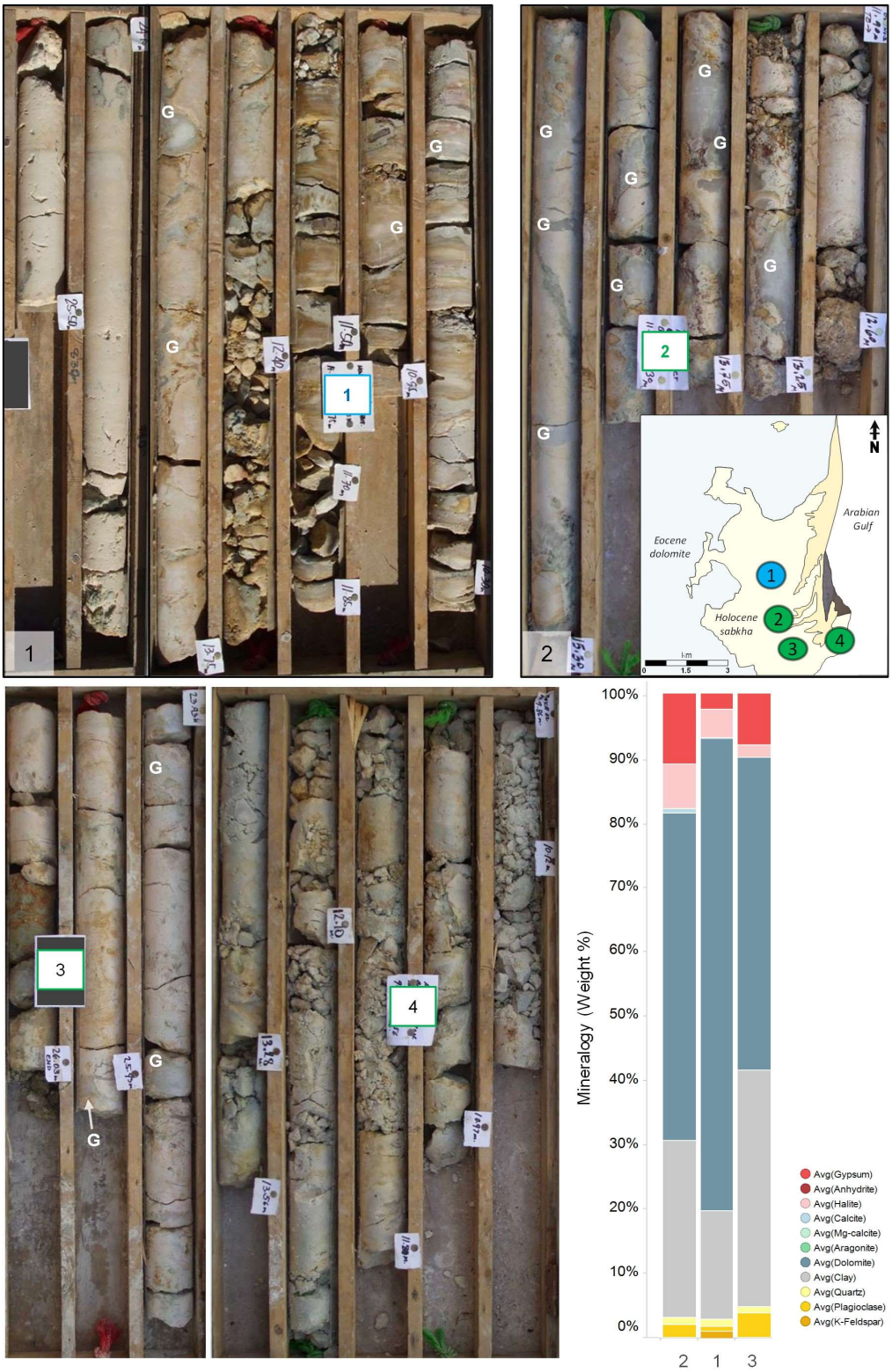

Figure 2-26. Representative cores of Dammam Formation underlying the middle sabkha which shows extensive distribution of diagenetic gypsum (labelled G) infilling cracks, joints, and dissolution voids. Each core section height is 3 m. Core 1 is from the middle sabkha while cores 2, 3 and 4 are from the lower sabkha. Accompanying XRD for the top 10 m are of the cores 1, 2 and 3.

Figure 2-27. Close-up photos of Dammam formation cores from borehole 109 and 104 underlying the middle and lower sabkha zone, which highlights complex diagenesis including cementation and vuggy porosity (V), post-depositional diagenesis infilling in dissolution voids and fissures (F) with gypsum precipitation (G) and arid clay precipitation (C), high Mg calcite or dolomite (D). (3) Massive gypsum cementing what may be a dissolution-driven karst (4) Core show horizontal fractures, burrows, and trace fossil infilled by gypsum precipitation. (5) Core show clear euhedral gypsum infilling voids.

2.6 Large-scale Surface Processes

2.6.1 Shallow Water Table

The water table height is quantified by the the vadose zone (VZ) thickness, which is the distance between the sabkha surface and the top of the water table. The VZ in Mesaieed averages at 0.44 m ± 0.20 (n = 58), which agrees with what is found in other Arabian Gulf sabkha (Sanford and Wood, 2001). Proximal and upper sabkha has the thinnest vadose zone with 0.26 m ± 0.11 (n= 7), followed by lower sabkha with 0.38 m ± 0.32 (n=8) and middle sabkha 0.56 m ± 0.56 (n=14). The outliers that have a maximum VZ of nearly 1.0 m are at sites that, due to water table, encountered localised gypsum cement heave, inverted topography drainage and heavy evaporites cementation, therefore, these are excluded from the mean measurements. The shallow water table is a typically observed in sabkhas (Al-Youssef, 2003; Sanford and Wood, 2001)

2.6.2 Marine Flooding and Evaporation

Satellite imagery shows cycles of marine flooding and ephemeral salt flats within Mesaieed (Figure 2-28). The presence of salt flat in the middle sabkha (and absence thereof) is observed in the field and on the satellite imagery by a white crust and smooth texture with sharp boundaries. Halite is the main mineralogy of the ephemeral salt crust. The transient salt flat appears to coincide with the areal upper limit of seasonal marine floods. This is confirmed by field observations of driftwood and flotsam, and from historic field observations by Jameson (in press) and Al-Youssef (2003).

Marine floods inundates the sabkha from the southeast, where the spits and barrier sands are absent (Figure 2-28). Although the satellite coverage is not temporally continuous, the marine flood is observed in the field to be driven by extremely high tide and winds, confirming previous workers' observations (Jameson and Puls, in press; Al-Youssef, 2003). The cited workers observed the occurrence of this event 6-10 times a year. Flood waters tend to pool in low-relief depressions, and this was commonly observed in the middle sabkha where the relief is the lowest as compared to other sabkha zones. These localised pools were then subjected to evaporation and, over time, become ephemeral, salt flats during desiccation. The most extensive salt flat is seen in 1991, 1998 and 1999 which is a result of a three-year drought during periods of 1992-1994 and 1998-2000 (Appendix 6-4). Satellite imagery shows that the maximum tidal flooding had reached the lower portion of the upper sabkha, just east of the highway, in 1989 (Appendix 6-4). This effect was most pronounced during storms where a combination of high winds, low barometric pressure and intense rainfall is believed to have caused maximum flooding. Using the ArcGIS polygonal calculator, the areal extent of maximum marine flooding is about 34 ± 1 km^2 with average marine flooding to occupy about 25 ± 1 km^2.

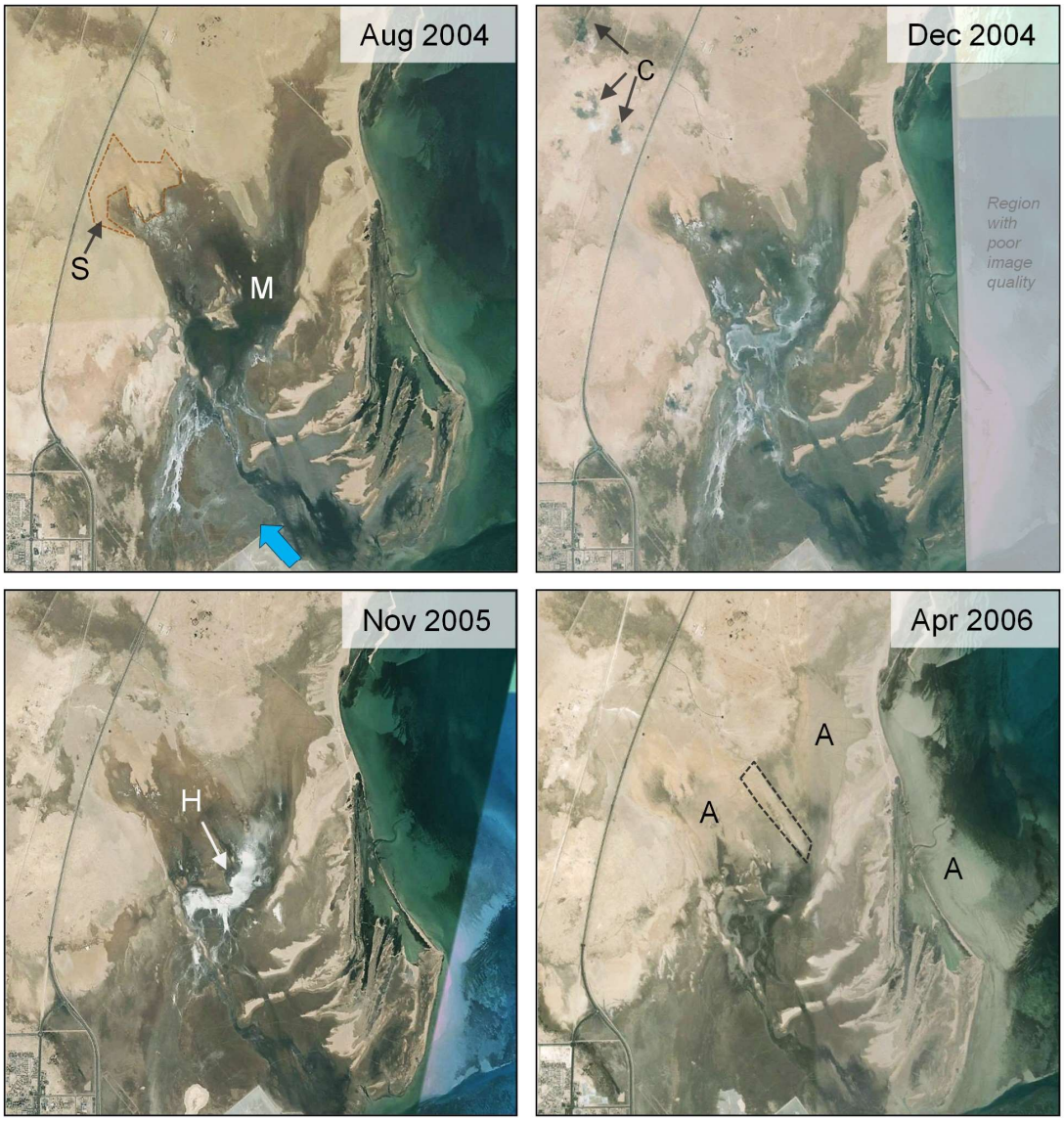

M: Marine flooding; A: Aeolian sand recently deposited; S: Stabilised sheet sand

Figure 2-28. Satellite imagery of two summer-winter season from August 2004 to April 2006. Surface processes that are highlighted include input of continental/meteoric waters (C), stabilised sheet sands (S) and recent aeolian deposition (A) in the upper and middle sabkha after a north-westerly shamal event showing sand sheets in lighter brown, with NW-SE oriented deposition with some spillover of sand (A) into the sea.

2.6.3 Meteoric Input in the Proximal Sabkha

Rainfall appeared to pond into the proximal sabkha with discharge from the continental Dammam aquifer into low relief areas through wadis (Figure 2-10, Figure 2-28 labelled C) and upper sabkha. This will be discussed further in Chapter 3 to combine with meteorology data.

2.6.4 Aeolian Deposition and Stabilised Sheet Sand

The dune complexes observed in Qatar are mostly crescent-shaped and are called barchan dunes. Barchan dunes form in regions where the surface underlying the dune is hard (limestone of the

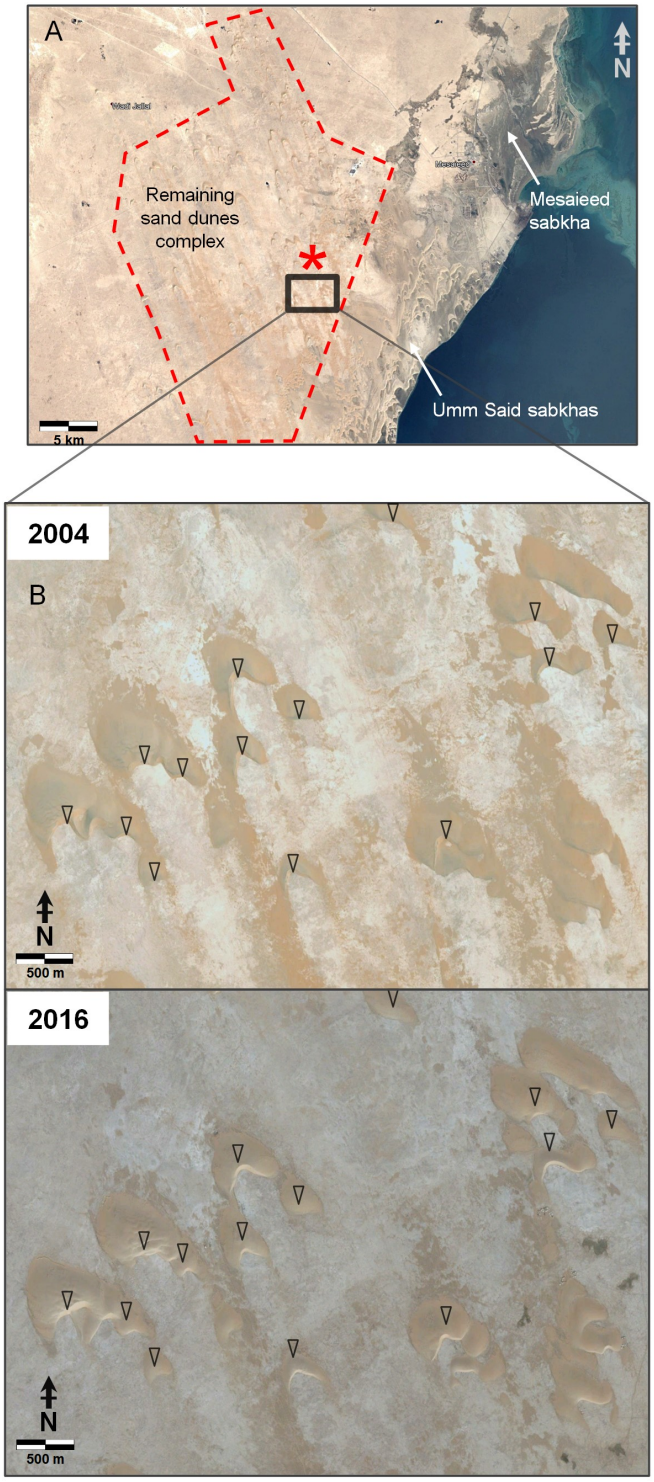

Figure 2-29. A: Map highlights the region where the northernmost sand dunes remain (red dashed line) in Qatar, relative to Mesaieed sabkha to the northeast and the Umm Said sabkha to the east. The black box zooms in to an example of the mobilizing barchan dunes in B. B: The pan view photos are captured in 2004 (left) and in 2016 (right). The inverted triangle symbol ∇ is marked at the highest angle of the dune slip face in 2004 in both photographs to highlight the distance that the barchan dunes have travelled in the direction of the prevailing shamal wind. Over 12 years, the time slice images in this sample area highlights that the barchan dunes have traversed between 50-150 m on the leeward direction of the prevailing wind.

Dammam Formation), there is a moderate supply of sand (from dust storms) and that there is a constant wind direction (the northwesterly shamal wind). The only remaining dunes that would have provided nearby aeolian source into the leeward coastal system in Qatar is located just southwest of Mesaieed (Figure 2-28). When comparing two time sliced photos (Figure 2-28b), the barchan dunes appear to have traversed between a range of 50 to 150 m in 12 years. Using the 4.17-12.5 m/year as an estimate for dune sediment mobilisation rate and 31 km as the furthest distance measured between the northernwestmost barchan dune to the leeward coastal sabkha, this means that it would take between 2,500 to 7,400 years to deplete all of the sand dunes in Qatar.

When accounting for the prevailing wind direction, this means that present-day Mesaieed is unlikely to receive any large supply of aeolian sediment within 50 km with the exception of dust storms events, strong summer shamal winds, and some reworked sand grains blown in the exposed Dammam Formation limestone in any erosional events. This indicates that any recently blown-in sediments driven by the prevailing shamal wind that are observed in Mesaieed is likely from the exposed Dammam Formation which currently forms the majority of Qatar's surface geology. The upper sabkha – which is mostly above the limits of flooding, have been observed to show thin veneer of wind-blown sand (Figure 2-28, labelled A). The deposition, encountered during the field season in February 2013, appears to have a NW-SE orientation which coincides with the prevailing shamal wind. These sediments consisted of well rounded, well sorted, medium to fine-grained quartz sand – which is similar to those found within the top 1 m of the sabkha sediments in the proximal and upper sabkha. Stabilised sheet sands underlying recent aeolian deposition were also observed (Figure 2-28, labelled S). This was observed in pit trenches whereby the sabkha sediment shows ripples and parallel lamination.

Aeolian transport has been studied for photovoltaic panels and for meteorology, but they are often to sample airborne dust, in which sampling station is about 1 m above ground. Shamal dust storms are believed to be a great mobiliser of aeolian input (Figure 2-29). The particulates in transport during dust storms in deserts are often saline and this adds another significant source of soil salinization (Liu et al, 2011). Aeolian input may provide nucleation sites for mineral precipitation, especially if combined with supersaturated porewaters or evaporation of standing waters, may provide loci for precipitation of evaporites and carbonates.

Four shallow standing PVC pipes of known volume were installed into the ground in the north and south of Mesaieed sabkha initially for groundwater monitoring, however the top of the wells (about 0.5 m above the surface) were not sealed and over time the pipes were filled with sand to different depths. This data is accidental, but it may provide a relative approximation to simulated aeolian input onto a bare sabkha. The volume of sand in the pipe was recorded after 9 months of exposure from February 2013 to November 2013. Daily average of sand accumulation rate into a salina averages about 1.03 ± 640 g m^{-2} d^{-1} and onto a dry sabkha at about 0.31 ± 160 g m^{-2} d^{-1}. For comparison, sand accumulation rate from other similar regions such as a bare saline lake at Ebinur, China is about 0.22 to

1.04 g m^{-2} d^{-1} (Liu et al, 2011) and at Negev Desert, Israel 0.57 g m^{-2} d^{-1} (Offer and Goossens, 2011). Sand accumulation rate in Qatar is known to be higher in the winter than in the summer due to higher relative humidity and lower wind speeds in the winter (Javed et al, 2017), so this agrees with our measurements on sabkha input from aeolian.

2.6.5 Marine Sediment Deposition and Shoreline Progradation

Figure 2-30 highlights at least 5 abandoned fully-formed spits (chenier barrier system) and 1 present-day spit on the seaward. It appears that the spits are sourced by movement of sediments down the coast from the north towards the south These spits are distinguished from the commonly interchangeable terminology 'cheniers' as the latter are typically generated from former spits and found on the windward side as they're mobilised by waves and migrated onshore, whilst spits are formed by longshore drift.

The first of the abandoned spit system is a landward spit attached to the exposed Dammam headland. The second abandoned spit is the largest of the coastal sabkha complex, with progressively seaward abandoned spits getting shorter in length but larger in width. Bigger wave heights are associated with longshore drift and lengthening of the spits while smaller, higher frequency waves refract the spits inland (Billeaud et al., 2014). The ^{14}C of the third abandone spit is 4360 yr BP while the sixth spit is 3060 yr BP. The seventh spit is presently being formed as evident in a series of crests of mobile, intertidal sand waves currently being transported southwards by the longshore currents. Breaches between the lengths of the spits are commonly observed, possibly formed by erosion. Channels were created most likely from tidal channels that transected older spits. The back fill deposit is fringed by areas of mangrove and microbial mats within the more protected lagoonal areas developed behind modern beach ridges.

Over time, each spit appears to create a protected back barrier area, which then allowed for sedimentation of fine-grained marine sands. Over time, during marine transgression, this allows for infill of aeolian sediment or marine sediment redistributed during storm events. This can be interpreted as cycles of beach prograding system alternating with sabkha deposition.

The longshore drift is observed to move sediments down to the Mesaieed coastline from the north in a series of crests of sand waves (Figure 2-30-7). This potentially contributes marine-sourced carbonates and reworked marine siliciclastics during wave refraction at the southernmost tip of the spits, which are observed in the cores for the middle and lower sabkha. The spits are mostly continuous, with the exception of a few broken ridges, as illustrated in Figure 2-30 as white arrows.

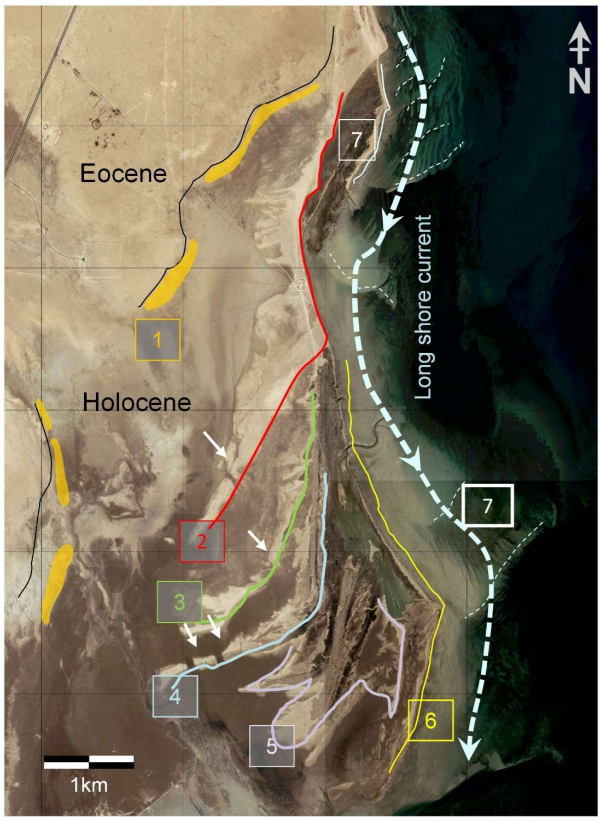

Figure 2-30. The evolution of spit system in Mesaieed coastal sabkha showing 7 depositional cycles (numbered in square boxes) with the accompanying back barrier sediment as a result of wave refraction. Light blue dashed arrows indicate the direction of the present day longshore current moving sediments down the coast from the north towards the south. White arrows indicate an example of subaqueous erosion. Channels were created most likely from tidal channels that transected older spit. Thin dashed lines indicate series of the crests of mobile, intertidal sand waves currently being transported southwards by the longshore currents. Yellow shaded polygons indicate earlier Holocene highstand beaches.

The map on Figure 2-31A highlights the spatial distribution of the age dates on the surface (top 15 cm), with contour lines representing isochronous ranges of age dates. Holocene sediments show some progressively younger facies southeast towards the coast, with a range of 8480 ± 50 yr BP in the upper sabkha to 1620 ± 30 yr BP in the lower sabkha. The ages are similar to the intertidal and supratidal Holocene deposits in the Gulf (Lokier et al., 2015) Bahamas and Florida (Evans, 2011). The transect plot on Figure 2-31B shows the distribution of the age dates with depth along the A-A' transect line – which appears to highlight the aggradation and progradation of the sabkha sediment. Holocene sediment ^{14}C age in Mesaieed is on average 4,380 ± 1800 yr BP (n= 46).

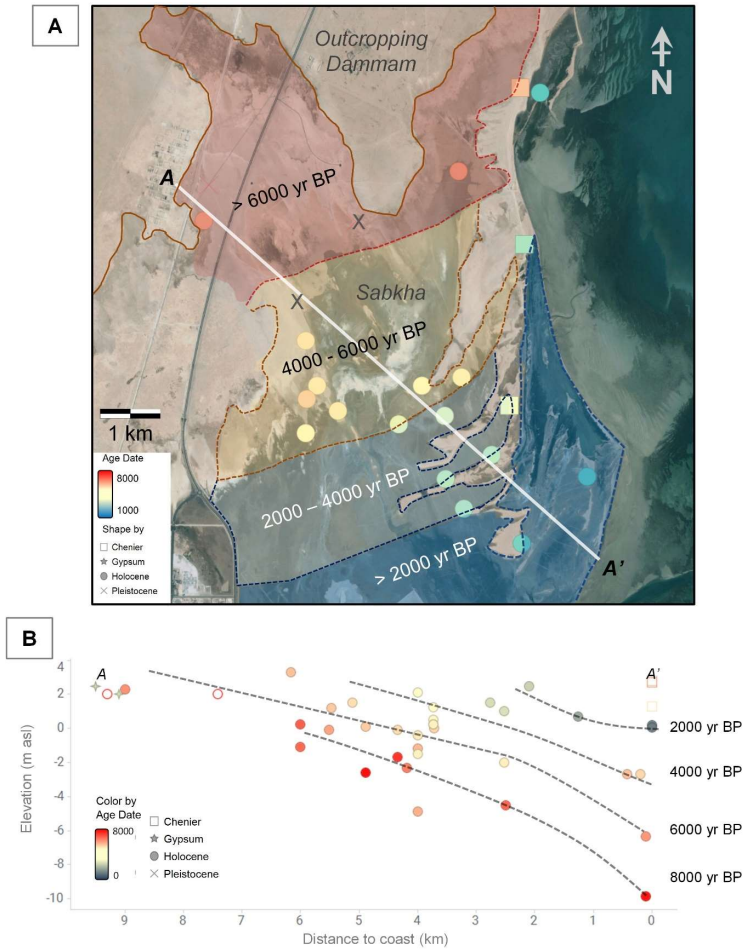

Figure 2-31. **A:** Contour map of ^{14}C age dates of the top 1 m illustrating the direction of the sabkha progradation which provides an extension of Strohmenger and Jameson, 2015. **B**: A to A' highlights the line of transect for plot below which highlights the distribution of sample points coloured by ^{14}C age date, relative to depth and distance to the coast, isochron contoured with dashed line.

3D Geocellular Model

Distribution of ^{14}C age dates, the orientation of spits and distribution orientation of stabilised sheet sands and recent aeolian deposition show that the Mesaieed sabkha forms a thin prograding wedge towards the southeast, perpendicular to the prevailing NW shamal wind. Using ^{14}C data, historic data from Jameson and Puls (2018), field mapping of erosional remnants and relict beach ridges – a framework of sabkha geocellular model was built to highlight progradation of the sabkha in 3-dimension. Using both surface and georeferenced age date distribution combined with well tops, a metre-scale 3D geocellular model of Mesaieed was created to understand the evolution of Holocene sabkha sediments since the last highstand. To create a reliable progradation model, the seven sub-key Holocene surfaces are subdivided by the ^{14}C age sampled dates (in yr BP): 0-2000, 2000-3000, 3000-4500, 4500-6000, 6000-8000, 8000-10000. These sub-key surfaces were mapped within the two main key surfaces - top Holocene sabkha and top Dammam formation. These surfaces were based on surveyed well data

(with precision 0.005 m). This would then allow the model to map the of individual sub-Holocene progradation beds separately.

The sub-Holocene surfaces that is utilized to create deterministic grid of the 3D geocellular model are based on both DEM and stratigraphic horizon grids which represent the different progradation cycle boundaries. The DEM were created using an algorithm called Minimum Curvature, with spacing of the grids being 25 x 25 m. Subsequently, the identified age dated zones were digitized for each zone by subtracting the Holocene zone from the surface distribution of the age dates. The inter-well horizon interpolations were simulated using the 'Across Segments' correction method whereby the residual surface is applied to the gridded horizon to create a horizon matching the wells. Subsequently, the adjustments were interpolated across segments.

The dimensions of the cells were defined using the dimensions of the minimum geologic feature needed to be resolved in the geologic or reservoir simulation model, typically by half (Fabuel-Perez, 2008). This may be especially important to capture heterogeneous distribution of facies. Hence, the horizontal dimensions were based on the smallest size of spits which were approximately 50 meter. Cell vertical dimension, z, is typically determined by the thinnest geologic beds, in this case the transgressive basal lag that averages about 2 m thick. The resulting geocellular model for Mesaieed has 994,301 defined 3D cells with each cell resolution size are 25 x 25 x 1 m.

Using the average direction of the shamal winds at 315° and the oblique position of Mesaieed, the orientation of the surfaces modelled is defined as 135° SE with a strike of SW-NE. An elevation histogram (Figure 2-9) highlights the sabkha surface being above present-day sea level while upper Dammam succession is about -5 m below sea level. 3D model (Figure 2-32) illustrates progradational cycle bedding which is a result of forced regression produced by a relative sea-level drop, falling stage systems tract (FSST). This illustrates that 8 km of steady outward progradation has occurred, with possibly some aggradation, since the last Holocene highstand, about 6,000 to 8,000 years ago.

The transect plot of ^{14}C relative and the 3D geocellular model does not pretend to be a Bayesian or 'classical' age-depth model (see Blaauw, 2010), but it is a good approximation of the evolution of sabkha system over time, highlighting coastward progradation of the sediments. This framework model is presently being used to input facies and diagenetic mineral distribution as a proxy for a reservoir model at ExxonMobil Upstream Research by Christine Ianello-Bachtel.

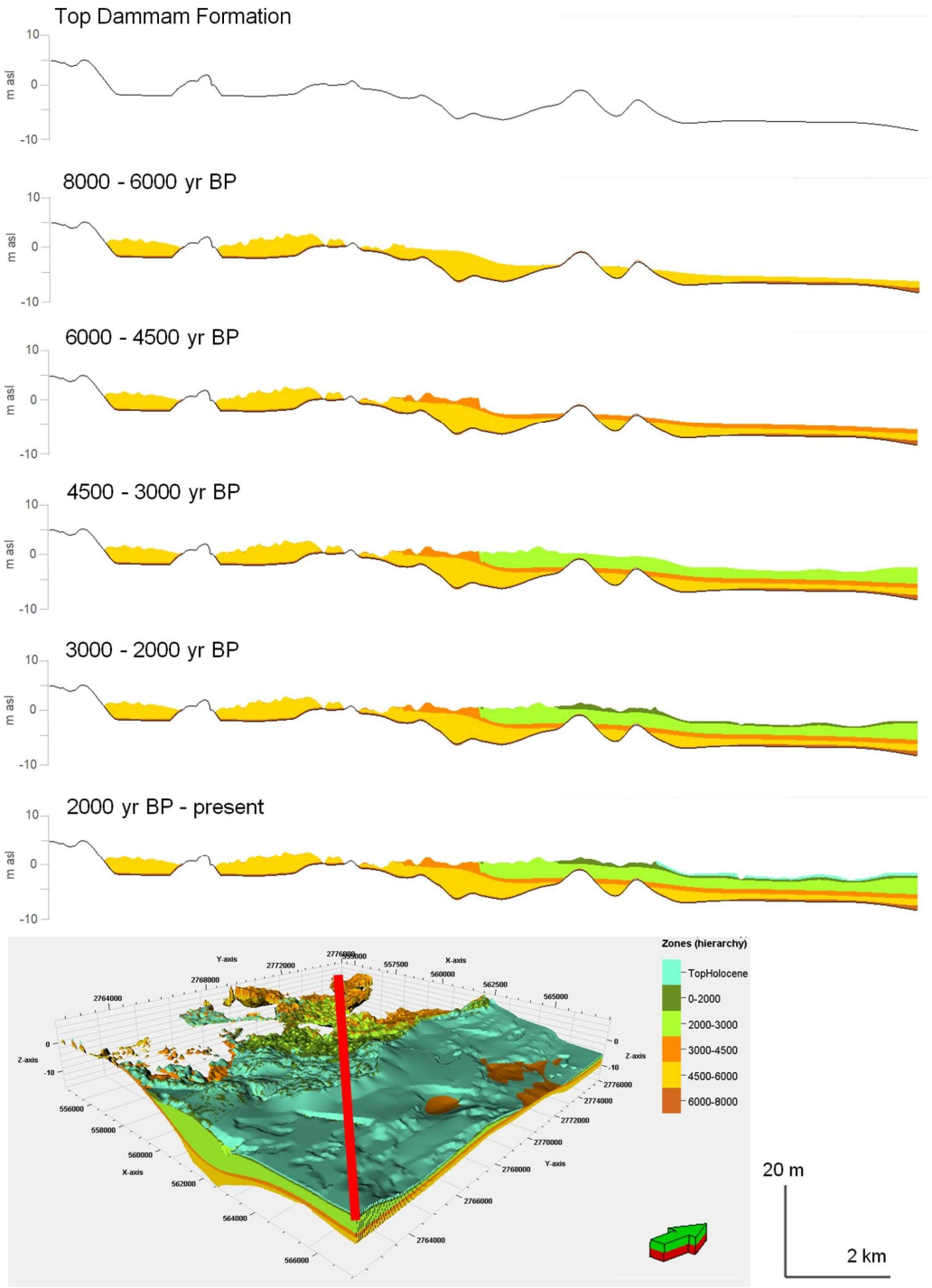

Figure 2-32. Time-series of NW - SE oriented cross-sections of 3D geocellular Mesaieed model showing the evolution of Holocene sabkha sediments in the last 8,000 yr BP.

2.7 Field-scale Permeability

The field-scale permeability is used here to demonstrate the spatial differences. Data is presented in Table 4. Permeabilities in the sabkha and Dammam Formation vary vertically as demonstrated by the core-scale permeability (Appendix 6-3),

2.7.1 Method Comparison

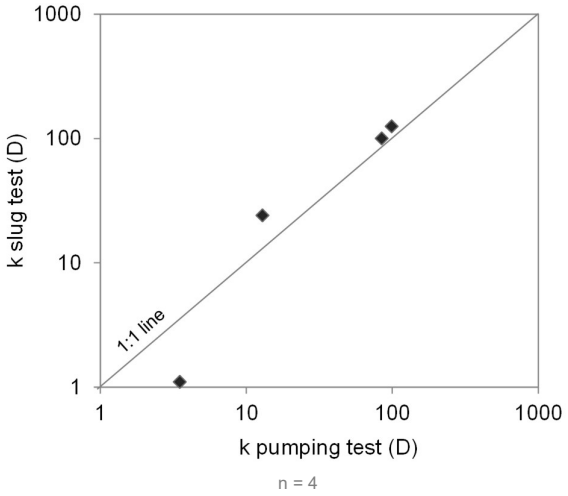

Figure 2-33. Significance of scale dependence in Dammam formation permeability as demonstrated by results from slug test performed on sites with existing pumping test site (G8, G26, G28, G29). Results show linear regression within the same order of magnitude which supports the validity of the quality of both slug and pumping test methods, and the use of slug test and pumping test data as one dataset to analyse Mesaieed.

Field-scale permeability tests for the Dammam formation underlying the sabkha were repeated in four groundwater wells screened within Dammam using both pumping tests and slug tests for comparison. Results show that they are within the same order of magnitude (Figure 2-33), with three of four samples showing a good 1:1 relationship between pumping test and slug test. Although the dataset is restricted (n = 4), this suggests that the scale dependency is insignificant for field-scale permeability within the Dammam formation. The results from both pumping tests and slug tests will be combined to explain the results for the Dammam formation.

2.7.1 Core-scale permeability in Proximal Sabkha

Figure 2-38 shows a vertical permeability distribution for one sabkha site in the proximal sabkha. Within the vadose zone, there is a decrease in small-scale permeability with depth from 90 D to 3 D. This coincides with decrease in total gypsum content (weight %) surface from 90 % to below 5 % with an increase in muddier sediment.

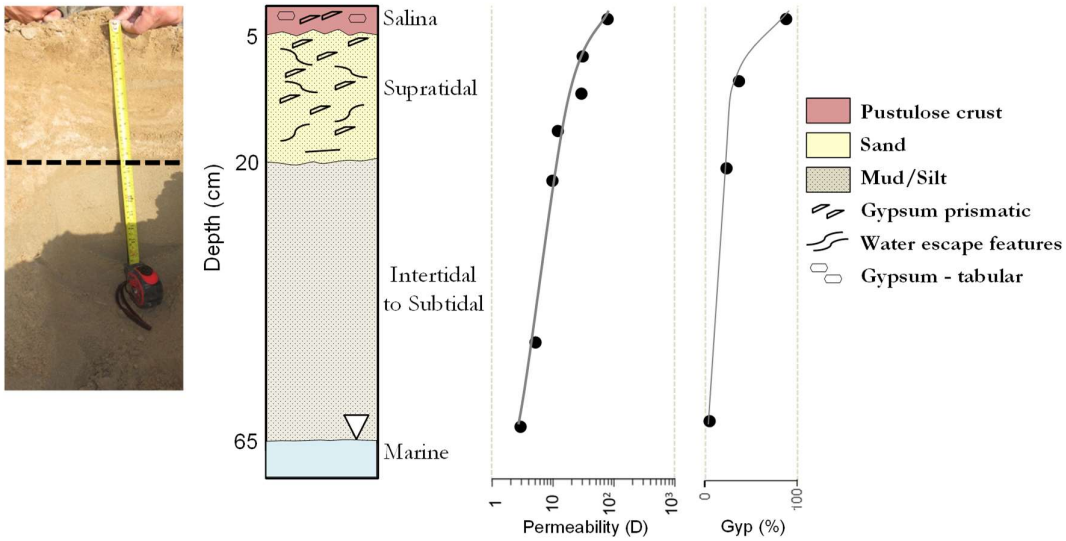

Figure 2-34. A representative site (JP) of the vadose zone in the upper-proximal sabkha about 200 m away from the edge of the exposed Outcropping Dammam Formation updip with GSA permeability measurements of unsaturated and capillary zones. L to R: Pit photograph with what may be a paleo water table as dashed line, subfacies with water table at 0.65 m below surface marked by inverted triangle, environment of deposition, core-scale permeability in log scale (Darcy), and gross gypsum (%). The paleo water table coincides with a drop-in gypsum 30 % to <5 %.

2.7.1 Vertical permeability in Eocene

Vertical distribution of field-scale permeability in three piezometer sites for the outcropping Dammam Formation, proximal sabkha and the lower sabkha were analysed (Figure 2-40). Updip of the sabkha, 7 km west of the coast, three piezometers screened at depths of 5, 15 and 50 m below the ground surface show a linear decrease of permeability with depth (Figure 2-40C). The highest permeability (90 D) is just below the water table, possibly reflecting dissolution from either from overland flow or direct recharge of meteoric water. Permeability is reduced to 36 D only 13 m deeper, and then to a meagre 0.06 D about 40-50 m below surface.

In the upper-proximal sabkha, two tests within the top 7.5 m of the Eocene shows the same permeability of 50 D. In the lower sabkha, the permeability measured at five depths within the range 16-27 m below the surface, show an increase with depth from 4 mD to 40 mD in 17 m (plot suggests range of depths >17 m at this site).

The deeper Eocene (<13 m) exhibits a somewhat greater permeability (26±30 D) in the middle sabkha than the shallower Eocene, while it is the opposite in the lower sabkha whereby the lower Eocene is lower (12±15 D). There is no relationship between depth and permeability measured (R^2 < 0.100) for both Eocene and lower Eocene.

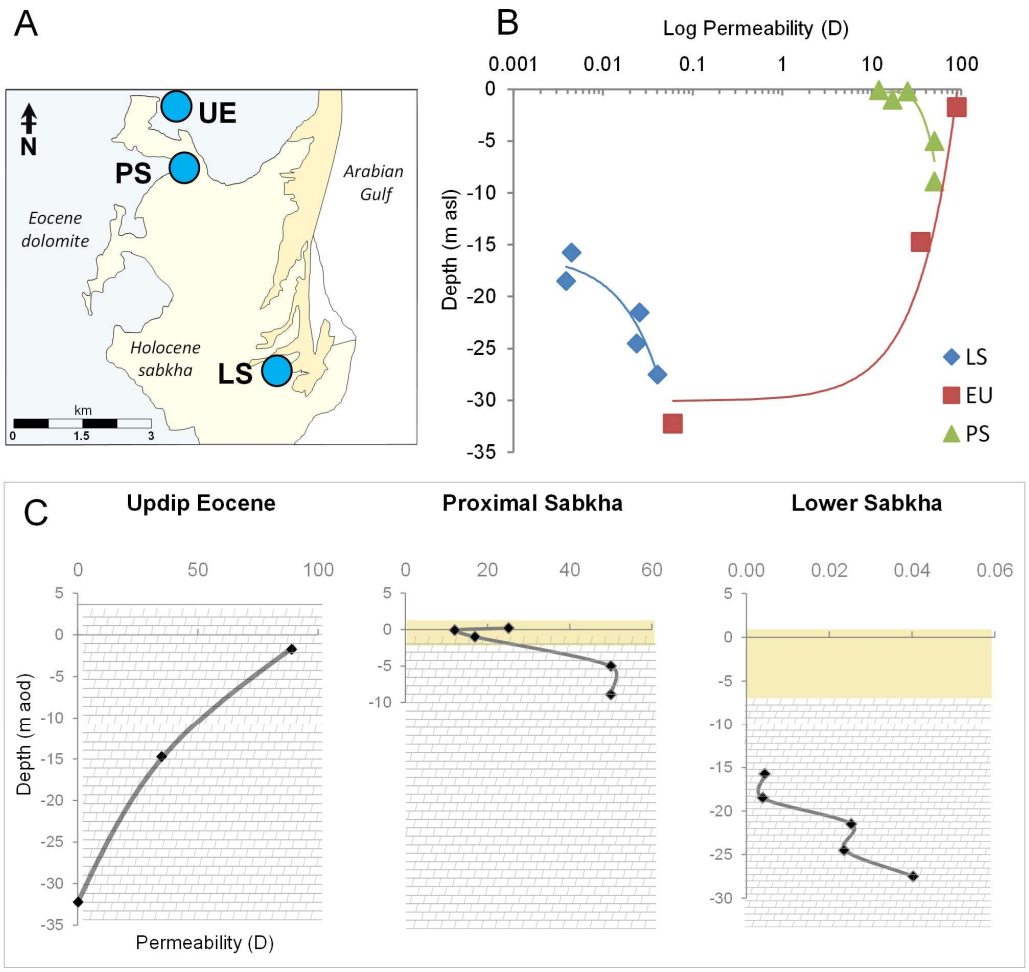

Figure 2-35. Vertical variation of field-scale permeability in outcropping Dammam Formation (EU), proximal sabkha (PS), and lower sabkha (LS) with depth in a single plot (**B**) and separate plots (**C**). (**A**) inset above showing its location. Points plotted are using the mid-point of the screen interval. Proximal sabkha is the only site with permeability tested in both Eocene and Holocene formations. Proximal sabkha has slightly higher permeability at the surface due to gypsum mush at the top 30 cm

2.7.2 Sabkha Sediment Permeabilities

The vertical depth resolution of a field-scale permeability is 3 m as reflected of the length of slotted core, and therefore the geometric mean permeability of the sabkha sediments is used. With a resolution of 3 m, this means that the permeability measurements here reflect the highest permeability of that sediment in that site.

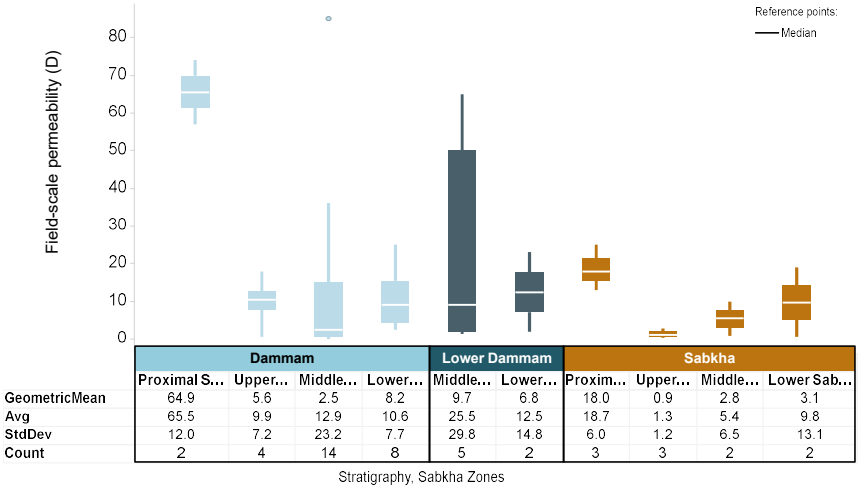

	Dammam				Lower Dammam		Sabkha			
	Proximal S...	Upper...	Middle...	Lower...	Middle...	Lower...	Proxim...	Upper...	Middle...	Lower Sab...
GeometricMean	64.9	5.6	2.5	8.2	9.7	6.8	18.0	0.9	2.8	3.1
Avg	65.5	9.9	12.9	10.6	25.5	12.5	18.7	1.3	5.4	9.8
StdDev	12.0	7.2	23.2	7.7	29.8	14.8	6.0	1.2	6.5	13.1
Count	2	4	14	8	5	2	3	3	2	2

Stratigraphy, Sabkha Zones

Figure 2-36. Box and whiskers diagram of field-scale permeability (in Darcies) within the Holocene sabkha sediments and Dammam Formation in different sabkha spatial zones. Geometric mean and its standard deviation is shown on the table below the plot. Plot excludes the outcropping Dammam Formation updip that are within 500 m proximity to the coast, which has an average of 204±141 D (n=6). The lower and upper limit of each box define the first quartile (Q1) and third quartile (Q3) percentiles, respectively. The white horizontal line within the box is the median. The whiskers extend to data that are not considered as outliers. Outliers (the data points that are not connected to the box and whiskers) were defined as a data value greater than Q3 + 1.5(Q3 - Q1) and less than Q1 + 1.5(Q3 - Q1).

Box and whisker plot (Figure 2-34) shows that the highest range of permeability is within the proximal sabkha of 13-25 D (geometric mean of 18±6.0 D), followed by the lower sabkha 0.5-20 D (geometric mean of 3.1±13.1 D) and middle sabkha 0.4-3.1 D (geometric mean of 2.8±6.5 D). The upper sabkha shows the lowest permeability 0.3 to 2.7 D (0.9±1.2 D). The geometric mean permeability of the sabkha is slightly lower than of the Dammam permeability in all sabkha zones except the middle sabkha. However, the relationship in the middle sabkha is not statistically significant ($p>0.05$).

Holocene permeability shows an inverse relationship with depth by $y = 0.25x + 6$ ($R^2 = 0.615$). Because the permeabilities of Holocene sabkha is derived from grain size analysis, this suggests that grain size, grain shape and cementation may account for the variability.

2.7.3 Dammam Formation Permeabilities

There are differences in permeability between outcropping Dammam Formation updip (without Holocene cover) with sabkha regions. In the outcropping Dammam Formation updip, the permeabilities are 200±140 D and it decreases as it approaches the sabkha, with measurements within 500 m of the boundary at 26±30 D. For the Dammam Formation underlying the sabkha (Figure 2-34), the permeability in the proximal sabkha (65±12 D) is distinctively higher than those measured in the lower sabkha (8.2±7.7 D), upper (5.6±7.2 D), and middle (2.5±23.2 D). Figure 2-35 shows the spatial distribution of log permeability. The low permeability sites are within the Dammam underlying the middle sabkha and this coincides with extensive amount of gypsum, carbonates and clay cementation (from core observations). The lowest permeability is found beneath and just slightly southwards of where the ephemeral salt flat is (0.01 to 1 D), which may indicate extensive cementation of joints and fractures.

A high permeability belt from the outcropping Dammam Formation updip north of the sabkha to the first generation of spit may indicate a large dissolution features which may introduce seawater into the sabkha.

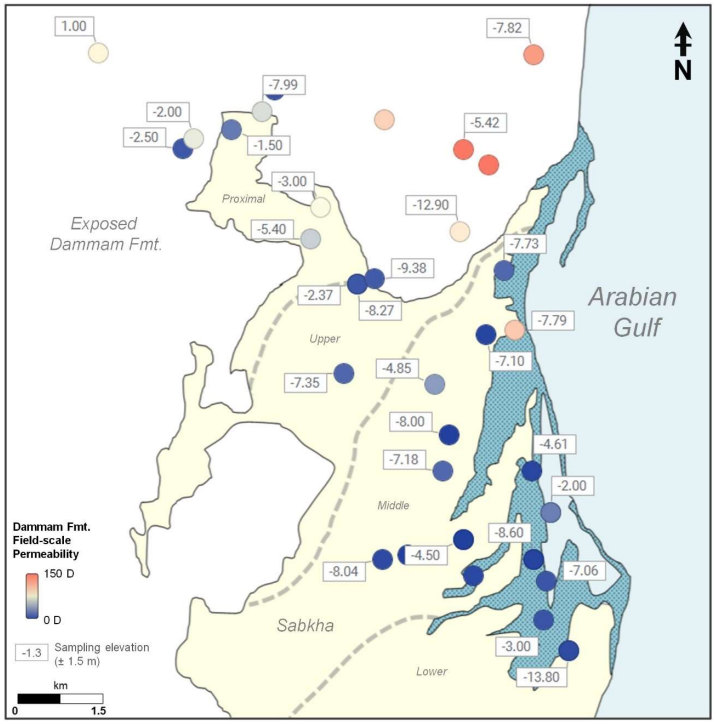

Figure 2-37. Distribution of well sites screened within the Dammam Formation aquifer, coloured by permeability (in Darcy) with sampling depth (m asl) as the labels of the map plot. Note that the sampling depth represents the mid-point elevation of a 3 m vertical screen within the well. The dashed lines represents the loose boundary to divide the sabkha zones.

2.7.4 Lost Circulation Zones

Of 110 NDP1 wells located within the middle and upper sabkha zones, 41 wells within the study area show occurrences of lost circulation (Table XX). Of these, 33 sites show total lost circulation (TLC) within the Dammam Formation underlying the sabkha (Figure 2-36). 3 sites show partial loss of circulation (PLC) within the basal transgressive lag (BTL) and 5 sites show 60-80% TLC within the Holocene. For the offshore wells, 30 % out of 24 wells show TLC. Figure 2-41A also shows that 50% of LCZ occur within the top - 8.0 m of the present-day surface elevation, and 80% within the top -10.0 m. There are no lost circulation zones in intervals where there are low permeabilities when compared with core descriptions provided by NDP (Appendix 6-3).

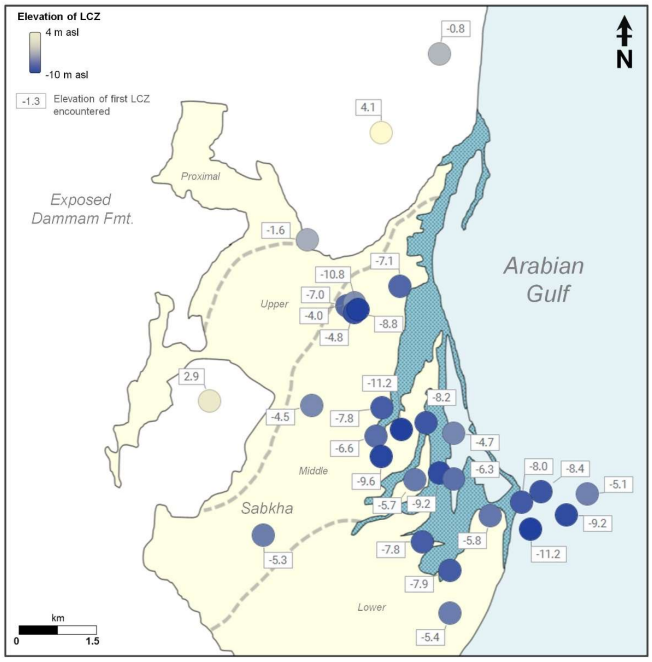

Figure 2-38. Map of the elevation that first occurrence of lost circulation zone (LCZ) is encountered (unit m asl) (n = 33). Data are only available within middle and lower sabkha hence an unmapped region in the upper and proximal sabkha. The dashed lines represents the loose boundary dividing the sabkha zones.

The spatial distribution of the first depth at which LCZ was encountered (Figure 2-35) mapped within the middle and lower sabkha highlights no spatial relationship. However, if we subtract the first occurrences of LCZ (Figure 2-37A) from the top surface of the Dammam stratigraphy using our core data, 50% of all LCZ occur within the top 3 m of the Dammam formation, and 80% within the top 5 m (Figure 2-37B). The top 0-5 m of the Dammam formation underlying the sabkha coincides with the majority of the high permeability values observed.

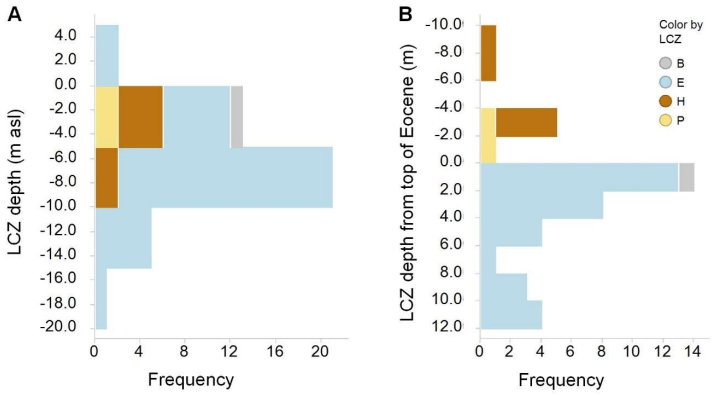

Figure 2-39. (**A**) Histogram of elevation relative to datum (m asl) at intervals where lost circulation zone is first encountered within both sabkha and Dammam. (**B**) Histogram of depth of first occurrences of LCZ from the top of Dammam Formation (as positive numbers), which includes basal transgressive lag (B). Negative numbers imply LCZ that occurs above the Dammam Formation, either within Pleistocene sediment (P), Holocene sabkha (H).

2.8 Discussion

2.8.1 Geomorphologic Zones

Mesaieed is a dynamic leeward coastal system in that it is developed along a coastline with an oblique orientation to the prevailing shamal wind. Mesaieed sabkha is formed from a unique combination of large-scale surface and small-scale near-surface processes (Figure 2-39, Figure 2-40).

The sabkha surface is characteristically planar and low-relief. Based on relatively constant vadose zone thicknesses, this is interpreted as an expression of Stokes surface, with ablation limiting accumulation of sediment above the height of the capillary fringe, the transitional zone between the unsaturated (vadose) and saturated (phreatic) zones (Fryberger et al., 1988). Thus, the capillary fringe of the sabkha appears to stabilise the sediments from aeolian erosion. Spatial variation do occur in that there is a slight thinness in the vadose zone (<0.5m) within the proximal and the lower sabkha which can be attributed to its proximity to groundwater discharging from the updip aquifer and from the coast, respectively. Following that, the thickness of the sabkha succession towards the coastline reflects the stratigraphy surface of the underlying formation, which in this case is the Dammam Formation (Figure 2-9). This highlights that as the Dammam Formation surface is lower in elevation, as observed in the well ad data and geologic model (Figure 2-9), the elevation of the sabkha succession thickens. This means that the thickness of the sabkha deposits is likely determined by a combination of the sediment accommodation space provided by the relict fluvial system of the Dammam bedrock and the sea-level fluctuations. In addition to the Dammam paleo-surface, the depth to the water table, which determines the height of the capillary fringe, play a factor in the preservation potential of the sabkha from aeolian and subaqueous erosion. With that, any existing sabkha topography that experiences either tectonic uplift or a drop in water table resulting in thick vadose zone (above 1.5 m), may encounter aeolian erosion in the future. The caveat to this is if there is localised cementation by evaporites that allows it to resist erosion, such as the erosional remnants observed in the upper and middle sabkha.

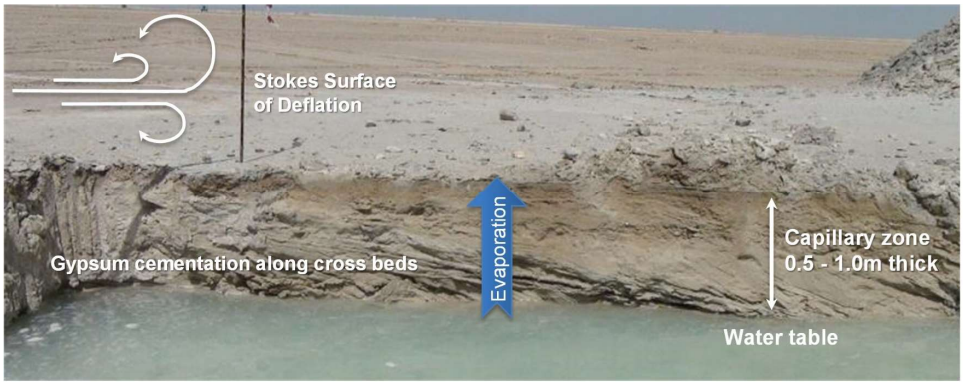

Figure 2-40. General characteristics of Mesaieed sabkha which includes the planar Stoke's surface driven by constant aeolian-driven erosion and height of the capillary zone. This positive feedback keeps water table relatively shallow, and thus allowing evaporation-driven gypsum cementation.

The sabkha study is a follow-up from Strohmenger and Jameson (2015) which provided the framework to further understand the sabkha region in detail. The sabkha zonation in the previous study loosely subdivided the sabkha spatially into upper, middle and lower zones on the basis of geomorphological differences (Figure 2-3, Figure 2-23). In their study, they identified that the upper sabkha zone is cemented by gypsum from the surface to the base of the sabkha sequence; the middle sabkha is cemented at the surface to the present-day water table, while the lower sabkha has insignificant gypsum crust often limited to the top. Their study extrapolated that the gypsum cementation in the landward portion of the upper sabkha is similarly pervasive when it is not the case. Therefore this study separated the landward portion of the upper sabkha into a proximal sabkha to reflect the geomorphology and sedimentological differences.

The *proximal sabkh*a is characterized by minor halophytic vegetation, gypsum pustulose crust, wadi and siliciclastic-dominant host matrix. Observations of xenophytes are not seen in other sabkha zones. The xenophytes and wadi on the proximal sabkha hints at possible source of brackish to fresh water from outcropping Dammam Formation. As marine flooding was not observed to reach the proximal sakha based on field observations and from historical imagery study, the evaporites are potentially sourced from evaporation of pooled meteoric waters resulting from the outcropping Dammam Formation, either as surface runoff, overland flow and/or from gravity-driven subsurface percolation process. Cores from the proximal sabkha hints that the sabkha likely deposited unconformably on the Dammam Formation, by the infilling the brecciated Dammam Formation, believed to be part of a basal transgressive lag. The host sediment is generally siliciclastic with minor carbonate.

Wavy, bioturbated sediment at the base of the sabkha succession transitions to planar laminations at the top 80 – 25 cm below the surface show paleoenvironment that began as an unrestricted subtidal to an intertidal environments. The presence of gypsum crust at the top 15-25 cm hints at the evolution of the subtidal-intertidal into a salina-like environment. This would have allowed lenticular gypsum mush to precipitate. With the loss of water in the proximal sabkha, this has now formed the crust seen at today.

The *upper sabkha* is a supratidal flat, characterised by the irregular surfaces that are filled with buckled gypsum crusts, erosional remnants of both Holocene and Pleistocene age, stabilised sheet sands, eroded Dammam Formation rubble and a small relict salt flat. The upper sabkha core and pit hints at a subtidal to intertidal paleo-environments. From satellite imagery and field observations, the upper sabkha is a supratidal flat, which marks the landward limit of maximum marine flooding. Today, this sabkha sucession is cemented by poikilotopic gypsum precipitation from the top surface to the base.

Buckled crust facies in Abu Dhabi typically consists of halite (Lokier, 2012), while in Mesaieed the gypsum is observed to be the dominant facies. The buckling of pre-existing gypsum crust is due to

lateral displacement driving the crust upward. This also suggests that the either the (1) halite has dissolved extensively, (2) brines have not reached halite saturation and/or (3) the dominant brine is not seawater, which is Na-Cl type. This indicate that the solutes sourcing the sabkha are rich in Ca and SO_4 ions and that the brine has reached saturation relative to the gypsum mineral. Aqueous geochemistry and hydrogeology study is required to quantify this hypotheses.

The upper sabkha has undergone about 1-2m of erosion leaving sediments that were previously cemented by gypsum now preserved as erosional remnants today. These erosional remnants comprise of heave structures, gypsum crusts, and nebkhas. Sediments of these erosional remnants are likely deposited in previously localised depressions and/or paleochannels, which over time the evaporatively concentration has resulted in gypsum precipitation. This localised depressions then became resistant to aeolian and tidal-driven subaqueous erosion compared to its surrounding less consolidated terrain, resulting in an inverted topography. Understanding of the erosional remnant is necessary when modelling the arid siliciclastic-carbonate system to avoid misinterpreting the gypsum-cemented structures and to not underestimate the amount of brine oversaturated with gypsum in the system.

The *middle sabkha* has an overall lower elevation than the other sabkha zones, including the lower sabkha zone. This phenomena may be due to a well-lithified but discontinuous outcrop belts of exposed carbonate of Pleistocene age that separates the upper and middle sabkha. The Pleistocene belt may potentially limit the erosion in the upper sabkha and thus cutting off aeolian supply into the middle sabkha from the prevailing wind. This then allow a positive feedback of marine floods pooling in localised depressions in the middle sabkha, resulting in the ephemeral halite observed today. The series of carbonate spits forming beach ridge successions on the eastern seaward side of Mesaieed driven by southward longshore drift is crucial to mobilize marine sand leading to the formation and maintenance of a coastal sabkha (Figure 1-43). The succession of spit formation and sabkha sedimentation cycle means that back barrier sequences have progressed from subtidal, intertidal and eventually a low-relief supratidal flat maintained by a combination of deflation of sediment above the capillary height of a shallow water table and the capillary zone itself.

The general observation of the Mesaieed sabkha highlights the contrasting geomorphology and diagenetic evaporite distribution that necessitates the division of the sabkha spatially into four distinct zones which are aligned perpendicular to the wind direction. The lateral zonation in the coastward direction is proximal, upper, middle and lower. This geomorphology and sedimentology study of Mesaieed provided an extension to previous work (Strohmenger and Jameson, 2015; Jameson and Puls, in press) with new information of the proximal, upper sabkha and the Dammam formation. They also grouped both the proximal and the upper sabkha as one and inferred that the proximal sabkha is equally cemented by gypsum from top to bottom, but this is not the case in the proximal sabkha that only has limited gypsum at the crust.

2.8.2 Sabkha Formation, Stabilisation and Preservation

The grains are well-rounded and well-sorted which hints at a reworked sediment, likely aeolian in the landward or marine in the coastward. The present-day aeolian deposits sampled today, although limited in samples (n=2), consist of a total of ~60% of carbonate and ~40% of siliclastic and the well-rounded. This however does not reflect the mineralogy proportion found in the sabkha, especially in the proximal which has about 80% of siliciclastic as the primary sedimentology (not accounting for evaporite content). This indicates that either erosion has occurred or that the supply source is different.

The position of Mesaieed sabkha just above the northernmost barchan dune complex (Figure 2.29) informs us that the near-source aeolian supply for Mesaieed has been cut off, thus allowing later sediment source to be largely the marine sediment and reworked siliciclastic transported from the north by the longshore drift. This aligns with the mineralogy observed in the middle and lower sabkha that increases in carbonate content towards the coast. The spatial distribution of primary mineralogy indicates that aeolian processes were crucial in supplying sabkha sediment in the landward side (proximal and upper sabkha) before marine processes become dominant in supplying and reworking sediments in the coastward part of Mesaieed sabkha (middle and lower sabkha).

Study of present-day surface processes provide an insight on the formation and possibly, the preservation of Mesaieed coastal sabkha over time. The schematic diagram of Mesaieed in Figure 2-41 highlights the formation of the sabkha over time and the role of spits beach ridges in the stabilisation of the sabkha. The series of carbonate beach spits on the eastern seaward side of Mesaieed observed today is driven by southward longshore currents and sediments supplied from the marine realm. The development of spit has resulted in the isolation of embayments that have subsequently developed into sabkha. As the sabkha have become progressively more isolated, and with sea-level regression resulting in marine flooding to proceed seawards, the sediments then become increasingly evaporitic (Figure 2-41). This process is only possible in a leeward coastal system where marine sediment supply is abundant. The low-relief sabkha surface is then maintained by a combination of deflation of sediment above the capillary height of a shallow water table and the height of the capillary zone itself. Considering the leeward coastal systems in Barr al Hikman only has one major spit that transforms it into a closed lagoon system, such spit and back-barrier process appears to be a unique characteristic of Mesaieed sabkha.

Well-sorted and rounded sabkha sediment grains, and events of wind-driven sand deposition observed on satellite imagery (Figure 2-28) and in the field, hints at a reworked processes either by aeolian in the landward or marine in the coastward. The present-day aeolian deposits sampled today, although limited in samples (n=2), consist of a total of ~60% of carbonate and ~40% of siliclastic and the well-rounded. This however does not reflect the mineralogy proportion found in the sabkha, especially in the proximal which has about 80% of siliciclastic as the primary sedimentology (not accounting for

evaporite content). This indicates that either erosion has occurred or that the supply source has changed.

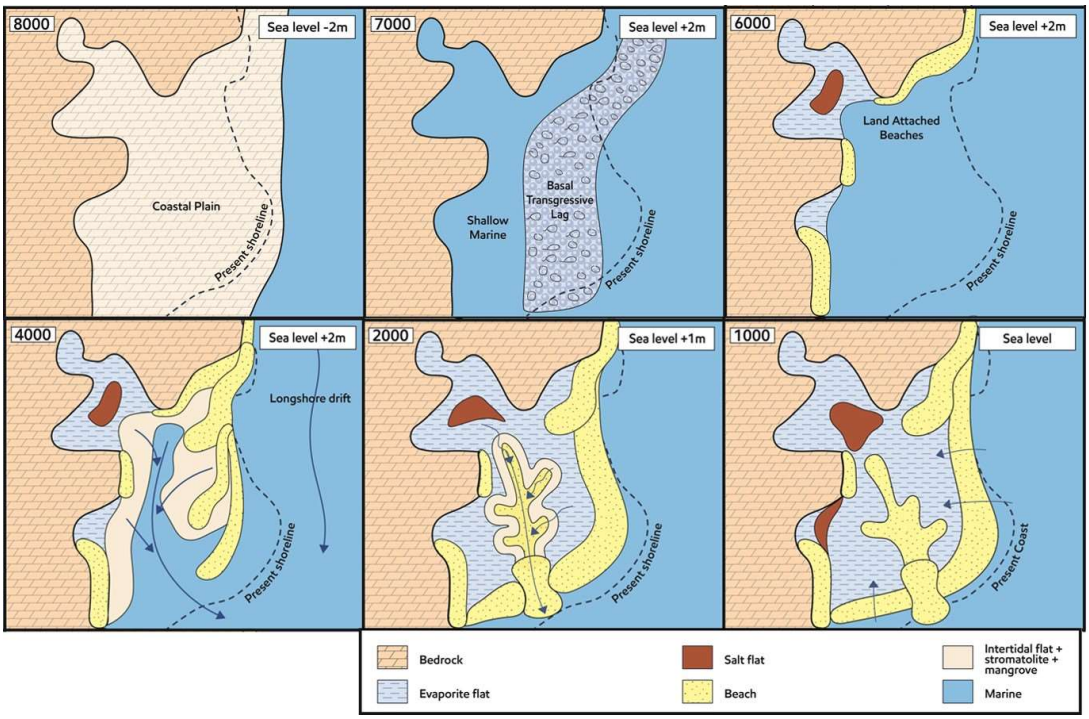

Figure 2-41. Evolution of Mesaieed sabkha (diagram source from Jeremy Jameson) highlighting events of basal transgressive lag from erosion of the Dammam formation and the aeolian sediments blowing in to infill the sabkha (evaporite flat) in the proximal and upper sabkha. Over time the longshore drift brings marine sediment and reworked siliciclastic from the north into Mesaieed through series of spits, allowing redistribution of sediments and creating barriers to stabilize further aeolian and marine deposition. Over time, sea-level fall and with continuously arid climate drove the connate waters to reach gypsum and halite saturation, thus creating salt flats.

Additionally, storm surges play a role in the redistribution of sediments and the preservation (or lack thereof) of the sabkha, and this can be observed in breaches in the spits (Figure 2-30). This is similar to observations in Abu Dhabi (Lokier, by personal comm.). The host siliciclastic sediments in Mesaieed, observed on the field as well sorted, rounded quartz-rich sands, hints of an aeolian source, likely driven by an accumulation of sand dunes that have migrated towards the southeastern part of the peninsula driven by the prevailing shamal winds. This has been postulated by previous workers (Yousef, 2003; Cavelier, 1970b; Shinn, 1973a; Kassler, 1973; Embabi and Ashour, 1985; Ashour et al, 1991) and can be confirmed by satellite observations on the sand dunes mobility over the last 12 years (Figure 2-29).

Local ponds in the proximal and upper sabkha after a heavy rain hints that continental waters are likely to influence the hydrology and therefore the geochemistry in the proximal and upper sabkha. In the upper sabkha, the rarity of tidal flooding may allow two processes: (1) minimal aqueous erosion in which the aeolian deposition can accumulate in the upper sabkha without constant denudation, and

thus allowing (2) evaporative concentration of brines which may drive the saturation of brine relative to gypsum and/or halite to cement the sediments.

Accumulation rate of sabkha sediments that is calculated from the geologic model using the median of the calibrated ^{14}C data concluded a 1.13 ± 0.61 mm/year with multiple age-dated sites. This is greater than the 0.29 mm/year measured in Abu Dhabi sabkha (Lokier and Steuber, 2008). This may be because of Abu Dhabi is experiencing the following reason(s): (1) Abu Dhabi sabkhas, by being windward, are subjected to relatively higher rates of aeolian erosion than Mesaieed that is protected by beach ridges from the spits, (2) the barrier island on the north of Abu Dhabi sabkhas provides a physical barrier for the aeolian influx into the sabkha during shamal events, (3) its windward position means that the aeolian supply is limited to what can be transported over the Arabian Gulf seawater and what is transported from the Hajar Mountains in the east during non-shamal events, and (4) the angle of the ramp in Abu Dhabi is lower than Mesaieed and therefore the accommodation space is limited. To further test these hypotheses, a geologic model of Abu Dhabi sabkhas using ^{14}C data from Lokier and Steuber (2008) and Strohmenger et al. (2011) can be built for comparison.

The average sediment accumulation rates have inconsistent variation over time, with 6000-8000 cal BP to experience a 0.64-0.69 mm/year, while the 6000-4000 cal BP to experience a 0.81-1.15 mm/year. The calculated progradation rates highlight a slight decline to 0.64-0.72 mm/year from 4000 – 0 cal BP year range. The only other comparison to the rates is over the past 1,400 years is Abu Dhabi (Lokier and Steuber, 2008) in which they see a sharp decline of 1.03 mm/year to 0.70 m/year. The limitation to Mesaieed's calculation as it does not consider correction for compaction and correction for evaporite cements.

Erosional remnants in the upper sabkha comprises of remnant subaqueous gypsum, heave structures, gypsum crusts, and nebkhas. With the top of the erosional remnant measured at 5867-6225 yr BP and the present-day surface at 3441-3593 yr BP indicates that about a minimum of 1-2 m of sabkha has been eroded in the last 2500 to 2800 years.

2.8.3 Sabkha Diagenesis and Implications to Preservation

The type of evaporite prectipitation, the fabric style of cementation and the timing of the events, either in the water table or at the surface, is crucial to the preservation of the sabkha post-depositional. The lack of halite observed in the upper and the proximal sabkha zones highlights that either halite saturation has not been reached or that Na and Cl solutes are not adequate. Minor relict halite observed in localised regions of the upper sabkha indicate that marine source is likely in local depressions albeit in minor proportions. The infiltration of marine flood up the the upper sabkha is proven by the extent of very rare marine floods captured on the satellite images.

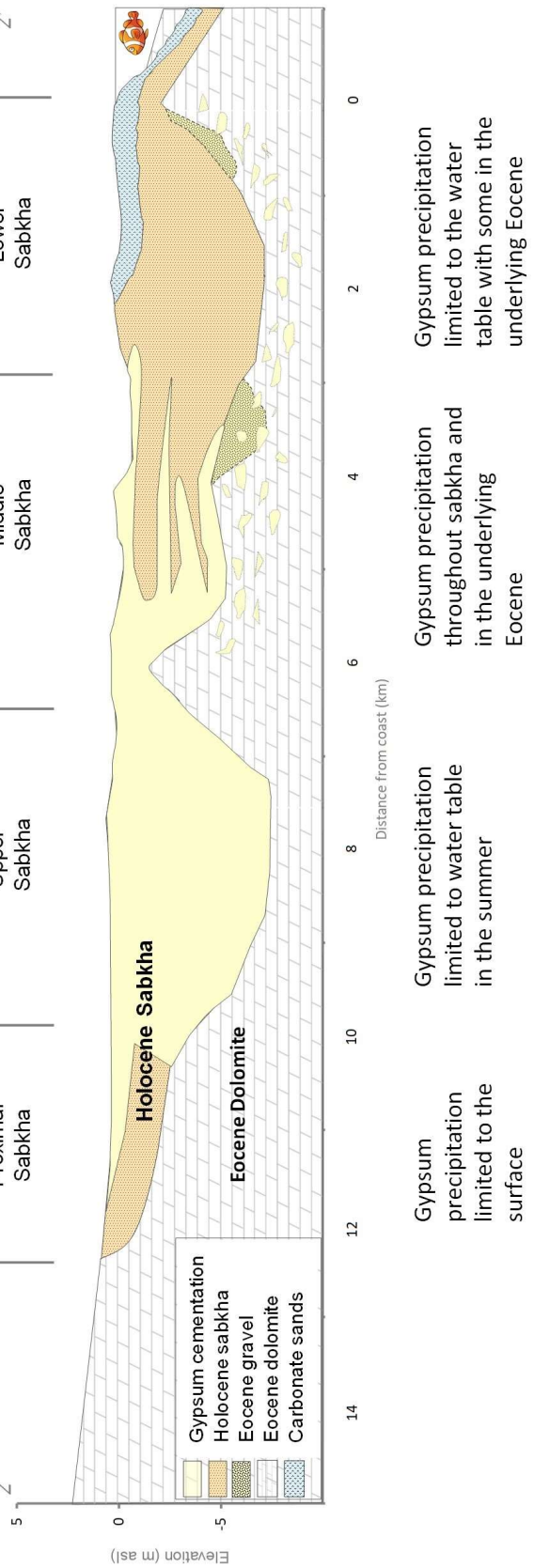

Figure 2-42.Cross-section of Mesaieed with vertical exaggeration showing distribution of diagenetic overprint by gypsum within the sabkha.

The ephemeral halite in the middle sabkha coincides with the present-day supratidal environment. Retrograde solubility of halite explains the ephemeral behaviour of the salt flat in the middle sabkha. The rate of halite flat formation and frequency of marine flooding may draw a preliminary conclusion that seawater may be the present-day source of solutes for the middle sabkha, at least within the top unsaturated zone (~0.5 m). However, this is misleading as gypsum is observed extensively cementing the subsurface, hinting that other sources of solutes are at play.

Observations of combined XRD, thin section, and cores indicate that gypsum mineral is the dominant evaporite in the proximal, upper and middle sabkha zones. Additionally, the lack of gypsum in the aeolian samples highlights that the gypsum is autochtonous. In the flowthrough pond, gypsum minerals were seen extensively cementing the sides of the pond, indicative that the source is likely $CaSO_4$-rich solutes. These combined observations discounts the classic sabkha model that the seawater (Na- and Cl-bearing) is the dominant source of solutes, while potentially highlighting that meteoric water is the main source, hinting at the greater supply of Ca and SO4 ions to the point of gypsum saturation. This can be confirmed with aqueous geochemical analysis.

The greater solubility of gypsum as compared to halite is crucial to the preservation of sabkha architecture. The extent of gypsum cementation is greatest in the upper sabkha explains the greater topography of the upper sabkha compared to other spatial zones. In the middle sabkha where the ephemeral halite is found, may explain why the middle sabkha is lower in elevation compared to the lower sabkha zone. As halite builds up at the surface of the middle sabkha over time, a rare storm and subsequent freshwater runoff can easily dissolve the halite crust causing the overall surface elevation to lower. The lower sabkha has a higher elevation than the middle sabkha which isn't typical of a low-angled ramp whereby a coastward dip is expected. This may be a combination of these events: 1) halite saturation is never reached in the lower sabkha; 2) sparse microbial mats observed in present-day, although only about few cm thin, may allow the lower sabkha to be resistant to subaqueous erosion; 3) the excess of sediment from the longshore drift may continuously feed into the lower sabkha at a sedimentation rate greater than the middle sabkha, as limited by the extent and frequency of tidal floods. Such dynamic relationship of events plays a role in the spatial preservation, or the lack thereof, of the sabkha sediments.

The gypsum cementation fabric often is observed as cross-cutting sediments, hinting at the pervasive nature of cementation which will result in reduction in porosity and permeability. The cementation nature indicates that the timeline of gypsum precipitation is likely syn-depositional to early post-depositional diagenetic events. The question of whether the gypsum distribution reflects the time since deposition or whether it is related to hydrogeochemical processes can be addressed with the hydrogeology and geochemical study of the processes (Chapter 3 and Chapter 4). The ability to predict the amout of gypsum is crucial in building a robust geologic model and hence understanding of hydrogeology and aqueous geochemistry can further consolidate our understanding in the modern system as

an analogue to ancient reservoirs. While the interplay between carbonate and silicicclastic will typically produce a mixed system of high lateral and vertical facies heterogeneity (Zeller et al., 2015), the lower reactivity of siliciclastics will have implications on the water-rock processes.

2.8.4 Impact of Sabkha on the underlying Dammam Formation

Groot (1973) and Al-Youssef (2003) assumed that the Dammam Formation underlying the sabkha is an impermeable layer and we found that with our permeability data and core observations disproves this hypothesis. Overall, the Holocene permeability for all sabkha zones were consistently lower than Dammam Formation permeability by at least 30 %. Permeabilities measured for the sabkha were in the order of 1 D (or hydraulic conductivity of 10^{-4} cm/s), in the range commonly associated with semi-confining layers (Cooper et al., 1965). Sediments with interstitial precipitation of gypsum would thus be expected to form a semi-confining layer to the Dammam. Permeabilities of about 50 mD observed within the deeper Dammam succession (30 m below surface) likely indicate unaltered dolomite, which are comparable to MoE (2006) study of deeper Dammam succession (0.2 to 50 D) and of Abu Dhabi's Dammam Formation (20-40 mD) (Alsharhan et al., 2003).

The core observations highlights that the Damman formation underlying the sabkha sediments comprises of mostly dolomite with minor clay particularly palygorskite, itself is a result of a complex multi-generational diagenesis. Palygorskite observed as common cementation clay mineral in the Dammam Formation coincides with previous study by Holaili and Al-Hajari (1997). Palygorskite, a Mg-rich clay, is typically associated to saline porewater precipitation (Warren, 2016). Processes related to subaerial exposure and erosion were observed in the cores as: (1) jointing and fracturing (2) dissolution, and (3) evaporite cementation. All three secondary processes are spatially non-uniform, resulting in aquifer characteristics that are extremely variably distributed and complexities in hydraulic continuity that are likely reflected in fluid flow pathways. Numerous irregular joints and dissolution-induced vuggy cavities of 1 to 20 cm in diameter are observed in the upper 10 m, indicating complex weathering zones.

These features were observed in the Dammam aquifer in Kuwait and other parts of the Arabian Gulf (Al-Awadi et al, 1998). This explains the higher permeabilities observed within the Dammam formation compared to the sabkha sediments. In Barr al Hikman, a two-permeability system is proposed from satellite imagery study of the lineaments (Mettraux, 2011). Lost circulation zones that is encountered in the Mesaieed Dammam Formation may be indicative of large joints or karstic features. Unfortunately, core observations could not be reconciled with lost circulation zone data due to the different sources of data from different wells.

The outcropping Dammam Formation updip shows larger-scale karstification, with dissolution vugs, and joints and fractures in the top 5 - 10 m, with permeabilities up to 340 Darcy. At the present

sea-level, such permeable pathways may have facilitated landward lateral flux of seawater in the eastern distal part of Mesaieed sabkha, potentially sourcing solutes as far inland as the middle of the sabkha. This is similar to the dual permeability system observed in the Barr al Hikman.

For the exposed Dammam Formation updip, the permeability found to be in the magnitude of 10^2 D is not uncommon for an exposed limestone that has been subjected to long periods of wet Pleistocene climate and subsequent meteoric diagenesis. For example, in the exposed Pleistocene Lucayan in the Bahamian Archipelago whereby it has been subjected to wet climate, the average permeability is 1.9×10^2 D (n = 244) (Whitaker and Smart, 1997).

When we compare just the data of the Dammam Formation underlying the sabkha itself, analysis of the permeability data and the frequency of the lost circulation zones indicates that the top 5 m of the Dammam underlying the sabkha generally has the highest permeability values. LCZ data itself is indicative of the highest weathering features such as dissolution voids and large karsts. The LCZ occurrences were cross-checked with descriptions of the core in NDP2 report (Appendix XX), which often cites 'moderate to highly weathered limestone with dissolution features and open and/or close-spaced fractures. This was supplemented by core observations on the NDP site by Jeremy Jameson and myself. This means that most of the very high permeability zones may have developed prior to sedimentation of the Holocene sabkha, possibly during the Pleistocene wet climate. The long period of exposure would have allowed recharge leading to extensive meteoric diagenesis during the wet climate Pleistocene lowstand. Whilst a karstic zone across the mixing zone is favourable for groundwater circulation and hence mixing, it may also allow a flow pathway for seawater into the mixing zone, depending on the hydraulic gradient established within the freshwater lens (Stringfield and LeGrand, 1971). Alternatively, groundwater flow along contact between sabkha and Dammam could have enhanced permeability after Holocene deposition. This may also lead to carbonate dissolution along a paleo-mixing zone (Smart et al., 1988) of the carbonate bedrock prior to dolomitization. It may also be an increase in pore-filling cementation by evaporites and clay from the middle of the sabkha downwards into the Dammam very high permeability zones.

The differences in permeability shown in the Dammam formation updip as compared to the permeability in the Dammam underlying the sabkha formation (Figure 2-34) highlights the potential impact driven by the overlying sabkha succession. The lower permeability observed within the Dammam underlying the sabkha coincides with extensive gypsum, carbonate and clay cementation as observed in core observations (Figure 2-27). In the updip Dammam Formation, gypsum and clay cementation is not observed on the outcrops. Additionally, the Dammam underlying the middle sabkha zone has a permeability of one to two orders of magnitude lesser than other sabkha zones (Figure 2-34). This is attributed to the precipitation of evaporites, clay and carbonate infilling the dissolution voids, joints, and fractures, observed in cores (Figure 2-27) and thus reducing permeabilities to as little as 0.01 Darcy. Extensive diagenetic overprint in the Dammam Formation underlying the middle sabkha appear to

contribute to the reduction of permeability by an order of two magnitude. Both the middle sabkha stratigraphy and underlying Dammam may locally form a semi-confining boundary to the underlying sub-formations, potentially inhibiting fluid flow.

Unlike the carbonate sabkha in Abu Dhabi (Sanford and Wood, 2002), siliciclastic-dominant Mesaieed sabkha highlights a relatively higher permeable medium where allowing significant lateral flow (either from the coast or updip aquifer) and vertical flow (from the surface or from the underlying Dammam Formation) to supply the mass of solutes required to precipitate the Quartenary evaporites of the coast sabkha.

2.8.1 Comparative Setting

The dominance of studies of the 3000 km² coastal sabkhas in Abu Dhabi have left an impression that most sabkhas are comprised of a carbonate host matrix, when the northeastern Arabian Gulf coastal system are siliciclastic (Warren, 2016). The dominant sedimentology in Mesaieed is detrital aeolian-derived siliciclastic sediment, with increasing carbonate content coastward, up to 60% in the lower sabkha.

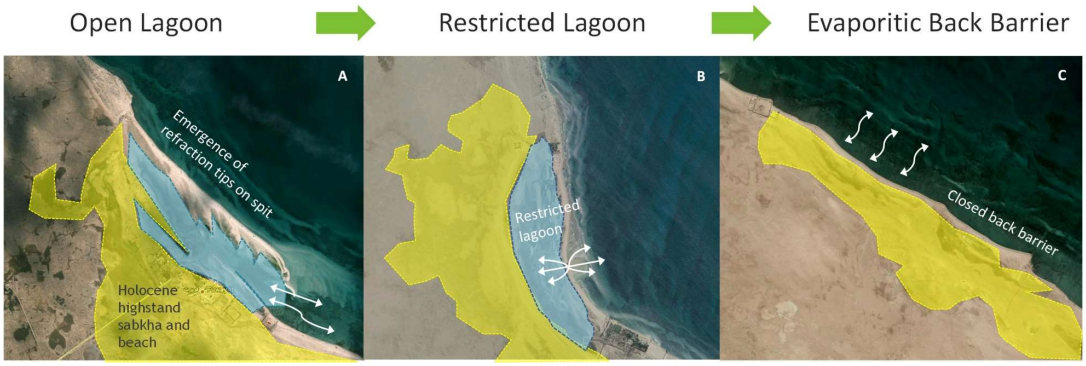

Figure 2-43. Illustration of different coastal system based on the maturity of the spits system: A) **Open lagoon** setting (Abu Dhabi and Mesaieed) where spits are emerging but there is limited barrier for marine flood and tidal influence to dilute any existing brines for potential evaporite-precipitation, (B) **Restricted lagoon** (Mesaieed) where marine influence is a function of the tidal inlets provided by incomplete spit formation, erosion of spits or breaches of the spit/barrier beach from storm events, (C) **Evaporitic back barrier** (Barr al Hikman) where the spits have completed closed the access of seawater to the beach and thus allowing evaporation-driven events to dominate the sytem (images provided by Jeremy Jameson).

Whilte both Abu Dhabi and Mesaieed are typically considered open lagoon (Figure 2-43), there are significant differences between the two coastal sabkha. Abu Dhabi's is a windward facing barrier island-protected coastline relative to the prevailing northwestern shamal winds. Mesaieed is a leeward system with limited physical barrier in the southeast. The formation of spits in Mesaieed has resulted in the progradation of the sabkha coastward, and being in the leeward position has likely resulted in the erosion of the landward parts of the sabkha, as observed in the erosional remnants. Aeolian erosion of Mesaieed, especially in the upper sabkha, keeps the water table close to the surface which is then

more susceptible to greater pore evaporation. The leeward setting allows sediments to accumulate directly onto the sabkha areas (Kendall and Skipwith, 1969) while being protected by the beach ridges formed by spits. This contrast means that the sabkha sedimentation rate are likely to be greater, more widespread and thus allowing it to span 50 times larger than Mesaieed that is on the leeward coast that Mesaieed would allow progradation rate to be greater. However, the sedimentation rate data from Qatar and Abu Dhabi (Lokier and Steuber, 2008) show that the rates are consistent.

While the only significant prior studies of the coastal sabkhas are in Abu Dhabi, the closest modern analogue to Mesaieed in terms of a leeward coastal setting with significant siliciclastics is the western sabkhas of Barr (or Bar) al Hikman. Barr al Hikman, a 34 x 40 km peninsula on the southeast Oman, receive a year-long prevailing winds from the south. The southern peninsula coastal system is recognized as a potential carbonate analogue for Middle East Cretaceous hydrocarbon reservoirs (Homewood et al., 2007).

Mettraux et al. (2011) is the only study of the four sabkhas in the peninsula and hence is limited to a reconnaissance-level study and only within 20-30 cm below the surface. The sabkha setting in Barr al Hikman is generally restricted lagoon to evaporitic back barrier (Figure 2-38), while in Mesaieed it is still an open lagoon (Figure 2-38). The western coastal sabkhas of Barr Al Hikman was observed to consist of halite polygons interbedded with wind-blown sand in the landward region, while ephemeral halite is found closer to the coast (Mettraux et al., 2011). In the near subsurface the wind-blown sediment has been deformed by gupsum nodules and crustal within the upper 10-20 cm.

In the coastward zones of Barr al Hikman sabkha, which is equivalent to Mesaieed's lower sabkha equivalent, algal mats increase in abundance towards the coast (Mettraux et al., 2011) which are largely driven by the restriction imposed by a large single spit. While Mesaieed has a small restricted lagoon on the northeast (Figure 2-22), the whole sabkha area is an open lagoon on the majority of the southeast coastline that allows marine flooding of tidal floods to reach the middle sabkha on a regular basis (Figure 2-28) and continental waters to drain back to the ocean.

2.8.2 Implications to Subsurface Characterization of Petroleum Reservoir Systems

To understand how this study can help us develop a better model of the subsurface reservoir quality for secondary or tertiary enhanced oil recovery, we can first ensure the environmental of deposition and its location relative to the prevailing wind direction and the host matrix. In the case of a mixed siliciclastic-carbonate petroleum systems that is located on the leeward coastline, Mesaieed would be a prime example to use instead of the classic sabkha model in Abu Dhabi.

The low-angled depositional slope and complex microtopography characteristic of carbonate ramps results in inherent sensitivity to even small-scale changes in relative sea-level, significantly altering the extent of exposure of the inner ramp leading to lateral migration of diagenetic zones. The

formation of diagenetic evaporites is therefore a key control in reservoir quality of arid environments, not just within the sabkha succession, but also within the underlying and the down-dip deposits through which brines can reflux and precipitate evaporites. This is especially true for similar shelf deposits that are found in Ordovician Williston Basin, San Andres, the Permian Basin in West Texas and New Mexico, and the Jurassic Gulf of Mexico. Similar ancient deposits that are analoguous to sabkha systems include the Permian Khuff, Jurassic Arab and Hith Anhydrite.

Holocene sabkha permeability is about two orders of magnitude higher than that measured in Abu Dhabi (3-10 mD) by Sanford and Wood (2002). This is reasonable as the Mesaieed sabkha matrix is predominantly siliciclastic grains which are shown to exhibit higher permeability (Ehrenberg and Nadeau, 2005) while sabkha matrices in Abu Dhabi are predominantly carbonate mud. Compared to coastal siliciclastic sands of the Holocene measured in West Bay, North of Doha (IoH, 1989), sabkha in Mesaieed ranges from 1 to 2 magnitudes lower in permeability (1-10 D) especially in the middle and lower sabkha. Low permeabilities in the range of 0.09-10 D applies to either diagenetic siliciclastic sabkha with evaporite cementing the sands (middle sabkha) or simply the primary deposition where there is high mud and silt content usually closer to the coast in the lagoon and behind spits in the lower sabkha. High permeabilities in the range of 10-20 D applies to either: (1) gypsum mush, a result of euhedral fish-tail evaporite precipitating in standing water, and/or (2) unaltered siliciclastic sand grains that have no intragranular evaporite precipitation, as seen in the upper and proximal sabkha. Primary depositional texture, diagenetic overprint and mud content are likely the main controls of permeability in the sabkha. The lower sabkha sees minor evaporite precipitation, but it contains more marine mud and lagoonal sediments and this may contribute to the lower permeability than the proximal and upper sabkha which have a coarse to medium grain aeolian sands.

In the unconventional reservoirs such as tight sands and tight carbonates, where permeabilities are in the micro-Darcy and nano-Darcy ranges, integrating subsurface characterization with this findings is evermore important for effective hydrocarbon recovery today. Driven by low profit margins in producing tight reservoirs, an understanding of a sabkha system is hence crucial in which unconventional techniques are being used to recover hydrocarbon. This thesis benefits not only to hydrocarbon recovery within the sabkha stratigraphy itself, but also the underlying limestone that is highly likely affected by the sabkha successions. This is notable in the Jurassic Arab Formation (Figure 2-42).

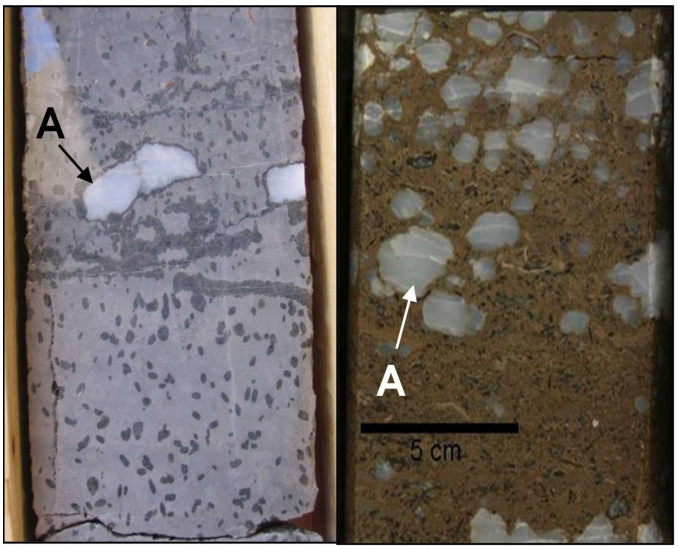

Figure 2-44. Subsurface examples of cores of carbonate with anhydrite cement (A), are shown here to occlude open marine facies in the Jurassic Arab formation. (Source: Jameson and Puls, 2013)

Additionally, our understanding of Mesaieed sabkha provides us the ability to improve geologic models of analogous subsurface reservoirs from an inter-well interpolation scale. The resolution from the high-density provided for this study in itself is one to two order of magnitude greater than any prior studies on sabkhas, thus providing a true 3-dimensional view of a costal sabkha system. Having another end-member of the coastal sabkha system that is both mixed siliciclastic-carbonate and on the leeward system makes Mesaieed a unique arid coastal system. Therefore it is crucial to develop a robust geologic model that is representative of a highly complex sabkha system, as the model will ultimately be used by reservoir engineers to simulate hydrocarbon flow, water injection and/or enhanced oil recovery using gas or water. A geologic model that is representative of the complex system, after accounting for compaction and geothermal trends, can therefore make a substantial difference in drilling a dry hole and economically producing well.

The usefulness in understanding the arid low-angle ramp deposits however comes with a caveat. This method assumes that the evolution and feedback of processes and environments through time are known, such as fluctuation in seawater composition, global eustatic levels, regional tectonic movements, and climate change. In addition, a geologic model is static in nature, whereby it represents a snapshot of the lithofacies at present-day. The limitations to this is that often times the processes such as erosion, displacement of sediment from cementation, inflated thickness from evaporite precipitation, sea-level rates is not accounted for. To build a model that is representative of the dynamic geologic events, a geological process modelling (GPM), also called stratigraphic forward modelling, will be a robust next steps. Detailed information on GPM can be referred to in Tetzlaff et al. (2014), Paterson et al., (2006), Jones et al., (2004), and Whitaker et al. (1997). Thirdly, understanding only sedimentology is inadequate for the reasons mentioned above, in which subsequent chapters will provide further insight integrating additional understanding from hydrogeology and geochemistry.

2.9 Conclusion

A Holocene-age leeward coastal sabkha with siliciclastic-dominant host sediment was studied in unprecedented detail using time-lapse satellite imagery, multi-scale permeability and lost circulation data, carbon-14 derived age dates, mineralogy, and geomorphology data. Over 150 boreholes at both the sabkha and Dammam Formation, combined with 40 sabkha shallow pits, and historic satellite imagery provided a unique opportunity to characterize the dynamic processes and the sabkha system in-detail. This is the first detailed study ever done on an arid leeward coastal system, which provides an insight of a new sabkha end-member as compared to the classic sabkha model in Abu Dhabi. Mesaieed, the 75 km^2 area of interest, consists of Dammam carbonate bedrock overlain by variably lithified Holocene sediments. The flat sabkha, with about 1:1000-1:5000 of relief, is a result of Stoke's type deflation that allows flooding of marine waters to reach up to 8 km inland on the sabkha, with residual flood waters often observed in the middle sabkha.

The formation of Mesaieed sabkha is a complex relationship between a spit system, aeolian sedimentation, sea-level fall arid environment with little rainfall, and subsequent evaporite cementation. Observations of the height of the exposed Dammam Formation updip of the sabkha, erosional remnants of both Holocene-aged deposits and ^{14}C-based younging direction of sabkha sediments towards the coastline hints at the sea-level fall in the recent history. The drop in sea-level, circa 6,000 years BP, and aeolian supply from shamal winds, combined with the interplay of wind-dominated environment of deposition and tide-dominated low energy environment, were crucial components to the forced progradation of the coastal sabkha in Mesaieed. During the middle of the Holocene highstand (~4,000 yr BP), the sabkha experienced rapid seaward progradation of aeolian siliciclastics. In recent years (<3000 yr BP), carbonate accretion in the form of spits drive the remaining back barrier deposits in the middle and lower sabkha, comprising of mixed carbonate and siliciclastic. Preservation of the sabkha is driven by a combination of extensive gypsum cementation driven by meteoric discharge, shallow water table and beach ridges.

The internal stratigraphic and diagenetic architecture of Mesaieed is clearly reflected in the dynamics of primary sedimentation and secondary evaporite formation episodes. The sabkha is characterized by a predominantly siliclastic host sediment and gypsum as the syn-depositional diagenetic evaporite, and in that their distribution is controlled by a unique combination of a leeward coastal location, an evolving spit system, and an irregular surface topography, shallow water table and a falling sea-level history. The sabkha is divided into four zones based on the combination of geomorphology, primary mineralogy and diagenetic overprint observations, which are likely the result of its proximity to the coast and the updip continental sabkha (Figure 2-44). The sabkha zones were: (1) proximal sabkha,

which is a semi-continental sabkha within upper part of valley in the Dammam Formation headland updip; (2) upper sabkha, which has extensive gypsum cementation, visible from the satellite imagery, and appears to act as a terminus between continental discharge and maximum and rare tidal flooding; (3) middle sabkha, a supratidal flat that is partially cemented by gypsum and within which ephemeral salt flat occurs, and (4) lower sabkha, which is supratidal to intertidal, with insignificant gypsum as crust and partially unprotected by beach ridges formed from a prograding spit system.

Previous study is limited to the Holocene sediments while this study attempts to understand the outcropping Dammam Formation updip and the Dammam underlying the sabkha. This study highlights the diagenetic features such as karsts and joints that will likely influence fluid flow while also highlight flow-inhibition features such as evaporite cementation, clay precipitation and possibly dolomite cements.

A similar relative to Mesaieed, the western sabkhas of Barr al Hikman would be another good modern analogue to further develop our understanding of the arid leeward coastal sabkha setting with mixed siliciclastic-carbonate host sediment (Mettraux et al., 2011). Bar al Hikman appears to represent the next geomorphology evolution for Mesaieed from a more open lagoonal setting to a more restricted evaporative environment. This new study has implications for facies and diagenetic overprint trends for similar ancient arid siliciclastic-carbonate reservoirs in terms of understanding reservoir quality in the upstream oil and gas industry. Additionally this study provides a foundation for the study of hydrology, hydrogeology and aqueous geochemistry, with focus on the provenance of diagenetic gypsum within Holocene sediments, which will be discussed in subsequent chapters in the thesis.

Table 2. Mineralogy data from a combination of XRD and petrography estimation from this study.

Well	Lat	Long	Clay	Quartz	K-Feldsp.	Plagio.	Calcite	Mg-calc	Aragonite	Dolomite	Gypsum	Bassanite	Anhydrite	Halite
Dust	N/A	N/A	0	28	4	6	35	0	0	25	2	0	0	0
Dust	N/A	N/A	0	26	3	10	31	0	0	27	1	0	0	2
B09	25.0207	51.5912	19	1	1	1	0	0	0	69	5	0	0	4
B09	25.0207	51.5912	15	1	1	0	0	0	0	78	0	0	0	5
B05	25.0284	51.5951	28	1	0	2	1	0	0	51	11	0	0	7
B19	25.0069	51.6184	36	1	1	4	0	0	0	48	8	0	0	2
P8	25.0301	51.5759	0	18	2	3	5	4	12	8	46	0	0	2
P8	25.0301	51.5759	0	48	4	5	12	1	26	4	0	0	0	0
M1	25.0243	51.5898	0	14	3	2	2	0	0	4	67	0	6	3
M1	25.0243	51.5898	0	56	6	5	20	0	0	8	2	0	0	4
M1	25.0243	51.5898	0	52	6	6	22	0	0	4	0	0	0	11
M1	25.0243	51.5898	0	53	7	7	19	0	0	7	0	0	0	7
M1	25.0243	51.5898	0	6	0	1	13	0	4	57	2	0	0	16
M1	25.0243	51.5898	0	68	3	6	18	0	0	4	0	0	0	1
M1	25.0243	51.5898	0	57	9	8	18	0	0	5	0	0	0	4
M1	25.0243	51.5898	0	45	6	13	25	0	5	5	0	0	0	2
M1	25.0243	51.5898	0	48	6	10	24	0	0	4	0	0	0	8
M1	25.0243	51.5898	0	60	9	5	17	0	5	2	0	0	0	2
M1	25.0243	51.5898	0	48	11	13	22	0	0	4	0	0	0	2
M1	25.0243	51.5898	0	60	5	9	14	0	0	10	0	0	0	2
M1	25.0243	51.5898	0	56	8	9	20	0	0	5	0	0	0	3
M1	25.0243	51.5898	0	53	5	6	19	0	11	5	0	0	0	2
M1	25.0243	51.5898	0	39	7	10	22	0	11	4	1	0	0	5
M1	25.0243	51.5898	0	7	1	1	16	17	39	11	0	0	0	8
M1	25.0243	51.5898	0	9	0	2	20	19	27	13	0	0	0	11
M1	25.0243	51.5898	0	48	5	9	18	5	10	4	0	0	0	2
M1	25.0243	51.5898	0	35	2	5	16	6	30	3	0	0	0	2
M1	25.0243	51.5898	0	10	3	7	15	17	26	11	0	0	0	10
M1	25.0243	51.5898	0	10	6	3	13	14	17	19	11	0	0	7
M1	25.0243	51.5898	0	12	3	5	14	11	5	27	18	0	0	4
M1	25.0243	51.5898	0	11	1	2	6	0	4	30	43	0	0	2
M1	25.0243	51.5898	0	54	6	12	15	0	0	10	0	0	0	3
M1	25.0243	51.5898	0	7	1	1	7	0	4	23	54	0	0	3
M1	25.0243	51.5898	0	57	9	13	14	0	0	5	0	0	0	1
M1	25.0243	51.5898	0	34	3	6	3	0	0	44	5	0	0	5
M1	25.0243	51.5898	4	3	2	0	1	0	0	85	2	0	0	4
M1	25.0243	51.5898	0	17	0	0	0	0	0	83	0	0	0	0
M1	25.0243	51.5898	0	18	0	0	0	0	0	82	0	0	0	0
P13	25.0225	51.5791	0	37	6	5	10	0	1	8	25	1	0	7
P13	25.0225	51.5791	0	62	6	5	16	0	0	5	1	0	0	5
P13	25.0225	51.5791	0	42	6	5	18	0	0	9	15	0	0	6
P13	25.0225	51.5791	0	68	4	6	14	0	0	5	0	0	0	4
P13	25.0225	51.5791	5	49	5	3	12	0	0	6	20	0	0	0
P16	25.0013	51.5822	5	35	5	5	8	0	0	3	18	0	9	11
P16	25.0013	51.5822	4	30	7	4	10	0	0	2	25	0	5	13
P16	25.0013	51.5822	6	40	9	7	7	0	0	4	11	0	11	5
P28	25.0013	51.5822	0	48	7	10	12	0	5	11	1	0	0	6
P28	25.0013	51.5822	7	19	7	4	32	0	13	5	4	0	0	9
P28	25.0013	51.5822	1	13	4	2	40	0	20	4	4	0	0	12
P28	25.0013	51.5822	8	9	2	2	38	0	17	3	6	0	0	15
P28	25.0013	51.5822	0	20	6	4	34	0	18	9	0	0	0	10
P28	25.0013	51.5822	4	12	6	3	36	0	18	9	0	0	0	13
P28	25.0013	51.5822	3	33	6	5	22	0	15	8	0	0	0	8
P28	25.0013	51.5822	4	11	5	5	33	0	18	8	1	0	0	15
P28	25.0013	51.5822	7	12	4	3	34	0	19	8	1	0	0	13
P28	25.0013	51.5822	0	41	2	2	18	0	10	6	20	0	0	1
P28	25.0013	51.5822	0	42	2	3	10	12	24	4	1	0	0	2
P22	25.0207	51.5765	0	41	9	11	17	0	0	11	0	0	0	10
P23	25.0214	51.5885	15	39	4	3	6	0	0	7	14	3	0	10
P23	25.0214	51.5885	0	61	6	8	20	0	0	3	0	0	0	2
P24	25.0284	51.5932	5	50	7	6	20	0	0	7	0	0	0	4
P24	25.0284	51.5932	6	53	8	11	14	0	0	6	0	0	0	1
P24	25.0284	51.5932	0	24	3	4	15	12	0	3	26	0	0	14
P1	25.0537	51.5926	0	38	5	7	7	0	0	24	7	0	0	13
P1	25.0537	51.5926	5	44	5	7	3	0	0	3	23	0	0	10
P1	25.0537	51.5926	0	17	3	5	13	9	0	3	41	0	0	9
M2	25.0802	51.5658	0	14	2	3	4	0	0	6	71	0	0	1
M2	25.0802	51.5658	0	11	1	3	4	0	0	4	76	0	0	1
M2	25.0802	51.5658	0	3	0	1	1	0	0	0	95	0	0	0

M2	25.0802	51.5658	0	77	4	4	13	0	0	1	0	0	0	0
M2	25.0802	51.5658	0	81	5	4	9	0	0	1	0	0	0	0
M2	25.0802	51.5658	3	54	8	14	18	0	0	2	1	0	0	1
M2	25.0802	51.5658	3	56	7	14	18	0	0	2	0	0	0	1
M2	25.0802	51.5658	4	52	9	19	15	0	0	1	0	0	0	0
M2	25.0802	51.5658	4	43	5	15	27	0	0	4	0	0	0	1
M2	25.0802	51.5658	4	49	5	14	23	0	0	3	0	0	0	1
M2	25.0802	51.5658	4	57	7	14	16	0	0	1	0	0	0	1
M2	25.0802	51.5658	2	55	6	18	16	0	0	2	1	0	0	1
M2	25.0802	51.5658	0	67	6	9	14	0	0	3	1	0	0	0
M2	25.0802	51.5658	3	50	8	20	18	0	0	1	0	0	0	0
M2	25.0802	51.5658	4	52	7	18	17	0	0	2	0	0	0	0
M2	25.0802	51.5658	1	68	7	9	14	0	0	2	0	0	0	0
M2	25.0802	51.5658	3	57	4	9	14	0	0	10	3	0	0	0
M2	25.0802	51.5658	7	16	1	1	1	0	0	73	0	0	0	1
M3	25.0724	51.5748	0	21	4	5	6	0	0	9	35	0	15	5
M3	25.0724	51.5748	2	63	6	12	14	0	0	3	0	0	0	0
M3	25.0724	51.5748	8	33	5	8	10	0	0	35	0	0	0	1
M3	25.0724	51.5748	4	12	2	2	2	0	0	77	0	0	0	1
P12	25.0310	51.5681	0	38	3	2	5	0	0	12	37	0	0	3
P12	25.0310	51.5681	0	47	5	6	18	0	3	19	0	0	0	2
P12	25.0310	51.5681	0	36	3	4	9	0	0	17	27	0	0	4
P12	25.0310	51.5681	3	52	6	7	17	0	3	0	5	0	0	7
P12	25.0310	51.5681	0	58	6	6	18	0	0	4	1	0	0	6
P12	25.0310	51.5681	0	48	4	2	10	0	0	3	30	1	0	1
P25	25.0431	51.5783	0	61	3	2	6	0	0	8	18	0	0	1
P26	25.0347	51.5915	0	23	0	0	8	0	0	3	12	8	0	47
P26	25.0410	51.5870	0	42	4	5	11	0	0	22	12	0	0	4
P26	25.0410	51.5870	0	16	3	3	14	10	0	3	38	0	0	12
P26	25.0410	51.5870	0	52	2	3	13	2	0	5	23	0	0	1
P27	25.0329	51.5866	0	31	2	4	6	0	0	8	36	0	0	14
P27	25.0329	51.5866	0	35	3	4	8	0	4	30	9	0	0	7
P27	25.0329	51.5866	0	46	5	6	12	0	0	4	24	0	0	4
P28	25.0329	51.5866	0	45	5	4	10	4	0	5	21	0	0	6
P17	24.9955	51.5865	0	32	4	6	20	0	8	9	18	0	0	3
P17	24.9955	51.5865	4	34	5	8	16	0	23	7	2	0	0	1
P17	24.9955	51.5865	0	24	7	4	34	0	19	3	6	0	0	3
P17	24.9955	51.5865	0	30	5	5	26	0	24	5	2	0	0	3
P17	24.9955	51.5865	0	16	4	4	26	0	39	8	0	0	0	4
P10	25.0305	51.5709	0	37	8	2	6	0	0	1	43	0	0	3
P11	25.0310	51.5681	5	15	3	6	4	0	0	8	53	1	0	5
P11	25.0310	51.5681	3	42	10	8	9	0	0	4	16	0	0	8
P11	25.0310	51.5681	4	35	4	8	4	0	0	8	30	0	0	7
P11	25.0310	51.5681	4	36	9	8	7	0	0	4	25	0	0	7
P11	25.0310	51.5681	0	27	4	2	11	0	4	14	35	0	0	3
P11	25.0310	51.5681	0	44	7	4	0	0	0	13	29	0	0	3
P14	25.0248	51.5747	7	35	5	5	6	0	0	3	38	0	0	2
P14	25.0248	51.5747	0	45	5	4	8	0	0	4	31	0	0	3
P4	25.0550	51.5719	0	37	2	5	8	5	0	9	32	0	0	2
P4	25.0550	51.5719	0	34	0	0	4	0	0	7	51	4	0	1
P19	25.0569	51.5722	0	22	2	2	2	0	0	24	10	0	10	28
P19	25.0569	51.5722	0	30	4	5	6	0	0	6	47	0	0	3
P19	25.0569	51.5722	0	45	4	7	11	0	0	5	25	0	0	3
P21	25.0252	51.5764	0	50	4	5	7	0	0	4	30	0	0	1
P2	25.0885	51.5476	0	20	2	3	11	9	0	7	34	0	0	14
P3	25.0628	51.5639	0	10	0	0	4	3	0	7	69	0	0	8
P3	25.0628	51.5639	0	42	4	4	8	0	0	10	22	0	0	9
P5	25.0539	51.5548	0	17	0	0	4	4	12	30	27	0	0	6
P5	25.0539	51.5548	0	42	4	5	7	0	0	3	36	2	0	1
P6	25.0772	51.5710	0	43	4	6	4	0	0	11	29	0	0	3
P7	25.0515	51.5690	0	24	3	4	6	2	0	14	46	0	0	2
P7	25.0515	51.5690	0	32	2	4	12	9	0	9	25	0	0	6

Table 3. Calibrated radiocarbon ^{14}C age ranges (2 σ) dataset using CALIB (Stuiver and Reimer, 1993) to 2 sigma employing a marine calibration curve and a regional reservoir age correction (ΔR) of 180 ±53 derived from east of Qatar (Hughen et al., 2004; Lokier et al., 2015).

ID	Distance to Coast	Stratigraphy	Latitude	Longitude	Elevation (masl)	Age Date	Error	Calibrated Range	Median Probability
L3-2	0.1	Holocene	25.001	51.6208	-6.36	5710	40	6408 - 6570	6497
L3-3	0.1	Holocene	25.001	51.6208	-9.86	7920	50	8604 - 8814	8760
L3-1	0.2	Holocene	25.001	51.6208	-2.67	4640	40	5299 - 5470	5404
Mes-PL		Pleistocene			2	35040	310		
M5-1	6	Holocene	25.0639	51.6005	0.25	6650	50	7437 - 7591	7629
M5-2	6	Holocene	25.0639	51.6005	-1.1	6490	50	7291 - 7490	7393
L4	1.26	Holocene	25.0052	51.6116	0.7	2090	30	1992 - 2142	2062
U5-PL	7.41	Pleistocene	25.056	51.5827	2	24920	160		
M7	2.77	Holocene	25.0154	51.5984	1.5	3280	30	3447 - 3577	3510
U6-PL		Pleistocene	25.0425	51.5706	2.2	26260	210		
L4	0	Holocene	25.001	51.6208	0.2	1170	40	486-670	579
L4	0	Holocene	25.001	51.6208	0.05	1170	40	686-890	788
U4-PL	9.3	Pleistocene	25.0617	51.5572	2	44720	1400		
L5	2.5	Holocene	25.0128	51.6012	-4.5	6500	30	7410 - 7471	7424
U1-Gyp	9.1	Gypsum	25.0562	51.5551	2	3280	40	3441 - 3593	3510
M1-1	4	Holocene	25.024	51.5901	2.1	4050	40	4421 - 462	4529
M1-2	4	Holocene	25.024	51.5901	-1.2	5130	40	5844 - 5944	5879
M1-3	4	Holocene	25.024	51.5901	-0.4	4320	40	4841 - 4890	4890
M1-4	4	Holocene	25.024	51.5901	-1.5	4210	40	3853 - 4243	4043.5
M1-4\5	4	Holocene	25.024	51.5901	-4.9	5290	50	5299 - 5257	
M3-1	2.53	Holocene	25.0192	51.6063	1	3330	30	3477 - 3637	3566
M3-2	2.53	Holocene	25.0192	51.6063	-2	4230	30	4806 - 4856	4821
L1-2	0.43	Holocene	25.0158	51.6229	-2.7	4980	30	5641 - 5752	5700
L1-1		Holocene	25.0158	51.6229	0	1840	30	1708 - 1835	1776
L2	2.1	Holocene	25.0107	51.6015	2.5	3010	30	3106 - 3258	3200
M4-1	3.72	Holocene	25.0315	51.6011	0	4690	30	5320 - 5424	5396
M12-2	4.89	Holocene	25.0262	51.5796	-2.6	8480	50	9431 - 9541	9495
M12-1	4.89	Holocene	25.0262	51.5796	0.1	4830	30	5476 - 5612	5581
M16-1	3.73	Holocene	25.0254	51.5981	0.5	4110	30	4523 - 4711	4632
M16-2	3.73	Holocene	25.0254	51.5981	0.25	4280	30	4822 - 4879	4849
M16-2B	3.73	Holocene	25.0254	51.5981	0.25	4240	40	4686-4868	4818
M16-3	3.73	Holocene	25.0254	51.5981	1.25	4040	30	4423-4581	4500
M17-2	0	Spit	25.027	51.6094	1.3	4360	40	4849 - 4986	4928
M17-1	5.11	Holocene	25.0227	51.574	1.5	4520	40	5046 - 5205	5162
M27	4.18	Holocene	25.0329	51.5866	-2.3	6120	40	6902 - 7157	7005
M8	5.47	Holocene	25.0301	51.5759	1.2	4880	40	5582 - 5664	5620
Spit-1	0	Spit	25.0524	51.612	2.8	3010	30	3106 - 3258	3200
U3-Gyp	9.5	Gypsum	25.0705	51.5701	2.5	3050	30	3174 - 3350	3262
Spit 2	0	Spit	25.0771	51.6113	2.7	5670	50	6316-6566	6454
U2	6.16	Holocene	25.0372	51.574	3.3	5000	40	5644-5892	5731
M2	4.35	Holocene	25.0301	51.5942	-1.7	7360	40	7510-7803	7648
M2	4.35	Holocene	25.0301	51.5942	-0.1	4550	40	5046 - 5205	5162
M6-1	5.52	Holocene	25.028	51.5742	-0.1	5480	50	6190 - 6354	6283
U1-1	9	Holocene	25.0562	51.5563	2.3	5810	60	5867 - 6225	6036
P11	6.4	Holocene	25.042	51.5728	0.9	5080	40	4962-5354	5180

Table 4. Field-scale data of permeability (in unit Darcy), depth of first occurrence of loss circulation zone (abbreviated as LCZ), elevation of the well screen in which the field-scale permeability is conducted. The dataset is categorized into geospatial zone (i.e. Updip = Outcropping Dammam updip of sabkha) and the stratigraphy succession (D = Upper Dammam, S = Sabkha = Lower D = Lower Dammam, OS = Offshore).

ID_1	Sabkha Zone	Stratigra-phy	Latitude	Longitude	Per-mea-bility (D)	Eleva-tion of screen (m asl)	LCZ stra-tigra-phy	LCZ depth	LCZ from Dammam
G01	Lower	Lower D	25.010511	51.604435	2.0	-16.78	E	-7.80	1.5
G10	Lower	Lower D	24.995535	51.586489	23.0	-16.94			
G04	Middle	Lower D	25.030874	51.602111	65.0	-16.54			
G07	Middle	Lower D	25.038922	51.579008	9.0	-17.76	E	-4.50	0.30
G09	Middle	Lower D	25.013062	51.588275	1.5	-17.09			
G14	Middle	Lower D	25.011884	51.567942	2.0	-17.27	E	-5.27	5.5
G20	Middle	Lower D	25.037329	51.594987	50.0	-13.02			
W7d	Updip	Lower D	25.102133	51.556667	0.1	-33.23			
G03	Lower	D	25.021192	51.610799	9.0	-7.06			
G05	Lower	D	25.040193	51.608046	2.5	-4.61			
G28b	Lower	D	25.064504	51.604803	110.0	-7.79			
B101	Lower	D	25.033060	51.611770	15.1				
B118	Lower	D	25.009220	51.615140	4.8				
G28	Lower	D	25.064504	51.604803	100.0	-7.79			
G30	Lower	D	25.074782	51.602793	16.0	-7.73			
A11	Lower	D	25.004610	51.610913			E	-7.90	0.1
A12	Lower	D	24.995764	51.610913			E	-5.38	1.0
A14	Lower	D	25.015933	51.620210			E	-5.79	0.5
A16	Lower	D	25.009186	51.624824			H	-1.52	-2.4
A17	Lower	D	25.020482	51.642571			E	-5.10	1.2
A101	Lower	D	25.033063	51.611775	25.0	-2.00	E	-4.70	2.1
A108	Lower	D	25.024902	51.608460	3.2	-8.60	E	-9.17	2.85
A117	Lower	D	25.018748	51.627293			E	-7.99	4.2
A118	Lower	D	25.009222	51.615136	9.4	-13.80	H	-1.42	-3.8
A121	Lower	D	25.020928	51.631773			E	-8.40	3.9
G06	Middle	D	25.040110	51.591141	16.0	-7.18			
G08	Middle	D	25.024937	51.579591	4.0	-8.04			
G22	Middle	D	25.046399	51.592349	0.4	-8.00			
G27	Middle	D	25.063714	51.599299	2.0	-7.10	E	-7.10	3.0
G29	Middle	D	25.056921	51.572203	13.0	-7.35			
G29b	Middle	D	25.056921	51.572203	18.0	-7.35			
Z03	Middle	D	25.058189	51.588936			E	-8.75	11.5
Z04	Middle	D	25.058792	51.589730			E	-10.75	11.5
Z05	Middle	D	25.059548	51.587086			E	-7.00	11.5
G25	Middle	D	25.060220	51.588932		-11.84	E	-4	8.5
B105	Middle	D	25.028380	51.595120	0.4				
B106	Middle	D	25.025740	51.584320	0.4				
B108	Middle	D	25.024900	51.608460	1.7				
B021	Middle	D	25° 0'25.06"	51°36'10.80"	0.0				
G15	Middle	D	25.039816	51.555536		-14.14	E	2.86	6.5
A01	Middle	D	25.038495	51.595235			E	-7.81	2.0
A02	Middle	D	25.033961	51.599650			E	-11.17	4.5
A03	Middle	D	25.031156	51.588158			H	-1.19	-3.8
A04	Middle	D	25.023499	51.602719			E	-5.66	0.5
A05	Middle	D	25.022097	51.596978	3.1		E	-13.45	8.2
A102	Middle	D	25.035363	51.605381			E	-8.22	2.0
A103	Middle	D	25.032558	51.593899			E	-6.56	0.1
A105	Middle	D	25.028376	51.595125	0.5	-4.50	E	-9.62	4.7
A107	Middle	D	25.023602	51.611745			E	-6.33	1.6
A111	Middle	D	25.013183	51.588005			H	-7.60	-7.1
122	Offshore	OS	25.016189	51.637751			E	-9.16	3.5
123	Offshore	OS	25.023273	51.651497			H	-1.55	-2.3
132	Offshore	OS	25.026936	51.655087			P	-4.40	-2.8
124	Offshore	OS	25.019851	51.657529			P	-4.30	-0.1
130	Offshore	OS	25.013161	51.629508			E	-11.20	3.4
133	Offshore	OS	25.041887	51.681538			H	-9.75	-8.3
134	Offshore	OS	25.030704	51.677850			E	-19.70	1.3
M2E	Proximal	D	25.080194	51.565814	57.0	-5.40			
W6	Proximal	D	25.085683	51.567767	74.0	-3.00			
W9	Updip	D	25° 7'30.12"	51°31'28.98"	0.7				
Gwa	Updip	D	25.014405	51.610282	14.0	-3.50			
GWb	Updip	D	25.014405	51.610282	2.6	-2.50			
M1E	Updip	D	25.097403	51.543481	68.0	-2.00			
W1	Updip	D	25.095767	51.541517	10.0	-2.50			
W2	Updip	D	25.099050	51.550767	23.0	-1.50			

W4	Updip	D	25.112217	51.525417	8.0	1.00			
W5	Updip	D	25.105800	51.559033	8.0				
W7m	Updip	D	25.102133	51.556667	36.0	-14.24			
W7s	Updip	D	25.102133	51.556667	89.0	-1.73			
M3Es	Upper	D	25.072398	51.574813	10.0	-2.37			
BH1	Upper	D	25.100800	51.579950	100.0				
M3ES	Upper	D	25.072443	51.574823	18.0	-7.27			
MS3ED	Upper	D	25.072443	51.574823	0.5	-9.27			
G31	Upper	D	25.073283	51.578009	11.0	-9.38	E	-1.62	0.1
24G	Updip	E-Coast	25.055172	51.589620	36.0	-4.85			
26G	Updip	E-Coast	25.062428	51.593864	85.0	-12.90	B	-1.8	0.1
1Z	Updip	E-Coast	25.058595	51.588808	250.0				
2Z	Updip	E-Coast	25.058551	51.588570	350.0		E	-4.75	11.5
G32	Updip	E-Coast	25.095601	51.595016	370.0	-5.42	E	4.08	0.1
G33	Updip	E-Coast	25.111951	51.608393	130.0	-7.82	E	-0.82	0.1
G11	Lower	S	24.990431	51.602114	0.5	-7.50			
A15	Lower	S	25.013105	51.624421	20.0	-2.00	E	-11.92	8.2
A09	Lower	S	25.006782	51.605856	19.0	-3.00			
A009	Lower	S	25.006901	51.615283	9.6				
B106	Middle	S			0.4				
G13	Middle	S	25.001323	51.582177	0.8	-7.50			
A05	Middle	S			3.1				
MP5/MS2	Proximal	S	25.080194	51.565814	25.0	0.45			
M2H	Proximal	S	25.080194	51.565814	13.0	-1.02			
M2HS	Proximal	S	25.080194	51.565814	18.0	0.08			
MDD7	Middle	S	25.051475	51.569028	10.0	0.37			
JP	Upper	S	25.053933	51.554750	2.7	0.18			
J06	Upper	S	25.067367	51.572333	0.3	1.75			
MD2	Upper	S	25.073378	51.562425	0.2	0.50			

3 Hydrology of Mesaieed Sabkha

Author Contributions: Time-series groundwater monitoring, water level, specific conductivity, local tide, and atmospheric pressure data for Mesaieed was collected by author with field assistance from Osa Ooi and Huw Pullin (UoB). Co-author Fiona Whitaker critically reviewed and provided direction during the progress of this study. Climate data (excluding tide data and atmospheric pressure) was provided by M. Fatima (AECOM). SEC and water level data for the middle and lower sabkha were provided by Anthony Watts (DAR). Jeremy Jameson reviewed the manuscript and suggested improvements. Didi Ooi Sher Mey is the lead author of this chapter and is responsible for the data mining, data collection, analysis and interpretation, subject to the above caveats. All figures were created solely by the author unless specified. Didi Ooi Sher is the lead author of this chapter and is responsible for the data mining, data collection, analysis and interpretation, subject to the above caveats. All figures were created solely by the author unless specified.

16,496 words

3.1 Introduction

The hydrology of arid systems, especially coastal sabkhas, is complex and poorly understood. A holistic and quantitative understanding is crucial to understand the mobility of solutes and associated water-rock interaction. A quantitative understanding of sabkha hydrology is important, not just for resource management, but also as an analogue to understanding ancient reservoirs.

The unique position of a sabkha allows a magnification of the magnitude of hydrological, hydrogeological and geochemical processes often not observed in deeper aquifers or groundwater systems. The position of Mesaieed sabkha between continental groundwater and seawater, reflects a possible commingling of two very different water bodies. Continental groundwater is generally less dense than seawater and consists of fresh to brackish water. The coastal sabkha can act as a zone of recharge and at other times a zone of discharge (Yechieli and Wood, 2002). Solutes may additionally be sourced from seawater, either introduced during episodic surface inundation or via subsurface flow. Because of this complexity, the hydrology of a coastal sabkha can be highly dynamic at a range of timescales.

Sabkha hydrology study is limited to those in Abu Dhabi (Sanford and Wood, 2001 and references) where the source of fluids is debatable. Several models for the Abu Dhabi sabkha were proposed (Figure 3-1) – evaporative "pumping", seawater inundation, and ascending brine. Many authors consider seawater to be the dominant source of solutes, either via seawater flooding of the sabkha surface (Kinsman, 1969; Butler, 1969; Patterson and Kinsman, 1977) or via evaporative-pumping of saline groundwaters (Hsü and Siegenthaler, 1969; Hsü and Schneider, 1973; Möller et al., 1990). None of these conceptual models were constrained by quantitative data characteristics of the hydrogeologic system, allowing fluid and thus solute fluxes to be budgeted (Wood et al, 2002; Warren, 2016). That study was limited and did not consider the proximal sabkha and the outcropping Dammam Formation aquifer.

In addition, older studies suggest that there are no solutes sourced from the continental updip groundwater (Patterson and Kinsman, 1977; McKenzie et al., 1980; Hardie, 1987), or they are an insignificant input to the system (Sanford and Wood, 2001). Sanford and Wood et al (2001) also assumed that within the proximal/upper sabkha the hydrology, and hence solute distribution, can be represented by studies of the lower sabkha. Previous workers who studied the aqueous geochemistry of sabkhas paid little attention to the geochemical nature of the input waters and trace ions to capture the processes occurring within the sabkhas system. A notable exception is Wood et al. (2003) and Sanford and Wood (2001) in which they found that solutes in the Abu Dhabi sabkha are found to be sourced by >95% from ascending brines by the underlying formation and that the system is vertically mixed.

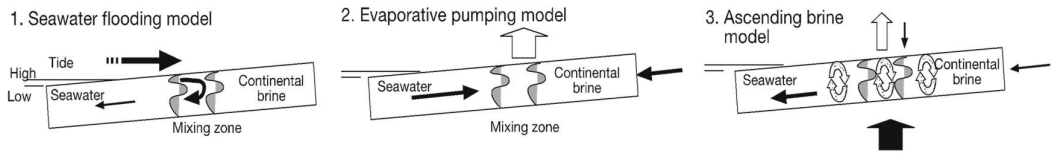

Figure 3-1. Hydrology models proposed by previous workers: (1) Seawater flooding model proposed by Kinsman (1969), (2) Evaporative pumping model proposed by Hsu and Siegenthaler (1969), (3) Ascending brine model proposed by Sanford and Wood (2001). Size of arrows indicate relative magnitude of fluxes. Figures modified from Warren (2016).

The focus area of this work is the coastal sabkha Mesaieed, a leeward coast east of Qatar. The hydrogeological formation consists of Paleocene Umm Er Rhaduma Formation, Eocene-aged Rus Formation, Eocene-aged Dammam Formation, and overlain uncomfortably by Pleistocene-Holocene sediments (Llyod et al., 1987). In a few parts of Qatar, Miocene Hofuf and Dam formations are seen overlying the Dammam Formation. Mesaieed is Holocene-aged sediment and is located proximal to the Southern Groundwater Basin province, where anhydrite and gypsum layers within the underlying Rus Formation are the thickest compared to the Southern Groundwater Basin (Eccleston et al., 1981).

The foundations of fluid fluxes in saline systems are very well summarized in Yechieli and Wood (2001). Environmental factors, such as weather and climate, are shown to affect the proportions of different fluid inputs (Tyler et al., 2006). Preliminary hydrological studies have previously been undertaken for Umm Said, the Greater Mesaieed area (Groot, 1973). That study was limited to 6 sites and only used the water table levels to understand flow without correcting for salinity. Groot (1973) found the water level varies very little and it was reported to be approximately 0.5 m below the sabkha surface in all parts of the sabkha, with minor decline from the coast towards the exposed Dammam Formation up-dip.

Preliminary analysis of the hydrogeology was completed in a previous co-authored extended abstract (Whitaker et al., 2013) with a limited dataset that was later found to be potentially affected by anthropogenic activities at the Hamad Ports. The conceptual hydrogeology model used a partially-corrected freshwater head from Fetter (2001) that did not reflect differences in density and depth (Post et al., 2007, 2013). Whitaker et al. (2013) suggests that the low groundwater head in the middle sabkha zone is due to a relatively permeable pathway provided by a basal transgressive lag, an average of 1m thick, a brecciated Dammam Formation layer in between the sabkha and Dammam. From Chapter 3, a detailed investigation at a 10-15m trenched area in Mesaieed showed the eroded Dammam Formation pebbly layer is cemented by a mixture of gypsum and dolomite, and groundwater was observed to flow either over or under this layer.

The aim of this study is to improve the fundamental understanding of the hydrogeology of the coastal sabkha systems developed on a leeward shore, where an input of aeolian siliciclastic sediment is significant. By combining temporal and spatial understanding, using new observations and analyses

of existing data, we can build a viable conceptual hydrogeologic model to yield an understanding of the sources and pathways of fluid flow. This provides a foundation for evaluation of the sources of solutes and implications for water-rock interaction evaluated in Chapter 4. This study will highlight contrasts with the classic Abu Dhabi sabkha model and Barr-al-Hikman, and thus, illustrates the broader variability of modern analogues than is generally appreciated.

3.1.1 Chapter Objectives and Structure

The goals of this chapter are to understand the hydrodynamics of Mesaieed sabkha aquifer, the Dammam Formation aquifer and to identify the full cycle fluid flow from source-to-sink. Chapter 3 presents fresh insights of using key components of Mesaieed's hydrogeological system, based on the analysis of a new dataset which is used to evaluate marine flooding and continental discharge, and how this is moderated by aquifer permeability (see chapter 2.7) to control groundwater flow and salinity. Unlike many prior studies, observations are extend beyond sabkha to include the hydraulically-connecting underlying and surrounding outcropping Dammam formation aquifer up-dip of the sabkha. The study is a result of detailed borehole fluid geophysical investigations, new observations, data collection and analyses, supplemented with unpublished historical data.

The chapter also examines the climate of Qatar in detail, providing a foundation for understanding the extent of seasonal variability in this arid system and the impact on sources and sinks of fluids and solutes. This will be important in refining the hydrological budget for Mesaieed and accurately specifying input fluxes in our sabkha model.

Analysis of the dataset is organised with consideration of the sabkha and Dammam Formation aquifers, considering firstly vertically and lateral variation, and then temporal effects. Such a multi-dimensional perspective will provide a broader understanding of the hydrological processes at play at any one point in space and time than has previously been attempted (Groot, 1973; Al-Youssef, 2001).

Analyses will be further divided based on the following sedimentological facies and hydrogeological zones (Figure 3-2): the Dammam aquifer up-dip of the sabkha (EU) and underlying the sabkha (sampled using groundwater monitoring wells), and the sabkha water table (sampled by hand-dug pits) and the sabkha phreatic zone (sampled by groundwater monitoring wells drilled with 3m long screens).

Preliminary analyses of specific electrical conductivity (SEC) and groundwater head indicated a systematic trend oriented along the direction of the progradation of the sabkha (to the southeast), reflected in the cross-section transect (Figure 3-2). Based on these trends we define four regions of the sabkha; furthest inland, the proximal which is partially isolated from the upper sabkha, which is separated from the middle sabkha by a Pleistocene sill, which also defines the upper limit of a salt flat, and the distal lower sabkha closest to the coast.

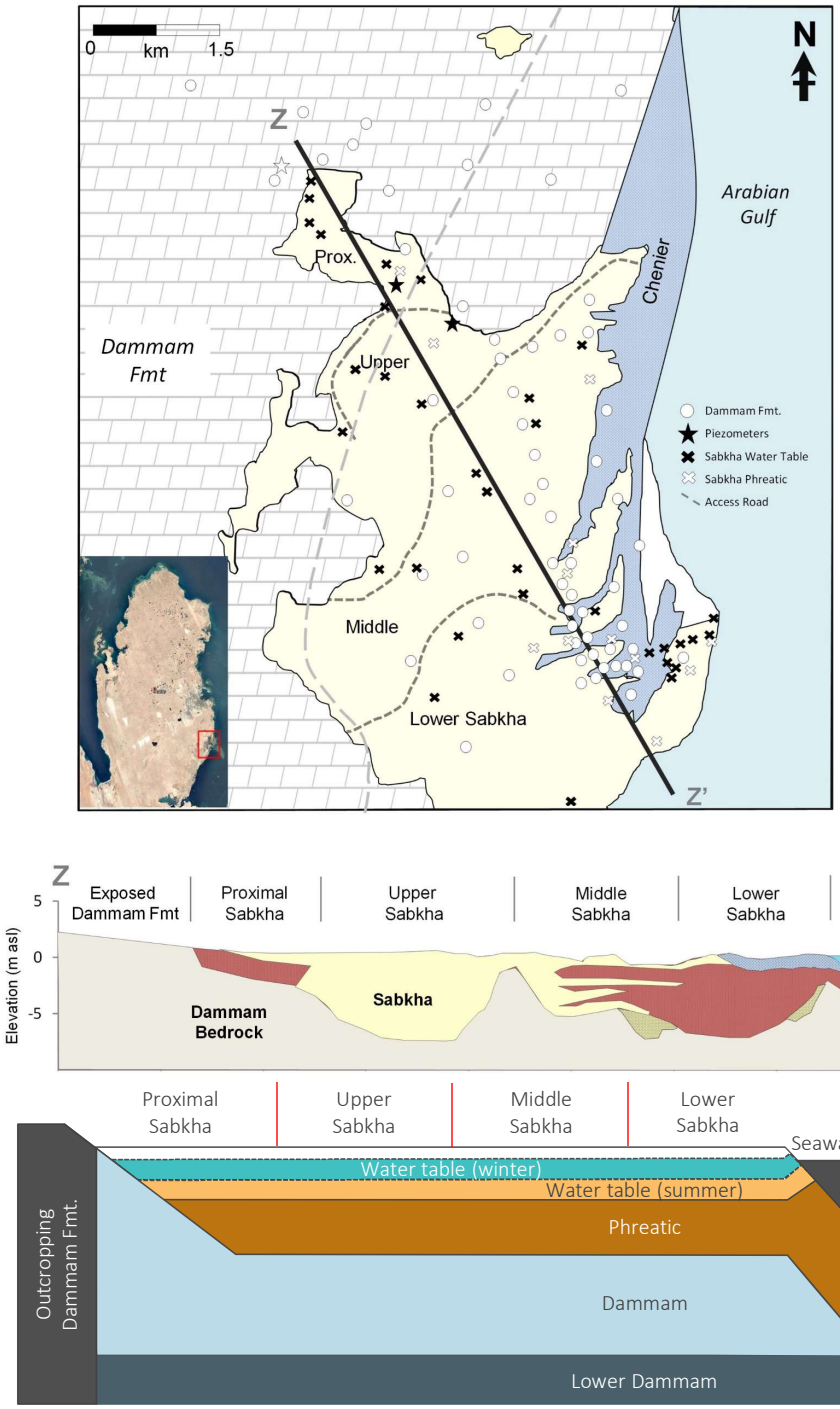

Figure 3-2. Map plan of spatial zonation subdivided by dashed line used in this study (**A**) showing sites and wells accessed for this study. Solid line traversing NW-SE highlights the cross-section Z-Z' shown below (**B**). Bold italic denotes the formations.

3.2 Methodology

Data set that accompanies this chaptere is in the electronic appendix (page 293).

3.2.1 Climate and Hydrology

Meteorological data for 32 years from 1983 to 2014 were obtained from the weather station at Doha International Airport 404280 (OTBD) with latitude 25.26^{O}N, longitude: 51.55^{O}E and altitude of 11 m QND (Qatar National Datum). It is located some 32 km north of Mesaieed sabkha. The height of the wind vane above the ground is 0.5 m. The dataset was analysed for annual and monthly variations, shown in box and whiskers plot. Outliers on the plots are designated based on data that is less than Q1-(1.5×IQR) or greater than Q3+(1.5×IQR) (Rousseeuw et al., 1998), with Q indicating quartile and IQR indicating inter-quartile. For the Arabian Gulf that often experiences extreme weather conditions, outliers can be the main controls of hydrology.

Evaporation (ET_o) rate (mm d^{-1}), is estimated using the Penman-Monteith equation (Allen et al, 1998);

$$ET_o = \frac{0.408\Delta(R_n - G) + \gamma u(e_s - e_a)\frac{900}{T+273}}{\Delta + \gamma(1 + 0.34u)} \tag{3.1}$$

where Δ represents the slope of the vapor pressure curve, R_n is the net radiation, G is the soil heat flux, γ is the psychrometric constant, u = wind speed (m s^{-1}) at 2 m above the ground, (e_s - e_a) represents the vapour pressure deficit of the air, T is the mean air temperature (°C), and u = wind speed (m s^{-1}) at 2 m above the ground.

3.2.2 Field Hydrogeology

Wells and sabkha sites are shown in Figure 3-2. To characterize variations in head and water chemistry within depth through the sabkha, and the interaction with the Dammam bedrock, multi-level water monitoring wells were installed at three sites. These provided data to supplement that from existing observation wells. Careful well design and planning was undertaken in October 2012 in accordance with Environment Agency Report SC020093 (2012) to optimize the understanding of hydrogeology.

Piezometers were drilled using rotary percussion (using Mach 44 hammer bit), with sealant to isolate zones of the slotted 75 mm diameter polyvinyl chloride (PVC) casing. Cement of the sealant is bentonite and cement slurry in 3 to 1 ratio. The annulus filling was washed Dammam Formation limestone aggregate and the slotted section was covered with a geotextile fabric liner. Shallower wells of <1

m with slotted intervals were statically-driven into the sabkha using a sledge hammer, with collapse of the unconsolidated sediment around the pipe providing backfill.

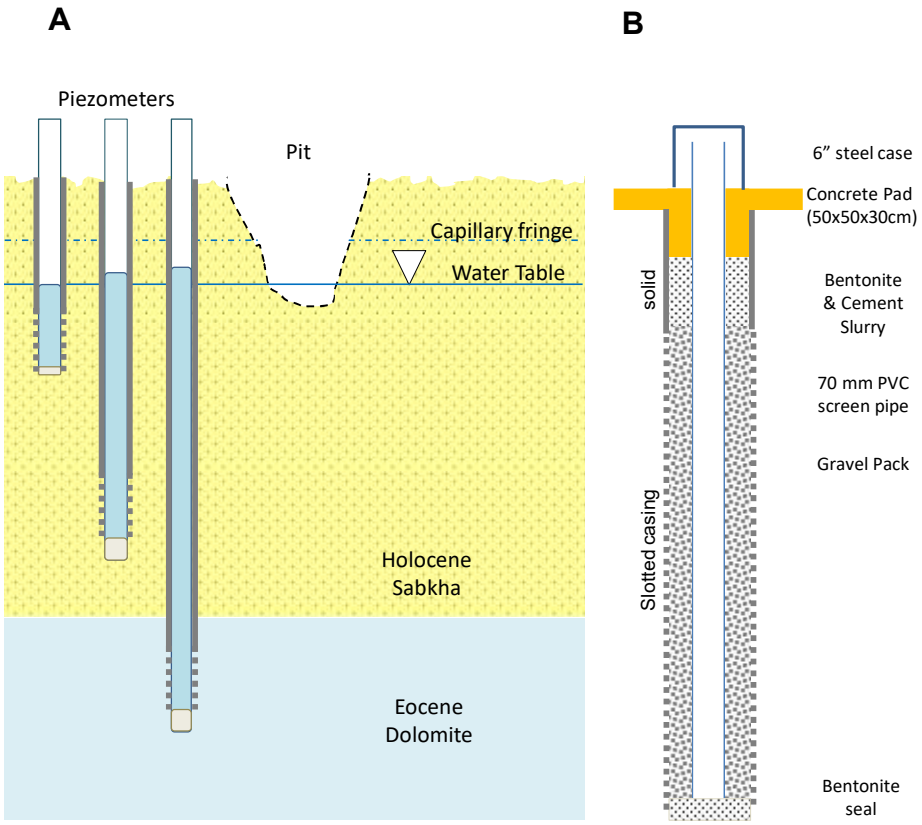

Figure 3-3. High resolution groundwater monitoring site consisting of (A) multi-level piezometers and hand dug pits, (B) well and construction diagram. Diagram is not to scale.

Groundwater changes were examined in terms of spatial (both lateral and vertical) distribution and their variation through time. Spatial data allows us to understand the flux and flow direction of the groundwater in the system, while time series analysis allows us to understand extent of atmospheric pressure, tidal effects and response to recharge events.

Water level measurements were collected at 126 wells using dipmeter (± 0.5 cm) during August 2009 by NDP for the middle and lower sabkha. For part of this project, we collected data in October 2012, February 2012, June 2013 and November 2013 for the proximal, upper and middle sabkha. However due to unexpected anthropogenic effects from settling basin construction in June 2013, all data collected from June 2013 and November 2013 had to be excluded.

Water levels relative to total organic content (TOC) were measured using a dipper, and heads were derived by subtracting the depth to water surface from the elevation of the top of the casing. The elevation was conducted by Gulf Labs for this study. The high-resolution elevation survey has made it possible to derive high-resolution groundwater head (with combined precision of±1 cm). In order to

have, as much as possible, a temporal snapshot, only data from summer and fall data during which no rainfall period occurred, were used to generate a potentiometric surface.

Three end-members which provide the fluid sources into the sabkha; seawater, precipitation and up-dip Dammam Formation ground waters, were sampled to understand the extent of the influence of these waters in the sabkha. This hydrogeology database is supplemented using historic data from NDPP (between June to August of 2009), after careful evaluation of the data quality. All data used in this study came from wells with only 3 m length of screen (including the historic data from NDPP) unless indicated otherwise, in accordance to Church and Granato (1996).

3.2.3 Salinity as Specific Electrical Conductivity (SEC)

In this study, an in-situ measurement of salinity is based on specific electrical conductivity (SEC) which is corrected to standard temperature (25 °C) and pressure (1 atm). In-situ measurements is crucial because dissolved ions are affected by storage periods at various temperatures (Rhoades, 1996). Salinity directly measures the concentration of dissolved salts in the water, whereas specific conductivity is the ability to conduct electrical current in which dissolved ions are the conductors (Rhoades, 1996). For hypersaline brines, Intellical™ CDC401 Field 4-Poles Graphite was used for measurement of SEC (±0.5% accuracy) with Hach® HQ40d meter but its limitation depends on reliable detection limit of only up to 200 mS/cm (total dissolved solids, TDS, of 50,000 mg/L as NaCl). Both NDPP and this study utilise dilution of hypersaline brine into within the detection limit of our equipment to get an accurate SEC. Historic data expressed as TDS were converted to SEC using relationships below hence were corrected using the relationship between SEC and chloride ion or total dissolved solids using data from this study and NDPP.

Most studies use total dissolved solids (TDS). For comparison, SEC relates to TDS by the following equation (Lloyd and Heathcote, 1985):

$$SEC = \frac{TDS}{k_r} \tag{3.2}$$

whereby TDS is expressed in g/l and SEC in mS/cm. k_r in this study was determined to be 0.637 (R^2=0.988). Linear correlations between in-situ SEC with laboratory-analysed chloride ion concentration and PHREEQC-derived density with R^2 = 0.988 and R^2 = 0.984 respectively (Figure 3-4), which indicates good data quality (Holzbecher, 1998).

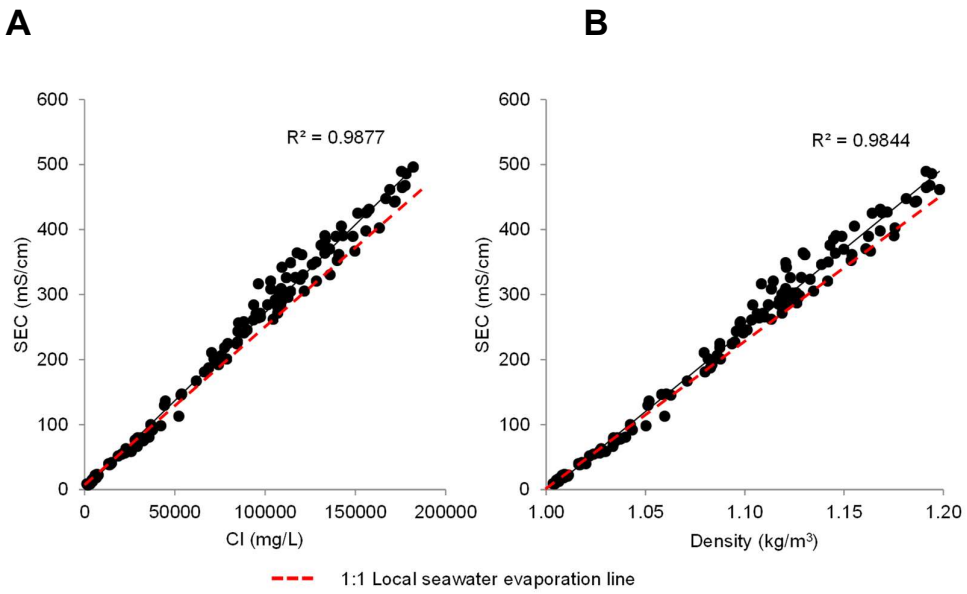

Figure 3-4. Linear regression plots of SEC versus chlorinity (left) and density (right) with R^2. Red dashed line indicates the conservative evaporation of local Mesaieed seawater in 1:1.

3.2.4 Groundwater Dynamics

Fluctuations of groundwater levels and ocean tide levels were recorded at high frequency with pressure transducer loggers left secured in boreholes and at Mesaieed harbour, respectively. Groundwater levels were monitored in wells screened within the Dammam up-dip, sabkha, Dammam Formation underlying sabkha superimposed on tide data from Mesaieed beach. High resolution groundwater monitoring (one-minute interval) using submersible data loggers (INW PT2X), was carried out using a network of 5 boreholes within the Dammam up-dip (M1E), proximal (M2H, M2E) and upper sabkha (M3E, M3ED) between February 24th to February 28th, 2013. In the middle and lower sabkha, medium resolution (30-minute interval) water levels were recorded by the NDP between April 8th and April 16th, 2012 (n=7). During both groundwater monitoring periods, marine flooding was never encountered.

Initial water level measurements are normalized to observed groundwater levels relative to sea level as measured on-site with elevation survey (precision 0.5 cm) and dip-meter (precision 0.25 cm).

Atmospheric Pressure Effects

Hydraulic head was corrected for atmospheric pressure effects. Atmospheric pressure was measured using a barometric pressure sensor (INW BaroSCOUT) installed within the well above the water

level. The pressure was logged every second to investigate high frequency responses. Barometric efficiency (BE), the ratio of water level differences to barometric pressure differences (Jacob, 1940), will be used to describe how water levels (h_i) in wells fluctuate in response to barometric pressure. In situations with variable ρ it is corrected to density, according to (Domenico and Schwartz, 1990) as;

$$BE = -\gamma \frac{\Delta H}{\Delta P_a} \tag{3.3}$$

whereby γ is the specific weight of water, which is a multiplication product of specific weight of the water in the well (N m^{-3}) and gravitational acceleration (m s^{-2}), ΔH is the change in water level measured in the well (m), and ΔP_a is the change in barometric pressure (N m^{-2}).

An alternative approach described by Clark (1967) and Gonthier (2007) is to obtain BE from an arithmetically scaled plot of groundwater level as a function of concurrent barometric pressure changes, in which BE is estimated from the slope of a least squares line fit through the data. For the sabkha this method is only possible if the water level used is corrected with the fluid density, for example making conversion from water level to equivalent freshwater head. The assumption inherent in both methods is that there is no time lag between water level changes in the well and the atmospheric pressure changes (Butler et al., 2011). This was checked by plotting a time series for depth from ground surface to water level and the atmospheric pressure. Effects of barometric correction are shown in Figure 3-5 for well 1E. The linear relationship shows no time-lagged responses between the drop in water level in the well and increased atmospheric pressure.

Atmospheric pressure, in units of m H_2O, is measured by barometric logger on-site, and conversion to SI unit of Pa is a multiplication of 9806.65. Barometric effect from atmospheric pressure was monitored within the well M1E above the static water level.

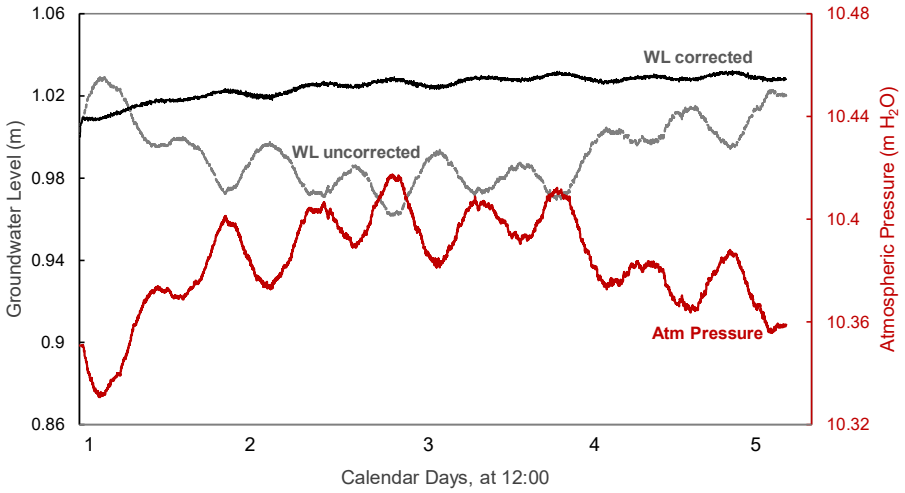

Figure 3-5. Time series of groundwater level in well 1E before (grey line) and after (black line) correction with atmospheric pressure (red line).

Ocean Tidal Effects

To understand the propagation extent of the tidal pressure signal inland from the sea, groundwater levels were corrected by removing the barometric effects;

$$W_{(t)cor} = W_{(t)uncor} - BE\ (\Delta P_a) \tag{3.4}$$

where $W_{(t)cor}$ is the water level at time t corrected for barometric pressure (m), $W_{(t)uncor}$ is the uncorrected water level at time t (m), BE is the observed barometric efficiency, and ΔP_a is the change in barometric pressure ($B_o - B_{(t)}$) at time t (Pa).

The time lag is calculated between the high tide and the peak of the piezometer head, according to Jiao and Tang (1999). Tidal oscillations and its effect on wells can be measured as tidal efficiency (TE), which is the ratio of water level changes ΔH (m) to the corresponding changes in tidal fluctuations ΔS (m) adapted from Ferris et al. (1962);

$$TE = \frac{\Delta H}{\Delta S} \tag{3.5}$$

Evaporation-driven convective flow

The onset of brine instability can be estimated using the non-dimensional Rayleigh number R_a (Simmons et al., 2001; Sanford and Ward, 2001; Nield, 2013), which is the ratio between buoyancy-

driven forces and resistive forces caused by diffusion and dispersion. The calculation was performed using the following equation (Nield, 2013):

$$R_a = \frac{k_i g \Delta\rho H}{\theta \mu D_0} \tag{3.6}$$

where k is permeability (m^2), g is gravitational acceleration ($m\ s^{-2}$), $\Delta\rho$ is the difference in density between fluids at two measurement points ($kg\ m^{-3}$), H is the saturated thickness of the porous layer (m) which is a subtraction of depth to water table from layer thickness, θ is the porosity, μ is the dynamic viscosity (kg/m s) and D_0 is the molecular diffusivity (m^2/s). Nield et al. (2008) suggested that the Rayleigh criteria R_a must attain at least a common stability criterion of $4\pi^2 = 39.48$ for free convection to occur.

Porosity averaged from this sabkha study is 0.40. Permeability K is derived from hydraulic conductivity k from

$$k = K \frac{\mu_{23}}{\rho g} \tag{3.7}$$

where ρ = fluid density, μ = dynamic viscosity and g = gravitational constant.

3.2.5 Groundwater Head

Hydraulic Head and Equivalent Freshwater Head

The hydraulic head, also called the absolute groundwater head or point-water head (Lusczynski, 1961), is the elevation to which water will naturally rise in a well to balance the pressure in the aquifer at that point. It is often measured in the field as the level of the water–atmospheric interface in a well relative to a common datum. For an unconfined aquifer like Mesaieed sabkha, the hydraulic head is interchangeably used as water table, the elevation of which often mimics topography of land surface above. The hydraulic head is defined by the following:

$$h_i = z_i + h_{p,i} \tag{3.8}$$

where hydraulic head h_i is a sum of elevation head z_i (mean level of the well screen at point i, with unit of meters) and point water pressure head $h_{p,i}$ (the length of water column in the well relative

to z_i). The point water head is related to the pressure of groundwater at the well screen by the following:

$$h_{p,i} = \frac{P_i}{\rho_i g} \tag{3.9}$$

where P_i is pressure (Pa), ρ_i is the density (kg/m^3) of water surrounding the well screen (or piezometer), and g is the acceleration due to gravity (m s^{-2}).

The above equation (3.9) shows that in a groundwater system where density varies spatially can result in different values of $h_{p,i}$. Hence, a correction needs to be applied to normalize using a reference density. In this case, the density of freshwater at 25° C is 1.00 kg/m^3. To assess the importance of density effects in variably-saline groundwater systems, groundwater heads (or hydraulic heads) measured need to be converted to equivalent freshwater head (h_f) using the following:

$$h_f = \frac{p_i}{p_f} h_i - \frac{p_i - p_f}{p_f} z_i \tag{3.10}$$

where p_f is density of freshwater (kg/m^3). From the equation above, for waters which are more saline than freshwater, z_i is always negative, the h_f is always equal or greater than point water head.

The assumption is that the equivalent freshwater head (EFH) is an imaginary level that would have been measured if the water in the aquifer and observation borehole had been fresh water. This means that the pressure of water at the point of measurement becomes uniquely related to the height of a water column for all observation boreholes. Measured SEC show significant variation in density throughout both the Dammam and sabkha aquifers due to changes in solute concentration from mixing, dilution and evaporation. When spatial differences in salinity exist, the influence they have on flow dynamics must be evaluated during the conceptualisation stage. However, this simplified understanding does not take account of the elevation of screen in factoring freshwater heads in variable-density groundwater flow conditions (Post et al, 2007).

It is crucial to use freshwater heads measured at the same depth when horizontal flow component is evaluated (Post et al., 2007). Contrary to groundwater with a homogenous density, the freshwater head varies with depth, even in hydrostatic conditions. The corresponding fresh water head at a reference depth, z_r is derived from Guo and Langevin (2002) and Post et al. (2007) using:

$$h_{f,r} = z_r + \frac{p_i}{p_f}(h_i - z_i) - \frac{p_a}{p_f}(z_r - z_i)$$

(3.11)

where $h_{f,r}$ is depth-corrected freshwater head and p_a is the average water density between measured point z_r and reference point z_r. From Darcy's Law, groundwater flows from high $h_{f,r}$ to low $h_{f,r}$ hence this allows us to understand a general flow direction of the groundwater.

In our data, there is no relationship between the density of the waters (which ranges between 1.01-1.20 kg m^{-3}) and the corresponding temperature (ranges 27.6-37.2 °C), with R^2 of 0.07. Thus, over a range of p which may be caused by differences in temperature are insignificant and is ignored in calculation of $h_{f,r}$.

3.2.6 Hydrology Budget and Solute Budget

To understand the horizontal and vertical groundwater flow and therefore, create a hydrology budget, the volumetric fluxes of the groundwater can be calculated. Following from Chapter 2, the study of flow will be done in more detail for each sabkha zone to capture the complexity of the system. This is due to the opportunity of greater data density, up to the proximal sabkha, in which previous workers did not have (see Sanford and Wood, 2001).

Fluxes were calculated for within individual zones, using piezometers or wells within 100 m proximity. For flow between different zones, using wells spaced within 2 m of each other but screened at different depths at separate zones. Hydraulic conductivity data will be used from Chapter 2 to derive flux from $h_{f,r}$.

Darcy's Law, the well-known expression of Newton's second law is a vital equation that relates to the fluid flow through a porous medium. The shorthand notation is as follows:

$$q = -K\nabla h$$

(3.12)

q denotes flux or Darcy velocity (volume of fluid per unit of cross-sectional area of porous medium per unit time $m^3/m^2/s$, or simply, specific discharge per time, m/s). K is the hydraulic conductivity (m/s) and ∇h the hydraulic gradient, which is the factor that drives groundwater flow per unit weight of groundwater (dimensionless). From here, we can calculate the volumetric flux Q by multiplying with width and length of the section.

Lateral groundwater flux, q_y (m/s), is estimated simply by:

$$q_y = -K_y \left(\frac{\Delta h_{f,r}}{\Delta z} \right)$$

(3.13)

where q denotes Darcy velocity, $\Delta h_{f,r}$ and Δz are the difference in freshwater head (m) and elevation head of the piezometers respectively (m) and K_y is the lateral hydraulic conductivity (m s^{-1}). Note that in equation 3.11 the $\Delta h_{f,r}$ takes account of density differences into account in equation 3

Vertical flow q_z uses a Darcy's Law-derived finite difference equation modified from Post et al. (2007) which includes a relative density contrast and the buoyancy effects on the vertical flow:

$$q_z = -K_z \left[\frac{\Delta h_{f,r}}{\Delta z} + \left(\frac{p_a - p_f}{p_f} \right) \right]$$

(3.14)

where $\Delta h_{f,r}$ and Δz are the difference in freshwater head and the difference in the measured elevation head, and p_a is the mean density of the groundwater between two piezometer mid-screens (kg m^{-3}). K_z is the vertical hydraulic conductivity (m s^{-1}). As measuring K_z in-situ is difficult, the net K_z is approximated by harmonic weighting of horizontal hydraulic conductivity K_y if the formation is relatively homogenous. If the K_y at two formations varies substantially, then the value used is for the least conductive layer (Sanford and Wood, 2001) as this will effectively limit flow rate.

Volumetric fluxes Q were calculated by multiplying either by the thickness of the formation (for lateral flux) or the vertical length of the section (for vertical flux).

Volume change, ΔV, over time, Δt, in the sabkha system can be calculated by the difference between total inflow and total outflow. The basis of hydrologic budget can thus be expressed by the water balance equation comprising of flux components:

$$\frac{\Delta V}{\Delta t} = Q_{rain} + Q_{inflow} + Q_{runoff} - Q_{etot} - Q_{outflow}$$

(3.15)

where Q_{rain}, Q_{runoff} and Q_{inflow} are rainfall, surface runoff and other inflow components respectively. Q_{etot} and $Q_{outflow}$ are total evaporation and other outflow components. The ΔV is related

to $\Delta h_{f,r}$ using porosity $\emptyset$ of aquifer. The nature of potential inflow and outflow components will be investigated in the results.

Similarly, the annual solute budget of the sabkha can be written as:

$$\frac{\Delta S}{\Delta t} = S_{rain} + S_{inflow} + S_{runoff} - S_{etot} - S_{evap} - S_{outflow} \quad (3.16)$$

whereby $S = C_i V$ is the solute mass in the lake (kg), represented by multiplying the average total dissolved solid concentration C_i (mg l^{-1}) by the volume of the sabkha.

3.2.7 Statistical Analysis of Variance

To understand the correlation between two variables, linear regression plots were used with least square regression calculated, summarised in a form of R^2. However, to further understand the statistical significance between different groups laterally (sabkha spatial zones and the adjacent saltwater or up-dip Dammam aquifer) or vertically (parts of the stratigraphy in which the water is hosted), statistical analysis of variance (SAV) methods such as parametric analysis of variance (ANOVA) or non-parametric analysis of variance (Kruskal-Wallis) are used. For ANOVA to be used, the criteria are that the data must be normally distributed, and the variances of the separate groups are equal. If this is not the case, then the Kruskal-Wallis method is employed. Analysis of variance attempts to assess whether to accept or reject the null hypothesis (H_o) which is that all variables distributed within different groups are identical (Lehmann and D'abrera, 1975) and are not statistically significantly different. To do this, a p-value is calculated which is a probability that measures the evidence against the null hypothesis. Statistical tests for our dataset were carried out with business intelligence TIBCO® Spotfire software, using an add-on Data Relationship tool, the significance is reported as probability (p) with two high confidence levels of 0.01 and 0.05. The lower the p-value, the stronger the evidence is to reject H_o. A very high confidence level of 0.01 indicates a 1 % risk of interpreting that a statistically significant difference exists when there is no actual difference (false positive). This analysis will frame the way where only significantly different results of the variables are discussed and presented.

3.3 Qatar Climate

3.3.1 Temperature

Analyses over the 32-year period of daily climate data show a high fluctuation in air temperature, both seasonally and annually (Figure 3-6). The mean daily temperatures ranged from a minimum of 9.8 °C in January to a maximum in July of 42.2 °C. The cool period of winter months extends from December to February, whilst hot summer months span from May to September.

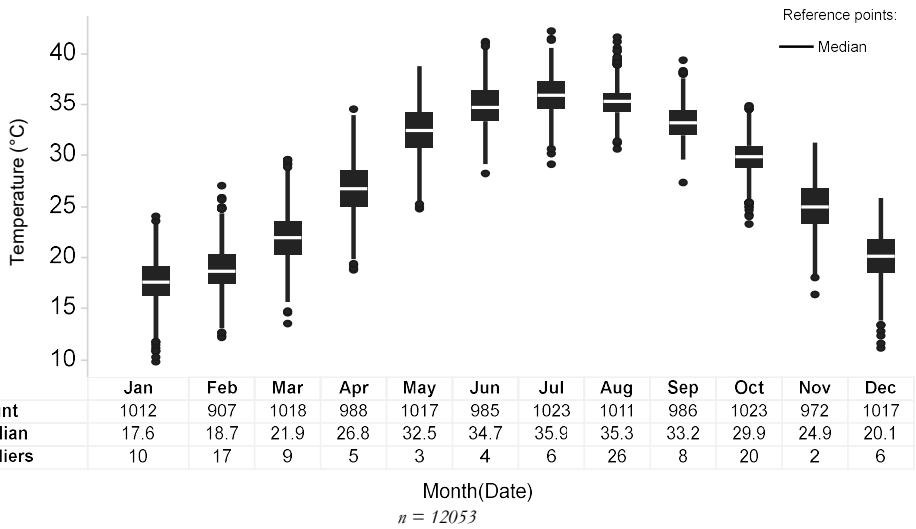

	Jan	Feb	Mar	Apr	May	Jun	Jul	Aug	Sep	Oct	Nov	Dec
Count	1012	907	1018	988	1017	985	1023	1011	986	1023	972	1017
Median	17.6	18.7	21.9	26.8	32.5	34.7	35.9	35.3	33.2	29.9	24.9	20.1
Outliers	10	17	9	5	3	4	6	26	8	20	2	6

Figure 3-6. Box and whiskers plot of monthly/seasonal variation in daily air temperature (°C) from 1983 to 2014 at the Doha International Airport meteorological station. The lower and upper limit of each box define the first quartile (Q1) and third quartile (Q3) percentiles, respectively. The white horizontal line within the box is the median (IQR = Q3 – Q1). The whiskers extend to data that are not considered as outliers. Outliers (the data points that are not connected to the box and whiskers) were defined as a data value greater than Q3 + 1.5(Q3 - Q1) and less than Q1 + 1.5(Q3 - Q1).

3.3.2 Relative Humidity

There is a seasonal variation in humidity, with lower humidity recorded in the summer months and higher humidity for the winter months, as shown in box and whisker plot (Figure 3-7). Being a peninsula, mean daily humidity can reach up to 95% and as low as 8%. Diurnal fluctuations are shown with mean hourly in Figure 3-8 with a greater variation in winter (σ = 15.4 %) than in the summer (σ = 5.1 %).

When compared to Abu Dhabi, humidity is greater than in Qatar (NOAA, 2013). Abu Dhabi has less marked seasonal variation, with mean monthly relative humidity of 68.0% in December and January and a mean of 55.0% in May. In Qatar, for three months between May and July, the mean monthly humidity remains ranges between 41 to 49%. The same period for Abu Dhabi records mean monthly humidity of 55 to 61%. (NOAA, 2013).

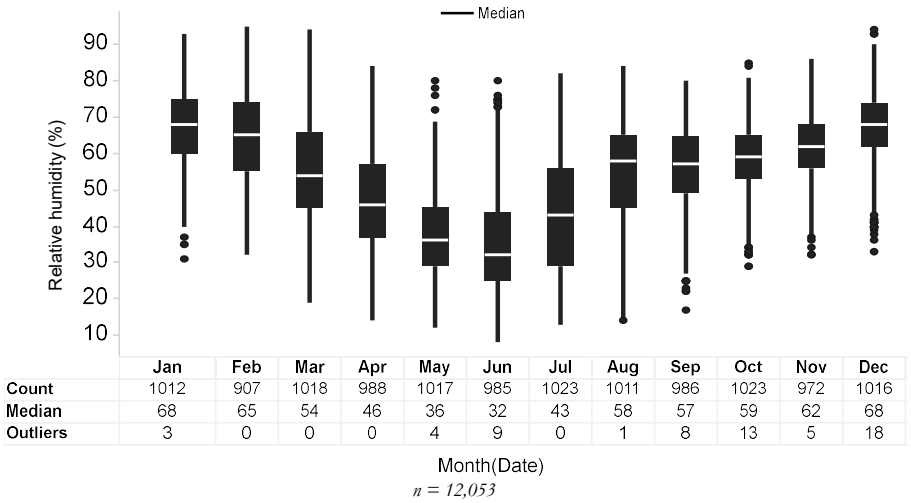

Figure 3-7. Box and whiskers plot highlighting monthly variation of average daily relative humidity (percentage) from 1984 to 2014.

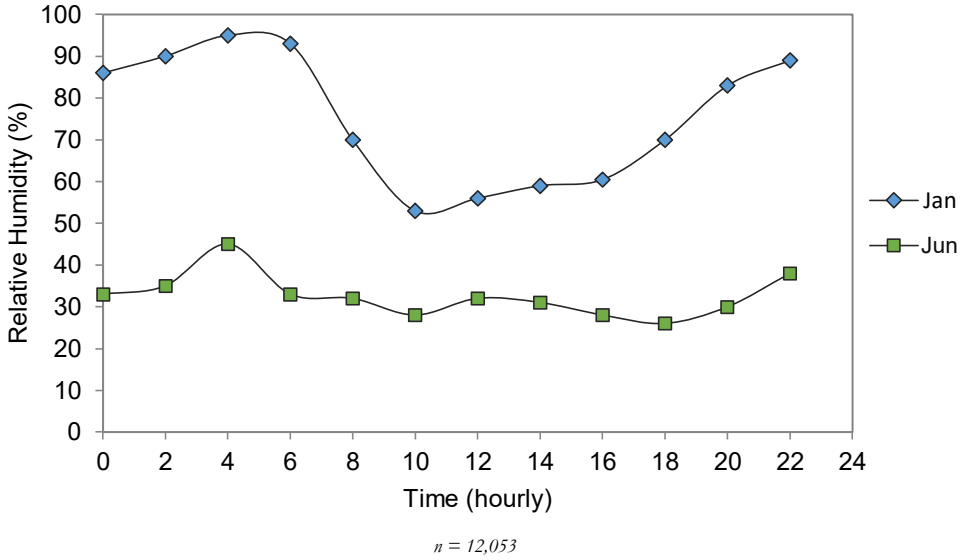

Figure 3-8. Mean hourly relative humidity in Qatar from 1980 to 2010 showing diurnal cycles.

3.3.3 Evaporation

Potential evaporation (PE_{to}) at sea level for the period 1983 to 2014 yields an annual average of 4364 mm/year, equivalent to a mean daily of 12.0 mm/day (Figure 3-9). During the summer, maximum PE_{to} can reach 45 mm/day in June, whilst in the winter minimum PE_{to} can be as low as 0.34 mm/day in January. This is comparable to the mean daily of 11.3 mm/d that was measured in Abu Dhabi (Sanford and Wood, 2001).

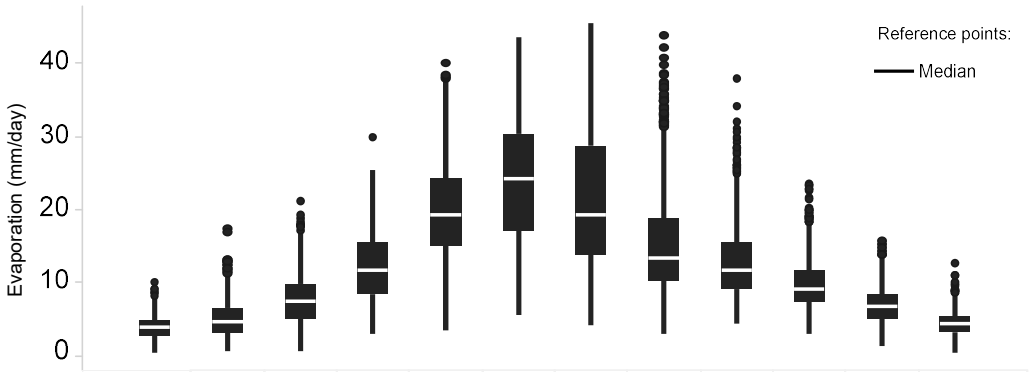

	Jan	Feb	Mar	Apr	May	Jun	Jul	Aug	Sep	Oct	Nov	Dec
Count	1012	907	1017	988	1017	985	1023	1001	958	1017	971	1016
Median	3.82438	4.73...	7.38...	11.6...	19.1...	24.147	19.2...	13.2...	11.7...	9.10...	6.75...	4.29988
Outliers	6	14	10	1	4	0	0	41	36	35	6	13

Month(Date)

n = 12,053

Figure 3-9. Box and whiskers plot showing the monthly variation of total daily evaporation, E_{to}, in Qatar (mm/day) from 1983 to 2014, calculated using Penman-Monteith method.

However, the rate of evaporation of sabkha pore waters is much lower than PE_{to}. Studies done by Sanford and Wood (2001) used humidity chamber technique, which measures the humidity and temperature beneath a clear dome placed upon the sabkha surface (Stannard, 1988). The total actual evaporation rate AE_{to} of pore waters held by capillary zone in sabkha is less than 3% of PE_{to} (Sanford and Wood, 2001). The effect of high salinity on evaporation results in lowered water activity, and hence reduce the saturation vapor pressure above the saline water (Mor et al., 2018).

Using this correction, this yields AE_{to} of Mesaieed at about 0.56-0.79 mm/day. A plot of monthly average AE_{to} shows a positive correlation with temperature, which is a function of solar insolation, but the highest AE_{to} occurs in June rather than when the temperature is highest in July. This is due to a higher humidity in July which inhibits evaporation.

3.3.4 Precipitation

Coefficient of variation in annual precipitation, which measures dispersion of values, is 1.71. This is higher than older studies which studied shorter periods, by Bazaraa and Ahmed (1991) and Lloyd et al (1987) which reported 0.85 and 0.75, respectively. The term 'mean rainfall' is hence meaningless in this region. Maximum rainfall in a 24-hour period is 183 mm in November 1994 followed by 170 mm on 21 March 1995.

Ratios of rainfall to potential evaporation (P:E) ranges from 120 during months of December and January, and up to 700 in the summer months (Figure 3-10). In a 32-year period, there are only four occurrences of daily precipitation greater than 120 mm. There are no precipitation events in June nor

July over the 32-year period, and only one each in August and September. For 10 out of 32 years, there was no rain that fell in Qatar. Measurable rain (> 0.25 mm) occurred for 196 days out of 11690 days studied using precipitation data from 1983 to 2014, yielding a probability of rainfall for any day at 1.7%.

Extreme variance can be observed from a 5-year drought (1984-1988) to thunderstorms that last up to 4-5 days. Figure 3-11 shows the annual sum of rainfall and monthly sum over the 32-year period.

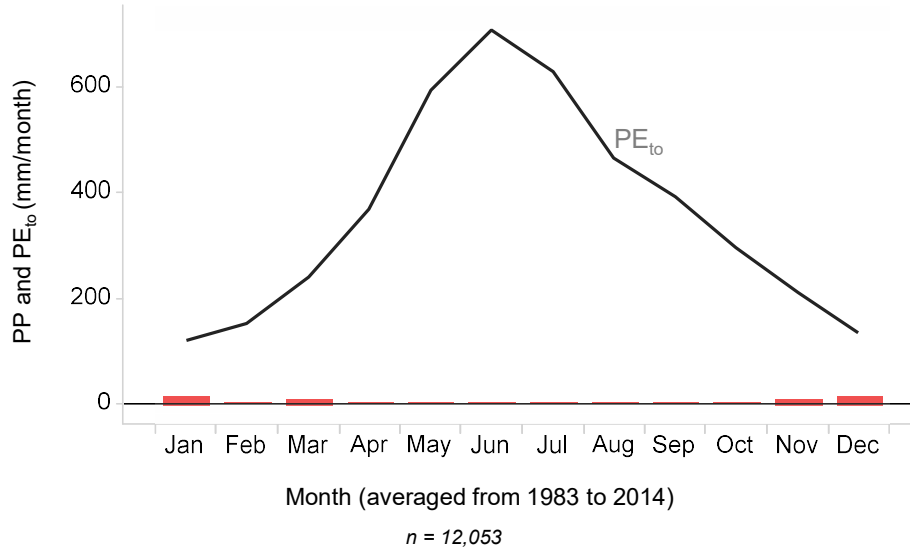

Figure 3-10. Monthly rainfall (as red bars) and potential evaporation PE_{to} (solid line) averaged over 32-year period between 1983 to 2014 in Doha Airport, Qatar.

Rainfall is mostly restricted to the winter months of November to March and is believed to be related to the Subtropical Jet Stream (Lloyd et al, 1987). Most rainfall occurs in short but intense thunderstorms and cloudbursts are common, up to 180 mm over a few hours. With the sabkhas located at the lowest of elevations in the country, the majority of recharge that occur in sabkha environments is related to surface to near-surface runoff during storm events. This means that heavy bursts of rainstorms can easily flood sabkha sediments from the up-dip Dammam Formation discharge, either via overland flow and as standing water from direct precipitation. This may then result in dissolution of highly soluble surface evaporitic salts, i.e. halite.

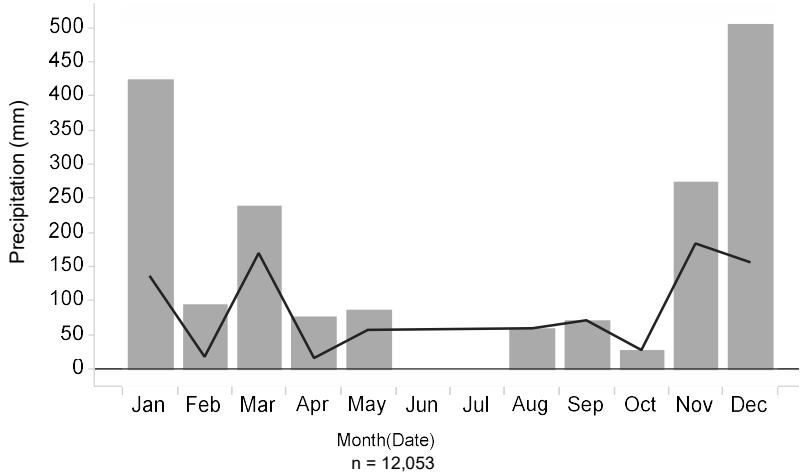

Figure 3-11. 1983 to 2014 analyses of rainfall (excluding zero rainfall days). Figure **(B)** highlights monthly sum of precipitation (bar) and maximum rainfall (solid line) over the 32-year period.

3.3.5 Fog

Fog was encountered in South Mesaieed and opportunistically sampled with a graduated cylinder laid on a tarp for two days in 27th January 2014 resulting in an average at 3.4±1.4 mm of dew waters per day (n = 17). The average humidity of that day was recorded at 88%, the highest of the year. Whilst this was only a short sampling period, this data provides a little-known information about which is one of the least studied aspects - the impact of fog on sabkhas. Lokier (2012) mentioned that high humidity results in the dissolution of halite crust, particularly at night. While periodic storms have more impact in dissolving surface salts, consistent moisture contribution from fog may help dissolve salts efficiently and possibly remobilize them downward into the vadose zone. Fog may be an important source of moisture to coastal deserts (Warren, 2016) and helps moderate the coastal air temperature. This however will not be explored due to the limited data available.

3.3.6 Tides

Tides were measured with a pressure transducer logger within a stilling well at Mesaieed harbour (25.0167° N, 51.6500° E). The data is presented in Figure 3-12 with lunar cycles obtained from www.tides.mobilegeographics.com (Mesaieed harbour location 3973). Tidal amplitude ranges from 0.6 m up to 1.9 m. It is characterised by two high and two low tides of different magnitude at every lunar day, which according to NOAA classification (2017) is typical of a mixed semidiurnal tide cycle. The maximum tidal range is just under 2 m, the tidal regime in Mesaieed is microtidal. Data accuracy was verified with www.wunderground.com historic data (location KQIR). The implication for Mesaieed sabkha is seasonal high tides and storm surges that are able to flow inland over the lower sabkha which is only 1-2 m above sea level.

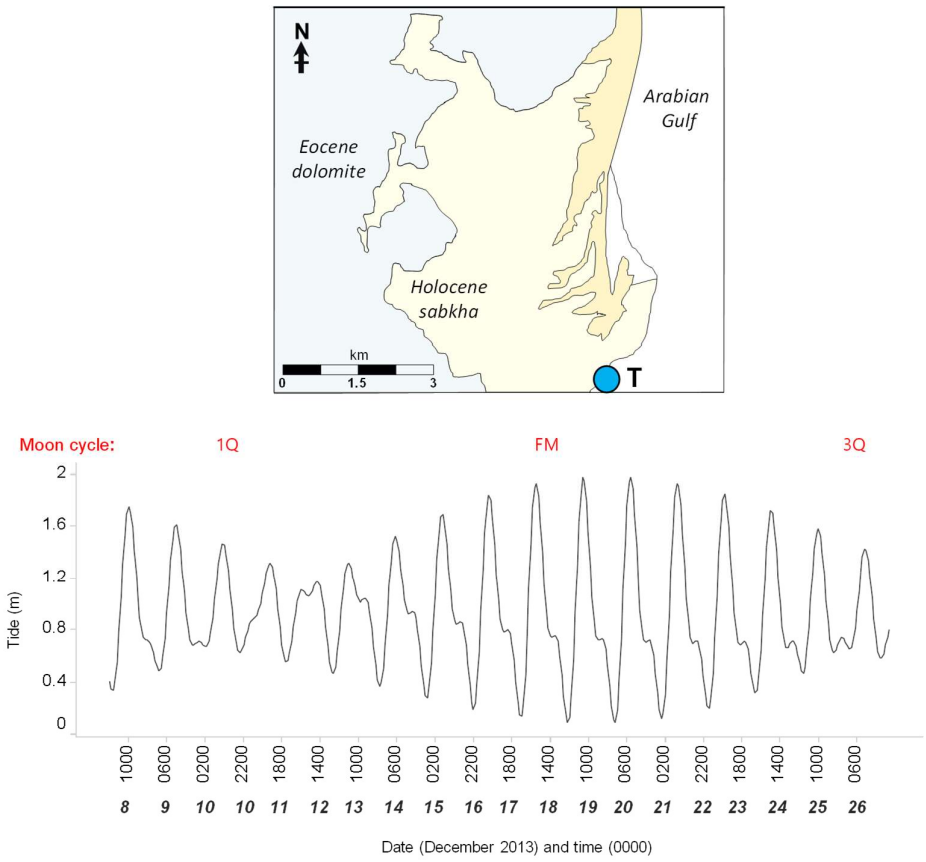

Figure 3-12. Tidal range measured hourly at Mesaieed harbour from 8th December 2013 to 26th December 2013 with the moon cycles: 1st quarter (1Q), full moon (FM), and 3rd quarter (3Q). Date is presented on the x-axis as time of day (vertically) above the corresponding day of month (horizontally).

3.3.7 Wind

The shamal ("north" in Arabic) is a prevailing wind that blows from a north to north-westerly direction. A shamal day is defined as typically exceeding 8.5 m s^{1-} in at least 3 hours throughout a 24-hour period (Rao et al, 2001).

Wind strength and duration affects relative humidity and thus evaporation of pore waters from the sabkha. Meteorological data was obtained from a local weather station onshore in Mesaieed near the tide station on Figure 3-12. Figure 3-13 represents a time series relationship between atmospheric pressure and wind velocities over a one-month period in March 2008. Atmospheric pressure shows a twice-daily variation of approximately 3 mB with an overall drop of 16 mB over the course of 1 month and 4 days. Wind velocities show daily variations but at a higher frequency and is inversely correlated with atmospheric pressure. This may represent local events associated with a cold front but cannot be verified without atmospheric temperature data.

Figure 3-14 represents wind direction and $\overline{x}$ velocities for over a calendar year of 2013, which confirms predominant northwesterly *shamal* winds (70%). Most measurement results are confined to the region of northwest to south-southeasterly, and very few within the S-NW region. Mean wind velocities are 4.5 m/s. 30% of prevailing wind is from the southeast to south-easterly direction, likely a result of sea breeze.

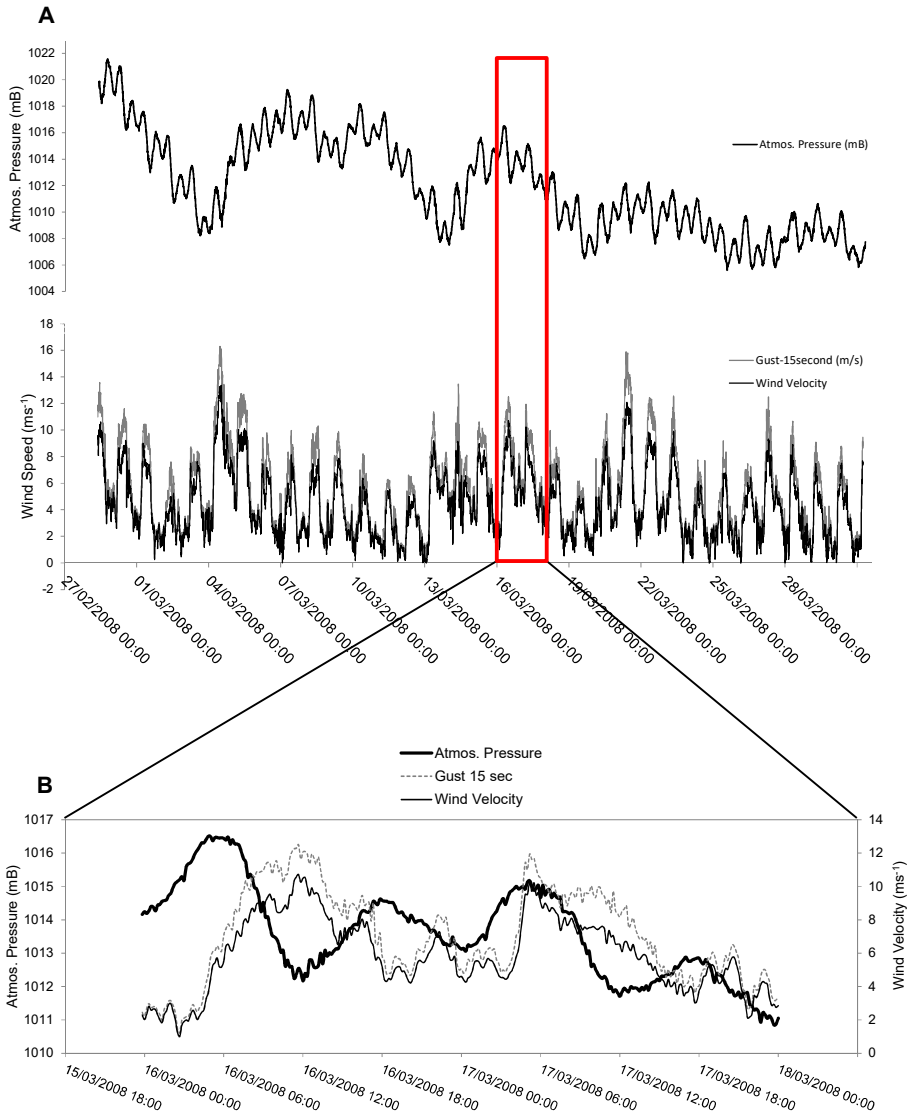

Figure 3-13. Time series plot of (A) atmospheric pressure and wind velocity with 15 seconds of sustained wind gust and (B) higher resolution data of a two-day period to highlight relationship between atmospheric pressure and wind. Data is taken from a local meteorological station in Mesaieed sabkha during the duration of 28th February 2008 to 31st March 2008.

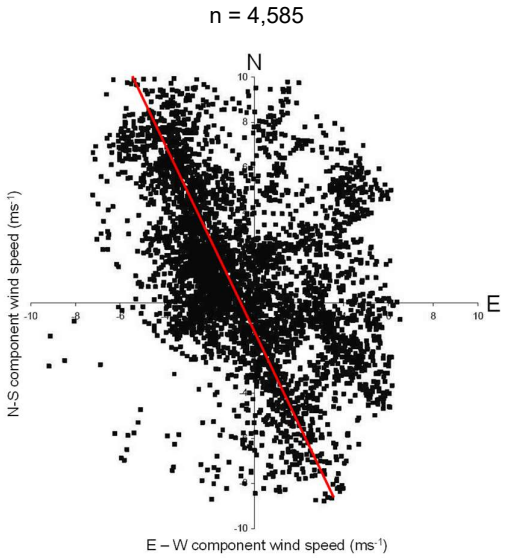

Figure 3-14. Scatter plot of recorded wind velocities and direction during the year of 2013 obtained from a local meteorological station in Mesaieed sabkha with a trendline through the prevailing wind direction in a NW–ES with dominant wind direction from NNW. NE and SE winds are due to effects of sea breeze.

3.4 Marine and Continental Charge in Mesaieed

Spring tides were observed on the field and using Landsat imagery to drive marine flooding landward of Mesaieed. This confirms previous accounts observed by Groot (1973) and Youssef (2003) for Umm Said sabkha just south of the field area. Annual variations of marine flooding in Mesaieed sabkha were studied using satellite images from 1985 to 2013 of the month of December.

Transient surface ponding is observed in parts of the proximal sabkha, sometimes without evidence of marine flooding, which suggests the effects of rainfall on continental meteoric groundwater. Figure 3-15 shows satellite images of Mesaieed proximal sabkha superimposed on rainfall plot from 1983 to 2014 highlighting the relationship between increased rainfall and darker sabkha sediments. The darkness of the proximal sabkha coinciding with times preceded by rain events, the most prominent ones in 1994 imagery.

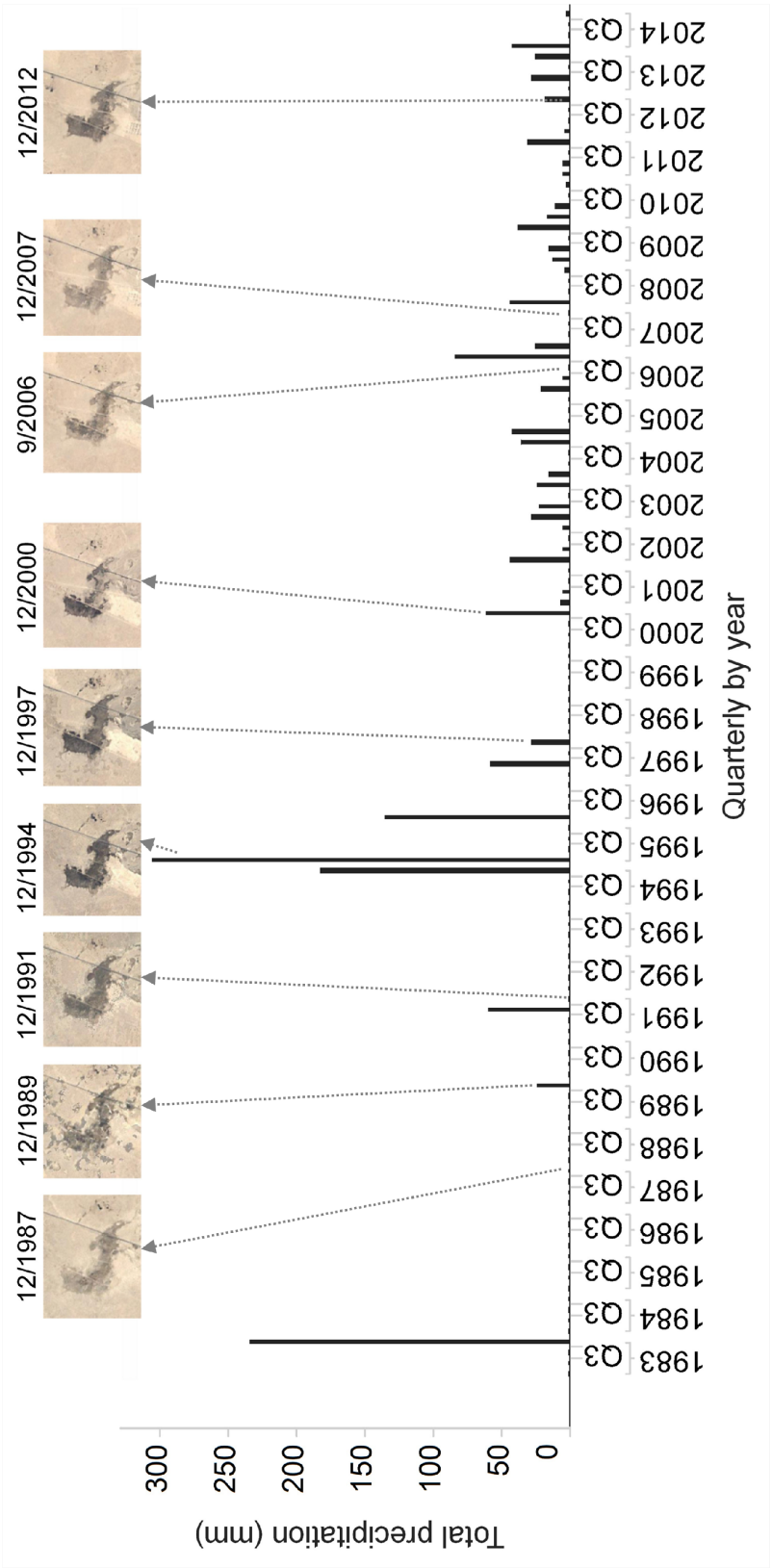

Figure 3-15. Rainfall data from 1983 to 2014 with satellite imagery of Mesaieed proximal sabkha above to highlight how the wet and dry seasons correlate with the darker and lighter colour, respectively. 12/1989 imagery coincides with maximum marine flooding and the 4th quarter 1989 rainfall which shows meteoric groundwater saturated to the point of flooding on the surface.

Marine flooding is the most prominent feature on the satellite imagery and in the field which indicates that the lower and middle sabkha is subjected to seasonal tidal flooding, driven by easterly winds. Most of the Mesaieed (98 %) sabkha lies above mean annual sea level. However, the lack of a fully developed spit as a major barrier between the sea and sabkha allows marine floods up to 10 km across the sabkha.

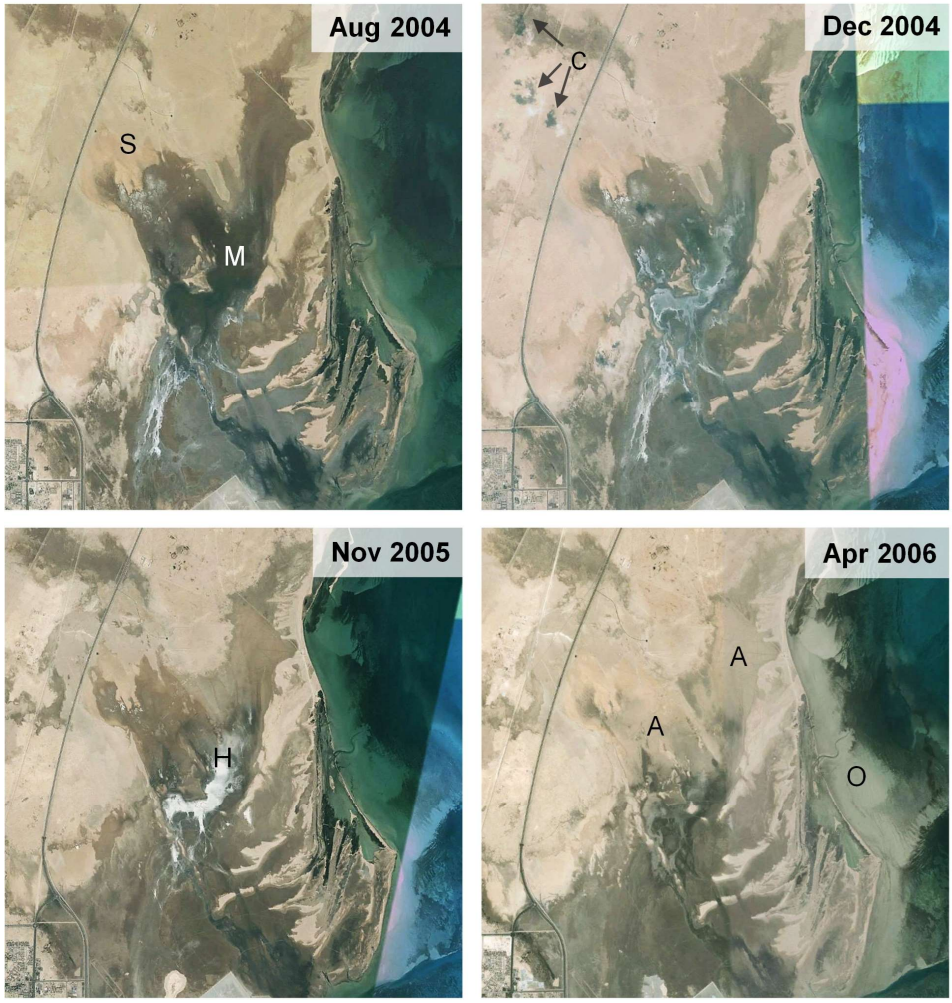

Figure 3-16. Satellite imagery montage of marine flooding (demarcated as M) from August 2004 to October 2006. The sabkha boundary can clearly be separated from outcropping Dammam Formation. Using the Munsell® Color Chart, the sabkha appears to be distinctively dark brown, with shades ranging from pale reddish brown (when dry and arid for years without rainfall) to grayish red or moderate brown (when saturated especially after a rainfall). Bedrock is light brown, between the shades of pale yellowish orange and moderate orange pink. Other important features are ponding of water especially after marine flooding, which dons a dusky blue green colour, and ephemeral salt which is yellowish grey to white.

Figure 3-16 highlights the pattern of marine flooding that occurs in Mesaieed and the development of salt flat at which coincides the upper limits of marine flooding. Middle sabkha is on the supratidal part where marine flooding occurs up to six times a year. The retreat of marine floodwaters is hindered by surface irregularities and the lowest relief in the middle sabkha allows pooling of seawater.

Maximum surface area occupied by marine flooding can be roughly estimated via GIS polygonal calculator to be about 32 ± 2 km² out of 50 km² with an average marine flooding to occupy about 20 ± 2 km².

The other persistent feature of the satellite images is the presence, and absence thereof, of **salt flat** (and absence thereof) which is characterized by white crust and smooth texture with sharp boundaries. The transient salt flat coincides with the upper limit of seasonal marine floods and in the field is evident by driftwood and strandline deposits. Figure 3-16 shows the ephemeral salt flat forming in November 2005 and October 2006 after a dry summer. A five-year drought ensued between January 1984 and December 1988 whereby salt flats are seen forming in 1986 and then subjected to marine flooding (captured by 1987 image, see Chapter 2) dissolving the salt flat. The cycle repeats for the following years. The most extensive salt flat is seen in 1991, 1998 and 1999 which is a result of three-year droughts during periods of 1992-1994 and 1998-2000.

3.5 Specific Electrical Conductivity (SEC)

3.5.1 Source waters

Figure 3-17 presents the distribution of measured specific electrical conductivity (SEC), a proxy for salinity, in both sabkha and Dammam formations, relative to those in potential source waters. Figures for SEC quoted here in the text are mean $\bar{x} \pm 1\sigma$.

The average SEC of the local near-shore surface seawater from samples collected within 200 m of the coastline at Mesaieed sabkha is 67.3±6 mS/cm (n=3). This is within the range of values reported for offshore waters in the Arabian Gulf with a SEC ranging between 57 mS/cm to 66 mS/cm in the summer (John et al, 1990), slightly higher than global surface seawater (52.9 mS/cm, Nordstrom et al, 1979; Drever, 2005) due to evaporation. Seasonal difference is notable with repeated measurement at the same site as the seawater ranges from 67 mS/cm in February 2013 to 74 mS/cm in June 2013. After heavy rainfall in November 2013, the seawater SEC went down to 61 mS/cm reflecting dilution from a combination of runoff and direct precipitation.

Waters in the Damamm aquifer updip of Mesaieed sabkha is found to be brackish, with an average SEC of 28 mS/cm±24 (n=20). The lowest SEC is found in the more landward wells (7 mS/cm) about 6 km inland of the sabkha. Eastward, there is a progressive increase towards the sabkha (reaching 55 mS/cm at W7d), only 0.4 km from the landward margin of the proximal sabkha. To the north of the sabkha, the SEC of waters in the Dammam aquifer is also affected by its proximity to the coast, with SEC increasing up to 50 mS/cm 1km from the coast.

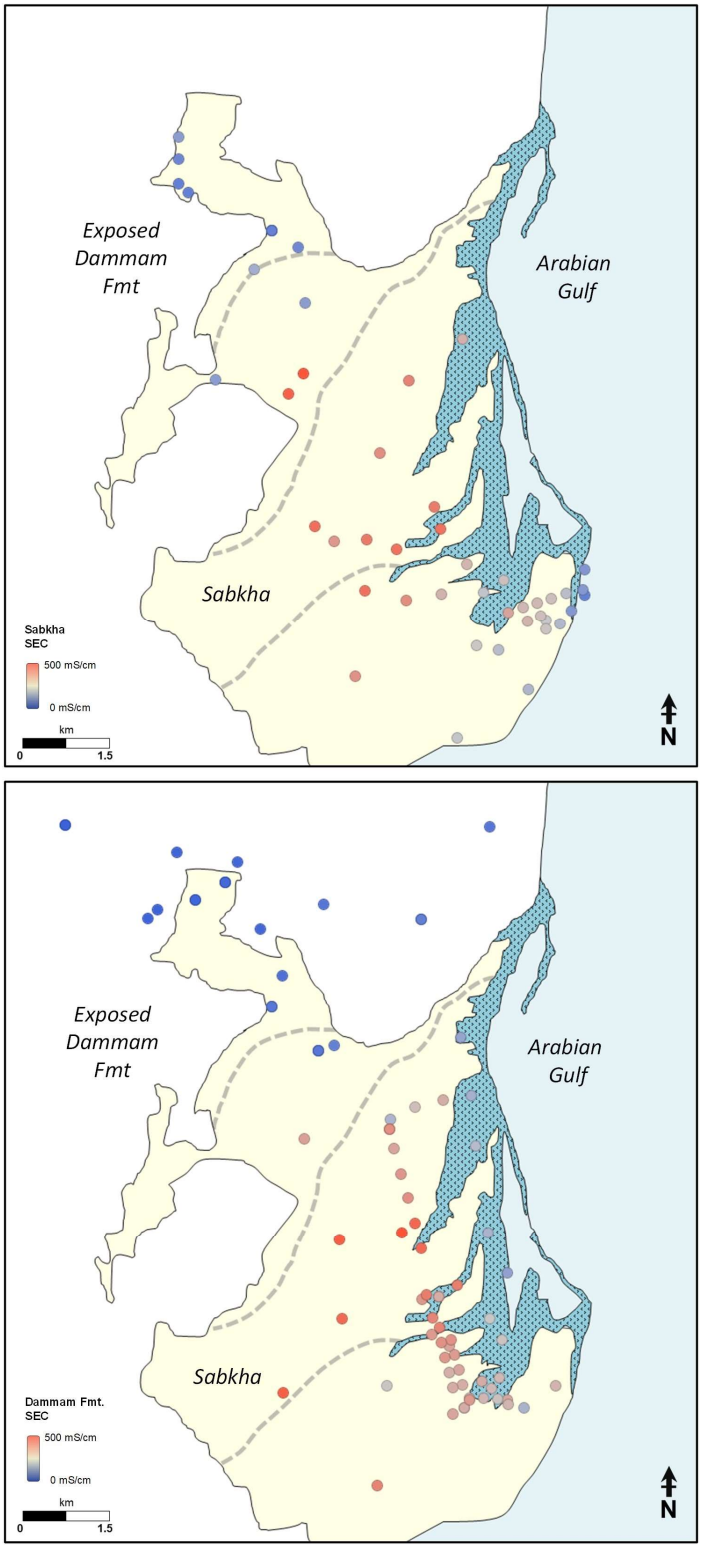

Figure 3-17. Contour map of Specific Electrical Conductivity (SEC) of groundwater hosted within sabkha and the Dammam formation. Dashed line represents irregular intervals. SEC of seawater (SW) is given in italic. The dashed lines represents the loose boundary dividing the sabkha zones.

3.5.2 Spatial distribution

Lateral distribution

The sabkha sediment isomap (Figure 3-17) of SEC shows that there is a progressive increase in the SEC of the brine under the surface of the sabkha from the proximal to the middle sabkha (R^2 = 0.74), and from the coast landward towards the middle sabkha (R^2 = 0.66) (Figure 3-18B). All sabkha pit waters are more saline than sea water. When comparing the lateral sabkha zones, the proximal sabkha shows the lowest SEC (81±47 mS/cm) followed by sabkha water table in the upper sabkha (114±40 mS/cm). However, the $\overline{x}$ SEC for sabkha water table in the lower sabkha is over twice of the sabkha water table (233±74 mS/cm), with sabkha water table in the middle sabkha (400±66 mS/cm) being the most saline (max = 496 mS/cm). The differences in SEC for pit waters within different sabkha zones are statistically significant, with differences between proximal and upper sabkha significant ($p<0.05$), and between the middle-lower sabkha ($p \ll 0.01$).

Within the Dammam Formation, SEC increases in a linear fashion converging from the outcropping Dammam Formation updip and the coast, into the middle sabkha. Waters in the Dammam Formation aquifer underlying the sabkha is lowest in the proximal (52±9 mS/cm), followed by the upper sabkha (66±10 mS/cm), lower sabkha (261±52 mS/cm) and in the middle sabkha (356±64 mS/cm) ($p<0.01$). SEC reaches up to a maximum of 489 mS/cm in the middle sabkha. The SEC isomap (Figure 3-17) highlights an increase of 85 mS/cm per lateral km from the proximal sabkha towards the middle sabkha which has the highest measurements of SEC (up to 490 mS/cm beneath the ephemeral salt flat). Landwards from the salt flat however shows a less sharp gradient of about 40 mS/cm per lateral km. Some 8 km inland, some sites (grouped as *aEU* in Figure 3-18B)) appear to have lower SEC which is indicative of influence of landward system whilst others have very high concentration.

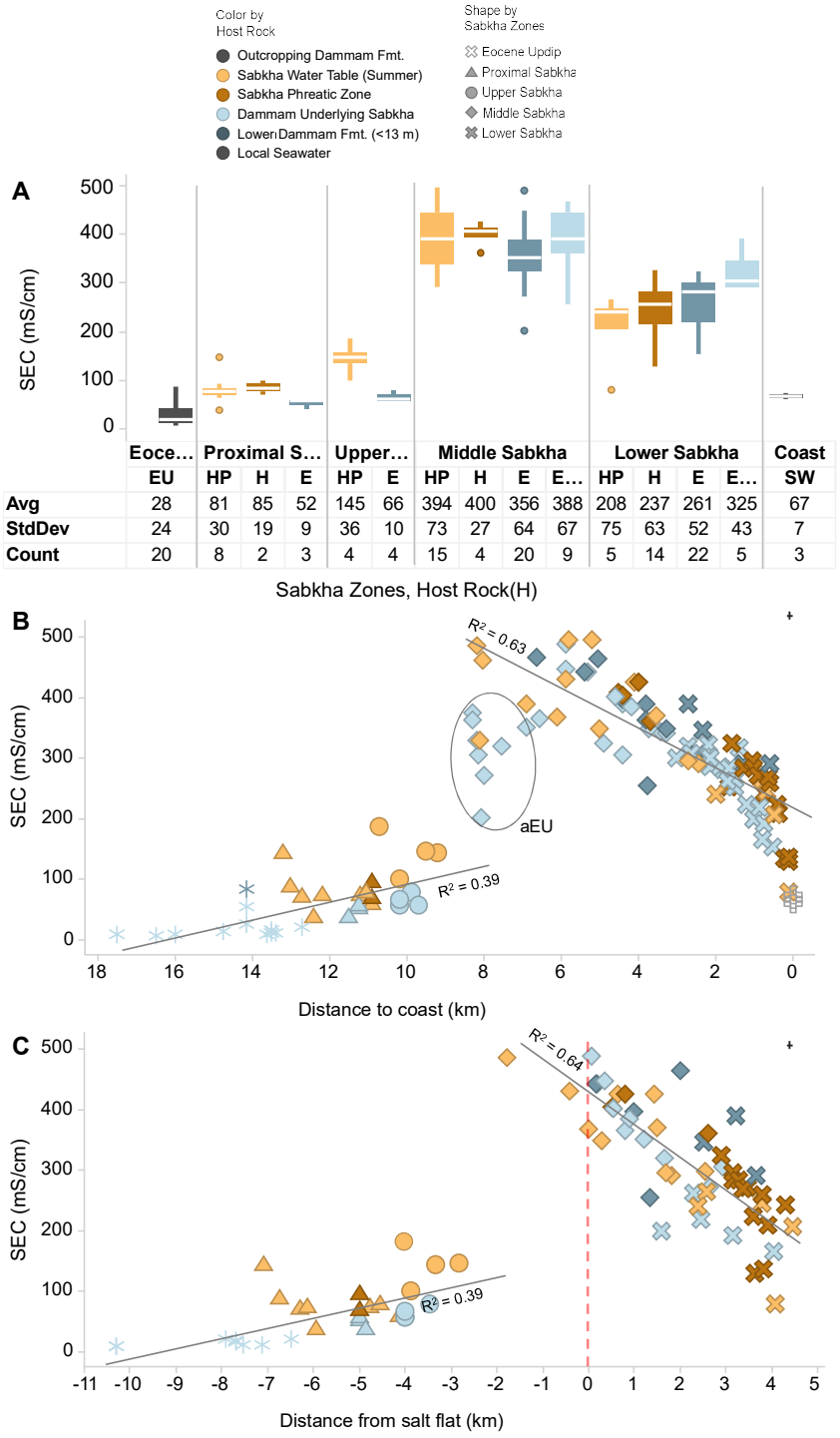

	Eoce…	Proximal S…			Upper…		Middle Sabkha				Lower Sabkha				Coast
	EU	HP	H	E	HP	E	HP	H	E	E…	HP	H	E	E…	SW
Avg	28	81	85	52	145	66	394	400	356	388	208	237	261	325	67
StdDev	24	30	19	9	36	10	73	27	64	67	75	63	52	43	7
Count	20	8	2	3	4	4	15	4	20	9	5	14	22	5	3

Figure 3-18. (**A**) Box plot of SEC subdivided by sabkha zones and the host formation, with end members outcropping Dammam Formation updip (EU) and seawater (SW). Tables highlight mean, standard deviation and count of data. Regression plots below show variation of SEC within sabkha with respect to (**B**) distance from the coast and (**C**) relative distance from the ephemeral salt flat (denoted by red dashed line) with positive distance indicating the south-eastward direction of sabkha progradation and negative distance being the updip of the salina towards the northwest. In both (B) and (C), best fit lines are shown for outcropping Dammam Formation updip and proximal-upper sabkha data set; and for the middle and lower sabkha (in the case of B), the quoted R^2 excludes the 8 outliners labelled (aEU).

Vertical Distribution

In the outcropping Dammam updip, in W7 the waters increase in salinity with depth, with SEC of 25 mS/cm at 2 m below sea level, 55 mS/cm at 15 m below sea level and 85 mS/cm at ~30 m below sea level.

There appears to be differences in the SEC within each formation in the sabkha (Figure 3-19). SEC in the proximal sabkha, upper sabkha and the middle sabkha, waters in the sabkha water table and wells show no statistical significance. However, when we look at two piezometers in the proximal sabkha screened at the sabkha, the shallow sabkha water table M2S (screened at 0.08 m asl) has SEC of 98 mS/cm while the sabkha phreatic zone M2H is 72 mS/cm (screened -1.02 m asl). The proximal sabkha has a low SEC compared to its source updip and since there are no low solubility salts (like halite) for dissolution, we can deduce that the greater SEC is due to evaporation at the surface.

Waters in the sabkha for these three sabkha zones show a greater SEC than in the Dammam Formation ($p<0.01$). This is further proven by piezometer well (M2 at the proximal sabkha) sampled in the summer, which shows that the shallowest sabkha water table is 98 mS/cm, followed by the sabkha phreatic zone (72 mS/cm), and the Dammam Formation well underlying it which is 56-59 mS/cm.

In the lower sabkha, this pattern is not observed. The waters in the pit shows the less saline (208 mS/cm±75) than in the sabkha (237±63 mS/cm) well ($p<0.05$) which shows dilution from recent marine flooding. The waters get more saline in the Dammam (261±52 mS/cm) ($p<0.05$) sabkha but less so than in the deeper Dammam Formation (325±43 mS/cm) ($p<0.01$). This vertical SEC profile within the lower sabkha shows that the associated density of the waters is stable.

3.6 Equivalent Freshwater Head

Static water level h_i (m asl) (uncorrected for density) for all of the sabkha aquifer is above sea level for all seasons. For wells screened within the Dammam Formation underlying the sabkha, the h_i is above sea level, except for the waters hosted within the upper sabkha and some of the middle sabkha.

When comparing between Figure 3-21B and Figure 3-21D, there is clearly a marked difference between h_i and equivalent freshwater head $h_{f,r}$. Using a reference depth z_r of -4 m for all the dataset, $h_{f,r}$ plot reveals that the heads are greater for both in the sabkha and Dammam (nearly 1 m greater than h_i), resulting in overall equivalent freshwater heads to be above sea level. $h_{f,r}$ plot shows that Dammam underlying the sabkha have greater head values than the sabkha as compared to the h_i within the lower sabkha over a zone of 2 km inland from the coast. The deep wells, at least within the middle and lower sabkha, are revealed to have much greater heads than the overlying wells, and this pattern

would not be recognized in using just hydraulic head calculation. The $h_{f,r}$ of the Dammam Formation deep wells are similar to $h_{f,r}$ of the outcropping Dammam Formation wells (13.5 to 15.0 km). These significant differences highlight the importance of using $h_{f,r}$ over h_i.

Figures quoted here use mean sea-level as reference, and corresponding tidal effects are minimal, ranging from ±0.01 to ±0.04. To understand the use of $h_{f,r}$, a greater sabkha $h_{f,r}$ than the Dammam, especially within the proximal, upper, and middle sabkha means that there is potentially a downward flow from the sabkha aquifer into the Dammam aquifer beneath it. Box plots, cross-section plots, and contour maps in Figure 3-20, Figure 3-21 and Figure 3-22, respectively, indicate that there is clear direction of fluid flow across and between the sabkha and the Dammam underlying it.

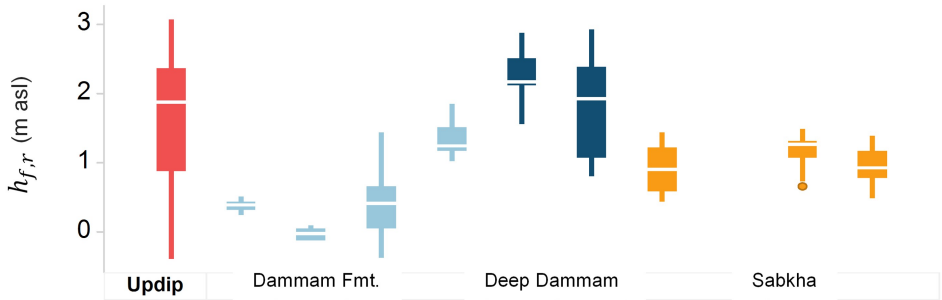

	Updip	Dammam Fmt.				Deep Dammam		Sabkha			
	Eocene...	Pro...	Upp...	Mid...	Low...	Mid...	Low...	Pro...	Upp...	Mid...	Lower...
Avg	1.59	0.38	-0.02	0.41	1.33	2.25	1.82	0.91	0.43	1.18	0.97
StdDev	1.09	0.20	0.11	0.52	0.25	0.40	0.79	0.39	(Em...	0.23	0.28
Count	17	2	4	13	15	9	8	7	1	15	20

Figure 3-19. Box and whiskers plot showing distribution of equivalent freshwater head $h_{f,r}$ within different formations and in different sabkha zones, with tables highlighting mean, standard deviation and count of data (n = 111).

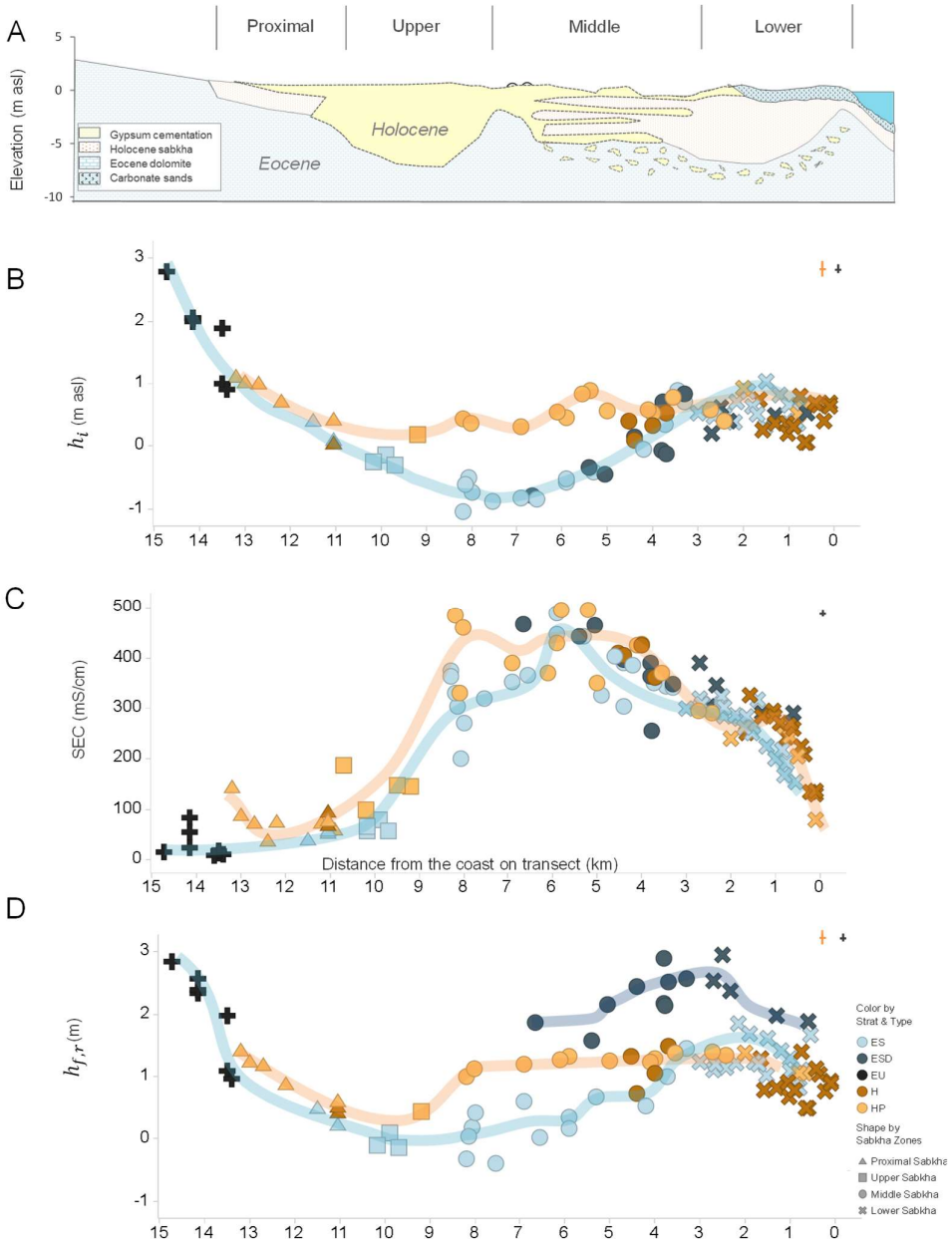

Figure 3-20. Cross-section plots through Mesaieed sabkha in the direction of progradation (to the southeast), to highlight the distribution of (A) stratigraphy and gypsum distribution as recorded in core logs, (B) absolute groundwater head h_i, (C) salinity as SEC, and (D) equivalent freshwater head $h_{f,r}$. Data is trellised by formation, ES - shallow Dammam under sabkha; ESD - deep Dammam Formation underlying sabkha >13 m; EU - Outcropping Dammam Formation updip of sabkha; H - sabkha phreatic and water table. Best fit lines on scatter plot represents average values for waters within sabkha (orange), shallow Dammam (blue), deeper Dammam formation (dark blue). Data is extrapolated perpendicular to the line of section from sampling points up to 500 m from the line of section. Cross indicate analytical uncertainty of data, with orange crosses for sabkha pits.

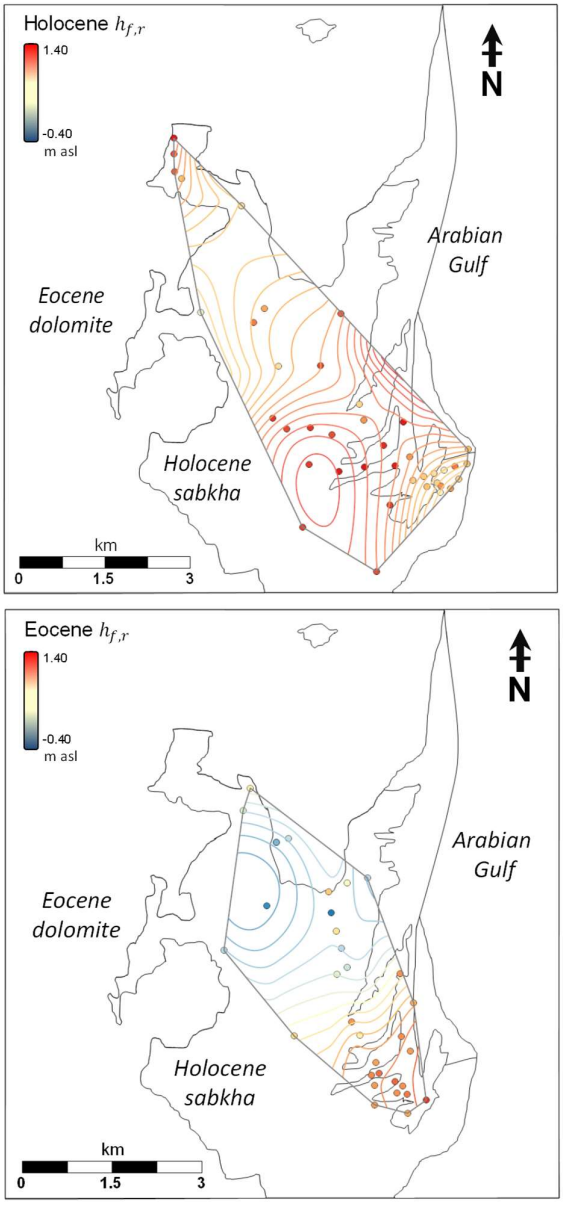

Figure 3-21. Geospatial distribution of effective groundwater head ($h_{f,r}$) with contour lines. Line interval is 0.05 m for sabkha and 0.08 m interval for Dammam.

The potential source of fluids, the outcropping Dammam Formation updip groundwater, has the highest equivalent freshwater head $h_{f,r}$ 1.59±0.39 m. $h_{f,r}$ within the outcropping Dammam Formation updip aquifer is seen to decrease sharply from 15 km to the edge of the sabkha at about 13 km, with gradient of 0.0013.

Within the sabkha, the proximal, upper, middle and lower sabkha $h_{f,r}$ are 0.91±0.39 m, 0.43 m, 1.18±0.23 m and 0.97±0.28 m respectively. When looking at the cross-section plots and maps, there are no systematic trends in the lower sabkha relative to the distance except that it is greater than mean

sea level. Further landward of this zone, sabkha $h_{f,r}$ stays relatively constant and elevated with respect to sea level at about 1.0 m until about 9 km before it drops to its lowest $h_{f,r}$, (0.43 m) within the upper sabkha. While there is only one data point within the upper sabkha, similar low $h_{f,r}$ is observed at 11 km inland in the proximal sabkha. Within the proximal sabkha, the $h_{f,r}$ increases with distance inland to 1.40 m at the edge of the proximal sabkha (lateral gradient 5.3 x 10^{-4}) where approaches that in surrounding updip aquifer. While it appears that sabkha within the proximal and the lower sabkha show similar $h_{f,r}$, the different $h_{f,r}$ observed from adjacent sabkha zones are statistically significant (p-value < 0.05).

Measurements of $h_{f,r}$ within the upper Dammam Formation have averages of 0.38±0.20 m, -0.02±0.11 m, 0.41±0.52 m and 1.33±0.25 m for proximal, upper, middle and lower sabkha respectively. $h_{f,r}$ in the Dammam Formation aquifer is seen to increase inland from the coast to its highest within the lower sabkha, before falling drastically from 3.5 km landwards to about sea level within the middle sabkha and upper sabkha where it stays fairly constant with deviations of±0.3 m. The $h_{f,r}$ then increases slightly into the proximal sabkha, which then increases sharply from the edge of the proximal sabkha boundary into the outcropping Dammam Formation updip aquifer (gradient 0.011).

For the Dammam Formation deeper than 13 m, the average is 2.25±0.40 m and 1.82±0.79 m for middle and lower sabkha respectively. Measurements of $h_{f,r}$ within the deep Dammam Formation aquifer may indicate a semi-confining layer, at least within the middle and lower sabkha. In chapter 2, we see that the shallow Dammam Formation has permeabilities down to 0.01 D.

Overall, it appears that the sabkha show greater $h_{f,r}$ than in the Dammam Formation. When considering each sabkha zone while comparing both the Dammam Formation and the sabkha aquifers, there are clear $h_{f,r}$ gradients whereby the upper stratigraphy has higher $h_{f,r}$ than the lower stratigraphy, which indicates vertical direction of groundwater flow (Figure 3-22).

Piezometers within the outcropping Dammam Formation updip aquifer show $h_{f,r}$ 4.8 x 10^{-3} m (Figure 3-22) per vertical m for the top 15 m of the formation and 0.13 m per vertical meter. In the proximal and upper sabkha, a downward gradient is observed within the piezometers, with vertical gradients of 0.08 m and 2 x 10^{-3} m, respectively. These vertical gradients are thus very steep—compared with lateral gradient between M2 (PS) and M3 (US) of 2.3 x 10^{-4} m in Dammam Formation.

In the middle and lower sabkha where there are no piezometers, two pairs of wells within 150 m proximity of one another which are screened at different depths in each formation were used to approximate the vertical $h_{f,r}$ gradient between the sabkha and Dammam Formation. In the middle sabkha, there is a downward gradient with an average of 0.11±0.05 m per vertical meter, while in the

middle sabkha it appears to be an upward gradient with an average of 0.10±0.03 m per vertical meter, which indicates that the lower sabkha is likely sourced from the Dammam.

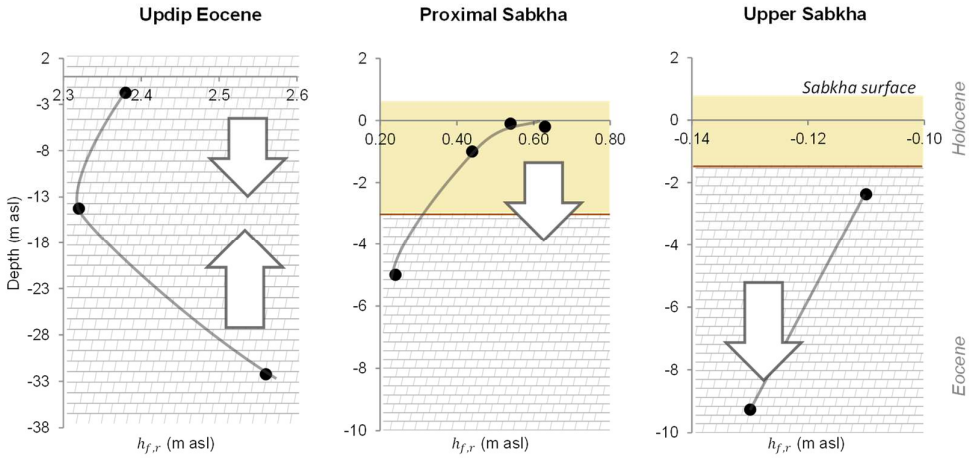

Figure 3-22. Vertical distribution of $h_{f,r}$ in three piezometer wells screened in three spatial zones – the outcropping Dammam Formation (well W7), proximal sabkha (well M2) and upper sabkha (well M3).

3.7 Groundwater Dynamics

Atmospheric pressure effects

BE closer to 0 can be inferred as unconfined water table conditions (at least at the unsaturated zone). High BE (closer to 1) often reflects confined aquifer conditions, which is often a result of fine-grained sediment. Calculations using static water level h_i shown in Figure 3-20 show that the well (well 1E) has a BE of 0.81, while the BE for the Dammam Formation underlying the proximal sabkha (well 2E) is also lower (0.42) than the Dammam wells in the middle (well 105) and lower (well 108) sabkha, 0.72 and 0.79 respectively. BE within the Dammam underlying the upper sabkha (3E and 3ED) are both 0.90. For the Dammam Formation <13 m bsl (well 118) in the lower sabkha, the BE is 0.50. The sabkha phreatic zone within the proximal sabkha (2H) have a lower BE (0.35) than in the middle sabkha (016) with BE 0.46. There was no data available in the upper sabkha. For sabkha phreatic zone within the lower sabkha (009) and within 200m (101 and 105) of the coast the BE could not be determined due to tidal effects affecting the groundwater behaviour being more dominant.

Tidal Effects

Tidal efficiency represents the pore pressure change caused by ocean tides (Merritt, 2004). Analyses are presented in Figure 3-23 and Figure 3-24. Tidal variations in Figure 3-23E show that the Arabian Gulf experiences one high and one low tide of different size every lunar day between the period of 24th February 2013 and 28th February 2013 and this is followed by diurnal cycle until 16th April. This shows that Arabian Gulf seawater experiences a combination of diurnal and mixed semidiurnal tides,

confirming studies by previous workers (Reynolds, 1993; Najafi, 1997). From both these plots (Figure 3-23 and 2-24) it is evident that minor propagation of tidal pressure on using static water level h_i is seen in all wells, and in both formations - affecting the sabkha aquifer more than the Dammam Formation aquifer. Tidal effects have caused fluctuations of about 0.006 m for the Dammam Formation (118) within the lower sabkha, and up to 0.100 m for the sabkha (site 015) <100 m the coast (Figure 3-23).

Within the Dammam Formation aquifer updip, propagation of tidal pressure variation is seen here to extend landward up to 7 km in 1E well (Figure 3-23B), with about 0.6±0.2 % tidal efficiency (TE) and 5.5±0.5 hours of tidal lag (TL) between the crest of the tide to the peak of the water level. For the Dammam Formation-hosted groundwater in the proximal sabkha (well 2E), there appears to be 3.0±0.2% TE with 2.5±0.5 hours TL. In the upper sabkha (wells 3E and 3ED), there appears to be insignificant tidal effects within the Dammam Formation. For the Dammam Formation underlying the middle sabkha (well 105), the TE is 1.9±0.2% with a TL of 10.0±0.5 hours. In the lower sabkha (well 108) the TE within the Dammam Formation drops to 1.5±0.2% slightly (TL 8.0±0.5 hours).

Within the sabkha in the proximal sabkha (2H), the tidal effect is similar to the Dammam, with about 3.1±0.2% % TE (TL 2.5±0.25 hours). The TE for in the middle sabkha is slightly higher (106, 1.6±0.2%) than the lower sabkha (009, 0.9±0.2%). TL for the middle sabkha (106) is 8.0±0.5 hours. For the sabkha well just 500 m inland of the coast (015), the TE is 1.5±0.2% (TL 11.0±0.5 hours).

Recharge and Evaporation Effects on the Water Table

Long-term groundwater monitoring data at Mesaieed that spans the period of recharge was affected by NDP construction. Therefore, we used a site in sabkha Dukhan to understand the effect of recharge on the groundwater level. The site DK2, with elevation of -1.1 m asl, has insignificant surface runoff observed. The sediments consist of mostly siliciclastic and it is located far (~4 km) from the contact with outcropping Dammam aquifer. The shallow well (25.427° N 50.874° E) has a 1 m screen with the middle of the screen at the average water table encountered during field observations and an unsaturated zone is about 0.50 m. The response to recharge is shown at Figure 3-25.

The water table is shown to decrease about 0.60±0.20 mm/day in March 2013 and this increased to 0.75±0.20 mm/day in April 2013. As there was no rainfall, this value can be inferred as the actual evaporation (AE_{to}) of the sabkha porewaters.

Evidence of minor salt dissolution due to rainfall is observed whereby sabkha waters SEC increased sharply by 4 mS/cm during the 14 mm rainfall, from 146 mS/cm to 150 mS/cm before falling to 148 mS/cm (Figure 3-25). During period of no rainfall, we see an increase of SEC of about 0.15 mS/cm per day during the period of May to June 2013, which is evidence of effects from sabkha waters evaporation.

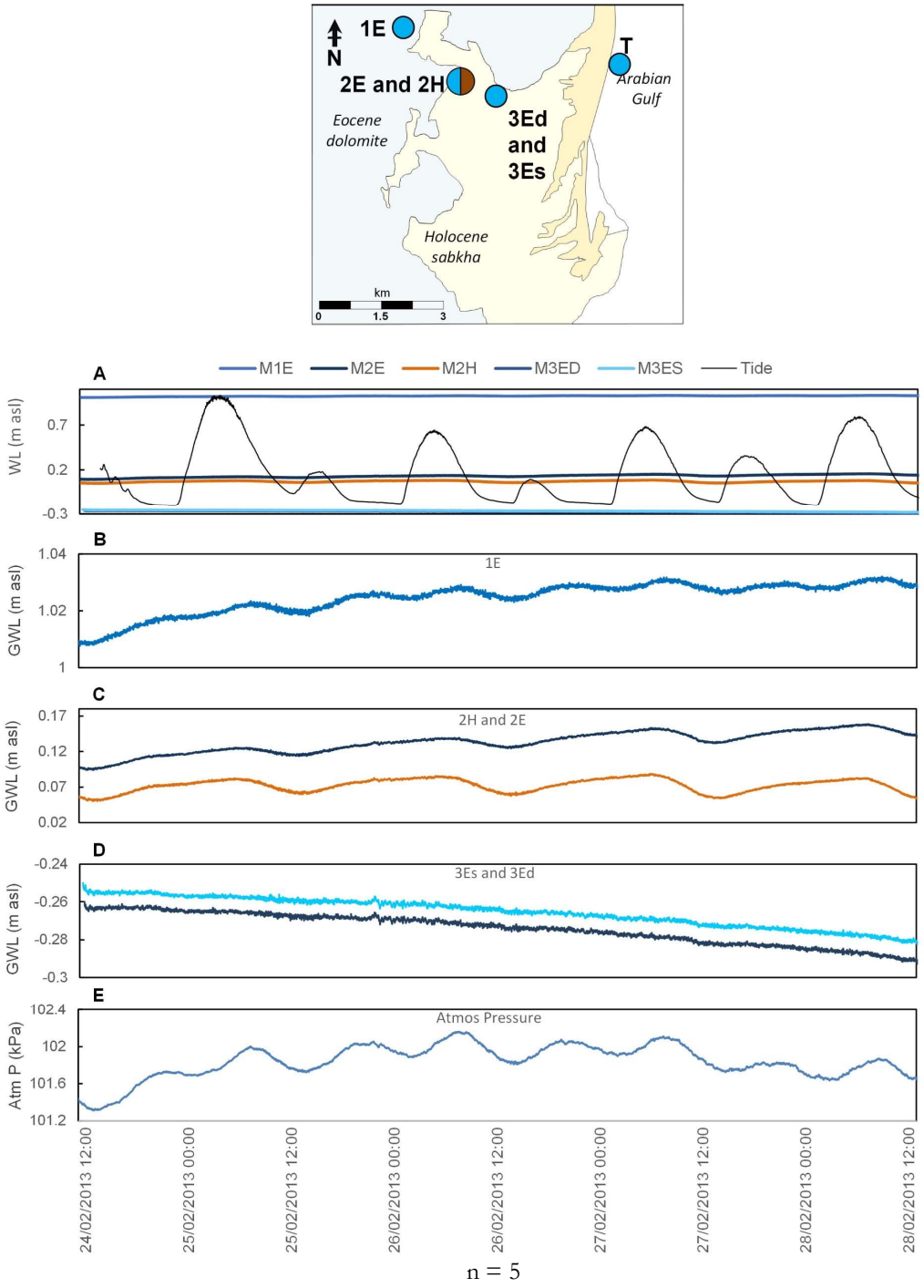

Figure 3-23. Groundwater monitoring network showing borehole hydrographs superimposed on tide data from Mesaieed beach and atmospheric pressure from February 24th to February 28th 2013. Well site number on the right corresponds with well site on the map above. **(A)** shows water level from all wells corrected with barometric pressure, with tide levels from Mesaieed harbour as solid black line, with each piezometer site shown in detail in **(B, C, D)** with salinity as SEC in dashed lines. Graph **(E)** highlights the barometric pressure and air temperature at well 1E. The increase of water level here relates to a local recharge event.

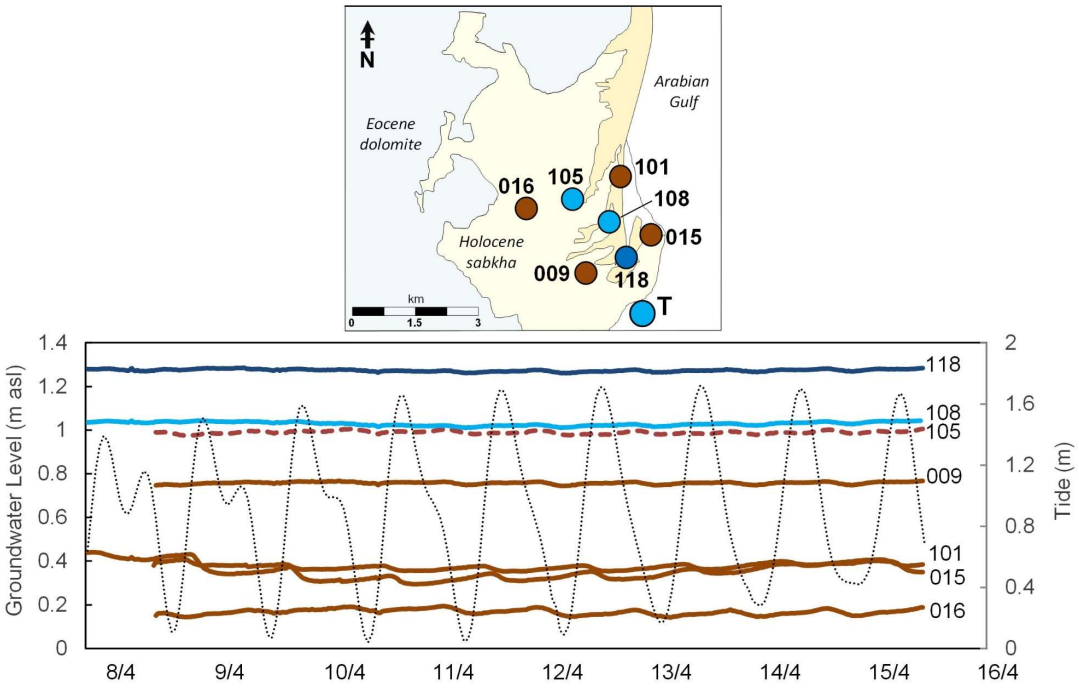

Figure 3-24. Medium resolution (30-minute interval) groundwater level monitoring network corrected with atmospheric pressure between April 8th to April 16th 2012 in the middle and lower sabkha, superimposed on tide data (in dotted black line) from Mesaieed harbour. Well site number on the right side of the corresponds with well site on the map above. The colour of lines corresponds to the formation the well is screened at, sabkha (brown), shallow Dammam Formation <13 m (light blue) and deep Dammam Formation >13m (dark blue). N = 5

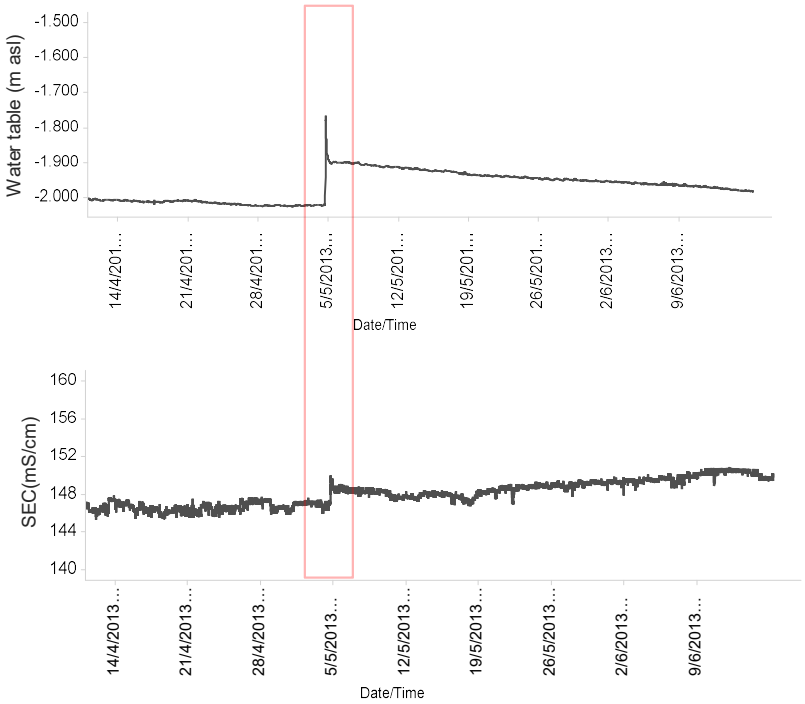

Figure 3-25 Response of groundwater table (barometric effects removed) and SEC at DK2 to 14 mm recharge (on 14th May 2013) highlighted in red box.

3.8 Discussion

3.8.1 Climate Implications on Evaporite Diagenesis

Qatar can be summed as subtropical dry and hot desert climate with highly variable but low annual rainfall, with a large range in maximum and minimum temperatures. Based on Wladimir Köppen's climate classification (Koppen and Geiger, 1930), Qatar is rated as BWh (hot desert). Qatar has an annual average temperature above 18 °C, in which the ratio of precipitation to evaporation is too low to sustain vegetation, or at most a very scant shrub.

The winter months occur between November and February, with the highest temperatures and greater humidity occurring between May and October. In the winter, the climate of the Arabian Gulf is characterised by arid-tropical systems called the 'cold fronts' which generate northwesterly shamal winds (Qatalum, 2010). The summer months see higher temperatures, higher wind speeds, lower visibility, higher total evaporation rate, lower relative humidity and insignificant precipitation.

Driven by low pressure cells with high atmospheric pressure gradients accompanied by strong winds (Pye, 1987), the *shamal* event is capable of mobilising large amounts of sand. The *shamal* plays a factor in not just creating low vapour pressures on surface of the sabkha and hence driving evaporation. It also provides a means for mechanical movement for detrital sediment which can settle in the usually low relief sabkha areas (Purser, 1985).

Groundwaters within sabkha and salina environments are inherently sensitive to solar evaporation due, respectively, to the shallow water table and restricted nature of the basins. The evaporation rate is not dependable only on solar energy (which is indicated by temperature) but also wind and relative humidity on the sabkha surface. Evaporation may play a crucial factor in (1) depressing the groundwater level which creates a hydraulic head gradient forcing marine water or continental waters to flow into the sabkha carrying dissolved salts, (2) raising salinity of groundwater, (3) driving concentrated fluids to supersaturation with respect to particular minerals, creating conditions whereby precipitation can occur.

The sabkha area, with a shallow water table (<0.5 m from the surface) and high evaporation to precipitation ratio, provides a perfect setting for net evaporation of waters. Shamal winds may provide sediment supply to the leeward coast of Mesaieed. Chapter 2 highlighted that progradation is largely a result of spit building related to longshore drift which allows back barrier accumulation of the aeolian sediment. Aeolian sediment that have high proportion of salts may act as nuclei for evaporite precipitation, but based on Chapter 2, the halite and gypsum are less than 5% of the total aeolian mineralogy. Southeasterly winds or a storm surge would push cause marine flooding landward and thus pooling of seawater in depressed parts of the sabkha. Fog may provide the moisture necessary to wet the unsaturated zone and bring surface salts into the capillary fringe if not into the water table. Summer weather

brings in high solar insolation and hence greater evaporation to drive shallow water table and pooled marine waters on the sabkha possibly towards the saturation threshold with respect to dolomite and evaporites.

3.8.2 Groundwater Tracer using Salinity

Mesaieed sabkha is comparable with the specific electrical conductivity (SEC) measured in Abu Dhabi, from 136 mS/cm and up to 445 mS/cm (Sanford and Wood, 2001), except for the proximal sabkha which sees a much lower SEC that is likely due to influences from up-dip meteoric waters. This observation in Mesaieed does not agree with Groot (1973) which highlighted that interstitial brines in Umm Said (south of Mesaieed) is greater in salinity seaward. SEC, related to total dissolved solids (TDS), can be affected by mixing processes (mixing of end-members), evaporation, and water-rock interaction.

SEC analyses suggests that there may be different sources of waters to the sabkha system. It also indicated statistically significant differences between adjacent sabkha zones and similarities within the same sabkha zone. Understanding equivalent freshwater head $h_{f,r}$ validated this hypothesis by highlighting (1) different flow regimes in the proximal, upper, middle and lower sabkha which complements the sabkha subdivision based on diagenetic overprint and primary mineralogy (Chapter 2), and (2) the magnitude of vertical groundwater flux of nearly one magnitude greater than lateral flux. This is difference is remarkably smaller than in Abu Dhabi which has vertical flux about 2 orders of magnitude larger than the lateral flux (Sanford and Wood, 2001), likely due to the greater hydraulic conductivity of our sediments as compared to that in Abu Dhabi.

Groundwater in the sabkha appears to consist of a mixture of two end-members, seawater to the east, and outcropping Dammam Formation groundwater to the west-northwest. The outcropping Dammam Formation updip waters are brackish while the seawater appears to be slightly evaporated. However, the linear increase of SEC within the Dammam aquifer updip of the sabkha indicates intrusion of sabkha waters. An increase of SEC within the Dammam aquifer north of the sabkha indicates seawater intrusion into the Dammam. In the outcropping Dammam Formation updip, it appears that the waters have salinity stratification with depth and are not well-mixed. This may indicate dominance of lateral flow within the outcropping Dammam Formation updip.

The position of the waters relative to the coast, the outcropping Dammam Formation updip, and ephemeral salt flat plays an important role in contributing to an increased SEC. Given the steep change in relationship between SEC in the middle and upper sabkha with respect to the distance to the coast, this suggests that dominant mixing and/or concentration of seawater. This also explains the high SEC in the middle sabkha. Within the lower sabkha, the higher SEC in the sabkha pits highlight the influence of marine flooding input with the fresher sabkha pit waters as compared to the deeper wells.

The increase in salinity observed within the sabkha may be a result of (1) evaporation and in the case of the middle sabkha, it can be due to (2) dissolution of low solubility halite salt. However, high SEC found at the water table in the proximal sabkha where there is insignificant evaporites indicate pore water evaporation and signifies that scenario (1) is more likely for most parts of the sabkha. Waters within the Dammam Formation underlying sabkha are generally fresher than in the sabkha within the proximal, upper and middle sabkha zones, indicating vertical density instability.

The Dammam-hosted waters have been evapoconcentrated throughout the sabkha, with ranges from 4 times that of continental groundwater updip within the proximal-upper sabkha, up to 50 times within the middle sabkha (~7.5 times seawater concentration). SEC within the Dammam underlying the sabkha are substantially higher than source waters, which means that sabkha brines concentrated by evaporation may reflux downward to mix with the underlying aquifer – as

The sharp divide of the SEC distribution between waters hosted in the proximal-upper sabkha and in the middle-lower sabkha reflects different sources of waters, with some mixing possible between the upper and middle sabkha. Such apparent discontinuity between two groundwater groups highlights separate hydrological regimes separated by the salt flat, which may indicate limited lateral groundwater movement and mixing between the two water bodies. This event is possible if vertical permeability is greater than horizontal permeability. Given the relationship of SEC with distance, it appears that the salinity of waters in the middle and lower sabkha is influenced by mixing and concentration of seawater, while the waters in the proximal and upper sabkha is influenced by the mixing and concentration of continental groundwater.

Three observations contradict previous work (Groot, 1973) whereby Groot observed in the south of Mesaieed that there is an increase in salinity downward and seaward – (1) less saline waters in the Dammam underlying the proximal, upper and middle sabkha aquifers, (2) within the same sabkha zones, there is also evidence of greater salinity closer to the water table than in the deeper sabkha, (3) salinity decreases from the middle sabkha to the lower sabkha.

3.8.3 Groundwater Dynamics

Due to the elastic properties of aquifers, both confined and unconfined aquifers that are located close to the coast respond to tidal cycles and atmospheric pressure effects (Lohman, 1979). Unconfined aquifers, especially with a shallow water table, are sensitive to effects of precipitation and evaporation. Wells that were tested are shown in Figure 3-23 and 3-24.

3.8.3.1 Reflux and Convective flow

Groot (1973) inferred that reflux of brines was occurring across the Umm Said sabkha. Vertical differences in head suggests a down-section flow from the sabkha in Mesaieed. High SEC found in the Dammam suggest dissolution of evaporites within the Dammam, or evaporation of fluids in sabkha which reflux downwards. The second scenario is more likely because high SEC is found at the water table of the proximal sabkha (section 3.8) where minimal evaporites are found as compared to the deeper waters in the sabkha.

Brine instability is controlled by the rate of evaporation, permeability of sabkha sediment, and density contrast between water bodies in the aquifer system (Van Dam et al, 2013). Instabilities can be measured by Rayleigh number.

To investigate if free convection flow driven by evaporation occurs within Mesaieed sabkha system, we start with the middle sabkha which hosts the highest salinity brines. The sabkha has an average of thickness at 5 m, has a minimum k of 9.9 x 10^{-15} m^2 (which is the main hindrance to vertical flow). Average brine density for the groundwater hosted in the middle sabkha is 1,170 kg m^{-3}, and hence we can derive $\Delta\rho$ = 145 kg m^{-3} for marine flooding scenario and $\Delta\rho$ = 160 kg m^{-3} for outcropping Dammam Formation updip discharge scenario. We will assume 0.38 for porosity, 0.002 kg/m-s for dynamic viscosity (Al-Amoudi, 1992), and for molecular diffusivity, we will use 1.4 x 10^{-12} m^2/s derived from the brines of similar salinity (Yechieli and Ronen, 1996). The resulting Rayleigh number is approximately 6,400 for marine flooding and 5,800 for outcropping Dammam Formation updip discharge.

For the sabkha aquifer within the proximal, upper and lower sabkha, using $\Delta\rho$ of 30 kg m^{-3}, 70 kg m^{-3} and 80 kg m^{-3}, respectively, and minimum of k of 2.0 x 10^{-12} m^2, 2.0 x 10^{-14} m^2, and 9.9 x 10^{-12} m^2, respectively, this yields a Rayleigh number of approximately 2.4 x 10^5, 1.9 x 10^3 and 5.7 x10^6 for the proximal, upper and lower sabkha subsequently. The Rayleigh numbers for all the Mesaieed sabkha zones are far greater than the commonly used stability criterion of $R_a = 4\pi^2 = 39.48$ (Nield and Bejan, 2006, Nield et al., 2008), thus the system is predicted to be unstable and free convection is expected to occur.

The Rayleigh numbers are about 1-2 magnitudes higher than what was measured in the sabkha system in Abu Dhabi (Sanford and Wood, 2001; Van Dam et al., 2009), with Rayleigh numbers of 3.65 x 10^2 - 4.0 x 10^4. This is due to greater salinity differences occurred within Mesaieed (average about ~400 mS/cm) than in Abu Dhabi (average 1.19 ~286 mS/cm).

Potential factors for instabilities in Mesaieed sabkha leading to free convection are: 1) dense brine overlying less-dense Dammam Formation groundwater driven by near surface evaporation processes

and 2) reflux of higher density waters from surface and near-surface salt dissolution events post-rainfall and post-runoff.

Physical instabilities play a major factor in understanding solute mobility. Short bursts of heavy rainfall can potentially tilt a normally steady state groundwater system by increasing its hydraulic gradient and dissolving the largely dolomitised surface of Qatar and thus mobilising both fluids and solutes. This hypothesis will be explored in Chapter 4.

3.8.3.2 Atmospheric pressure effects

Barometric efficiency (BE) tells us the extent of which atmospheric pressure could propagate through the aquifer (Sanford and Wood, 2001; Spane, 2002). The sabkha phreatic zone within the proximal sabkha (2H) have a lower BE (0.35) than in the middle sabkha (016) with BE 0.46. There was no data available in the upper sabkha. For sabkha phreatic zone within the lower sabkha (009) and within 200m (101 and 105) of the coast the BE could not be determined due to tidal effects affecting the groundwater behaviour being more dominant. Within the proximal sabkha, it appears that the BE for both within the sabkha and in the Dammam Formation is relatively lower than in the middle sabkha. This is likely due to the greater gypsum cementation and fine-grained mud disseminated throughout the unsaturated zone within the middle sabkha (Chapter 2.5). This link can be further elucidated with the very high BE within the Dammam Formation underlying the upper sabkha, in which the sabkha pore spaces is mostly filled by gypsum cementation.

3.8.3.3 Tidal Effects

Tidal efficiency represents the pore pressure change caused by ocean tides (Merritt, 2004). Analyses are presented in Figure 3-23 and Figure 3-24. Tidal efficiency in Mesaieed highlights that minor propagation of tidal pressure is seen in all wells, and in both formations. The tidal effects is slightly more noticeable in the sabkha aquifer than in the Dammam Formation aquifer.

No attempt was made in the present study to apply the relationship of TE to estimate hydraulic conductivity in accordance to Carr and Van der Kamp (1969) due to a lack of information available. However, for the limited sample available, we can deduce that the tidal effects of the sabkha and Dammam aquifers are similar within each sabkha zone (especially in wells 2H and 2E which are piezometric wells). This indicates a more dominant vertical flow component than a horizontal component.

Tidal effects are strongest within the sabkha aquifer closest to the coast (015) and weakest in the outcropping Dammam aquifer, which affects the water level from about ±0.01 to ±0.04. Tidal effects are the strongest within the proximal sabkha, and this may be due to tidal propagation effects from the seawater east of the proximal sabkha through the Dammam bedrock.

3.8.3.4 Recharge and Evaporation Effects on the Water Table

When compared to the average pan evaporation for March at 8.84 mm/day and for April at 16.6 mm/day, this means that AE_{to} in the sabkha is approximate 4.5-6.7 % of PE_{to}, which is at least 50 % greater than what is measured in Abu Dhabi (Sanford and Wood, 2001). This can be hypothesized with increased surface evaporation area. This may also be attributed to sealing of carbonate surface in Abu Dhabi with evaporites and high salinity concentrations in the sabkha (Van Dam et al., 2014).

A 14 mm rainfall, measured by the nearest climate station in Doha some 78 km away, occurred on the 4th of May 2013. Response to this rainfall reveals about 0.13 m of net rise in the water table level was followed by with a decline of 20 mm/day.

Using the period of 3rd March 2013 to 19th March 2013, the water level declines at about 0.7 mm/day while the average pan evaporation for the week was measured as 9.3 mm/day. Dividing the water level changes by pan evaporation rate results in specific yield (Walton, 1970) of 32 % which falls within the average range of 26-33 % range for unconsolidated sand (Morris and Johnson, 1967; Johnson, 1967). By dividing total rainfall for the day by the specific yield, we can get the potential water table rise of the site by 42 mm which contradicts the 120 mm rise seen at the site. This means that it is likely that while nearly 100 % of the rainfall is captured by the sabkha via downward percolation, there may be either (1) water contribution from the outcropping Dammam Formation aquifer (which was likely receiving the rainfall as well) percolating through the Dammam formation, or (2) a localised rainfall greater than 14 mm.

Sharp increase in SEC indicates minor salt dissolution during the 14 mm rainfall. (Figure 3-25) During period of no rainfall, the increase of SEC of about 0.15 mS/cm per day during the period of May to June 2013, which is evidence of effects from sabkha waters evaporation.

3.8.4 Hydrological Budget

Factors that may affect flow components other than evaporation and precipitation include the hydraulic conductivity of aquifer, contact of sabkha zone with the Dammam updip, distance of the sabkha to the coast and the Dammam up-dip, elevation of the sabkha, relative hydraulic gradient of sabkha with the outcropping Dammam Formation updip et cetera.

To calculate the hydrological budget, flow components are first quantified prior to calculating Darcy fluxes from $\Delta h_{f,r}$ with hydraulic conductivity values from Chapter 2 prior to determining volumetric fluxes. Due to the heterogeneous nature of the permeabilities within the sabkha and the Dammam, the smallest permeability will be used to quantify vertical flow (Sanford and Wood, 2001). This is because that layer is likely to impede flow up or down the system.

We can assume a linear system and develop the budget for a cross-section, which based on the direction of propagation, is oriented NW to SE of about 12 km in length (from Figure 3-2). This will have a unit width of 1 m and sabkha thicknesses that range from 4-9 m. There is geometric justification of considering a 1 m wide slice of the sabkha, especially within the middle and lower sabkha. However, the proximal and upper sabkha is surrounded by outcropping Dammam Formation up-dip. Therefore, runoff and drainage possible from the north and the east of outcropping Dammam into the sabkha. Therefore, since it is inherently a 3D system, as we shall see below, we will consider inflows from both the west and the north Dammam Formation.

Lateral fluxes will be calculated from the Dammam up-dip into the sabkha and from the lower sabkha towards the coast. Within the sabkha, the vertical fluxes will be considered using piezometer wells and since the lateral fluxes are insignificant it will be ignored. In the middle and lower sabkha where there are no piezometers, two pairs of wells within 150 m proximity of one another which are screened at different depths in each formation were used to approximate the budget.

Porewater evaporation is assumed to help balance the budget within the proximal and upper sabkha through two scenarios: (1) salinity increases in the summer leads to a lower water activity, and thus lowers the porewater evaporation; (2) during periods of no rainfall, water table should decrease at a rate equivalent to the rate of evaporation divided by the specific yield of the aquifer (Sanford and Wood, 2001), hence this increases the vadose zone thickness which will leads to a lower potential porewater evaporation. Within the middle and lower sabkha, the amount of input from marine flooding will depend on the saturation level of the vadose zone which dictates the amount of seawater input to the groundwater. Thus, marine flooding will be used to balance hydrology budget.

Undoubtedly uncertainties will exist from (1) range of hydraulic conductivities, (2) averages in evaporation and precipitation, and (3) averaged flux values or representative values from wells (head variability can be up to 10 %). However, with using Darcy's Law we can at least quantify the relative flux components to demonstrate the relative inflow and outflow balances in the hydrologic budget.

Calculations of Darcy fluxes, the hydraulic conductivity used and resulting volumetric fluxes are shown on Table 3-1.

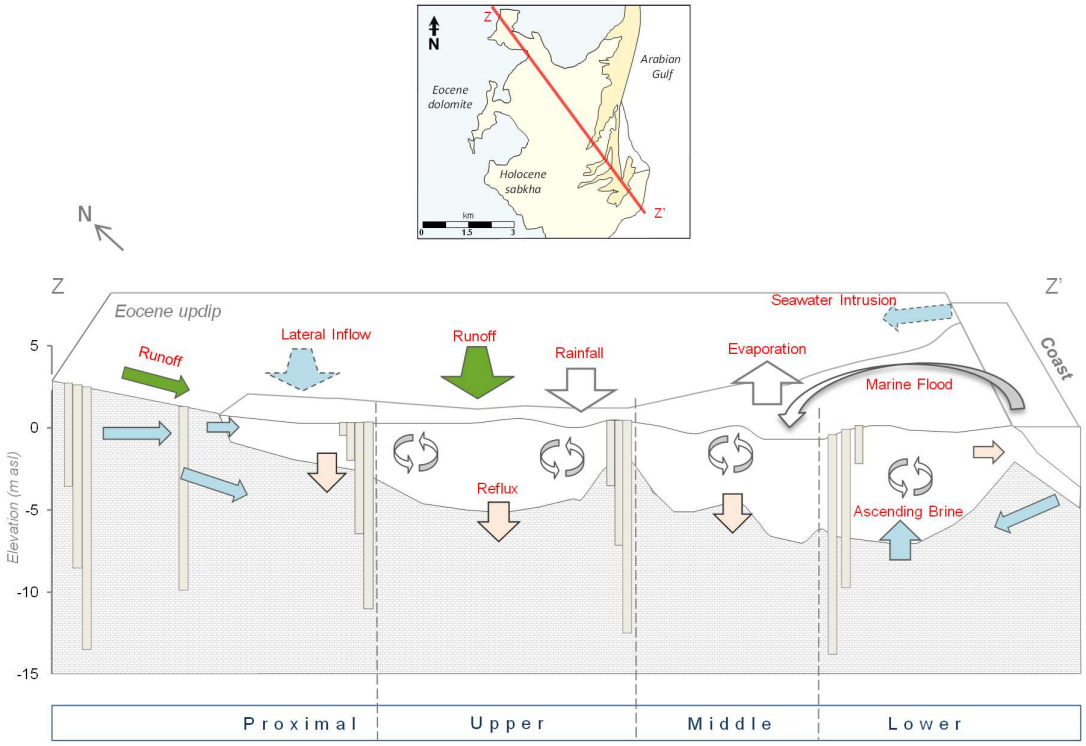

Figure 3-26. Components of hydrologic budget in Mesaieed with blue arrows showing subsurface flow within the Dammam, green arrows showing overland runoff and beige arrows showing outflow from the sabkha.

Table 3-1. Table of hydrology budget calculations.

	Outcropping Dammam proximal to Proximal Sabkha	Outcropping Dammam up-dip North to Upper Sabkha	Middle Sabkha	Lower Sabkha Outflow
Lateral Flow				
Site #	M1E, M2H	W7, W6	-	S07, Coast
Hydraulic Gradient	-3E-04	-9E-04	-	1E-03
Hydraulic Conductivity (m/d)	2E+01	6E+01	-	9E+00
Darcy Flux, q (m/yr)	2E+00	2E+01	-	-4E+00
Thickness (m)	3.5	4.5	-	6
Volumetric Flux, Q (m^3/yr)	7	89	-	-10
Vertical				
Site #	M2E, M2H	M2E, M2H	25, B149	S07,118
Hydraulic Gradient	4E-02	4E-02	8E-03	-4E-02
Hydraulic Conductivity (m/d)	4E-03	4E-03	9E-04	9E-04
Darcy Flux, q (m/yr)	1E-02	1E-02	-2E-02	-2E-02
Length (m)	2500	4000	3000	3000
Volumetric Flux, Q (m^3/yr)	36	58	60	-60

3.8.4.1 Outcropping Dammam Formation updip

From the $h_{f,r}$ within the outcropping Dammam Formation updip formation, and the density stratification seen in W7 – we can assume that lateral flow is dominant. The proximal and upper sabkha are surrounded by the outcropping Dammam Formation updip on three sides. We can thus expect lateral flow from the Dammam up-dip in the west and in the north, towards the proximal sabkha, and from the Dammam up-dip in the north towards the upper sabkha.

3.8.4.2 Proximal-Upper Sabkha

The inflow components in this section include rainfall, runoff and flux from outcropping Dammam updip. The volumetric flux from rainfall is the product of 1 m width of the section, annual mean rainfall (0.04 m/year) and the proximal-upper sabkha section length of about 6,000 m, which yields 240 m^3/yr. The runoff into the sabkha can be estimated at roughly 22% of the annual rainfall in Qatar (Eccleston, 1981), which yields 53 m^3/yr.

Subsurface inflow of meteoric groundwater from western outcropping Dammam aquifer to the east of the sabkha is 7 m^3/yr while from the northern up-dip aquifer is 270 m^3/yr. The outflow component includes the downward flux from the sabkha sediment into the Dammam of about 36 m^3/yr within the proximal sabkha and 58 m^3/yr within the upper sabkha. The potential pore evaporation from this section of the sabkha is estimated to be 1200 m^3/yr, based on a conservative estimate of ~4.5% of 4.4 mm/yr along the section length and width. However, using evaporation to balance the hydrology budget this yields about 642 m^3/yr of water for the sabkha aquifer for the section.

3.8.4.3 Middle Sabkha

The volumetric flux from direct rainfall for the sabkha section length of about 3,000 m is about 120 m^3/yr. The outflow components are the downward reflux which is about 60 m^3/yr and evaporation of 655 m^3/yr.

The lower topographies (~0 m asl) of the middle sabkha means that overland flow driven by high tides can occur, which allows more volume of seawater to be retained within the sabkha as compared to the lower sabkha.

Using satellite imagery, the volume contributed by marine flooding up to the middle sabkha can roughly be quantified by assuming a frequency of flooding events of 6 times a year. Based on DEM maps and for a given high tide and observations by Jameson during such event (verbal comm.), we assumed 0.1 m height of marine waters above the middle sabkha surface, on the basis of tidal height and minimum elevation. Most of this water returns to the sea when the tide ebbs, and thus using GIS, we can approximate the waters retained by dividing the polygon of frequently observed areas subjected to floods by the area of the sabkha zone, which is about 20% of the surface area. The depth of the actual retained water varies depending on depth of local depressions. This observed flooding at the

surface means we can assume that the vadose zone is saturated (with porosity 0.4). Using the mean vadose thickness along the section of about 0.65 m, the potential fluid flux is about 4740 m^3/yr.

However, to balance our current hydrology budget, the influx from marine flooding will be a minimum of 595 m^3/yr.

3.8.4.4 Lower Sabkha

The inflow from precipitation for this section length of about 3,000 m is 120 m^3/yr, and ascending flux from the Dammam (60 m^3/yr). The outflow components include minimal lateral outflow to the sea (25 m^3/yr) and evaporation (655 m^3/yr).

The lower sabkha elevation is about 1-2 m greater than in middle sabkha. Using the same method as the last section, we estimate about 10% of the surface area in the lower sabkha that gets filled by about 0.05 m of residual marine floods. With an average vadose zone thickness of 0.4 m and porosity of 0.4, this yields a potential marine source of 3,000 m^3/yr. A minimum of 50 m^3/yr is required to balance the hydrology budget. In the Dammam, there appears to be a lateral inflow out to the coast of about 10 m^3/yr.

Table 3-2. Table of solute budget calculations by different sabkha zones. Blue boxes indicate inflow while red boxes indicate outflow

Proximal	Q Flux (L/yr)	TDS (kg/L)	Solutes (kg/yr)	**Upper**	Q Flux (L/yr)	TDS (kg/L)	Solutes (kg/yr)
Rain	80000	0.0006	48	Rain	160000	0.0006	96
Runoff	53000	0.0006	31.8	Runoff	53000	0.0006	31.8
Dammam	270000	0.02	5400	Dammam	180000	0.047	8460
Reflux	94000	0.053	4982	Reflux	60000	0.086	5160
Evaporation	309000	0	0	Evaporation	333000	0	0
Total			**-500**				**-3400**

Middle	Q, Flux	TDS	Solutes (kg/yr)	**Lower**	Q Flux (L/yr)	TDS (kg/L)	Solutes (kg/yr)
Rain	120000	0.0006	72	Rain	120000	0.0006	72
				Ascending Brine	60000	0.10	6000
Marine Flood	595000	0.04	23800	Marine Flood	50000	0.04	2000
Reflux	60000	0.25	15000	Lateral Outflow	25000	0.2	8072
Evaporation	655000	0	0	Evaporation	655000	0	5000
Total			**-8900**				**-3000**

3.8.5 Solute Budget

To quantify loss of solutes from the system, we can quantify the solute budget of the inflow components using total dissolved solid measured with the method explained in Section 3.2.7. As halite

is not found in aeolian sediments, aeolian-derived salt will be insignificant in the budget. The calculations are shown on Table 3-2 for the same section length of 11,000 m and 1 m width.

Using equation 3-16, there appears to be about net gain in 500 kg of solutes (Table 3-2) within the proximal sabkha.

We can semi-quantify the vertical thickness of gypsum precipitation we can expect over a sabkha zone, using ^{14}C age date model from Chapter 2. Gypsum, with a density of 2320 kg/m^3, tends to precipitate when TDS (total dissolved solid) of the sabkha waters is about 0.13 kg/l (which will be shown in Chapter 4). The uncertainty in evaporite estimation will be from: (1) assuming that hydrology and solute fluxes remain unchanged over the period of sabkha progradation; (2) saturated vadose zone from marine flooding, the salts may have dissolved and retreat to the coast and/or into the low elevation middle sabkha; (3) aeolian processes could possibly remove some of these surface salts, especially in its early phase of precipitation. As the proximal sabkha waters is below the gypsum precipitation threshold, only the upper, middle and lower sabkha will be discussed.

With about 3,000 kg of solutes surplus within the upper sabkha, this equates to 0.75 kg/year/m^2. Using mineral density ϱ of 2320 kg/m^3 for gypsum and 2160 kg/m^3 for halite, we would expect a layer of gypsum with a thickness of 1.9 - 2.3 m or halite of 2.1 - 2.4 m thick since its deposition in the last 6,000 years. As only minor halite is observed in the field, we shall focus only on gypsum. With an average porosity ($\emptyset$) of 0.4 (Jameson and Puls, in press), this means about 4.8-5.8 m of sabkha thickness would have been partially-cemented by gypsum. Since the average thickness of the upper sabkha is 4 m, what this means is that the whole upper sabkha is expected to be completely cemented by gypsum. This confirms the current observation today where the upper sabkha is cemented by gypsum from the surface to the bottom, with interbedded gypsum layers in between. The erosional remnants observed in the upper and middle sabkha (Section 2.15) appear to account for the excess gypsum cementation not seen today, which are the antecedent topography of surface crusts (see Chapter 2) relative to the modern Stokes surface.

Estimation of gypsum precipitation assumes that there is only an input flux with no output towards the sea or the surrounding Dammam aquifer, and the latter is confirmed by insignificant lateral movement within the upper sabkha to the surrounding sabkha zones (Section 3.9.4.2). H_{fw} data also shows us that the equivalent freshwater head is the lowest in the upper and middle sabkha zone indicating that input into these sabkha zones significantly dominates the output.

The middle sabkha aquifer shows a greater annual gain in solutes, at about 8,800 kg (2.93 kg/year/m^2). Using mineral density ϱ of 2320 kg/m^3 for gypsum and $\emptyset$ of 0.4, we would expect a sabkha thickness of 12.6 to 19.0 m cemented by gypsum in the last 4,000-6,000 years. Sabkha thickness in the middle sabkha range from 4-8 m and only about 40 % of the pore spaces are cemented by gypsum.

The lower sabkha appears to a surplus of 7,000 kg of solutes a year. However, to maintain the solute budget it will need ~7 m of sabkha be cemented by gypsum in the last 1,000 to 3,000 years. There is no erosional remnant and the average sabkha thickness is 6 m.

What this means for the middle and lower sabkha is that the solute budget is not at a steady state. As there is no observed outflow using equivalent freshwater head data (Figure 3-26, Table 3-1), this means that the solutes should increase with time (Sanford and Wood, 2001), concentrating the brines within the sabkha.

Within, water rises upward onto the lower sabkha surface driven by both evaporation and greater head pressure from the Dammam, the solutes are assumed to be deposited as evaporite salts even after accounting for the outflow drainage. The insignificant amount of evaporite observed on the on the sabkha surface and within the pits indicates that these salts were dissolved during marine flooding or rainfall events, which reflux back down to the water table.

Using an upward flux value of 0.02 m/year, this means that about 60 m of brine would have ascended into the lower sabkha in the last 3000 years. Using porosity values at 40% and 9 m of mean sabkha thickness, this means that about 16 pore volumes of brine may have sourced the lower sabkha. This is double of the pore volumes observed in Abu Dhabi sabkhas (Sanford and Wood, 2001), which is due to lower hydraulic conductivity values. Conservative element Br data is limited to shallow sabkha pit waters. However, we can use Br from our solute budget to check with our hydrologic budget. Br in the top 0.5 cm of the lower sabkha is ~4 times of the seawater. This means that a total of about 4 pore volumes of marine flooding would have sourced the lower sabkha in the last 3000 years. This assumption implies a closed and a one-way system. The difference between the pore volume numbers highlight that marine flooding is crucial in sourcing the sabkha aquifer, at least at the water table.

Using the total hydrologic outflow of approximately 2100 m^3/year, we can estimate using the sabkha volume of 61,000 m^3, that the residence time of the sabkha waters is about 30 years. For the solute residence time of the solutes, we can calculate using the average porosity of 0.4, mean TDS values of the proximal (66 g/L), upper (90 g/L), middle (246 g/L) and lower (150 g/L) sabkha to derive a total of 3.7 x 10^6 kg solutes that are currently contained within the sabkha. Using the solute budget of 15,200 kg/year, this yield approximate 245 years. The solutes residence time is approximated to be nearly 8 times the hydrologic budget, which indicates that the brines within the sabkha is likely homogenous from mixing, similarly to those seen in sabkhas in the Abu Dhabi.

3.9 Conclusion

Quantifying groundwater flow systems is important to understanding fluid movement in the subsurface. The key importance of this study is the attempt to capture the sabkha groundwater flow components from a broader perspective. This includes understanding the climate and considering interactions between the waters hosted within deeper underlying aquifers and the updip meteoric aquifers.

Mesaieed is about 25% lower humidity than Abu Dhabi in the summer months, has about 30% lesser rainfall and is located on the leeward side of the prevailing wind. This aridity, combined with the siliciclastic nature of sabkhas and greater hydraulic conductivity, allows for the sabkha to be highly responsive to hydrologic events, such as rainfall, and also evaporation, compared to sabkhas in Abu Dhabi. Evaporation of pore waters is twice as high as that of Abu Dhabi evidence from time series water level data.

The drivers of flow within the sabkha system include evaporation, rainfall, lateral flow within the Dammam Formation, marine flooding, density-driven refluxes, ascending brine, and minor runoff. Empirical evidence using equivalent freshwater head and SEC as tracer confirms that the groundwater within both sabkha and Dammam formations is flowing from two different sources; outcropping Dammam Formation groundwaters and seawater via marine flooding and likely from the Dammam (in the lower sabkha). Brackish meteoric waters from the outcropping Dammam Formation updip discharges laterally into the proximal and upper sabkha, either as surface runoff or through the permeable aquifers. Seawater appears to enter laterally from the coast through the more permeable Dammam underlying the lower sabkha and equivocally through percolation from the surface through seasonal marine flooding events.

The hydrogeology model derived from field data shows vertical flow of approximately one order of magnitude greater than lateral flow and that Rayleigh number shows that there is brine refluxing as a result of evapoconcentration of waters from the shallow sabkha. Lateral groundwater input from the outcropping Dammam Formation is important in sourcing the proximal and upper sabkha, while vertical flow dominates the sabkha and Dammam aquifers. For the proximal, upper, and middle sabkha it appears that downward flow is the dominant vertical component whereas upward flow into the lower sabkha from the Dammam is the main vertical component.

While barometric effects and tidal effects tell us the nature of the aquifer, their magnitudes are very small relative to the spatial differences in groundwater head (less or equal than 3 % of change in head Δh) Recharge, although rare, can give greater effects on two timescales, instantly and over several weeks. This demonstrates the necessity of correcting water levels before calculation of $h_{f,r}$.

In summary, the unsaturated zone of a sabkha is highly dynamic and responds to rainfall events quickly, which allows infiltration through the unsaturated zone. Salts on the surface or within the unsaturated zone are subject to undergo minor dissolution during rainfall. This inference may be important for calculation of solute budget especially in areas with high solubility evaporite minerals such as halite, but for Mesaieed this is insignificant.

In response to lateral hydraulic gradient by evaporation in sabkha, the solute budget indicates precipitation of minerals is likely driven by evaporation at the water table. This results in lowering of equivalent freshwater head and increasing brine salinity. The evapoconcentrated brines result in density instability and followed by reflux in most parts of the sabkha. In the lower sabkha this is not the case. Ascending brines dominate the vertical flow which allows the sabkha to increase in solutes over time. However, as gypsum precipitation is insignificant in the lower sabkha and is only limited to surface crusts, this means that the brines in the lower sabkha are increasing in concentration over time.

The importance of any groundwater head correction are often overlooked in major textbooks and papers (Simmons, 2005). This is the first study to attempt to understand groundwater flow in a sabkha system within a theoretical framework with necessary corrections of density referenced to well screen depth, using methods adapted from Post et al (2007). Groundwater level in a well varies over time and can be affected by barometric pressure, recharge, seasonal affects, local or regional pumping, earth and ocean tidal fluctuations, evaporation effects, and surface water fluctuations. Being a coastal sabkha with relatively permeable units, it is expected that some tidal influences would be felt landward. The extent of the tidal influence, requiring simultaneous monitoring of groundwater level wells in a sabkha system and the adjacent sea, has not previously been investigated.

Given the distribution of equivalent freshwater head $h_{f,r}$, the flow in the lower sabkha of Mesaieed agrees with the 'ascending brine model' theory proposed by Sanford and Wood (2001), in which upward leakage provides the source of solute. However, the evidence of evaporation-driven descending brine is observed in most parts of Mesaieed, which does not fit this model. The model based on the Abu Dhabi sabkha rests upon the assumption that the flow components within the updip of the sabkha (landward) would be the same with the lateral outflow (Sanford and Wood, 2001). These conclusions are not consistent with the budget fluxes for Mesaieed hydrology. This new model is based on hydrogeology data that are accessible in the outcropping Dammam Formation updip. The Mesaieed sabkha, although smaller than Abu Dhabi sabkhas by about one order of magnitude, highlights the heterogeneity in fluid and solute flow within a sabkha system.

As there is a mixture of evaporation-driven reflux flow within the proximal-upper-middle sabkha and an ascending brine recharge in the lower sabkha, I propose an empirical model of the hydrology of Mesaieed sabkha that is based on '**mixed evaporative-driven**' model. Upon examination of the hydrology models of Mesaieed, as well as comparison to the well-studied Abu Dhabi sabkha, there is

no single flow system in any one sabkha or within the sabkha system. Different sites within the same sabkha may be subject to different flow systems, depending on the distance to the coast and the outcropping Dammam Formation. At any one time, one flow mechanism may dominate but the dominance of different flow systems is also likely to change through time, subject to shifting conditions such as sea level and climate, as well as diagenetic changes in porosity and permeability. The new hydrological framework will provide a proxy to understanding geochemical evolution of the brines in Chapter 4.

4 Geochemistry of Mesaieed Sabkha

Author Contributions: Waters were sampled by the author while analysis was done by the author in University of Bristol and Scientific Analysis Laboratories (SAL). Additional samples and analysis were provided by NDPP to the author for analysis. Co-author Professor Fiona Whitaker critically reviewed this manuscript and provided direction during the progress of the writing. Didi Ooi Sher is the lead author of this chapter and is responsible for the data mining, data collection, statistical analysis and interpretation, subject to the above caveats. All figures were created solely by the author unless specified.

18,076 words

4.1 Introduction

Study of saline near-surface water bodies, like Mesaieed, warrants a special treatment of groundwater chemistry due to the variations in sabkha system relative to space and time (Post and Abarca, 2009). Previous studies of sabkhas have focused largely in the Abu Dhabi region. In Abu Dhabi, the geochemistry of sabkha pore waters and sediments has often been studied to understand dolomitization (Hsü and Siegenthaler, 1969; Butler, 1969; Groot, 1973; McKenzie et al, 1980; Illing and Taylor, 1993, Geske et al, 2015), but rarely have these studies addressed evaporite precipitation. An exception to this is the study by Gunatilaka (1990, 1991) for the Sabkha Al-Khiran in Kuwait.

Saline clay authigenesis is driven by the same evolving saline hydrology that forms evaporites (Warren, 2016). However, associated arid clay diagenesis and seasonal effects on sabkha brines have not been previously been studied with regards to water-rock interaction processes. Clay formation is commonly observed in downdip areas of the prevailing Shamal wind (Warren, 2016). Occasional dust storm which were observed to rapidly infill depressions with detrital clay sediments in Mesaieed sabkha (Chapter 2). Additionally, attempts to understand the system as a whole, the source waters and the waters hosted in formations underlying the sabkha, or mass-balance quantification of water-rock interaction, is rare. Existing sabkha geochemical studies often present just molar concentration of major ions (Groot, 1973; Illing and Taylor, 1993; Al-Youssef, 2003; Basyoni and Aref, 2016) and occasionally use isotopes in their interpretation (McKenzie et al., 1980; Wood et al., 2002), but molality and molar activity, phase diagram and thermodynamic potential were very rarely integrated in our understanding of sabkha aqueous geochemistry.

Evaporation is widely recognized as an important driver of converting normal coastal plains into sabkha (see Chapter 2 and 3; Babel and Schreiber, 2014). Evaporation factor, the ratio of Chloride, Cl, of the sabkha relative to that of seawater Cl, can be used to ascertain the extent of evapoconcentration (evaporation-driven concentration) of the brine. However, the majority of studies mentioned earlier used Cl as their reference ion to understand the loss of other ions into the system. The limitation to this method is that little effort has been done to ascertain the degree to which Cl behaves in a conservative manner.

In Qatar, geochemistry of coastal sabkhas have been studied in the northwest (Illing and Taylor, 1993), Sabkha Faishakh and in Umm Said, located in the south of Mesaieed (Groot, 1973; Al-Youssef, 2003). These studies provide a broad hydrogeochemical characterization in relation to dolomitization. Groot (1973) inferred that the sabkha brines are stagnant, based on the high salinity. Chapter 2 clearly highlights that there is movement of brine between the sabkha and the Dammam aquifer, in both the proximal and lower (coastward) zones. Both workers offer contradicting conclusions on the movement of solutes: Al-Youssef (2003) inferred that the proportion of Na and Cl increases landward and that

there is a seaward discharge through the sabkha (assuming the Dammam was impermeable), while Groot (2003) hypothesised that recharge into the sabkha comes from the seawater. Groot's (1973) study was focused on implications of sabkha system to dolomitization. He highlights that the loss of Mg ions is due to recent dolomite precipitation that is unrelated to reflux of porewaters. In addition, chloride concentration from just 5 wells and 5 pits in Groot (1973) inferred that the sabkha is "saturated, or almost saturated with halite", rather than using actual thermodynamic calculations to quantify potential of precipitation relative to halite minerals. Al-Youssef (2014) mentioned that high concentrations of Ca and SO_4 ions may facilitate the formation of gypsum. The work attributed the main source of these two ions to gypsum dissolution process with a secondary source from carbonate dissolution. This conclusion was made based on high concentrations of the ions without establishing geochemical mass balance thermodynamic calculations or an attempt to compare with the input waters to quantify these processes.

The goals of this chapter are to understand the key factors in the formation of gypsum cements in the Mesaieed sabkha system and any associated mineral precipitation (such as dolomite and clay precipitation). Here we present a high-resolution geochemical study of multiple zones within a single coastal sabkha to understand how brine chemistry varies along flow paths and within the sabkha and the adjacent aquifer both laterally and vertically (for example mixing, evaporation, water-rock interaction). From our previous hydrogeologic study (Chapter 3), we can expect our source and thus the composition of fluids surrounding Mesaieed sabkha to differ between the landward (proximal and upper) zone and the seaward (middle and lower) zone. Such an understanding is important to evaluate the water-rock interaction processes affecting the concentration of solutes and the input waters, both continental and coastal waters, vary spatially and temporally.

The methodology undertaken for this chapter is to investigate the geochemistry signature of waters within the sabkha in different spatial zones and how it behaves in the sabkha aquifer and the underlying Dammam Formation aquifer. We will then compare with the sabkha geochemistry to the Dammam aquifer and seawaters—both updip aquifer and sea water. Capturing the geochemical signature of the sabkha waters allows us to understand: (1) whether the modern sabkha groundwater has the chemical potential to precipitate or dissolve gypsum and, thus, whether gypsum observed within the upper and middle sabkha is a product of relict process operating in the past or an ongoing process; (2) what other associated diagenetic reactions are occurring within the sabkha and in the underlying Dammam Formation that are likely affected by fluids sourced from the sabkha and (3) what are the controls on the reactions and what the spatial distribution tells us about dominant processes relative to the source waters.

4.1.1 Study Area and Stratigraphic Framework

The distribution of groundwater chemistry in Mesaieed was evaluated both laterally and vertically, on the basis of our understanding of the fluid sources and flow paths from the previous hydrological study (Chapter 3). As described in Chapter 1 and 2, Mesaieed sabkha is about 6 - 10 km wide, 3 to 15 m thick coastal plain consisting of an onlap prograding wedge of sabkha sediments which overly and partially-confined groundwater within the permeable Dammam bedrock. Gypsum is observed to cement both the vadose and phreatic zones extensively in the upper and middle sabkha. The sediments get progressively younger in the southeast direction from our calibrated ^{14}C study (Chapter 2).

Mesaieed sabkha, located south of Doha, is divided into four spatial zones: (1) proximal sabkha (PS), the inner continental sabkha adjacent to the exposed or outcropping Dammam Formation that occurs updip from the sabkha; (2) the upper sabkha (US), where gypsum is cemented from the surface to the base of the sabkha; (3) middle sabkha (MS), the central part of the sabkha where gypsum cementation occurs intermittently with depth, possibly reflecting relict water tables and (4) the lower sabkha (LS), within 3 km of the modern coastline (Figure 4-1).

The predominant mineralogy in the sabkha is siliciclastic, with increasing carbonate grains towards the coast. Diagenetic minerals consists of primarily gypsum ($CaSO_4.H_2O$) with minor dolomite ($CaMg(CO_3)_2$) and calcite ($CaCO_3$), with minor halite and clay (refer Chapter 2), and hence the major water-rock interactions can be described by the stoichiometric equations presented in Chapter 1.

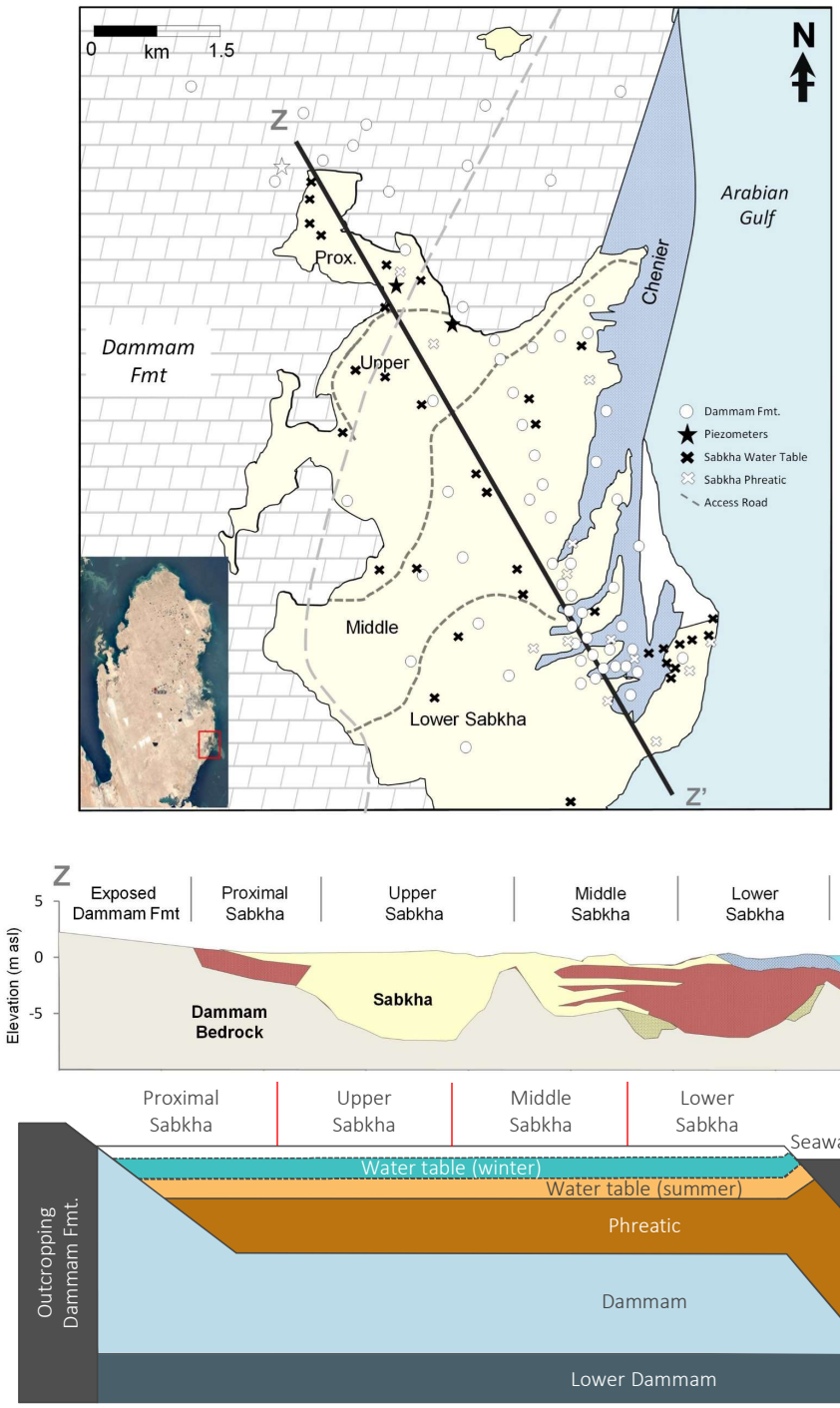

Figure 4-1. Map plan of spatial zonation subdivided by dashed line used in this study (**A**) showing well locations with legend indicating which stratigraphy the waters were sampled from. Solid line traversing NW-SE highlights the cross-section Z-Z' shown below (**B**). Bold italic denotes the formations. The second cross-section of Z-Z' from Figure 4-1A showing the hydraulic flow units or sub-aquifers that are being studied in detailed for this chapter. These sub-aquifers are based on the stratigraphy (sabkha - water table and phreatic zone; Dammam: outcropping or exposed Dammam Fm. that occurs updip from the sabkha, Dammam underlying the sabkha and Lower Dammam)

4.2 Methodology

Across Mesaieed, four types of waters were sampled: seawater, sabkha at the water table, rainfall, and groundwater that are hosted in both sabkha and Dammam aquifer. The sampling sites include vertically nested piezometers of sabkha-hosted waters (Figure 4-2A, 4-2B): wells screened at the Dammam Formation (Figure 4-2C); using hand-dug pits accessing the water table in the sabkha sediments (Figure 4-2D). Wells from the deeper Dammam aquifer were screened at deeper than 13 m below the top Dammam paleosurface. The 13 m cut-off differentiates the Dammam Formation into the shallower highly fractured and jointed stratigraphy (Chapter 2) and the deeper stratigraphy that typically does not observe such dissolution features weathered upper formation and the tighter lower formation as determined by regional permeability study (see Chapter 2).

All the samples were taken in the summer, in June 2013 (this study) and June to August of 2011 by NDP. 10 waters from the sabkha pits were taken in the winter (October 2012 and February 2013) for seasonal comparison. Deep waters hosted within the Dammam formation (< 13 m below surface) underlying the middle and lower sabkha were opportunistically sampled on NDP wells.

After drilling and casing of the groundwater monitoring wells (n=6), they were left for a month to stabilize before sampling of pH, salinity, heavy metals and volatile organic compounds to check for contamination. All samples have VOC < 0.1 µg/l, heavy metals element < 0.005 mg/l, except for boron (an important constituent in siliciclastic due to the preference to concentrate in clay minerals).

Figure 4-2. Field photos: (A) 2.0 mm width slots being sawed in PVC pipe used for wells in sabkha. (B) Installation of slotted PVC pipe into sabkha with sledgehammer to minimize sediment disturbance. (C) Preparation of water sampling through a flowthrough cell (arrow). (D) Process of in-situ measurements of the chemistry at water table in a freshly dug sabkha pit (arrow)

Groundwater sampling was carried out using a low-flow pumping method from piezometers and existing observation wells according to stabilization criteria set out in the USGS National Field Manual (2010). Groundwater was pumped slow at the rate of <0.001 L/s with a Van Walt Geopump2 peristaltic pump through a pre-rinsed polyethylene tube and on the surface the samples were immediately passed through a flowthrough closed cell system (Figure 4-2C), modified from Garske and Schock (1986), in which field parameters (section 4.2.1) were determined. Seawater samples were sampled from Mesaieed coastline about 100 m away from the Mesaieed beach. Sabkha vadose zone waters were obtained from digging of pits until the first sight of porewater is observed.

4.2.1 Field Geochemistry

Well installation specifications were detailed in Chapter 3. These wells were left to stabilize for one month prior to sampling of its pH, salinity, heavy metals, volatile organic compounds (VOC) to test for contamination. All samples have VOC < 0.1μg/l, heavy metals element < 0.005 mg/l

Parameters that were analysed in the field, pH (± 0.01 pH units), temperature (± 0.1°C), specific electrical conductivity (SEC, ±1 μS cm^{-1}) and dissolved oxygen (DO, ±1.5%) used Hach HQ40d multi-parameter meter. The meter probes were standardized using pH 7 and 10 buffers, SEC standard of 12.88 mS/cm and 111.3 mS/cm and calibrated in 100% O_2, respectively. For samples under >200mS/cm, field SEC measurements with the 4-pole graphite sensor were backed up by determinations after dilution in the field lab with deionised water using a high precision micropipette. These values compared with those determined with downhole multi-logging probe YSI 600XLM in-situ confirmed no change in chemistry composition.

Dissolved oxygen is temperature dependent and thus it varies with temperature. DO concentrations are then corrected with temperature and ionic composition of the waters based on equation of state and experiments described by Sherwood (1992, 1991) to study its variation independent of the two parameters.

Bicarbonate alkalinity samples were stored in glass in a cooler and were analysed in triplicate within two to four hours post-collection, using inflection-point (Gran) titration, which is more suitable for seawater or water with low carbonate concentrations than the more widely used colorimetric method (USGS, 2010). The Gran method, used a calibrated Hach IntelliCAL™ pH probe to measure the pH change, with addition of the 0.01 M HCl acid to bring the sample to titration point at pH 4.5 using high precision micropipette. The volume of acid added is then used to calculate the alkalinity (HCO_3^-) with an error±0.20%. For rainfall samples (n=2) with a pH lower than 4.5, alkalinity was calculated using ion balance error, assuming zero analytical error for all other ions.

High-density polyethylene (HDPE) bottles were triple rinsed with sample before being filled up to the top with a meniscus level to exclude any atmospheric interaction during temporary storage and

transportation. Samples for cation and anion analyses were prepared by pressure-filtration through 0.22 μm Millex®GP Milipore Express PES cellulose nitrate membrane filter into a pre-rinsed HDPE container before being stored at <4 °C. Primary filtration using 0.45 μm cellulose nitrate filters was used if there was a high proportion of suspended sediment in the raw samples, before a second filtration using the 0.22 μm filters.

4.2.2 Laboratory Geochemistry

Given the high TDS concentrations, most samples were diluted with Milli-Q water by weight using a calibrated four decimal point balance, with error from dilution being 0.20 %. Analyses for major cations (Na^+, Ca^{2+}, Mg^{2+}, K^+) was undertaken ICP-AES Agilent 710 while major anions Cl^-, Sr^-, Br^- and $SO4^{2-}$ were measured via Dionex ICS-5000. B, Ba, and Al were analysed by Gulf Labs using US EPA 3005/6010C method (SMWW, 2012). Analytical errors associated with each ion is presented in Table 4.1. Uncertainty is obtained by running blanks and a select few samples across the TDS range six times. Alkalinity has a relatively very low uncertainty, and this is due to alkalinity being measured on-site undiluted. This data is supplemented by raw data made available for this research by NDP, after careful evaluation of data quality using IBE (see section 4.2.4).

Table 4-1. The analytical uncertainty for the major ions including errors from dilution (except for bicarbonate which was not diluted).

Elemental Ion	My PhD Analytical Uncertainty (%)	NDP Analytical Uncertainty (%)
Sodium (Na^+)	0.76	0.98
Chloride (Cl^-)	1.05	1.21
Calcium (Ca^{2+})	0.90	1.08
Sulphate (SO_4^{2-})	1.34	1.29
Magnesium (Mg^{2+})	0.64	0.76
Potassium (K^+)	1.20	1.16
Bicarbonate (HCO_3^-)	0.20	0.87
Strontium (Sr^{2+})	1.28	1.35
Bromide (Br^-)	1.56	1.98
Boron (B)	1.80	2.0
Silica (SiO_2)	0.98	1.26
Aluminium (Al^{3+})	0.91	1.17

4.2.3 Statistical Analysis of Variance

To understand the correlation between pairs of variables, linear regression plots were used with least square regression calculated, presented in a form of R^2. However, to further understand the statistical significance of differences between values for a single variable from different groups of samples, laterally (within different sabkha zones) or vertically (parts of stratigraphy in which the water is hosted), statistical analysis of variance (SAV) methods such as parametric analysis of variance (ANOVA) or non-parametric analysis of variance (Kruskal-Wallis) were used. For ANOVA to be used, the criteria

are that the data must be normally distributed, and the variances of the separate groups are equal; if not then the Kruskal-Wallis method will be employed. Analysis of variance assesses whether to accept or reject the null hypothesis (H_o), which is that all variables distributed within different groups (Lehmann and D'abrera, 1975) are not statistically significantly different. To do this, a p-value is calculated, which is a probability that measures the evidence against the null hypothesis. Statistical tests for our dataset were carried out with a business intelligence TIBCO® Spotfire software, using an add-on Data Relationship tool, the significance is reported as probability (p) with two high confidence levels of 99% and 95%. A very high confidence level of 99% indicates a 1 % risk of interpreting that a statistically significant difference exists when there is no actual difference (false positive). Based on this analysis, only variables where significant differences are calculated will be discussed and presented.

4.2.4 Uncertainty Analysis

Ion balance error (IBE), or sometimes called charge balance error, is used to check the accuracy of major ion analysis, based on the neutrality of waters which means that the sum of positive and negative components should be balanced (Appelo and Postma, 1993). It is important to note that IBE is a relative error, rather than an absolute error. This is calculated where the concentrations of cations and anions are expressed as meq/l;

$$Ion\ Balance\ Error\ \%\ (IBE) = \frac{(\sum cations + \sum anions)}{(\sum cations - \sum anions)} \times 100 \quad (4.1)$$

IBE of±2 % are generally considered inevitable in most analysis (Appelo and Postma, 1993) representing the effect of analytical errors. An error of±5-10 % is considered acceptable in groundwater analyses (Nielsen and Nielsen, 2006). Samples with IBE greater than±10 % were excluded from further analysis. Most of the samples were less than±5 % mean of IBE was 0.52±2.94 %. Higher IBE commonly occurs in analysis of samples with lower ionic strength or near instrument detection limits, such as those of the outcropping Dammam Formation aquifer, and therefore IBE of up to 15 % have been included for those subset of samples (n = 5). For these samples, the positive errors are likely due to higher concentrations of cations than anions. Possible causes for ion imbalances may be lab errors, dissolved solutes that are not measured or contaminated samples that may contain particulate matter. As the errors were not systematic, therefore lab errors during analysis are excluded. Historic samples from Ports were included provided their IBE was less than±5 %.

Total fractional errors ($\sum fe$) associated with the XS calculations, saturation index, and pCO2 were calculated using the following root mean square error formulas where the absolute is the sum of all fractional errors (fe);

For adding or subtracting: $$\sum fe = \sqrt{fe_{\mathrm{A}}^2 + fe_{\mathrm{A}}^2 + fe_3^2 + \ldots fe_n^2} \quad (4.2)$$

For multiplying or dividing: $$\sum fe = \sqrt{\left(\frac{fe_A}{A}\right)^2 + \left(\frac{fe_B}{B}\right)^2 + \left(\frac{fe_C}{C}\right)^2 + \ldots fe_n^2} \quad (4.3)$$

4.2.5 Dimensionality Reduction with Unsupervised Learning

Piper trilinear diagrams are commonly used to explore the brine evolution of the sabkha, but it has limitations in that it can only classify up to 4 variables. Sabkha system that is highly dynamic requires a more robust statistical analysis, like PCA, to capture as many variables as possible for a first-pass exploratory analytics.

Deriving regression and important information from an interrelated but large complex dataset is facilitated by dimensionality reduction statistical technique, called principal component analysis (PCA). PCA is an unsupervised learning, a subset of machine learning, that attempts identify associations between variables by understanding the extent of variance. This pattern recognition method was applied here to the geochemical composition of the groundwater using $decomposition.PCA$ function in the Scikit Learn library in Python (Pedregosa et al., 2011). This was carried out by orthogonal transformation of data to a new set of variables that focuses on variances, called principal components (PCs) in which the first-derived component retains the majority of the variation present in all the original variables (Jolliffe, 2002). This is akin to finding Euclidian distances using Singular Value Decomposition (SVD) or K-Means technique.

Due to the different units of measurement and the large range spanned by some elements of the dataset (up to four order of magnitude), a variance scaling is performed to give each variable equal weight in the analysis. For the variance to be within the same order of magnitude between each set of variables and thus contributing equally to the analysis, the variables are normalized by subtracting the mean of each value from the measured variable and then divide each value within the variable by its standard deviation (Chen et al., 2007, Moore et al., 2009). This also ensures that the data is re-centered so that the mean is zero.

The resulting calculated principal components are defined as eigenvectors of the correlation matrix of the data. They denote correlation coefficients in the form of loadings between each variable and its corresponding PC (Moore et al., 2009). The scree plot of eigenvalues helps with identifying the number of principal components needed. To characterize the system in our data, each line is described by the values in the respective columns. If all these lines were to be represented in a single chart, there will be a plot in hyperspace with as many axes as there are columns in the data and as many points as there are lines in the data, in which all the points together will form a 'cloud'. PCA allows us to understand the shape of this 'cloud' and most importantly the portrayal of the positions from where we

should look at the 'cloud' to see it at its largest significance of interest. For example, from which angle does the 'cloud' look the biggest and that the variability of the data is the greatest.

The importance of such positions forms PC 1 which accounts for the greatest variance observed in the correlation matrix and the second most important forms subsequent principal component (PC 2) and simulating with PC 3 to PC n. The inclusion of further PCs is determined by the value of its eigenvalue, in which should be above 1 for inclusion (Cattell and Jaspers, 1967). A simplification to interpreting PCA is that it is based on finding which variables are most strongly correlated with each component. Thus, the higher the component loadings for a variable, the greater the influence that the variable has on that principal component. Loadings that are positive indicate they show a direct relationship, whilst negative loadings indicate an inverse relationship.

4.2.6 Analytical and Numerical Geochemical Modelling

To understand potential for the groundwater to precipitate or dissolve host rocks, we need to identify its activity potential. The saturation indices (SI) relative to a mineral indicates whether the waters sampled in that space and time have the thermodynamic potential to dissolve or precipitate the minerals. The aqueous geochemical speciation code PHREEQC version 3.3.12 (Parkhurst and Appelo, 2013), was used to determine the distribution mineral saturation state (log (IAP/*K*)), partial pressure of CO_2, aqueous species, and ion-activity products. All the sabkha waters are above >130‰, hence thermodynamic database PITZER was used for geochemical modelling (Plummer et al, 1988). Saturation indices for gypsum is calculated as such;

$$IAP = (mCa^{2+})(mSO_4^{2-}) \tag{4.13}$$

$$K_{sp_{gypsum}} = [Ca^{2+}][SO_4^{2-}] \tag{4.14}$$

$$SI_{gypsum} = log\left(\frac{IAP}{K_{sp_{gypsum}}}\right) \tag{4.15}$$

Positive SI with respect to an individual material implies a supersaturation relative to the source mineral and that it has a potential to precipitate, while negative SI indicates an undersaturation state and no precipitation will occur and that it will remain as solutes. It is noteworthy that waters may remain supersaturated with respect to a material phase if kinetic factors limit the rate of precipitation. It may also remain undersaturated and if it has not been in contact with that material, no dissolution can occur. Even if there is presence of that material, dissolution rate can be limited by kinetic factors.

Dolomite is the prime example of facing kinetic barriers in limiting its formation, and this problem is due to factors including (1) extremely low concentration and activity of carbonate ion (Lippmann, 1973), (2) high hydration energy of Mg ion (Zhang et al., 2012; Roberts et al., 2013) and (3) presence of sulphate (Kastner, 1984; Morrow and Ricketts, 1988; Wang et al., 2016).

The amount of water-rock interaction that a fluid has already been involved in can be examined using Ca_{XS}, SO_{XS}, and Mg_{XS} calculated relative to concentrations predicted from conservative processes (Whitaker and Smart, 1990, 2007, McClain et al., 1992). The excess or depletion (negative excess) of ions relative to concentration calculation from the simple dilution or mixing, or concentration of solute sources, provides direct evidence for reactions between gas, dissolved solutes and mineral phases.

XS was calculated using chloride as a chemically conservative tracer. This assumption is reasonable since lithologies on Mesaieed are primarily quartz, gypsum, carbonate and dolomite. It will be tested by comparing Cl^- and Br^-. Hydrological studies (and subsequent analysis of geochemical data) suggest a groundwater divide at 7 km from the coast. At sites <7 km from the coast we thus use average seawater composition as a source, and at sites >7 km inland we use averaged updip groundwater from wells in the Dammam Formation as a source. Thus, for example $SO_{4\,XS}$ can be expressed as

$$SO_{XS} = SO_{4\,i} - \frac{SO_{4\,o} \cdot Cl_i}{Cl_o} \tag{4.16}$$

Whereby $SO_{4\,i}$ is the molar concentration of sulphate in the sample, $SO_{4\,S}$ is the average sulphate concentration in the source water, and $Cl_i \,/\, Cl_S$ is the ratio of chloride in the sample to the chloride in the source water. Negative values for SO_{4XS} indicate a sink of SO_4, for example potential to precipitate of gypsum, whilst positive values indicate dissolution of gypsum. If a water is depleted in both Ca_{XS} and SO_{4XS} in a 1 to 1 molar ratio, it is likely that the gypsum has precipitated out of the water, whereas positive Ca_{XS} and SO_{4XS} suggests that gypsum has dissolved. In either case, a 1:1 relationship suggests no other reactions add or remove SO_4 or Ca from the water.

4.2.7 Activity Phase Diagram

While calculations of XS tells us the extent of the loss or gain of solutes, phase diagrams show which minerals may have reacted with groundwater. Activity phase diagrams presented here comprise of four components of the system Mg-Ca-SO_4-HCO_3. The Mesaieed system can be readily represented in two dimensions as a function of log [aCa/aMg] and log [a^2SO_4/a^2CO_3]. Phase diagram of log [aCa/aMg] and log [a^2SO_4/a^2CO_3] for waters from the different sabkha zones show the relative stability of carbonate and evaporite minerals at 25 °C and 1 atm as a function of the molar activities of Ca, Mg, SO_4 and CO_3 of the waters. Activities of Ca, Mg and SO_4 are primarily driven by precipitation and dissolution processes, while the activity of CO_3 is driven by pH and the magnitude of CO_2 dissolved in groundwater, in the form of pCO_2. Phase boundaries between dolomite, calcite and evaporites are derivatives of (1) equilibrium rate constants (k) of water-rock interactions and (2) ionic activity of the associated aqueous elements (a) (Moore, 2010);

$$\log k = \log\left(\frac{a_{product}}{a_{reactant}}\right) \tag{4.4}$$

For calcite-dolomite phase boundary using equation 4.4:

$$\log k_{calc-dolo} = \log\left(\frac{a\ \mathrm{Ca}^{2+}}{a\ \mathrm{Mg}^{2+}}\right) = 0.38 \tag{4.4}$$

Gypsum-calcite phase boundary can be derived from equation 4.6:

$$\log k_{gyp-calc} = \log\left(\frac{a^2 {SO_4}^{2-}}{a^2\ {\mathrm{CO_3}}^{2-}}\right) = 7.99 \tag{4.6}$$

While the gypsum-dolomite boundary is derived from (4.7) in the following steps:

$$\log k_{gyp-dolo} = \log a\ \mathrm{Ca}^{2+} + 2\log a^2\ {SO_4}^{2-} - \log a\ \mathrm{Mg}^{2+} - \log a^2\ {\mathrm{CO_3}}^{2-} \tag{4.7}$$

$$\log k_{gyp-dolo} = \frac{\log a\mathrm{C}^{\ 2+}}{\log a\mathrm{Mg}^{2+}} + \frac{\log\ {}^{2}{SO_4}^{2-}}{\log a^2{\mathrm{CO_3}}^{2-}} = 8.37 \tag{4.8}$$

Rearrange the formula (4.19) in the form of $y = mx + C$.

$$\log\left(\frac{a^2 {SO_4}^{2-}}{a^2{\mathrm{CO_3}}^{2-}}\right) = -\log\ \left(\frac{a\ \mathrm{Ca}^{2+}}{a\ \mathrm{Mg}^{2+}}\right) + 8.37 \tag{4.9}$$

Activity of CO_3^{2-} is a function of pH ($\log(H^+)$) and the amount of dissolved CO_2 in the water, which can be represented by;

$$H_2CO_3 \leftrightarrows 2H^+ + CO_3^{2-} \tag{4.10}$$

Or in the logarithmic form to represent the K,

$$\log K_{H_2CO_3} = 2\log a_{H^+} + \log a_{CO_3^{2-}} - \log a_{H_2CO_3} \tag{4.11}$$

$\mathrm{Log}\ K_{H_2CO_3}$ has value of -16.68, $a_{H_2CO_3}$ can be represented by $K_{CO_2}.p\mathrm{CO_2}$ (Drever, 2002), $\log K_{CO_2}$ thus has a value of -1.47, and $\log a_{H^+}$ is pH, thus the equation can be rearranged with the substituted K values which gives,

$$\log a_{CO_3^{2-}} = \log P_{CO_2} + 2\ \mathrm{pH} - 18.15 \tag{4.12}$$

Equation (4.23) shows how $a_{CO_3^{2-}}$ relates to pH and pCO_2 for each sample. The log k values are all derived from Plummer and Busenberg (1982).

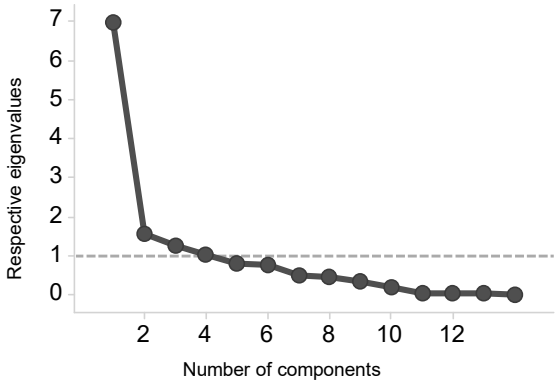

Figure 4-3. Scree plot of the PCA eigenvalues and component number. Dashed horizontal line intersecting at eigenvalue of 1 indicating insignificance. For PC loadings see Table 4-2.

4.3 Exploratory Data Analyses

4.3.1 Principal Component Analysis (PCA)

PCA is calculated for the geochemistry dataset including concentration of anions and cations, pH, temperature, dissolved oxygen (DO) and also the distance from coast (zCoast). The scree plot (Figure 4-3) highlights a sharp drop in eigenvalues from the first PC to the second. The first three PCs (6.14, 1.55, and 1.30, respectively) make up a total 64% of the variance observed, which justifies the eigenvalues of a three-component solution. PC loadings that are sufficiently large, i.e. which show a high correlation between the PC and individual variables, are highlighted in table 4.2. A threshold of ±0.4 is found to the most reasonable number to delineate variations meaningfully. Within PC 1, pH and HCO_3 are highly correlated with strong positive loadings, while temp, Na, Cl, SO_4, Mg, K, Br and B are highly correlated with strong negative loadings. The association between the latter is as expected from evaporative concentration. Na and Cl have the highest negative loading which indicates the strongest control of variances in the system, suggesting their relative conservative behaviour, followed by K and Mg. In PC 2, only pH and Ca are positively correlated, while B and distance from the coast are correlated with a negatively loading, which indicates that there may be a driven of pH and Ca simultaneously by its distance away from the coast. Ca is not observed in PC 1 which suggests that the dominant influence on Ca concentration may be a process unrelated to evaporative concentration. In PC 3, Sr and Br are strongly correlated with a negative loading.

Table 4-2. Principal component loadings, eigenvalues and % of variance for Mesaieed chemistry dataset. Strong factor loadings, i.e. greater than ≥ ±0.4 are highlighted in blue (positive) and red (negative). Black box areas represent ≥ ±0.8.

Variables	PC 1	PC 2	PC 3
zCoast	0.32	-0.61	0.09
pH	0.58	0.44	0.04
Temp	-0.43	0.16	0.23
B	-0.44	-0.56	0.23
Na	-0.98	0.07	0.08
Cl	-0.98	0.06	0.07
Ca	-0.32	0.74	0.09
SO4	-0.84	0.00	0.08
Mg	-0.96	-0.08	0.11
Sr2	-0.24	0.13	-0.84
HCO3	0.63	-0.09	0.03
Br	-0.55	-0.24	-0.60
K	-0.96	-0.01	0.07
DO %	-0.01	0.11	0.27
Eigenvalue	6.14	1.56	1.30
% Variance	**43.8**	**11.1**	**9.3**

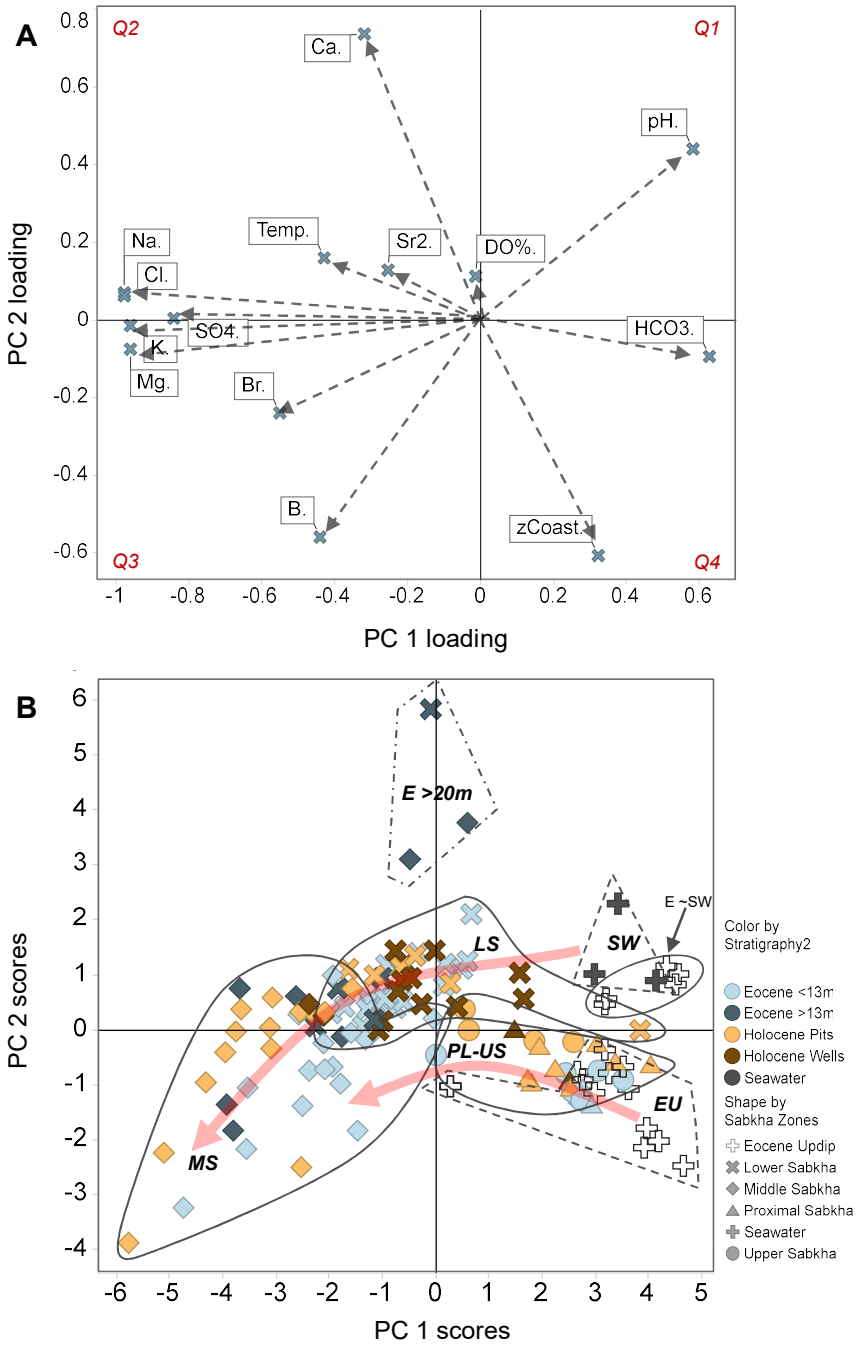

Figure 4-4. (**A**) Principal component loadings for PC 1 and PC 2 showing the relationship for each variable and (**B**) principal component scores for PC 1 and PC 2 showing the relationship for each sample displayed by colour (highlighting the stratigraphy hosting the waters) and shape (highlighting the spatial distribution by sabkha zone). Quadrants of the plot are represented by Q1 for first quadrant to Q4 for fourth quadrant. Dotted arrows stem from the origin represents its relationship (see text). Three samples grouped by E>20m indicates the outlier presented by the deepest Dammam Formation samples. In (B) the plots are grouped according to their sabkha zones and labeled by its acronyms, with proximal and upper sabkha grouped as one (PL-US) and the red arrows suggest geochemical evolution from sources of solute.

The PC loadings plot (Figure 4-4A) highlights that some variables cluster with similar loadings and others plot as outliers. The distance of each variable from the origin of the loadings plot indicates its relative contribution, whereas the spacing between adjacent lines (which are represented as dotted arrows in Figure 4-4A) stemming from the origin for each variable signifies the strength of their reciprocal association (Ravikumar and Somashekar, 2015). Many variables plot within the second and third quadrants (negative PC 1 loadings).

Strong negative loadings (>-0.4) of Cl, Na, Mg, K and SO_4, gives rise to a clear cluster on PC 1, which is balanced by a strong positive loading on PC 1 for HCO3. Ca and Sr plot in the second quadrant and appear to be inversely correlated with distance from the coast (quadrant 4). This is clearly true for Ca, but it is less convincing for Sr. Finally, there appears to be a negative correlation between Br and B (quadrant 3) and pH (quadrant 1).

The plot of PC scores in Figure 4-4B highlights the most distinguishable angle that best represents every line for each sample incorporating the effect of all the variables. The PCA scores plot shows a clear geochemical divide between the middle-lower sabkha and the proximal-upper sabkha. Most of the samples lie within a clear cloud which is in a shape of a chevron. The further the point is from the origin, the more different it is relative to the rest of the samples. For example, three deepest waters (all >20 m in depth) from the Dammam aquifer (wells B144, B147 and B150) are clear outliers. Though not distinguishable from the other samples in terms of PC 1, these have very high positive loading for PC 2, which indicates a distinct separate source of water whose geochemical makeup is distinguished by an anomalously high pH and Ca.

Unlike the PCA analyses for middle and lower sabkha, the Ca is clustered with the rest of the major ions. However, the B and Br lies closer to most of the major ions in the middle and lower sabkha.

When comparing the two plots, negative PC1 scores appear to correlate with increase in evaporation which is seen within sabkha pit waters, more significantly in the upper sabkha. This can be inferred that processes at the water table (pits) accounts for the increase in majority of the solutes.

Summary The first-pass analyses of all the variables suggest that while the major control on the aqueous geochemistry of the sabkha groundwater is evaporative concentration process, explaining the tandem increasing in concentration of Na, Cl, Mg, Ca, SO_4, Br, B and K, the existence of the second PC with significant eigenvalues suggest other processes and these appear to affect Br, Sr, B, HCO3 and pH. This provides a first step framework to further investigate the geochemistry relative to conservative evaporation of the input waters using regression analysis.

4.3.2 Statistical Analysis of Variance (SAV)

Statistical analysis of variance (SAV) using both Kruskal-Wallis and ANOVA tests were initially performed for aqueous solutes Na, Cl, K, Mg, HCO_3, SO_4, Ca, Br, B, Sr, pH, and DO (%) for (1) different sabkha zones (outcropping Dammam Formation updip, proximal, upper, middle and lower sabkha) and (2) different host rock in which the waters were sampled in (sabkha water table, sabkha phreatic zone, shallow Dammam Formation aquifer <13 m and deeper Dammam aquifer >13 m).

Results showed an extremely low p-value, with 50 % of the ones with the lowest p between 1 x 10^{-9} to 2 x 10^{-18} (Table 4-3). This means that all variables for most subgroups have very significant statistical difference. However, as observed in the PCA analysis, a strong geochemical divide between proximal-upper and middle-lower sabkha exists means that analyzing all the sabkha waters in one bulk may fail to capture a realistic geochemical picture of this statistical analysis.

The unequal number of samples between middle-lower sabkha samples (n=89) and proximal-lower samples (n=21) also means that the dataset is slightly skewed may introduces bias as the weight lies with the middle-lower sabkha data. Hence, for accurate p-values to be obtained, the groups were further divided and re-analyzed. This increases the p-value substantially with p-values of the top 50 % being between 1 x 10^{-2} to 3 x 10^{-9}, rather than some inflated statistical differences.

For the middle-lower sabkha the Kruskal-Wallis method is used, sabkha zone groups show the lowest p-values than the host rock groups. Most of the variables within the sabkha zones show the lowest p-value ($p \ll 0.01$), and DO % and Sr with $p < 0.05$, while Ca shows no statistical significance ($p = 0.5$). For variables within the host rock groups, only pH has the lowest p-value ($p<0.01$) and B, DO %, Br, SO_4, Mg and HCO3 have low p-value ($p<0.05$) while the other variables show no statistical significance with which host rock the water resides in.

This means that the differences of all solutes (except Ca) are statistically significantly different between middle and lower sabkha, and that for only B, Br, DO %, SO_4, Mg and HCO3 solutes residing in sabkha water table, sabkha phreatic, shallow Dammam and deep Dammam – the differences between these host rocks are statistically significant while the rest of the solutes are not.

For the outcropping Dammam Formation updip and proximal-upper sabkha, the ANOVA method is used for most except for Na and Cl (which uses Kruskal-Wallis). The results are opposite whereby the host rock groups generally show the lowest p-values than the sabkha zone groups. K, pH, HCO3, SO_4 and Cl show statistically significance within different host rocks ($p<0.05$) while only Mg show statistical significant between different sabkha zones ($p<0.05$). What this tells us is that for the proximal and upper sabkha zones, the different host rock from which the fluids were sampled are an important factor in the differences observed in the aqueous geochemistry than in the different lateral zones.

Table 4-3. Results of statistical analysis of variances for the ions as y-variables within sabkha zones (SZ) and host rock (HR) as x-variables. The corresponding method of either Kruskal-Wallis (K-w) or ANOVA is presented with probability value (p-value) and H-stat. Results are only shown are those that satisfy the confidence level of 0.05 and with ascending order of p-value.

Middle-Lower Sabkha					**Outcropping Dammam Formation updip and Proximal-Lower Sabkha**				
Y	X	Method	p-value	H-stat	Y	X	Method	p-value	H-stat
Na	SZ	K-W	2.8E-09	35.33	K	HR	ANOVA	1.7E-04	12.22
Cl	SZ	K-W	5.5E-09	34.01	pH	HR	ANOVA	5.0E-03	6.14
K	SZ	K-W	1.2E-08	32.43	Mg	SZ	ANOVA	1.0E-02	8.14
Mg	SZ	K-W	6.4E-08	29.25	HCO3	HR	ANOVA	1.8E-02	4.41
HCO3	SZ	K-W	8.3E-07	24.29	SO4	HR	ANOVA	3.3E-02	3.68
B	SZ	K-W	1.1E-04	14.91	Cl	HR	K-W	4.3E-02	8.14
pH	HR	K-W	1.4E-04	22.81					
SO4	SZ	K-W	9.0E-04	11.03					
pH	SZ	K-W	2.0E-03	9.56					
Br	SZ	K-W	4.0E-03	8.26					
HCO3	SZ	K-W	8.3E-07	24.29					
HCO3	HR	K-W	1.5E-06	35.03					
pH	HR	K-W	3.7E-06	33.04					
B	SZ	K-W	1.1E-04	14.91					

4.4 Results: Major Ions

Discussion for the major ions will be based on the stratigraphy of the aquifer (updip Dammam aquifer, sabkha aquifer, and the Dammam aquifer underlying the sabkha) and the spatial zones that it is located (proximal, upper, middle and lower) (see Figure 4-5A). Data set that accompanies this result is located in electronic appendix (page 293).

4.4.1 Chloride (Cl^-) and Sodium (Na^+)

Some of the sabkha groundwaters are very saline (5019 mmol l^{-1}), up to 7 times the concentration of local seawater. Chloride concentrations for all water samples are summarized in Figure 4-5A. Na concentrations within the sabkha system show a strong linear relationship with Cl (Figure 4-5B) which indicates a conservative behaviour, with the same source for Na and Cl. Two thirds of the samples lie within one standard deviation of analytical uncertainty of conservative evaporation of seawater. However, some 18% of the 129 samples have Na concentrations more than the 2σ analytical uncertainty higher than expected from conservative evaporation of seawater (CESW), with only 10% showing significant Na depletion.

Local seawater has a mean of 738±150 mmol l^{-1} (n=3) Cl^-, while rainwater ranges from 4.3 mmol l^{-1} during the first 10 minutes of rainfall (R_1) to 0.2 mmol l^{-1} after 4 hours of continuous heavy rainfall (R_2). Of all the groundwaters sampled, the outcropping Dammam Formation updip waters to the northwest of Mesaieed show the lowest Cl concentrations at 114±58 mmol l^{-1} (n=17).

Four wells located in the outcropping Dammam Formation wells to the north of Mesaieed sabkha, which is not surrounded by sabkha areas, have groundwaters with relatively elevated Cl concentrations (380 to 951 mmol l^{-1}, n=4). To the north where there is no sabkha, the ionic concentration is similarly elevated (about a three-fold) within 2.5 km toward the coast. To the northwest of the Mesaieed sabkha, there appears to be about a four-fold increase within the same distance from the proximal sabkha. The high Cl levels are likely due to the greater proximity to the coast and the sabkha than the waters located to the northwest of Mesaieed. Cl concentration is found to be increasing from 200 mmol l^{-1} (2.5 km away from the coast) to 600 mmol l^{-1} (0.5 km away from the coastline) (Figure 4-6). The outcropping Dammam Formation updip to the northwest of Mesaieed sabkha, the increase of Cl concentration is observed to be from 35 mmol l^{-1} to 200 mmol l^{-1} over 4 km towards the upper boundary of the proximal sabkha.

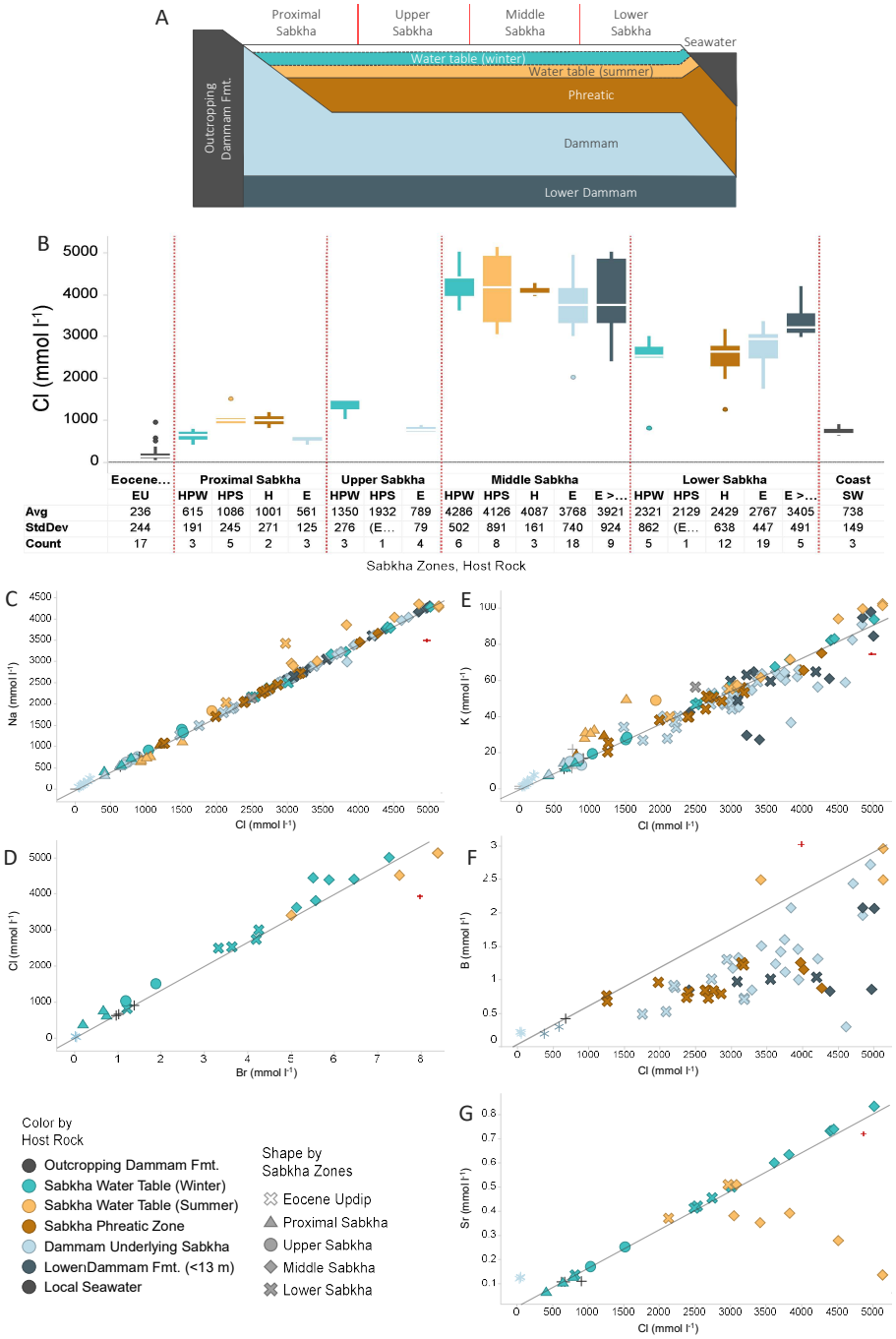

	Eocene…	Proximal Sabkha				Upper Sabkha			Middle Sabkha					Lower Sabkha					Coast
	EU	HPW	HPS	H	E	HPW	HPS	E	HPW	HPS	H	E	E >…	HPW	HPS	H	E	E >…	SW
Avg	236	615	1086	1001	561	1350	1932	789	4286	4126	4087	3768	3921	2321	2129	2429	2767	3405	738
StdDev	244	191	245	271	125	276	(E…	79	502	891	161	740	924	862	(E…	638	447	491	149
Count	17	3	5	2	3	3	1	4	6	8	3	18	9	5	1	12	19	5	3

Figure 4-5. (**B**) Box and whiskers plot of chloride, Cl, concentration. Host stratigraphy that were sampled include outcropping Dammam Formation updip (**EU**), sabkha water table sampled in the winter (**HPW**), sabkha water table in the summer (**HPS**), sabkha phreatic zone (**H**), Dammam formation (**E**), and deeper Dammam (> 13 m from top Dammam) and local Mesaieed seawater (SW). (**C, E, B, Sr**) Plots of Cl, K, B (n=54), Sr (n=24) concentration (mmol l^{-1}) as a function of chloride Cl, with symbols coloured by the host rock and shaped by sabkha zones. Solid gray line in each plot represents conservative evaporation of average of local concentrations of seawater samples. (**D**) Chloride as a function of conservative bromide, in mmol l^{-1}. The red cross symbol represents the combined analytical uncertainty of the point (x, y). For box plot (B) the lower and upper limit of each box define the first quartile (Q1) and third quartile (Q3) percentiles, respectively. The white horizontal line within the box is the median (IQR = Q3 – Q1). The whiskers extend to data that are not considered as outliers. Outliers were defined as a data value greater than Q3 + 1.5(Q3 - Q1) and less than Q1 + 1.5(Q3 - Q1).

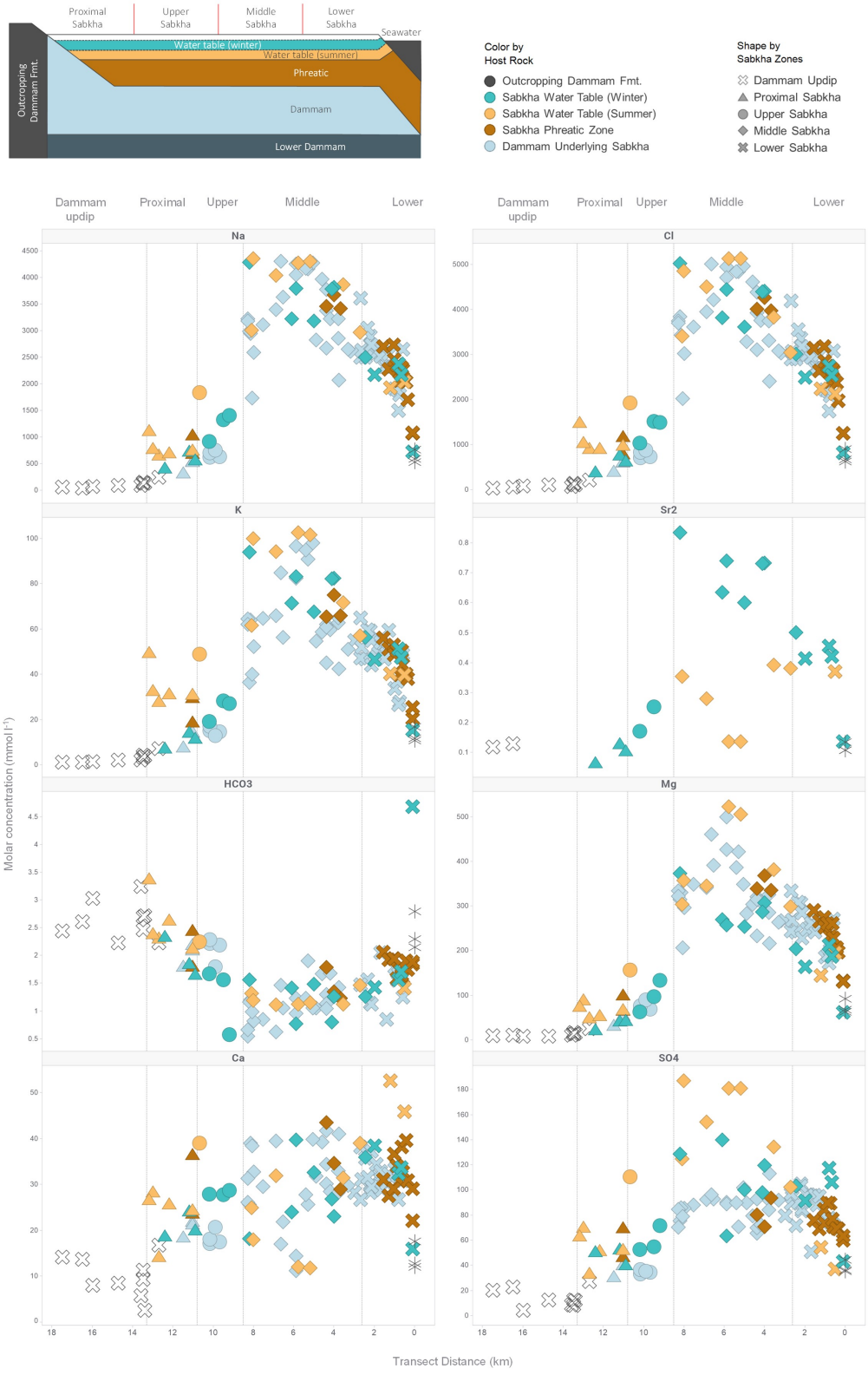

Figure 4-6. Cross-plot of Na, Cl, K, Sr, HCO3, Mg, Ca and SO4 concentrations (mmol l^{-1}) with distance from the outcropping Dammam updip of the sabkha to the coast. Samples are coloured by the host rock the waters were sampled from. Dashed line divides the distance cross plot into sabkha zones.

Local seawater has a Na to Cl molar ratio of 0.85±0.02 (n=3) which is indistinguishable from the global Na:Cl of 0.858 (Nordstrom et al., 1979). The initial rainwater (first 4 hours) has a ratio of 0.71±0.03 which falls within the range of rain waters worldwide of 0.50-1.00 (Moller, 1990) and the similarity to seawater reflects the location of Qatar surrounded by seawater. Groundwater within the outcropping Dammam Formation aquifer has a higher ratio (1.06±0.26). In the sabkha pits the Na:Cl ranges between 0.92±0.11 within the proximal-upper sabkha to 0.87 ±0.05 within the middle and lower sabkha. In the Dammam Formation underlying the proximal-upper sabkha this ranges between 0.9±0.01, to 0.86±0.02 within the middle-lower sabkha.

For all of the sabkha zones, an insignificant water table samples (<2%) are enriched in Cl relative to the sabkha groundwater Figure 4-5C), hence the Cl concentrations hosted in both the sabkha aquifer and the water table will be discussed as one sabkha aquifer unit (as mean $\overline{x}$). In the proximal sabkha, the sabha aquifer has a mean Cl concentration 959±302 mmol l^{-1}. Cl sampled in the Dammam aquifer underlying the sabkha is (561±125 mmol l^{-1} n=3). The Cl in the Dammam underlying the sabkha is twice as concentrated compared to that of the Cl in the updip aquifer (236±244 mmol l^{-1}). Within the upper sabkha, the sabkha aquifer (1330±495 mmol l^{-1}) similarly shows a two-fold increase in Cl concentrations compared to the underlying Dammam aquifer (869±712 mmol l^{-1}).

In the middle sabkha, Cl concentrations in the shallow Dammam have a mean of 3820±7190 mmol l^{-1} while in the overlying sabkha the Cl is only slightly higher (4175±661 mmol l^{-1}). However this is not statistically significant ($p>0.05$). In the lower sabkha, the deeper Dammam aquifer samples, located <13 m below the top Dammam, shows a much greater Cl concentration (3410±491 mmol l^{-1}) than in the Dammam Formation (2690±511 mmol l^{-1}), and sabkha has lowest Cl (2410±662 mmol l^{-1}).

4.4.2 Chloride vs Bromide

For Br, we tested a subset of 26 samples that are randomly selected from the sabkha water table, 2 local seawater samples and 3 samples from the outcropping Dammam Formation updip, which include four samples from the summer season of which three are from within the salt flat in the middle sabkha. Br in local seawater is high (0.71 mmol l^{-1}) compared to global seawater, 0.03 mmol l^{-1} (Hem, 1986) indicating that the local seawater is partially evaporated. Cl:Br ratios within the local seawater has a mean of 657±10 while Cl/Br varies within the outcropping Dammam Formation updip (1580±700). Within the sabkha the proximal zone's Cl/Br reflects closer to the outcropping Dammam Formation updip (1370±607), while it appears that Cl/Br of the rest of sabkha reflects closer to the seawater's (upper sabkha 838±41, middle sabkha 685±61 and lower sabkha 695±41). These differences are all statistically significant ($p<0.01$). Cl is shown to have good correlation with Br ($R^2 = 0.98$) in Figure 4-5D, with 24 samples lying within 2σ of the analytical uncertainty of the CESW. Only 2 samples in which minor depletion is seen is where the salt flat is located.

4.4.3 Potassium (K^+)

Concentrations of K in the seawater is 39.6±26.4 mmol l^{-1} while in the rainwater it is 0.72±0.99 mmol l^{-1}. Within the outcropping Dammam Formation updip K concentrations are about 5.76±4.58 mmol l^{-1}. K within K/Cl ratio in the seawater is 0.018±0.001, while for the rainwater the K is higher (K/Cl = 0.200±0.184). K/Cl within the outcropping Dammam Formation updip is 0.028±0.008. Potassium concentration for almost 80% the waters lies within 2σ of analytical uncertainty of predicted evaporation of seawater, with 34% samples above 2σ of the analytical uncertainty and 17 % samples below 2σ. The outcropping Dammam Formation shows a very minor enrichment of K relative to conservative evaporation of seawater (CESW) (31% of samples) with mean of K_{XS} 2 mmol l^{-1}. Within the sabkha, most waters are aligned with CESW line (Figure 4-5E). Greatest depletion of K is observed in waters sampled in the Dammam underlying the middle sabkha (K_{XS} = -16.5±10.6 mmol l^{-1}). Some 30 % of sabkha water table in the proximal sabkha show minor enrichment of K ($\bar{x}$ K_{XS} = 1.5 mmol l^{-1}).

4.4.4 Boron

A subset of samples (n=69) that were randomly chosen was analysed for Boron, B. The rainwater typically consist of about 4.5 x 10^{-4} mmol l^{-1} (Neal et al., 1997). For comparison, B in the outcropping Dammam Formation is 0.23 mmol l^{-1} while in the local seawater it is 0.43 mmol l^{-1}. Many samples appear to be depleted in B relative to Cl in seawater (Figure 4-5F), with ~50% of the samples containing about half the B concentration that is expected from CESW. For the middle and lower sabkha, most of the samples show a greater concentration of B in the Dammam aquifer than in the sabkha phreatic zone. Only one sabkha sample (Q4) lie above the CESW indicating a minor enrichment of B at this site.

4.4.1 Strontium

Due to well destruction from NDP construction, only a limited number of samples (n=29) were tested for Strontium, Sr, at the sabkha water table in the summer and winter, 3 outcropping Dammam Formation updip and 2 from the local seawater. Sr appears to be conservative relative to CESW except for sabkha aquifer in the middle sabkha sampled in the summer which are mostly depleted (Figure 4-5G). The cross plot shows a trend of a minor decrease in Sr with an increased Cl which signifies a retrograde solubility trend (R^2 = 0.67).

4.4.2 Magnesium (Mg^{2+})

Mg in local seawater is 74.4±15.4 mmol l^{-1} (Mg/Cl of 0.101±0.001) while Mg/Cl of the rainwater is significantly higher (0.5 to 0.18). The molar ratio Mg:Ca in the rain water and in the Qatar dust is 0.52 and 0.55 respectively. Mg increases systematically with increase Cl until 500 mmol l^{-1} Cl when

waters deviate away from CESW, and the degree of depletion appears to increase with increasing Cl concentrations (Figure 4-7A). 74 % of the samples have Mg less than 2σ of the analytical uncertainty lower than expected from CESW indicating minor depletion, and 22 % of samples are depleted by more than 2σ of analytical uncertainty. In all sabkha zones except the lower sabkha, Mg concentrations appear to be higher within those sampled in sabkha water table than the sabkha phreatic and Dammam aquifer (Figure 4-7A).

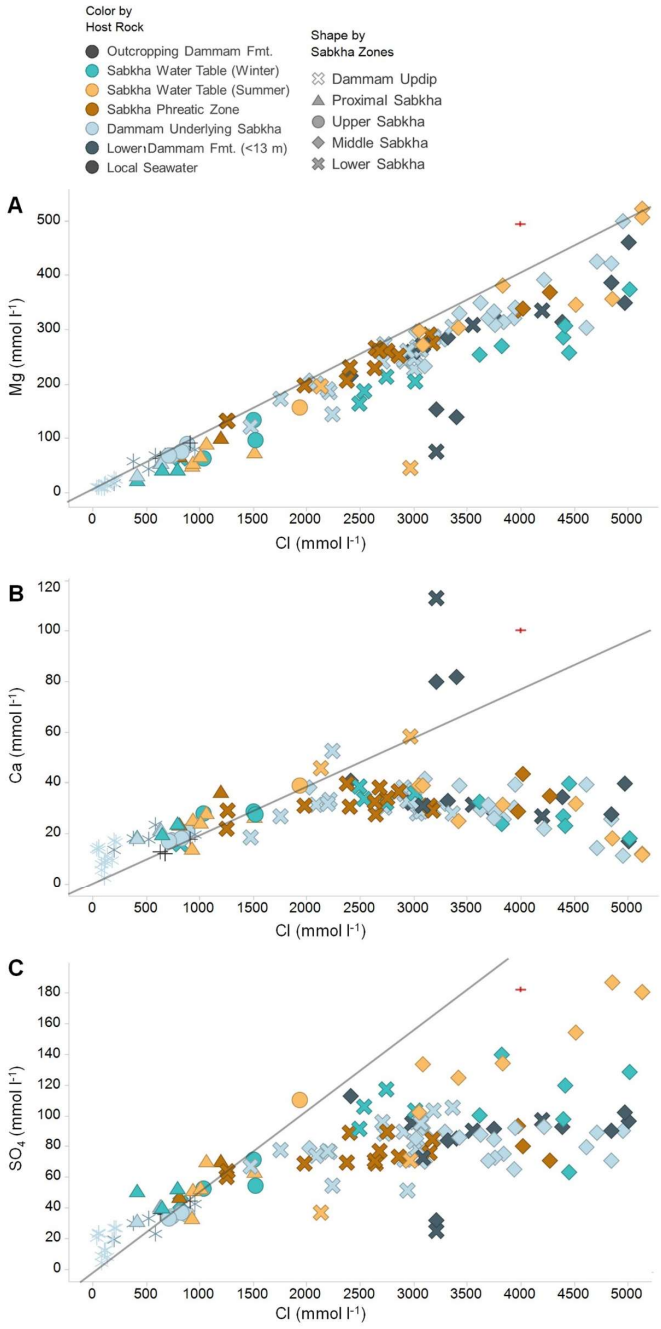

Figure 4-7. Relationship of magnesium, calcium and sulphate with chloride (mmol l^{-1}) with gray line representing the trend of a conservative evaporation of seawater. Red crosses are a representative uncertainty at point (x, y). Mg *n = 127*; Ca *n = 127*; SO4 *n = 127.*

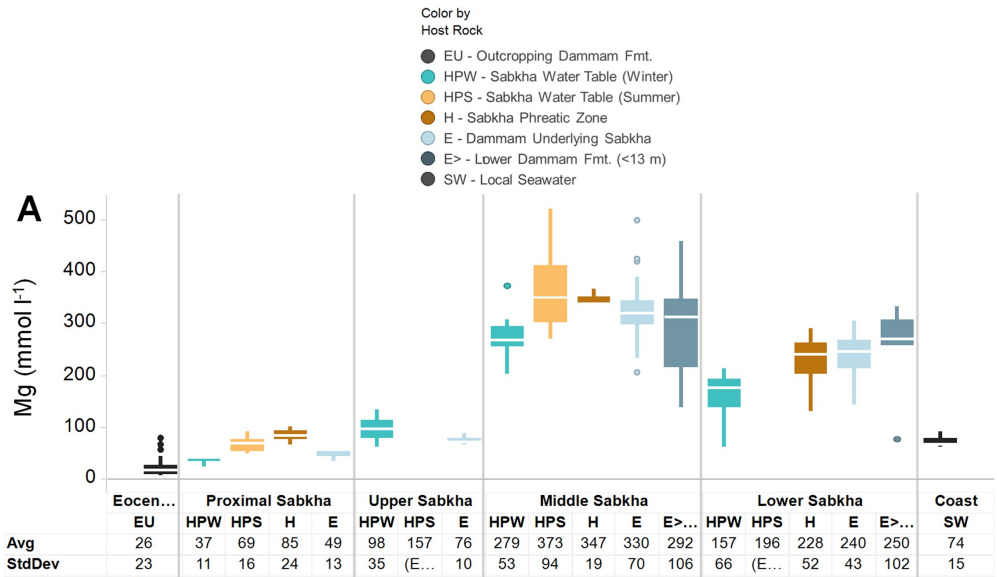

	Eocen...	Proximal Sabkha				Upper Sabkha			Middle Sabkha					Lower Sabkha					Coast
	EU	HPW	HPS	H	E	HPW	HPS	E	HPW	HPS	H	E	E>...	HPW	HPS	H	E	E>...	SW
Avg	26	37	69	85	49	98	157	76	279	373	347	330	292	157	196	228	240	250	74
StdDev	23	11	16	24	13	35	(E...	10	53	94	19	70	106	66	(E...	52	43	102	15
Count	17	3	5	2	3	3	1	4	7	8	3	18	9	4	1	12	19	5	3

Sabkha Zones, Host Rock

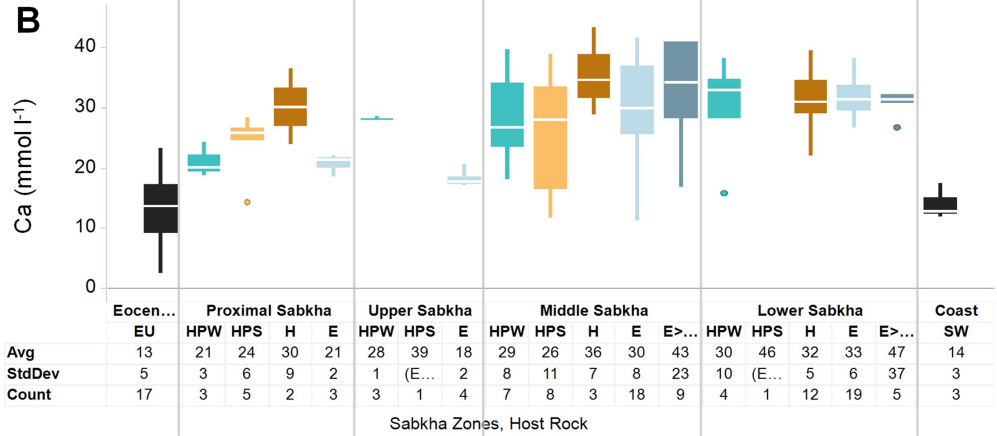

	Eocen...	Proximal Sabkha				Upper Sabkha			Middle Sabkha					Lower Sabkha					Coast
	EU	HPW	HPS	H	E	HPW	HPS	E	HPW	HPS	H	E	E>...	HPW	HPS	H	E	E>...	SW
Avg	13	21	24	30	21	28	39	18	29	26	36	30	43	30	46	32	33	47	14
StdDev	5	3	6	9	2	1	(E...	2	8	11	7	8	23	10	(E...	5	6	37	3
Count	17	3	5	2	3	3	1	4	7	8	3	18	9	4	1	12	19	5	3

Sabkha Zones, Host Rock

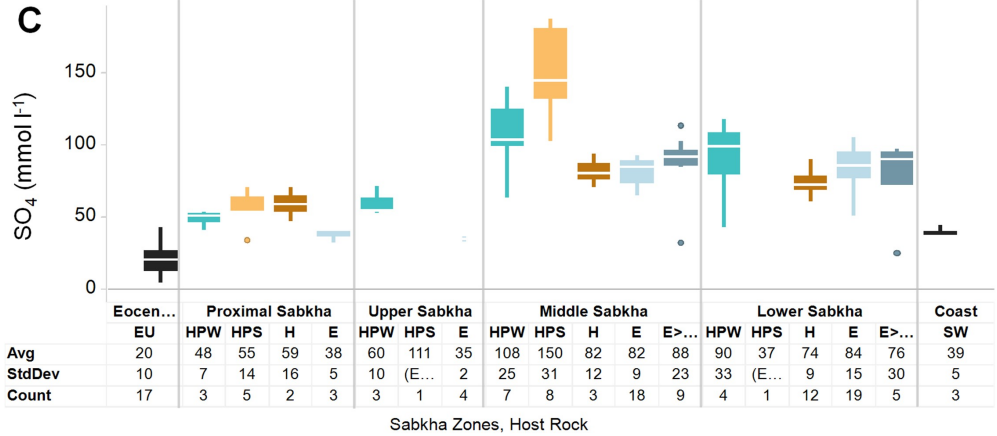

	Eocen...	Proximal Sabkha				Upper Sabkha			Middle Sabkha					Lower Sabkha					Coast
	EU	HPW	HPS	H	E	HPW	HPS	E	HPW	HPS	H	E	E>...	HPW	HPS	H	E	E>...	SW
Avg	20	48	55	59	38	60	111	35	108	150	82	82	88	90	37	74	84	76	39
StdDev	10	7	14	16	5	10	(E...	2	25	31	12	9	23	33	(E...	9	15	30	5
Count	17	3	5	2	3	3	1	4	7	8	3	18	9	4	1	12	19	5	3

Sabkha Zones, Host Rock

Figure 4-8. Box and whiskers plot of Mg, Ca, SO_4 by sabkha zone and stratigraphy the waters are hosted in. Sabkha zones include outcropping Dammam Formation updip (**EU**), sabkha water table in the winter (**HPW**), sabkha water table in the summer (**HPS**), sabkha phreatic zone (**H**), Dammam underlying the sabkha (**E**), and deep Dammam (**E > 13 m**) and sea-water (**SW**). Ca box plot has been scaled and does not include deep Dammam outliers. Mg *n = 127*; Ca *n = 127*; SO4 *n = 127.*

4.4.3 Calcium (Ca^{2+})

Local seawater contains 14.1±3.0 mmol l^{-1} of Ca while rainfall samples have an average 1.24±1.58 mmol l^{-1}. Figure 4-7B highlights that the outcropping Dammam Formation updip waters are above the CESW line but the general trend shows that there is an increase of Ca in all waters along the CESW, until about 1800-2000 mmol l^{-1} of Cl when Ca starts falling below the CESW and then at Cl > 2350 $mmol^{-1}$ it decreases with increasing Cl.

All waters within the middle and lower sabkha appears to be significantly depleted with calcium and thus depletion increases with increasing Cl. 52 % of them are below 2σ of the analytical uncertainty higher than expected from CESW indicating minor depletion while 37 % of samples lie above 2σ

Box plot shows not much discernible differences across the middle and lower sabkha as compared to upper and proximal sabkha (Figure 4-8B). Vertical variation within the proximal and upper sabkha show that Ca concentrations are higher in the sabkha than in the Dammam, whereas the Ca distribution between the sabkha and Dammam within the middle sabkha and lower sabkha are not statistically significant ($p>0.05$).

There appears to be no seasonal difference affecting the distribution of Ca within the sabkha water table (Figure 4-8B), except for the proximal sabkha. However, there are only two data points, and this is not statistically significant ($p>0.05$)

4.4.4 Sulphate (SO_4^{-2})

Local seawater contains 38.7±5.10 mmol l^{-1} of SO_4 which is higher than of global seawater at 28.9 mmol l^{-1}. SO_4/Cl within the local seawater is 0.053±0.004. Outcropping Dammam Formation updip shows a higher ratio (0.194±0.154) of SO_4/Cl than seawater which closely reflect rainfall sample 0.375±0.010.

The outcropping Dammam Formation updip waters appears to be above the CESW line indicating excess of SO_4 (Figure 4-7C). The SO_4 appears to increase with Cl but do not appear to follow the CESW line. Cl of approximately 1500 to 1700 mmol l^{-1}, after which the SO_4 falls below the CESW with increasing Cl for most waters. 61 % of the samples below 2σ of the analytical uncertainty than expected from CESW indicating minor depletion, and 21 % of samples are depleted by more than 2σ of analytical uncertainty. In general, sabkha water table show a slightly less SO_4 depletion as compared to those hosted within the Dammamand are also subjected to seasonal variations with the summer pit waters having a trend closest to the CESW line.

Box plots (Figure 4-8C) shows that SO_4 concentrations are generally higher in the sabkha water table than in the deeper sabkha phreatic zone or the Dammam for all sabkha zones, with the highest

SO_4 found within the middle sabkha pits. A notable exception is the proximal sabkha samples, where this difference is not statistically significant.

There appears to be seasonal variations especially in the middle sabkha with SO_4 in the summer having greater concentrations than in the winter ($p<0.01$).

4.4.5 pCO_2, HCO_3, and pH

Plots of pH, pCO_2, and HCO_3 against Cl and its box plots are shown in Figure 4-9 and Figure 4-12, respectively.

pCO_2

Partial pressure of carbon dioxide, pCO_2, calculated for local seawater is 0.057±0.012 % close to atmosphere while the outcropping Dammam Formation aquifer have a very high pCO_2 (0.91±0.29 %). Rainwater contributes the highest amounts of pCO_2, from 218 % in R_1 (first 10 minutes of rainfall) to 41.8 % in R_2 (after 4 hours of continuous heavy rainfall). There is no significant relationship between pCO_2 and Cl ($p>0.05$). Box plots show that the pCO_2 of Dammam aquifer is greater than the sabkha waters within the proximal and upper sabkha, and pCO_2 is lower from outcropping Dammam Formation through proximal to upper and middle sabkha. In the middle and lower sabkha, pCO_2 concentration is highest in the sabkha phreatic, followed by sabkha water table waters and in the Dammam aquifer ($p<0.05$). Within the Dammam aquifer, the deep Dammam aquifer shows higher concentration of pCO_2 than in the shallower Dammam.

Sabkha water tablesampled in different seasons show that the winter waters have no change of pCO_2 with Cl. The winter samples have lower concentration of pCO_2 compared to the summer samples ($p<0.01$). While this attribute to more degassing, this may indicate that there is not much evaporation to draw waters upward and possibly diluted by input of low pCO_2 seawater during marine flooding.

HCO_3

82% of samples (n = 128) were analysed for alkalinity. As the 98% of the groundwater pH are between the ranges of 6.4 to 8.7 this means the total alkalinity comes most from bicarbonate (HCO_3^-) species rather than H_2CO_3 (Drever, 2002). HCO_3 concentration in the local seawater is 2.42±0.34 mmol l^{-1}, which is similar to that of the outcropping Dammam Formation updip waters (2.20±0.34 mmol l^{-1}). HCO_3/Cl within the outcropping Dammam Formation updip is the highest, at 0.022±0.02, while the local seawater has ratio of 3.4 x 10^{-3}±0.0010. Within the proximal and upper sabkha, HCO_3/Cl is about an order of a magnitude lower than of the outcropping Dammam Formation updip while in the middle and lower sabkha it is about an order of a magnitude lower than of seawater. The lowest HCO_3/Cl appears to the within the middle sabkha (0.0003±0.0001), indicating that there is degassing within the sabkha through the vadose zone pore network.

Its relationship with Cl shows a systematic trend, which decreases with increasing Cl. In the proximal sabkha, HCO_3 decreases with depth from the the sabkha into the underlying Dammam aquifer while in the upper sabkha the trend is the opposite. In the middle and lower sabkha, the HCO_3 is about the same vertically with the highest concentrations in the deeper Dammam than in the sabkha water table and the shallow Dammam aquifer.

pH

pH of local seawater is 8.20±0.04 which is about that of global seawater pH of 8.22. In the outcropping Dammam Formation groundwater pH is 7.25±0.15 while rainwater has a pH of 4.35 - 4.56. pH decreases with increasing Cl, from 7.25±0.15 (outcropping Dammam Formation updip) to 6.90±0.20 in the middle sabkha (~10 times H^+ concentration).

The box plot (Figure 4.12A) highlights that in all zones except the lower sabkha, the pH trend is sabkha water table ≥ sabkha phreatic ≥ Dammam Formation aquifer. The underlying Dammam formation waters in the lower sabkha have greater pH than the overlying sabkha ($p<0.05$) which may indicate seawater percolating through the Dammam Formation. The highest pH is found in the proximal sabkha pit waters (7.57±0.10), which is closest to that of the outcropping Dammam Formation (7.25±0.15). The lowest pH is found within the Dammam aquifer underlying the middle sabkha (6.74±0.31).

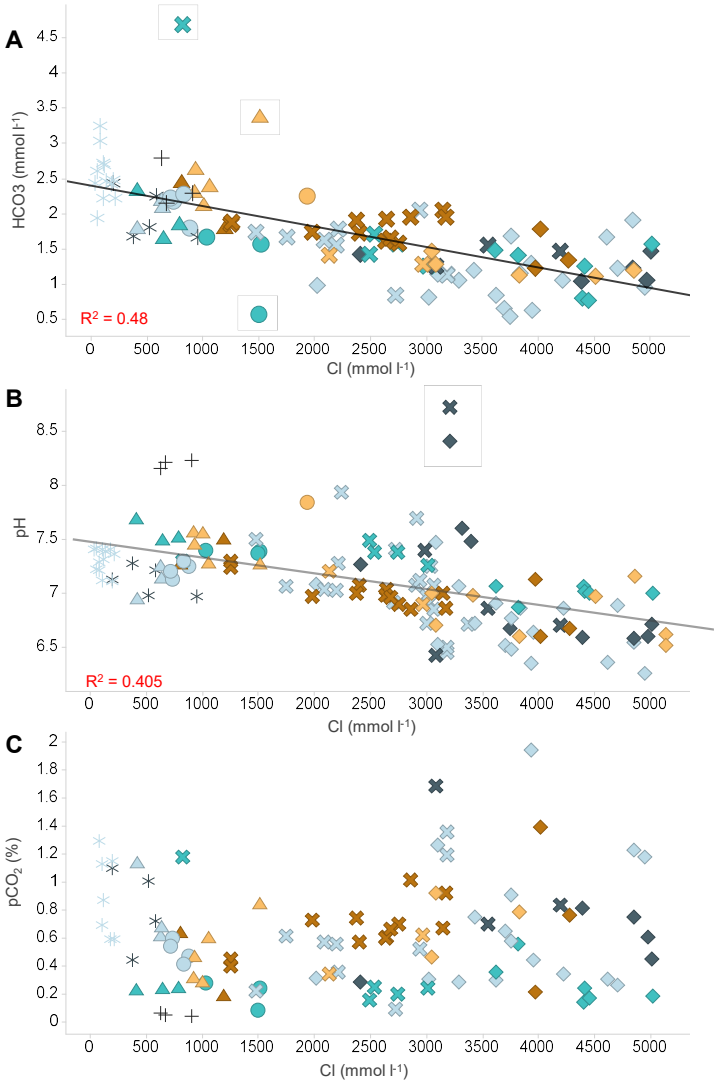

Figure 4-9. Plots of pH, partial pressure of CO_2 (as pCO_2) and bicarbonate (HCO_3) with Cl (mmol l^{-1}). Solid gray line in each plot represents conservative evaporation of seawater. The red cross represents the uncertainty of the point (x, y). PCO2 n = 101;

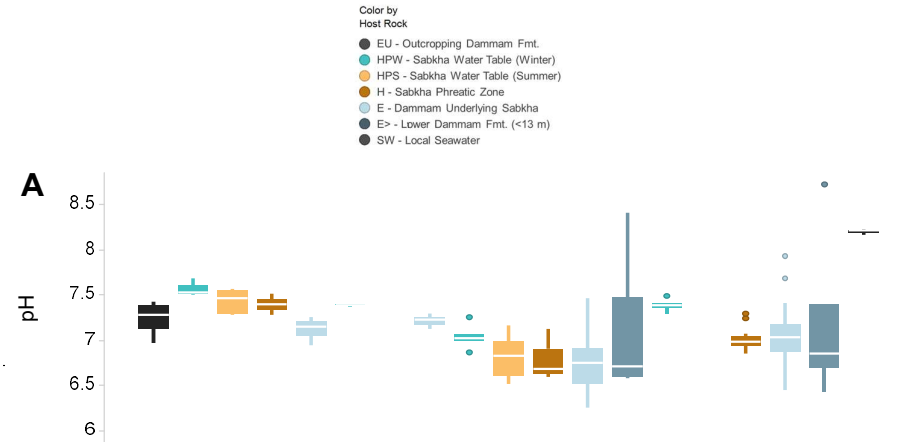

	Eocen...	Proximal Sabkha				Upper Sabkha			Middle Sabkha					Lower Sabkha					Coast
	EU	HPW	HPS	H	E	HPW	HPS	E	HPW	HPS	H	E	E>...	HPW	HPS	H	E	E>...	SW
Avg	7.25	7.57	7.43	7.40	7.12	7.39	7.84	7.22	7.04	6.82	6.80	6.74	7.10	7.39	7.20	7.01	7.05	7.22	8.20
StdDev	0.15	0.10	0.14	0.16	0.16	0.02	(E...	0.07	0.12	0.24	0.29	0.31	0.64	0.08	(E...	0.14	0.36	0.91	0.04
Count	17	3	5	2	3	3	1	4	7	8	3	18	9	4	1	12	19	5	3

Sabkha Zones, Host Rock

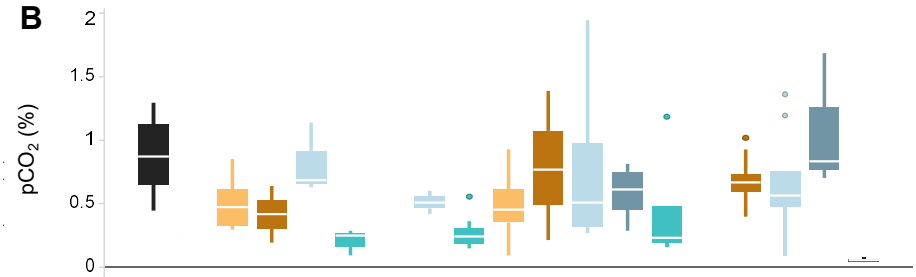

	Eocen...	Proximal Sabkha				Upper Sabkha			Middle Sabkha					Lower Sabkha					Coast
	EU	HPW	HPS	H	E	HPW	HPS	E	HPW	HPS	H	E	E>...	HPW	HPS	H	E	E>...	SW
Avg	0.88	0.25	0.51	0.42	0.82	0.21	(E...	0.51	0.28	0.49	0.79	0.69	0.58	0.45	0.34	0.68	0.66	1.08	0.06
StdDev	0.28	0.01	0.23	0.32	0.28	0.10	(E...	0.08	0.14	0.27	0.59	0.49	0.22	0.49	(E...	0.17	0.42	0.53	0.01
Count	11	3	5	2	3	3	0	4	7	8	3	16	5	4	1	12	8	3	3

Sabkha Zones, Host Rock

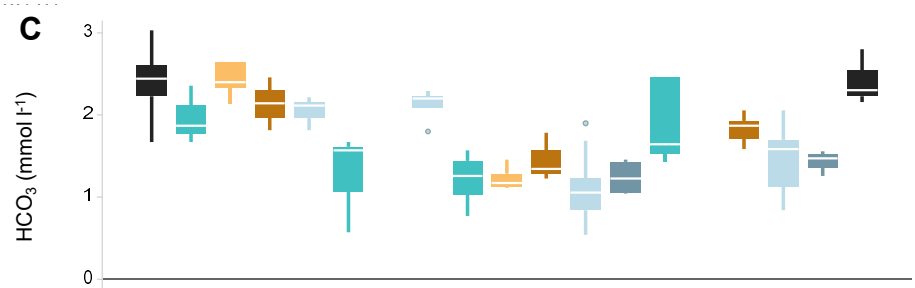

	Eocen...	Proximal Sabkha				Upper Sabkha			Middle Sabkha					Lower Sabkha					Coast
	EU	HPW	HPS	H	E	HPW	HPS	E	HPW	HPS	H	E	E>...	HPW	HPS	H	E	E>...	SW
Avg	2.37	1.96	2.58	2.14	2.05	1.27	2.24	2.12	1.22	1.22	1.45	1.11	1.25	2.35	1.42	1.82	1.47	1.43	2.42
StdDev	0.44	0.36	0.49	0.46	0.21	0.60	(E...	0.22	0.32	0.13	0.29	0.38	0.20	1.56	(E...	0.15	0.40	0.16	0.34
Count	17	3	5	2	3	3	1	4	7	8	3	17	5	4	1	12	8	3	3

Sabkha Zones, Host Rock

Figure 4-10. Box plots of pH, pCO_2 (%) and bicarbonate alkalinity (HCO_3) in mmol l^{-1}.

4.4.6 Dissolved Oxygen

Local seawater is oversaturated with DO (>100 %) while the outcropping Dammam Formation updip has 63±32 %. DO is independent of Cl within the sabkha system (Figure 4-11A). Box plots (Figure 4-11B) shows that the sabkha system is oxic, 92 % of the waters with DO above 20 % (n = 97) and 55 % of the waters have DO above 50 %. Box and whiskers plot shows that DO in the sabkha water table within the middle sabkha is the highest (68±17 %). The second highest DO is found within Dammam Formation in the proximal, middle and lower sabkha (65±27 %, 61±13 % and 56±22 % respectively). In the middle sabkha, the DO is highest within the sabkha water table (68±17 %) and lowest in the deep Dammam-hosted waters (48±20 %). The lowest DO is found in the sabkha phreatic waters of the lower sabkha (37±18 %). While within the Dammam Formation, the DO appears to be the same for the waters found in the deeper and shallower wells (p>0.05). Seasonal effects on DO was not available.

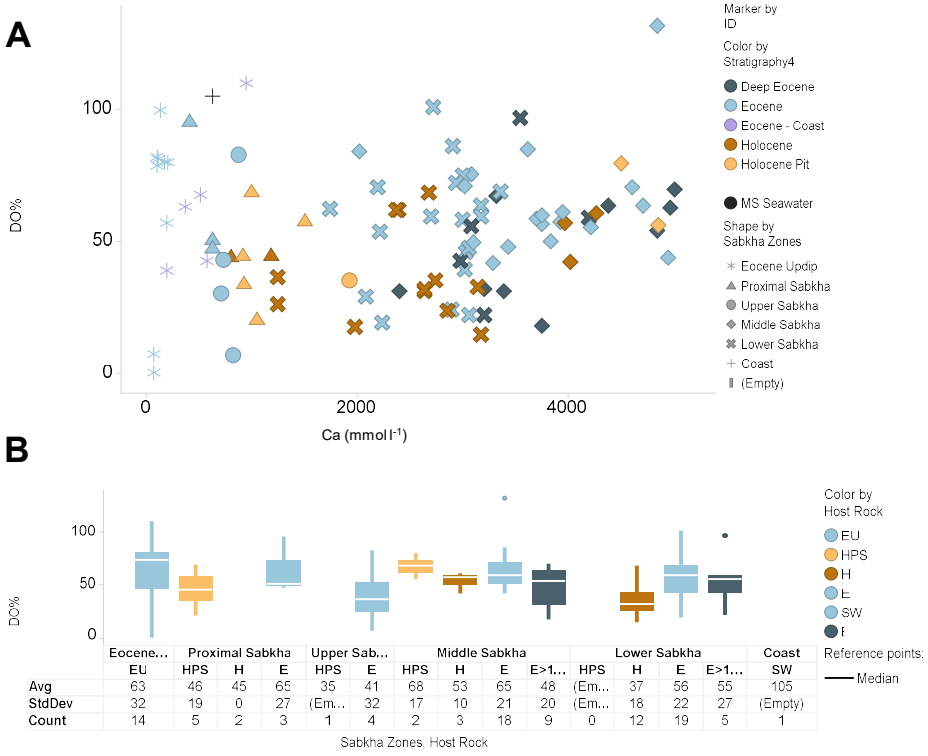

	Eocene...	Proximal Sabkha			Upper Sab...		Middle Sabkha				Lower Sabkha				Coast
	EU	HPS	H	E	HPS	E	HPS	H	E	E>1...	HPS	H	E	E>1...	SW
Avg	63	46	45	65	35	41	68	53	65	48	(Em...	37	56	55	105
StdDev	32	19	0	27	(Em...	32	17	10	21	20	(Em...	18	22	27	(Empty)
Count	14	5	2	3	1	4	2	3	18	9	0	12	19	5	1

Figure 4-11. (**A**) Dissolved oxygen (DO %) against Cl concentration (mmol l^{-1}) and (**B**) as box and whiskers plot to shows its distribution laterally (sabkha zone) and vertically (stratigraphy) in which the waters are hosted in.

4.4.7 SiO_2 and Al

Samples from the middle and lower sabkha for SiO_2, and Al to understand its relationship with arid clays (palygorskite, illite and chlorite) that were observed in the field (Figure 4-12).

SiO_2 Seven samples were tested for dissolved silica, as SiO_2. Molar ratio SiO_2/Cl for outcropping Dammam Formation updip of 0.006 to 0.001, while for the local seawater it is 5 x 10^{-4}, which indicates that the outcropping Dammam Formation updip waters have greater dissolved silica than seawater. Within the middle sabkha, there is a depletion of SiO_2 in the middle sabkha pits, where SiO_2/Cl ratios are about 1 x 10^{-4}.

Al Although aluminium concentration in outcropping Dammam Formation updip waters and local seawater are Al, 0.005±0.002 mmol l^{-1} and 0.004 mmol l^{-1} respectively, 90 % of the samples (n = 76) were below instrument detection limit (<2 x 10^{-4} mmol l^{-1}). With increasing Cl, only three water table samples in the middle sabkha show a depletion relative to CESW having Al/Cl ratio of (3.1-3.9) x 10^{-6} as compared to 6.0 x 10^{-6} for seawater and (2.6-7.6) x 10^{-5}.

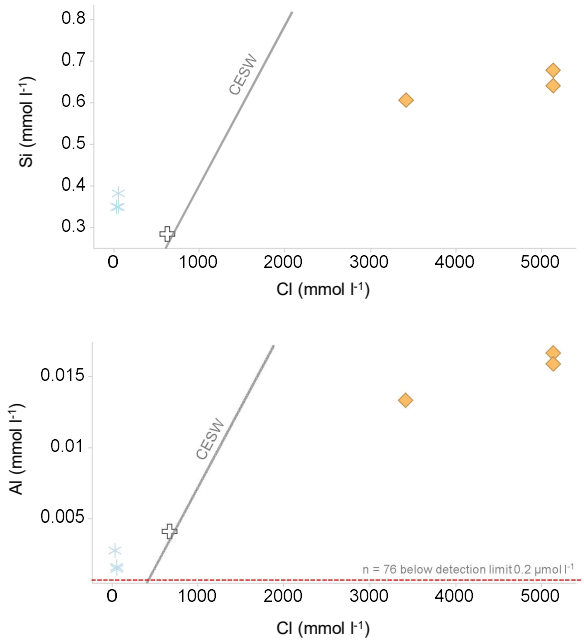

Figure 4-12. Plots of trace elements silica (as SiO^2) and aluminium (Al) relative to Cl. Grey line represents conservative evaporation of seawater containing these chemical constitutents.

Table 4-4. General summary of aqueous geochemistry results per each sabkha zone and end-member sources of solutes for section 4.5. Seasonal samples apply only to sabkha water table samples.

	Outcropping Dammam Formation updip	Proximal Sabkha	Upper Sabkha	Middle Sabkha	Lower Sabkha	Seawater
PC1* (+)		Na, Cl, K, Mg, SO4, Ca, pH		Na, Cl, K, Mg, SO4, Br, B		
PC1 (–)	HCO3, pH			pH		HCO3, pH
PC1 (A)		Sr, Br, B		Sr, Ca		-
Na	Enriched+	Conservative with CESW#				-
Cl		Conservative with CESW				-
K	Enriched	Conservative with CESW				-
B	Enriched	Depletion with CESW				-
Sr	Enriched	Conservative with CESW, depleted in the summer only				-
Mg	Enriched	Minor depletion	Minor depletion	Depleted	Minor depletion	-
Ca	Enriched	Conservative	Conservative	Depletion with CESW		-
SO_4	Enriched	Conservative	Conservative	Depletion with CESW winter depletion ≫ summer		-
pH	7.25	Depletion with CESW			NR	8.2
pCO2	High	No relationship; Sabkha winter < summer				Low
HCO3	2.37	Depletion with CESW			NR	2.42
DO	-	NR		Higher in Dammam Formation		-
SiO_2	Enriched	-		Depletion	-	-
Al	Enriched	-	Below DL	Depletion in Hpit	Below DL	-
Phase Diagram	Dolomite field	Dolomite field; parallel to gypsum boundary with ↑ CESW				Dolomite field
SI_{GYP}	Undersaturated	Undersat.	Equilibrium	Oversat.	Equilibrium	Undersat.
SIdol	Slightly oversaturated	Minor oversat.	Minor oversat.	Oversat.	Oversat.	Oversat.
SI_{DOL}	Equilibrium	Slightly oversat.	Slightly oversat.	Slightly oversat.	Slightly oversat.	Oversat.
Ca_{XS} v $SO4_{XS}$	Minor Gypsum Dissolution	Gypsum precipitation; with sabkha water table on the 1:1 line				-
Mg_{XS}	Minor excess	Minor depletion	Minor depletion	High depletion	Depletion only in water table	-
ΔCa_{XS} v Mg_{XS}	Minor Dedolomitisation	Clay formation	Clay formation	Secondary dolomitisation		-
aCa/aMg	≪ 1	<1	<1	>1	≥1	<1
ΔCa_{XS} v $HCO3_{XS}$		Increase of delCaxs with decrease $HCO3_{XS}$				-
[X]/Cl v pH		Mg/Cl decreases with pH while SO4/Cl and Ca/Cl increases with pH especially within the sabkha waters				-

*PC = principal component; +EU relative to seawater; #CESW =conservative evaporation with seawater
NR = no relationship;

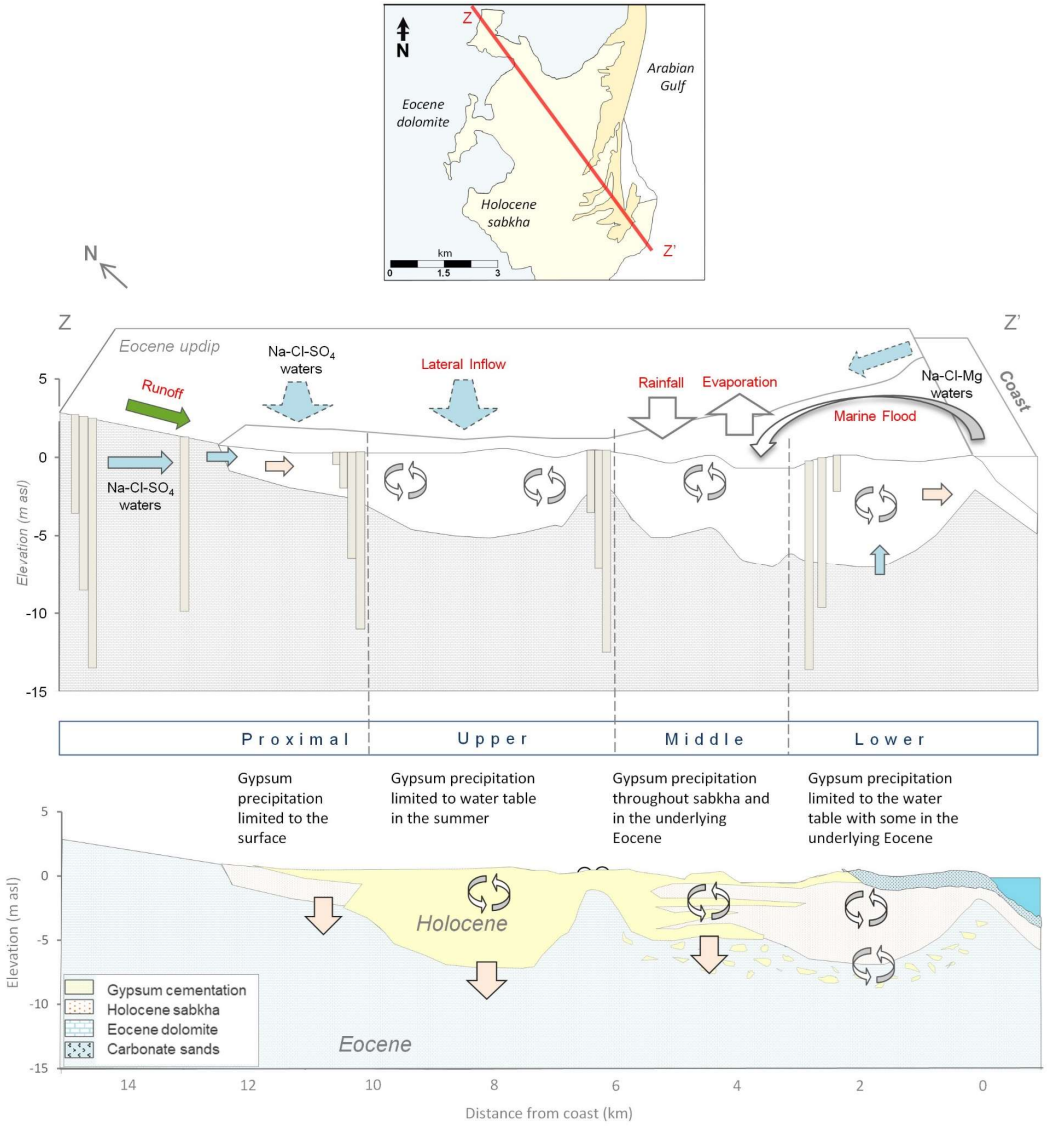

Figure 4-13. Summary of end-member waters which sources solutes to the sabkha, conservative processes and geochemical-driven water-rock interaction processes occuring within sabkha. This accompanies discussion in section 4.5. Highlighted here is the major process of gypsum cementation.

4.5 Discussion

Table 4.4 and Figure 4-14 provides summarized table and illustration that accompanies the following discussion.

4.5.1 Conservative Processes

Evaporation

This study evaluated the assumptions of using Cl as a conservative ion by comparing the relationship between Cl and conservative ion Bromide, Br, in the waters. The assumption of using just Cl as the conservative ion is that halite, NaCl, does not precipitate nor does it dissolve. With using Br ion, the lattice layers of halite is not suited for Br in substituting the Cl ion, hence the potential Br loss to halite precipitation is very insignificant (Braitsch, 1971). Loss of Br to resorption does not occur near neutral pH and only starts at pH 4.7 and lower (Boggs and Adams, 1992). The pH of the sabkha does not fall below 5.0. Hence, Br has no tendency to precipitate out or undergo complexation with other ions or clays in Mesaieed's sabkha system. Majority of previous studies (such as Groot, 1973; Illing and Taylor, 1993; Al-Youssef, 2003; Basyoni and Aref, 2016) used Cl as their reference anion to understand the sources and sinks of other ions, but little has been done to ascertain the degree to which Cl behaves in a conservative manner. This limitation should be considered more closely by future workers in areas where halite is often found in greater proportions in other sabkhas including Abu Dhabi.

Given that both our hydrogeological studies (Chapter 3) and prior PCA analysis (Section 4.3.1) have demonstrated that the outcropping Dammam Formation meteoric waters are an important source for the proximal and upper sabkha, and that seawater is an important source for the middle and lower sabkha, we also consider contribution from evaporation to the groundwater. Linear increase of Cl with conservative Br implies that evaporation process is driving up concentration of ions and not halite dissolution, thus allowing Cl to be considered as a conservative ion. The concentration of most solutes in the sabkha system, especially Na, K, Mg and SO_4 increases with increase in Cl. Evaporation can thus be used to explain the dominant mechanism driving geochemical processes in the sabkha system.

While the two end-member source waters have an abundance of Na and Cl that are readily available for halite precipitation, the waters however would require 10 degrees of evaporation of seawater (Warren, 2016). The highest measured degree of evaporation, using Cl, at the water table is 6.96 (Q3 and Q4) which means that the ephemeral salt flat that we observed on the field is limited to the localised depression during marine inundation events. Marine waters that are unable to retreat nor infiltrate quickly enough is left to evaporate. Consequently, there is more SO_4 available from the outcropping Dammam Formation updip source waters for gypsum precipitation within the proximal and upper sabkha and more Mg available from local seawater for clay or dolomite to precipitate, assuming the thermodynamic and kinetic conditions are met. Identifying Cl as a reliable conservative tracer allows

us to then cement our understanding of water-rock interaction processes using the concept of excess (XS) ions of Mg, Ca and SO_4 in following sections (see Whitaker and Smart, 2007; Moore, 2009).

Vertical Mixing and Brine Reflux

Evaporation-driven brine reflux is a major process in the system, as observed in PCA analysis and in the Br and Cl relationship. In addition to the findings from Chapter 3 that the vertical fluid flow dominates the sabkha system as compared to lateral fluid flow, the greater similarity in conservative ion concentration within a sabkha zone than when compared to other sabkha zones signifies a relatively well mixed solutes between the Dammam aquifer and sabkha aquifer.

When focused on just one sabkha zone, the greater Cl concentration within the Dammam Formation aquifer underlying the sabkha as compared to the sabkha itself and the greater Cl concentration at the water table as compared to the phreatic zone within the sabkha, indicates that there is an unstable density constrast in both aquifers. The density contrast hints at a downward movement of waters from the sabkha to mix with the fresher waters coming in from the outcropping Dammam Formation updip. Evaporation of top of the sabkha surface draws water molecules upward through the capillary fringe which it then draws water through the thin unsaturated (vadose) zone from the top of the water table. It leaves the remaining solutes at the water to table become more saline and denser and eventually sink downward through the permeable sabkha over time, with its position previously at the water table replaced by a less dense brine from the Dammam formation allowing the cycle to continue.

It is difficult to envisage how the relative higher Cl concentration, especially within the proximal sabkha or the Dammam underlying the stratigraphy, can be explained by halite dissolution, given very minor halite is observed within this sabkha zone. Brine reflux is further evident by the high dissolved oxygen (DO) content found in the sabkha waters providing hints of aeration or oxygenation of groundwater and the lack of microbes presence (Rounds et al., 2013). The lack of vegetation in the sabkha, except for minor xenophytes in the proximal sabkha, tells us that the source of oxygen is entirely from the atmosphere. Sabkha's shallow water table (about 0.5 m below surface) means that the groundwater is in contact with the atmosphere and thinness of unsaturated zone allows the infiltration of O_2 and thus oxygenating the system.

The highest DO observed in the middle sabkha thus indicates that evaporation-brine reflux is more dynamic in the middle sabkha and thus allowing greater oxygenation of groundwater. DO tends to decrease with depth (Drever, 2002), hence the greater DO observed in the Dammam Formation indicates that there is likely a (1) greater aeration due to greater groundwater flux within its karstified layer compared to its overlying sabkha and underlying deep Dammam and/or (2) lateral groundwater mixing with local seawater infiltrating the shallow Dammam from offshore landward.

Lateral Mixing in the Dammam Formation

Increases in conservative ion concentrations with Cl within the outcropping Dammam Formation updip groundwater, with increased proximity to the sabkha and coast, indicates lateral mixing of meteoric waters with sabkha and seawater respectively. The waters within the Dammam underlying the sabkha show a sharp increase in Cl concentrations from the proximal (northwest) to the distal (southeast) where the ephemeral salt flat is. When compared to the sabkha waters between the upper and middle sabkha, the increase of Cl in the sabkha is sharper with a three-fold increase, ~2300 mmol l^{-1} per km. The Cl increase between the Dammam underlying the sabkhas at the same boundary zones show less of a gradient than in the sabkha over the same distance (~1500 mmol l^{-1} per km). This lateral contrast in Cl highlights that at least within the sabkha, the reflux of high salinity waters from the overlying sabkha is greater than the lateral mixing.

The lateral mixing within the Dammam Formation underlying the sabkha is evident by the Cl ion concentration within the proximal sabkha is twice greater than in the underlying Dammam Formation. This unstable density contrast suggests that the flow down rate (reflux) in the proximal sabkha is smaller compared to the lateral flow of the freshwater in the Dammam, confirming our hydrogeologic results in Chapter 3.

The seawater inundation and percolation through the Dammam underlying the sabkha appears to control the Cl concentrations in the lower and middle sabkha. This is reflected by a gradual decrease in Cl within the Dammam from the middle sabkha to the coastline (~1000 mmol l^{-1} per km decline). This also indicates mixing of seawater with hypersaline brines. The mixing at this interface from salinity in the hydrogeology study shows that the middle sabkha is a brine plume of "ionic soup mix" of SO_4 from the outcropping Dammam Formation updip and Ca from seawater or calcite dissolution for gypsum precipitation.

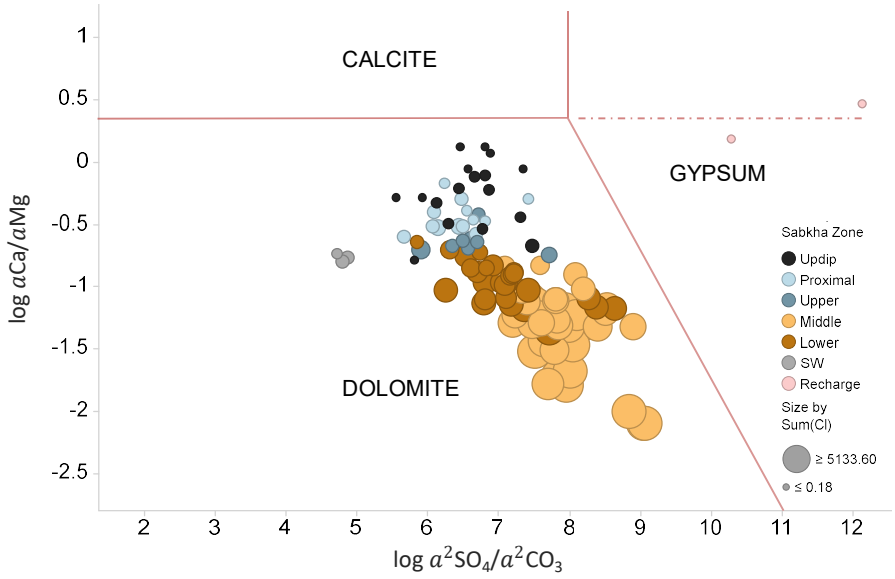

Figure 4-14. Phase diagram of water-rock interaction between waters sampled in different sabkha zones and reactive minerals in the Mesaieed system – gypsum, dolomite, calcite. Marker colours are used for sabkha zones the waters are hosted in instead of stratigraphy due to greater discernible differences. Symbol size increases with increased Cl concentration. Red solid lines represent phase boundaries between minerals, and represent chemical equilibrium between different mineral phases. The horizontal semi-dotted line represents an extension of metastable dolomite-calcite phase boundary into the gypsum stability field (see Moore, 2009).

4.5.2 End-member solute sources

All sabkha waters fall within the dolomite stability field on the phase diagram (Figure 4-14), which indicates that these waters have primarily reacted with dolomite, reflecting the majority of the source waters from the dolomitised Dammam Formation underlying the sabkha.

According to groundwater head model in Chapter 2, the dominant source of solutes to the proximal and upper sabkha is the meteoric groundwater within the outcropping Dammam Formation aquifer. The Dammam Formation brackish waters have Na > Cl > SO_4 > Mg > Ca in 1.00 : 0.94 : 0.13 : 0.12 : 0.08 molar proportions. The dominance of Na and Cl mirrors the rain waters that in itself has Na and Cl as its main dissolved species, which reflects the proximity of coastal sources (Drever, 2002). There is a possibility of a direct lateral mixing with waters within the highly permeable pathways in the Dammam as seen in natural fractures and joints of the cores.

XS calculations provide direct indication of ion/gain by process other than evaporation. The aqueous chemistry for the Dammam aquifer highlights a positive XS for K, SiO_2, Al, B, Sr, Ca, SO_4, and HCO_3 relative to local seawater indicating minor enrichment of the ion relative to conservative evaporatrion processes (Figure 4-5, 4-7). The Dammam aquifer appears to have an insignificant enrichment in Na as compared to Na:Cl ratios found in rainfall and seawater samples which likely indicate cation exchange with clay. When we look at the Ca and SO_4 ions separately (4.06±11.0 mmol l^{-1} for SO_{4XS} and 6.10±6.90 mmol l^{-1} for Ca_{XS}), it may tell us that processes such as calcite dissolution or secondary

dolomitisation replacing calcite provide the source of Ca and that process like H_2S oxidation helps with sourcing the SO_4. The 1:1 relationship of the Ca_{XS} and SO_{4XS} waters observed in the XS plot (Figure 4-16) confirms that gypsum dissolution process dominates the system within the aquifer. Vertical groundwater head study within Chapter 2 highlights an upward movement of waters, so it is logical that SO_4 and Ca -rich natural waters reflects gypsum dissolution from within the deeper formations. The process is observed by Eccleston et al (1981) within the underlying Rus Formation. Although there is an excess of Ca and SO_4 in this aquifer, the potential for gypsum precipitation within the outcropping part of the Dammam Formation is low (SI_{GYP} = -0.47). This provides solutes for the proximal and upper sabkha for potential evaporative-driven gypsum precipitation.

Enrichment of K within the Dammam Formation updip of the sabkha indicates that sources of K in the proximal sabkha could be clay dissolution, dry deposition (dissolved in rainfall) and/or aeolian siliciclastics blown over from the mainland up dip, specifically from mica, potash and K-feldspar (Warren, 2016). However, with less than <5% of clay found in the XRD Aeolian clays can be due to the minimal clay found in XRD data in Chapter 2. Enrichment of Al and B indicates clay dissolution (Uhlman, 1991; Leyshon and James, 1993; Gupta, 1993 for B) while SiO_2 indicates silica and/or clay dissolution. The sabkha system shows that higher HCO_3 is observed within the outcropping Dammam Formation as compared to the ones found in the sabkha which indicates relatively less degassing of CO_2 through the vadose zone.

As discussed in Chapter 2, the second source of waters for the middle and lower sabkha is dominantly seawater. Local seawater chemistry shows that the Arabian Gulf waters are more evaporated compared to global seawater. It is Cl > Na > Mg > Ca > SO_4 > Ca type, with 1.00 : 0.85 : 0.10 : 0.05 : 0.02 molar ratios. As there is an infinite amount of seawater used to source the sabkha and that enrichment and depletion of ions were calculated using seawater as the conservative element, there is little to discuss regarding seawater except the potential for precipitation/dissolution (using saturation indices, SI). Like the outcropping Dammam aquifer, the current local Mesaieed seawater has no potential for gypsum precipitation (SI_{GYP} = -0.48). The slight negativity state of the SI indicates potential of the water to initiate minor gypsum dissolution. Additionally, the waters indicate for dolomite and calcite precipitation potential (SI_{CAL} = 1.08 and SI_{DOL} = 3.02). In the phase diagram (Figure 4-14), local seawater samples plot well more central within the dolomite stability field as compared to other waters which is attributed to greater Mg than Ca ionic activities controlling saturation indices. This explains why seawater has the highest saturation index with respect to dolomite (SI_{DOL} = 3.02±0.08) relative to other minerals.

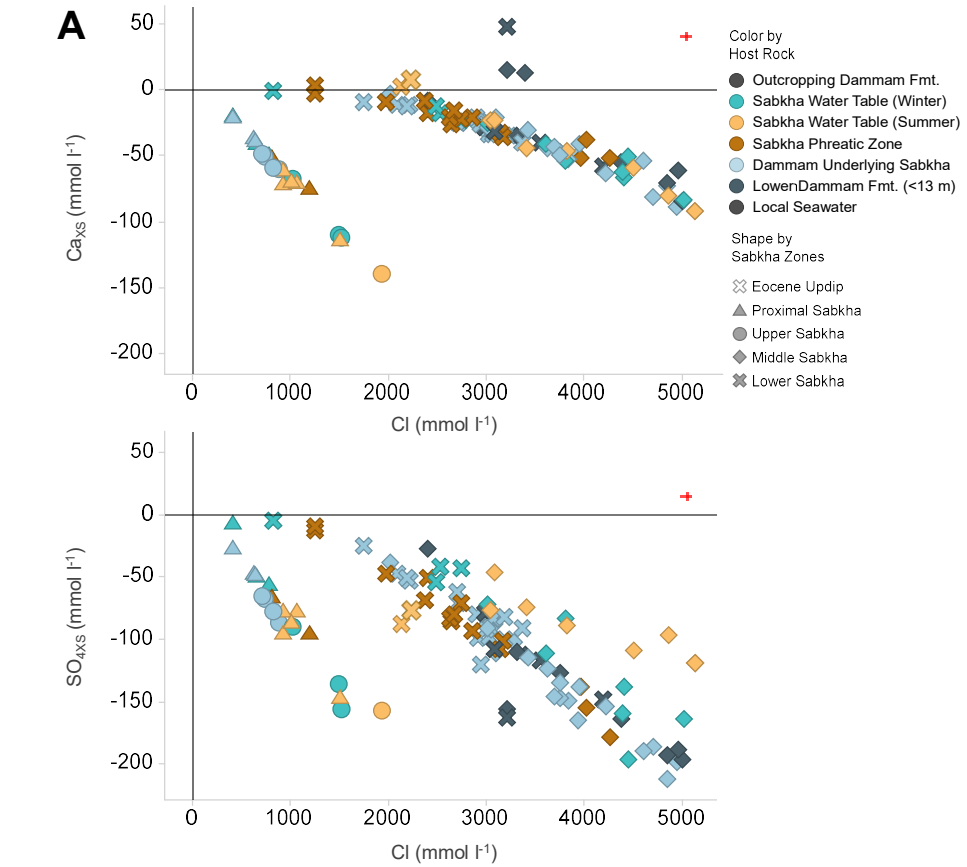

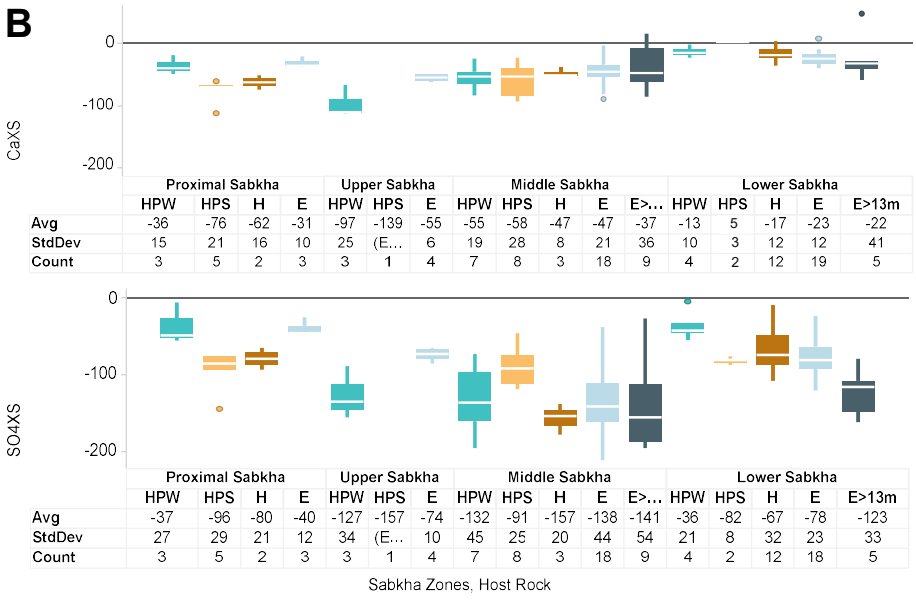

	Proximal Sabkha				Upper Sabkha			Middle Sabkha					Lower Sabkha				
	HPW	HPS	H	E	HPW	HPS	E	HPW	HPS	H	E	E>...	HPW	HPS	H	E	E>13m
Avg	-36	-76	-62	-31	-97	-139	-55	-55	-58	-47	-47	-37	-13	5	-17	-23	-22
StdDev	15	21	16	10	25	(E...	6	19	28	8	21	36	10	3	12	12	41
Count	3	5	2	3	3	1	4	7	8	3	18	9	4	2	12	19	5

	Proximal Sabkha				Upper Sabkha			Middle Sabkha					Lower Sabkha				
	HPW	HPS	H	E	HPW	HPS	E	HPW	HPS	H	E	E>...	HPW	HPS	H	E	E>13m
Avg	-37	-96	-80	-40	-127	-157	-74	-132	-91	-157	-138	-141	-36	-82	-67	-78	-123
StdDev	27	29	21	12	34	(E...	10	45	25	20	44	54	21	8	32	23	33
Count	3	5	2	3	3	1	4	7	8	3	18	9	4	2	12	18	5

Figure 4-15. (**A**) Plot of Ca_{XS} and SO_{4XS} with Cl (mmol l^{-1}) and (**B**) box and whiskers plot of its XS (mmol l^{-1}) for each sabkha zone and stratigraphy the waters are hosted in, with statistical table highlighting the mean (Avg), standard deviation (StdDev) and number of sample (Count). Red cross on cross plots indicate analytical uncertainty. Seasonal differences in the winter (HPW) and summer (HPS) were tested within the sabkha pits. Plots with Cl show a systematic depletion in both Ca and SO_4 with increase in Cl, which indicates an evaporation-driven water-rock interaction. Box plots with statistical table show that both in the upper and proximal sabkha show a greater depletion of both Ca_{XS} and SO_{4XS} in the sabkha than in the Dammam aquifer.

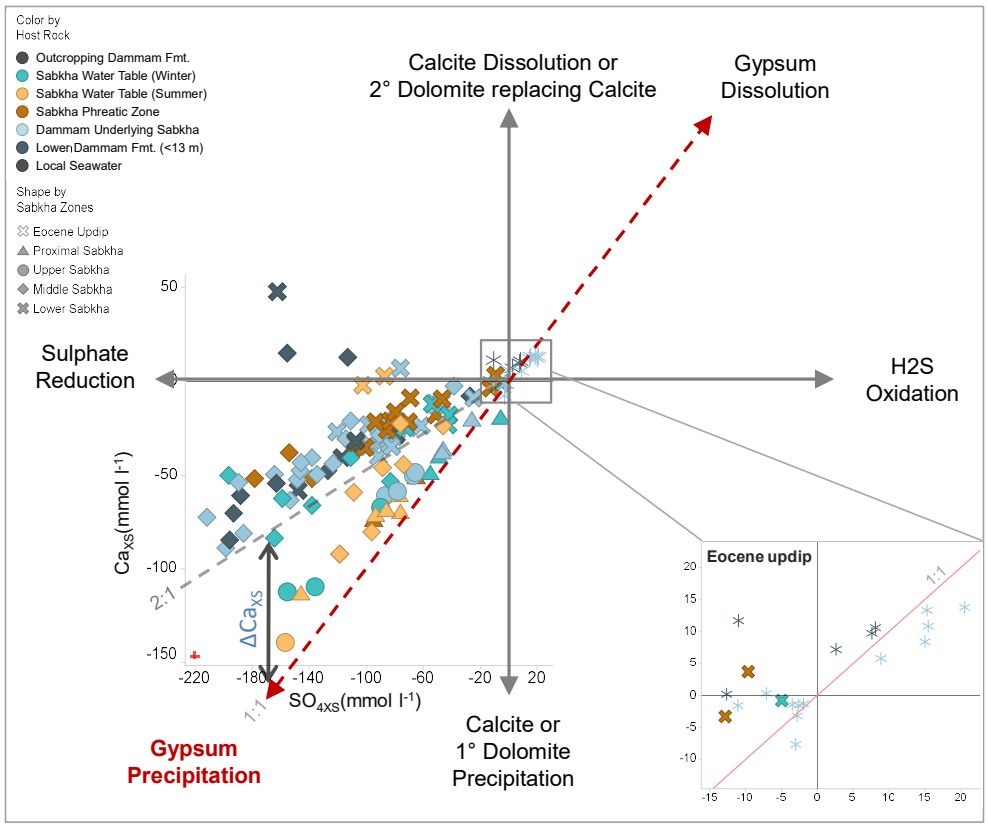

Figure 4-16. Plot of Ca_{XS} against SO_{4XS} with water-rock interaction processes involved. Grey line highlights the regression line with $R^2 = 0.638$. Inset on the bottom right shows a close-up of Outcropping Dammam Formation updip waters. All waters in the proximal and upper sabkha, including waters in the underlying Dammam, fall slightly to the left of the 1:1 depletion line for both CaXS and SO_{4XS}. The differences between the 1:1 line for expected gypsum precipitation and the sampled waters are denoted by ΔCa_{XS}. Most of the samples lie to the left of the 1:1 depletion line indicating that the major process in this system is gypsum precipitation.

4.5.3 Gypsum Precipitation

The sources of aqueous Ca in the sabkha aquifer include aeolian or precipitation of gypsyum, dolomite and calcite while the sink of SO_4 within Mesaieed can include bacterial-mediated sulphate reduction, gypsum or anhydrite dissolution. Insignificant proportions of gypsum is found in the aeolian sample (Chapter 2), abundant of gypsum found throughout the sabkha as pore cements (Chapter 2) and relatively high dissolved oxygen in the sabkha pore waters in Mesaieed indicate that gypsum dissolution, aeolian source and sulphate reduction are unlikely to source aqueous Ca to the waters.

Phase diagram in Figure 4-14 provided us a clue on water-rock interaction as evaporation drives the increase in salinity. All the waters, from within and below sabkha zone, falls along a trend which runs parallel to the phase boundaries of gypsum indicating reactions with this mineral. Marker sizes in Figure 4-14 are based on Cl concentration, which we know is primarily controlled by the degree of evaporation. With the increase in Cl, the waters trend not just away from the phase boundary of calcite but also closer towards the phase boundaries of gypsum indicating that greater degree of salinity is crucial for gypsum precipitation. a^2SO_4/a^2CO_3 ratios of the waters vary about 50% more than

aCa/aMg ratios, suggesting that most aqueous geochemical variation within the zone results from changes in SO_4 concentration. We can extrapolate from this observation that SO_4 is likely the limiting ion in reactions.

Gypsum precipitation can be inferred from SO_{4XS} for these reasons: (1) Ca ions can be involved in other water-rock interaction, (2) data from dissolved oxygen (DO) says that sulphate reduction is not possible (Rose and Long, 1988), and (3) SO_4 loss to celestine is insignificant (<2 mmols l^{-1}). This means that the varying degrees of SO_4 depletion, especially with increasing in conservative ion Cl, can be explained by gypsum precipitation (Gomis-Yagües et al., 2000) driven by evaporation.

Ca_{XS} and SO_{4XS} plotted against Cl (Figure 4-15A) shows a systematic depletion of both ions for all the waters sampled within the sabkha aquifer and the underlying Dammam Formation. Additionally, there is a 1:1 depletion for 30 out of 107 samples taken from the water table of the sabkha (or the sabkha pits). This indicates that these waters lost most of its Ca and SO_4 solutes to gypsum precipitation. For the present-day water table, it appears that gypsum precipitation is the most dominant process as sinks to Ca and SO_4. The reason for dominance of gypsum precipitation process can be driven by low pH conditions and limited HCO_3 from degassing, which acts as an important buffer that is preventing or slowing down calcite or aragonite precipitation. Taking into account of ~10% of marine inundation that is ponded within the lower sabkha (see Chapter 3) and ~50% of the waters observed within the pits that are slightly oversaturated with respect to gypsum, we can roughly estimate the proportion of gypsum precipitation. Using the average SO_{4XS} -36 mmol l^{-1} in the sabkha water table (from sabkha pit samples) in the winter yields ~2 mmol of gypsum expected to precipitate per liter of present-day brine.

The greatest depletion of both solutes and positive SI_{GYP} within the proximal-upper sabkha pit waters show that gypsum precipitation is at present occurring within the sabkha water table, at least during the summer. The waters in the deeper sabkha stratigraphy and underlying Dammam Formation are undersaturated with respect to gypsum, and yet are depleted in Ca and SO_4, indicating that the waters in which gypsum has precipitated from have likely refluxed downwards and mixed with the fresher and less depleted waters from the Dammam. From XS calculations, we can predict that about $\overline{x}$ of ~100 mmol of gypsum have precipitated within the proximal sabkha and up to ~160 mmol of gypsum within the upper sabkha per liter of brine in the summer. Field observations confirm that gypsum is limited to the surface and in the vadose zone of the proximal sabkha while the extensive gypsum observed cementing the upper sabkha is partly a relict process.

In the middle sabkha, the combination of the depletion seen in SO_{4XS} data and positive SI_{GYP} (showing an oversaturated state) indicate that gypsum precipitation is actively occurring within the sabkha and the Dammam formation. The present-day brine appears to contribute between 90 to 130 mmol of gypsum per liter of brine. The geochemical data confirms the Dammam core observations of

gypsum cementing dissolution voids and the intermittent gypsum cementing the sabkha. This is further supported by field evidence from areas like the flowthrough pond located south of the upper sabkha zone, whereby centimetre-sized gypsum crystals have been noted to form over half a year.

In the lower sabkha, SI_{GYP} appears to be thermodynamically in equilibrium to slightly undersaturated with respect to gypsum minerals for most waters. Some waters within the Dammam and in the pits sampled in the winter show minor oversaturation. Paradoxically, these same waters also show depletion state relative to SO_4. However, from our hydrogeologic study there is an upward influx of waters from the Dammam. The ascending brines, likely from the deep Dammam, are much depleted in SO_4 and oversaturated with respect to gypsum, are mixing with the evolved marine porewaters within the overlying sabkha. The gypsum precipitation is thus limited to parts of the surface driven by evaporation of ponded marine inundation (as highlighted with some pits waters). This is confirmed with field observation of the sabkha and core observations of extensive diagenetic gypsum within the Dammam formation.

Gypsum Precipitation Potential

Saturation indices tells us the present thermodynamic state of the waters and their potential to precipitate and dissolve minerals. SI_{GYP} of seawater is -0.48±0.09 is undersaturated while the rainfall is very undersaturated (-2.44±1.59). These conditions mean that rain waters and seawater has the potential to dissolve any gypsum upon contact, however large differences with the oversaturation states of sabkha waters indicate the evaporation of these waters are rapid and thus dissolution reactions are expected to be very minimal. Within the sabkha zones, there are clear differences between the proximal-upper sabkha and the middle-lower sabkha. As lateral mixing within the sabkha spoatial zones are minimal, they will be discussed as separate zones.

The waters within proximal and upper sabkha are relatively in equilibrium with respect to gypsum. The Dammam aquifer underlying the sabkha however, show a higher degree of undersaturation (SI_{GYP} = -0.43±0.02). Within the proximal sabkha, the differences of the SI_{GYP} between the sabkha water table, sabkha phreatic and the seasonal effects are statistically insignificant. Altogether they have $\bar{x}$ of -0.16±0.15. Within the upper sabkha, the sabkha pit sampled in the summer shows minor saturation (0.15) compared to the winter samples (-0.15±0.04). Although, there is only one data of the summer to support this, this indicates that greater evaporation rate in the summer is likely to provide conditions for increasing gypsum precipitation potential.

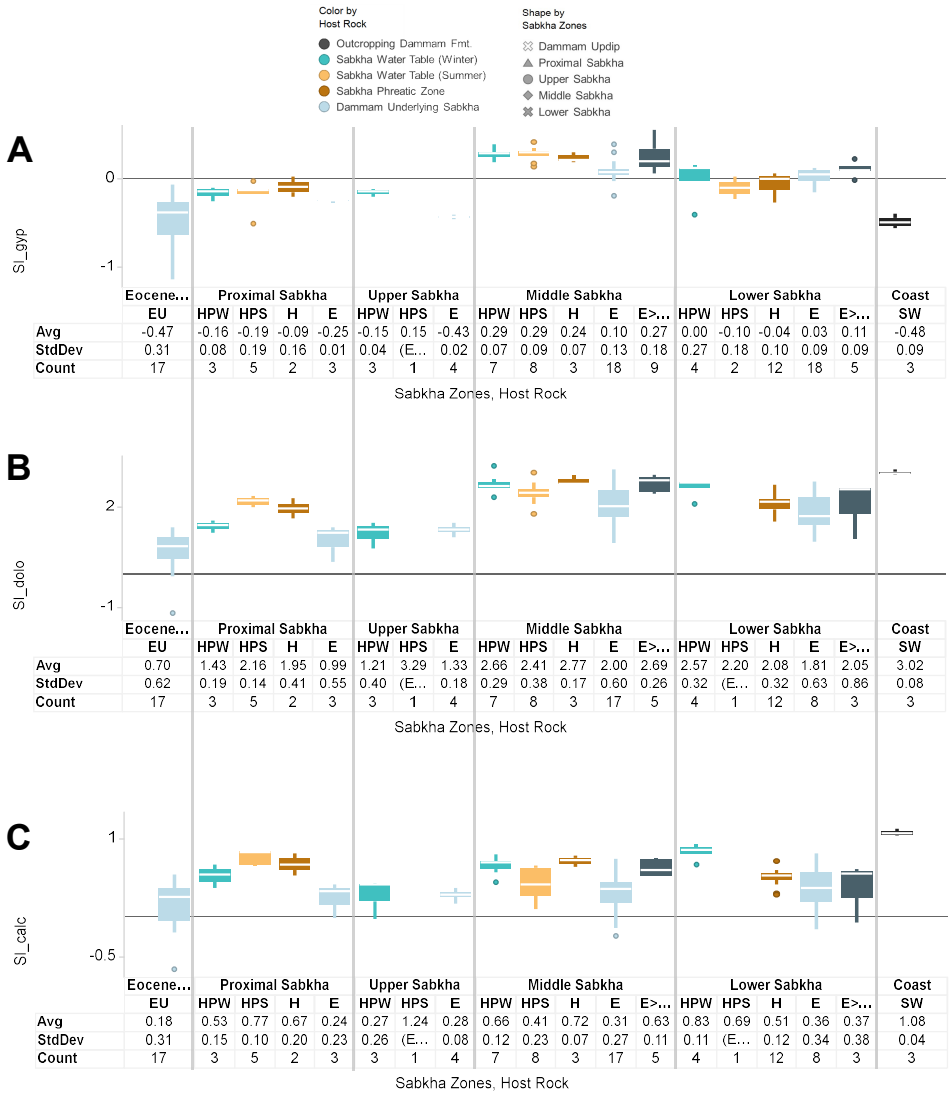

	Eocene...	Proximal Sabkha				Upper Sabkha			Middle Sabkha					Lower Sabkha					Coast
	EU	HPW	HPS	H	E	HPW	HPS	E	HPW	HPS	H	E	E>...	HPW	HPS	H	E	E>...	SW
Avg	-0.47	-0.16	-0.19	-0.09	-0.25	-0.15	0.15	-0.43	0.29	0.29	0.24	0.10	0.27	0.00	-0.10	-0.04	0.03	0.11	-0.48
StdDev	0.31	0.08	0.19	0.16	0.01	0.04	(E...	0.02	0.07	0.09	0.07	0.13	0.18	0.27	0.18	0.10	0.09	0.09	0.09
Count	17	3	5	2	3	3	1	4	7	8	3	18	9	4	2	12	18	5	3

	Eocene...	Proximal Sabkha				Upper Sabkha			Middle Sabkha					Lower Sabkha					Coast
	EU	HPW	HPS	H	E	HPW	HPS	E	HPW	HPS	H	E	E>...	HPW	HPS	H	E	E>...	SW
Avg	0.70	1.43	2.16	1.95	0.99	1.21	3.29	1.33	2.66	2.41	2.77	2.00	2.69	2.57	2.20	2.08	1.81	2.05	3.02
StdDev	0.62	0.19	0.14	0.41	0.55	0.40	(E...	0.18	0.29	0.38	0.17	0.60	0.26	0.32	(E...	0.32	0.63	0.86	0.08
Count	17	3	5	2	3	3	1	4	7	8	3	17	5	4	1	12	8	3	3

	Eocene...	Proximal Sabkha				Upper Sabkha			Middle Sabkha					Lower Sabkha					Coast
	EU	HPW	HPS	H	E	HPW	HPS	E	HPW	HPS	H	E	E>...	HPW	HPS	H	E	E>...	SW
Avg	0.18	0.53	0.77	0.67	0.24	0.27	1.24	0.28	0.66	0.41	0.72	0.31	0.63	0.83	0.69	0.51	0.36	0.37	1.08
StdDev	0.31	0.15	0.10	0.20	0.23	0.26	(E...	0.08	0.12	0.23	0.07	0.27	0.11	0.11	(E...	0.12	0.34	0.38	0.04
Count	17	3	5	2	3	3	1	4	7	8	3	17	5	4	1	12	8	3	3

Figure 4-17. Box and whiskers plot of saturation indices (SI) of the waters relative to gypsum (SI_{GYP}), dolomite (SI_{DOL}) and calcite (SI_{CAL}).

In the middle sabkha, all the waters hosted in sabkha water table are oversaturated (0.28±0.08), with no statistical significance in the differences between waters sampled within the summer, winter and of those sampled within the pits and the wells. Within the Dammam, the deep Dammam (0.27±0.18) show greater saturation than the shallower Dammam (0.10±0.13) ($p<0.01$). In the lower sabkha, the waters sampled within the sabkha are approximately in equilibrium (-0.04±0.14), with no statistical significance in the differences between the waters sampled. The waters are clearly affected by frequent marine flooding as they are undersaturated as compared to the Dammam aquifer (0.03±0.09) ($p<0.01$). Within the Dammam, the deeper aquifer show slight oversaturation (0.11±0.09) as compared to the shallower Dammam ($p<0.05$) which may indicate influence from marine waters.

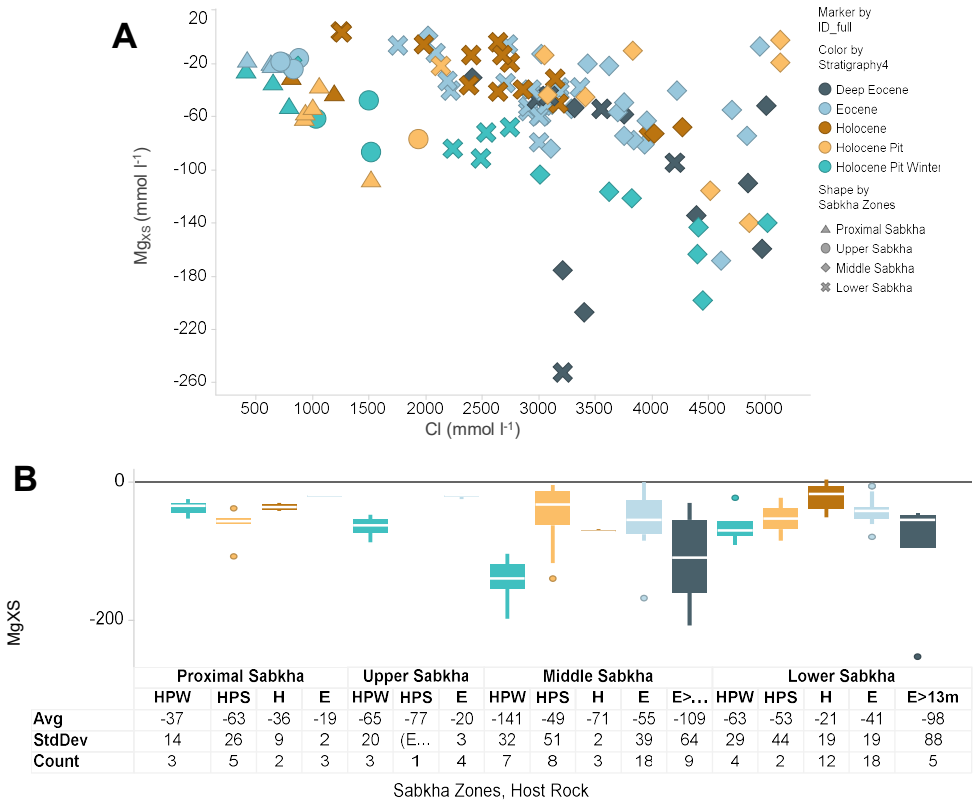

	Proximal Sabkha				Upper Sabkha			Middle Sabkha					Lower Sabkha				
	HPW	HPS	H	E	HPW	HPS	E	HPW	HPS	H	E	E>...	HPW	HPS	H	E	E>13m
Avg	-37	-63	-36	-19	-65	-77	-20	-141	-49	-71	-55	-109	-63	-53	-21	-41	-98
StdDev	14	26	9	2	20	(E...	3	32	51	2	39	64	29	44	19	19	88
Count	3	5	2	3	3	1	4	7	8	3	18	9	4	2	12	18	5

Figure 4-18. (**A**) Plot of Mg_{xs} vs Cl and (**B**) box and whiskers plot for Mg_{xs}. See Figure 4-3 for legend description.

4.5.4 Secondary Dolomitisation

Low pH and pCO_2 in an aquifer, especially if compared to the source waters, can indicate water-rock interaction with carbonates, for example carbonate precipitation. This is explained by the linear relationship between HCO_3 and pH (as log (H^+)) whereby $HCO_3^-(aq) \leftrightharpoons H^+(aq) + CO_3^{2-}(aq)$, and therefore the increase in evaporation leads to decrease of carbonate species allowing greater free hydrogen ions to lower pH (Drever, 2002). In local seawater and the outcropping Dammam Formation updip waters, Ca concentration is about one third of the SO_4 which means Ca should be a limiting ion within the sabkha system. Wells (1962) concluded that dolomitization and gypsum precipitation are concurrent processes, both representing sinks for calcium ion.

Dolomitization can occur if the brine meets the many often-debated conditions: (1) Mg/Ca >10 (Bush, 1973) or >6 (Patterson and Kinsman, 1982) or >5 (Warren, 2016); (2) Molar activity ratio of aMg/aCa > 1 (Drever, 2002); (3) High HCO_3 or abundance of $CaCO_3$ to be replaced (Machel, 2004); (4) High source of Mg, i.e. from seawater or dissolution of very high magnesium calcite; (5) pH more than 6.4, because the activity of HCO_3 is required to be more than H_2CO_3 (Drever, 2002).

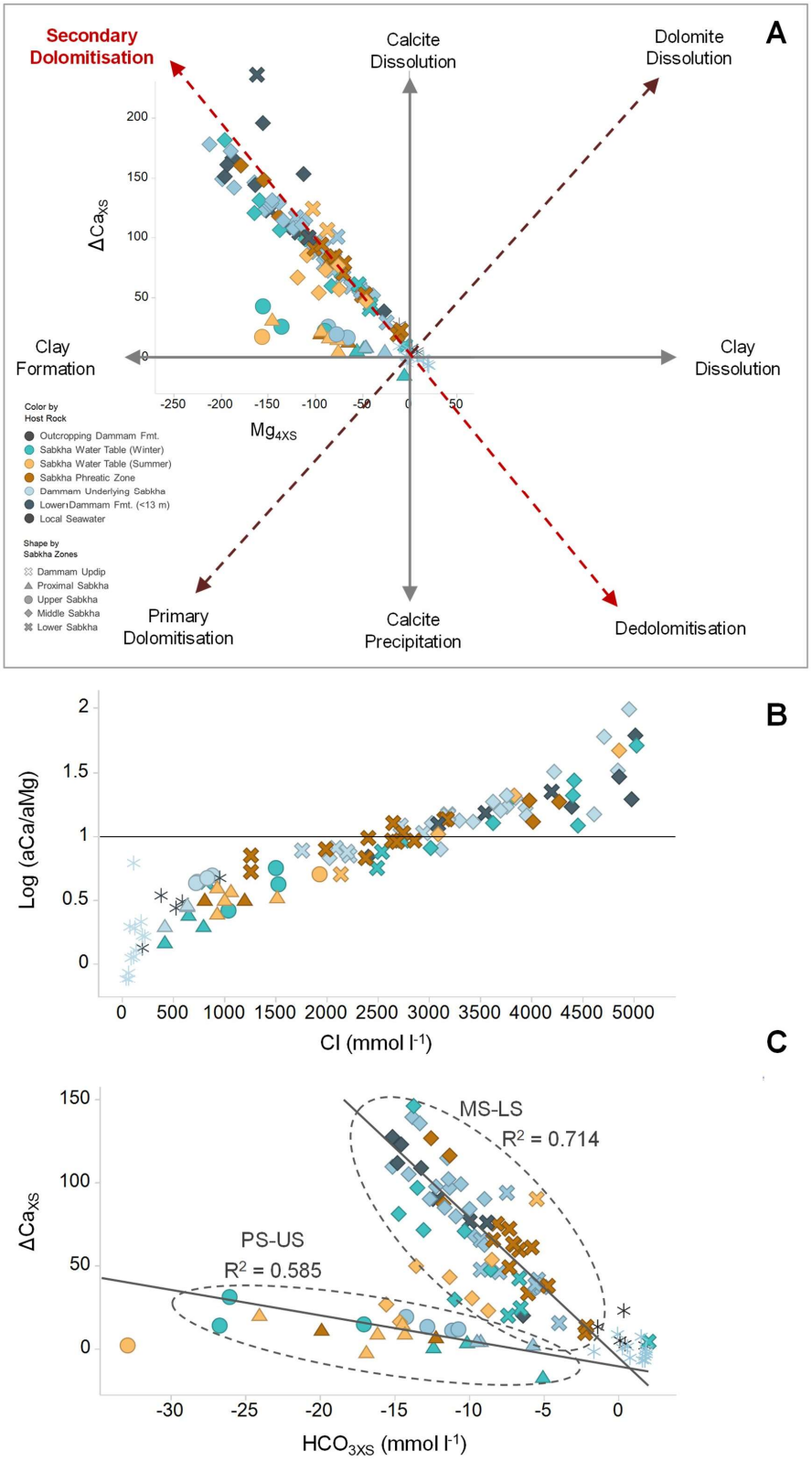

Figure 4-19. Plot of (**A**) ΔCa_{XS} against Mg_{XS} for all waters with the water-rock interaction processes expected based on 0:1 or 1:1 XS molar ratios. (B) Log of $\alpha Mg/\alpha Ca$ against Cl concentration, with a f(γ) = 1 line highlighting one of the "criteria" for dolomitization by Drever (2002). (C) Plot of ΔCa_{XS} against HCO_{3XS} with two grey regression lines and R^2 for PS-US and MS-LS.

The waters in the middle sabkha have Mg/Ca of >10 while the lower sabkha has Mg/Ca >6 due to seawater sourcing Mg into these sabkha zones. Marine flooding occurs 6-12 times a year when high tides coincide with low atmospheric pressure, providing the excess of Mg. The molar activity ratio aMg/aCa increases linearly with increasing Cl, surpassing 10 at 3600 mmol l^{-1} of Cl (Figure 4-19B). It highlights 41 % of samples have <1, with most of them being middle sabkha (85 %) samples and some 40 % of lower sabkha waters meaning that these waters have thermodynamical potential to precipitate dolomite.

HCO_3 is finite within the sabkha system compared to those of the source waters, which means that replacement dolomitization is more likely than primary dolomitiation. Figure 4-19C highlights the $HCO_{3\ XS}$ depletion of down to -30 mmol l^{-1} coinciding with increased ΔCa_{XSj} indicating replacement dolomitization. Hence a dolomitization replacement of calcite is the only process able to provide the bicarbonate ions needed. In the summer, temperatures of the water table reach up to 35 °C while the capillary zone sees waters reaching upto 45 to 50 °C. All the waters in the middle sabkha, except two samples, are above pH 6.4 concluding that calcite dissolution would have to supplement the dolomitization. This is important, because a pH < 6.4 means that H_2CO_3 species are more stable than HCO_3 (Drever, 2002).

However, there is of course the kinetic constraints that often accompany the '*dolomite problem*'. Therefore we can use XS calculations to constraint geochemical mass balance and provide us with clues of dolomitization within the sabkha system. SO_4 is observed within the sabkha and Dammam aquifers to be much more depleted, often double than of Ca. XS plots in Figure 4-16 show that samples fall to the left of the 1:1 gypsum precipitation line which means there is more depletion of SO_4 than Ca ions or that there is an additional source of Ca. After accounting for gypsum precipitation, there is either (1) additional loss of SO_4 via another process such as sulphate reduction, or an (2) excess supply of Ca from mineral dissolution or ion exchange. Scenario (1) is unlikely as we do not see evidence of sulphate reduction from DO data. The source of Ca can either be from secondary dolomitisation replacing calcite precipitation or dissolution of calcite. Although dissolution of calcite can be sourced by rainfalls providing the acidic conditions for dissolution of calcite grains within the sabkha and within the outcropping Dammam Formation updip, rainfall in Qatar is rare. To quantify additional sinks for Ca depletion, we can calculate ΔCa_{XS}, which is the amount of Ca_{XS} after accounting for gypsum precipitation. This assumes the SO_{4XS} is a representative molar of gypsum precipitated, which is reasonable given the linear relationship seen in Figure 4-18.

Mg_{xs} in the proximal-upper system and middle-lower system is calculated with two different reference waters (seawater and Dammam aquifer updip) to reflect the source of solutes. It appears that in general there is a progressive decrease with Cl (Figure 4-18A), at least for the waters within the sabkha water table and sabkha phreatic. This means that Mg is being removed from the waters for possibly

dolomite and clay. The decrease in Mg_{xs} with Cl is not straightforward within the shallow Dammam aquifer and in the deep Dammam.

Within the sabkha system, the ΔCa_{XS} correlates with Mg enrichment in all the waters along the 1:1 line (Figure 4-19A). This suggests that secondary dolomitization is the the dominant water-rock interaction occurring today after accounting for gypsum precipitation, with minor clay formation. Note that all the samples that align with secondary dolomitization are waters from the middle and lower sabkha, while waters within the proximal and upper sabkha fall to the left of the 1:1 line toward the clay formation. This depletion discrepancy within sabkha zones reflects that the mineral precipitation is limited by the source waters, seawater has greater supply of Mg while the outcropping Dammam Formation waters have a greater supply of Ca.

ΔCa_{XS} plotted against Mg_{XS} show that within the fourth quadrant, the outcropping Dammam Formation updip waters lay on the 1:1 line which indicates the waters have undergone minor dedolomitization and hence providing the excess of Ca into the proximal and upper sabkha (Figure 4-19A). These updip waters show a range of Mg_{xs} relative to the seawater (1 ± 8 mmol l^{-1}).

While there is abundance of dolomite within the Dammam Formation and the sabkha, at present there is a challenge in our ability to differentiate between primary and secondary (replacement) dolomitization, because the dolomites observed in XRD are a combination of detrital and authigenic. However, the possibility of authigenic dolomite as grain-coating phase in the sabkha has been shown with SEM and EDAX analysis (Jameson and Puls, in press). In the Dammam Formation however, it is even more difficult to delineate between authigenic dolomite and the host matrix which is a micro-crystalline dolomite.

Dolomite Precipitation Potential

The sabkha phreatic zone, especially in the middle sabkha and during the winter, appears to be where dolomitisation has a greatest chance of occurring based on SI calculations (Figure 4-17). Seawater has the highest SI_{DOL} ($+3.02\pm0.08$). The outcropping Dammam Formation updip has the lowest SI_{DOL} (0.70 ± 0.62) which is in contrast with rain samples, which has the lowest SI_{DOL} (-4.19). All waters within the sabkha system are very oversaturated with respect to dolomite (Figur 4-17). Within the proximal sabkha, the waters sampled in the pit (2.16 ± 0.14) is slightly more oversaturated than of the sabkha well (1.95 ± 0.41) ($p<0.05$). The waters sampled in the pits during the winter are lower (1.43 ± 0.19) than of the summer ($p<0.01$). The Dammam underlying the proximal sabkha show lower SI_{DOL} (0.99 ± 0.55) which is closer to the outcropping Dammam Formation updip waters SI_{DOL}. Within the upper sabkha, the single pit data shows a very oversaturated set of waters with respect to dolomite (3.29) as compared to the Dammam (1.33 ± 0.18) and the waters sampled in the winter (1.21 ± 0.40).

The middle sabkha shows a greater SI_{DOL} within the sabkha than of the shallow Dammam samples (2.00±0.60) ($p<0.01$). The waters in the sabkha pits, both summer (2.41±0.38) and in the winter (2.66±0.29), have lower SI_{DOL} than of the waters in the phreatic zone (2.77±0.17) ($p<0.01$). The seasonal effects within the pit samples are different as compared to the SI_{DOL} observed in the proximal and upper sabkha, whereby the winter waters have higher SI_{DOL} ($p<0.01$). The SI_{DOL} within the lower sabkha shows similar patterns with the middle sabkha, whereby the sabkha shows a very oversaturated with respect to the Dammam samples, with SI_{DOL} of +1.81±0.63 ($p<0.01$). Within the sabkha, the sabkha pits (2.57±0.32) are greater than the sabkha wells (2.08±0.32) ($p<0.01$).

4.5.5 Minor Clay Precipitation

About half of the waters have low $a\mathrm{Mg}/a\mathrm{Ca}$ low, especially within the lower sabkha aquifer, and therefore do not have the right conditions for replacement dolomitization (Figure 4-14B). Hence for these waters most of the Mg depletion observed is most likely due to Mg-clay precipitation which ties back with our core observation of palygorskite, illite and minor chlorite. Clay minerals observed in cores may reflect paleodrainage detrital deposition of argillaceous materials during exposure in the Pleistocene era prior to sabkha deposition (Warren, 2016). However, the concurrent depletion of K, Al, B and Si relative to source waters (i.e. Dammam Formation updip and seawater) support the recent occurrence of authigenic clay precipitation in the sabkha system, at least within the middle and lower sabkha and in the underlying Dammam aquifer. This supports field and XRD observations of chlorite, palygorskite and illite (see Chapter 2) within the Dammam core and sabkha (Al-Youssef, 2003). Arid clays such as illite and palygorskite is typically formed in-situ in highly evapoconcentrated brine environments whereby magnesium ions are aplenty (Fisher, 1988). It is noted that sylvite (KCl) precipitation is highly unlikely as it is not observed within the cores and would require a concentration of seawater by 20-fold (Warren, 2016).

Aqueous Si and Al ions within the outcropping Dammam Formation updip waters are enriched relative to conservative seawater evaporation and may provide additional solutes for clay precipitation in the proximal and upper sabkha. Another supporting evidence for clay precipitation is that the major constituent of the primary deposition in Mesaieed is silica, from quartz (SiO_2) (refer to Chapter 2), especially in the proximal to the middle sabkha. Marine flooding, especially in the summer, provides the necessary pH (pH > 8.0) and temperature conditions for minor silicate weathering and hence, the slow dissolution of quartz silica (Boggs, 2009; Abed, 2002). This theoretically could contribute to excess of SiO_2 in the system. However, the fact that Si in the sabkha aquifer is depleted indicates that the loss of SiO_2 out of solution to arid clays like palygorskite, illite and chlorite.

Depletion of K observed in the Dammam Formation aquifer is likely due to the precipitation of arid K-clay such as illite and palygorskite which were observed within the cores underlying the middle sabkha Brine depleted in boron can indicate borate evaporite or palygorskite and illite precipitation

under marine conditions (Fleet, 1965; Harder, 1970). However, borate evaporites tend to form in cooler conditions, lacustrine environment and usually at high elevation (Warren, 2010). Mg-clays deposited under marine conditions have higher boron incorporated into clays by a factor of 2 - 10 and are deposited in meteoric or continental waters (Fairbridge, 1972). Therefore, the loss of solutes to barite is ruled out for Mesaieed sabkha system. Additionally, borate evaporites were not detected in XRD, while diagenetic palygorskite, chlorite and illite are present in the sabkha and the Dammam underlying the middle sabkha with concentrations up to 5% (Al-Youssef, 2003).

The depletion of Al ion relative to measurable concentration of end-members beyond the lower detection limit hints that Al in the sabkha system is the limiting ion.

Palygorskite (or attapulgite; $Mg_{1.5}\,Al_{0.5}\,Si_4\,O_{10}\,(OH)\,4(H_2O)$) is commonly found in arid regions with hypersaline brine rich in Mg and Si, and with the presence of carbonate and sulphate minerals (Velde, 1985) and it is the major clay constituent in Mesaieed. Authigenic palygorksite often requires capillary action and continuous evaporation to concentrate solution to form magnesian silicate minerals (Velde and Meunier, 2008). Mg and SiO_2 are necessary components for palygorskite formation, preferably with near exclusion of other constituents and between 1:2 to 1:5 ratio (Galan and Singer, 2011). Depending on the pH, the former can be sourced from quartz which constitute half of the host rock matrix in the sabkha, while Mg can be sourced from local seawater (which is the third most abundant ion). Si ions are potentially liberated into solution which further supplement the formation of palygorskite. However, for SiO_2 dissolution to be possible, a pH of below 4 or above 8 is needed for dissolution of Si-minerals (Drever, 1992, 1994; Velde and Velde, 1995) and the middle sabkha water table has the lowest pH of the entire system, which is to say only marine inundation of local seawater, with a pH of 8.2, is necessary to facilitate silica dissolution and palygorskite formation. The rare recharge events ($pH<4.5$) may assist in dissolving calcite grains which may raise the alkalinity at the capillary zone and water table.

Although Si was not analysed in most of the waters, silica dissolution may provide a minor factor in explaining the decrease of siliciclastics from proximal sabkha (65 %) towards the coast (<35 %), even though active aeolian deposition of siliciclastics is still occurring today.

Chlorite, $(Mg,Fe)_3(Si,Al)_4O_{10}(OH)_2\cdot(Mg,Fe)_3(OH)_6$, the second most abundant clay in Mesaieed, is another Mg-rich clay that is usually formed from early diagenetic reactions during evaporitic conditions (Hillier, 1993). Chlorite is often an indication of a strong Fe content in the absence of Al or conditions of low Al activity with minimal alkaline conditions input. Illite ($K\,H_3O\,(Al, Mg, Fe)_2\,(Si, Al)_4\,O_{10}\,[(OH_2),H_2O]$), the third most abundant clay in the sabkha system (~5 %), is a potassium silicate clay usually formed by alkaline conditions and high concentrations of Al and K, and/or weathering of silicates, primarily from K-feldspar (Wilson et al., 2013, Velde and Meunier, 2008):

$$K - Feldspar\ +\ H^+ + Mg\ \longrightarrow Illite + K^+ + Si^{4+} \tag{4.17}$$

4.5.6 Minor Celestine Precipitation

Decrease in Sr with an increase in Cl signifies either aragonite and/or celestine ($SrSO_4$) precipitation. In M1 pit (Chapter 2), neither celestine nor aragonite is found in the top 60 cm where the brines were sampled, but in deeper samples, 2 % of celestine is found near the base of the sabkha (6.8 m bgl) and 7% of aragonite is found throughout M1. This means that minor amount of celestine is precipitating.

In seawaters aragonite precipitation can lead to removal of Sr compared to Ca in a molar proportion of 1.1 x 10^{-2} to 1 (Budd, 1988), which would suggest that for samples Q2 and Q3, with a Sr_{XS} of -0.652 mmol, fluids should also be depleted by 60 mmols of Ca. Such depletion is not seen in the waters (see section 4.6.3)

As per observation of aragonite within the sabkha, Ca_{XS} and SO_{4XS} plot is nearly 1:1 indicating gypsum precipitation which supports core and field observations. This indicates the aragonite analysed is detrital or a relict. The Sr depletion in the brines is likely from celestite precipitation in a minor amount of just less than a mole per volume only occurring in the summer.

4.5.7 Validation of Field Study using Inverse WRI Modelling

To verify our models of fluid flow pathways and brine evolution, an inverse modelling technique for water-rock interaction (WRI) is used to understand the thermodynamic feasibility of water-rock interactions discussed. This technique is used to further validate XS and SI calculations. This numerical simulation uses mass balance to reconstruct reactions that may have happened to relate two solutions and phase assemblages along a known flow path (Figure 4-20). It assesses changes in major dissolved constituents as a means to estimate gypsum and associated carbonate precipitation between identified input solution in the outcropping Dammam Formation updip and seawater, and the sabkha brines. The assumptions made when modelling any mass-balance processes is that we assume a closed system, which means that the input solutions are in somewhat a steady state. This translates to an assumption that longitudinal and lateral dispersion and diffusion of species through porous medium is thus insignificant. Each solution is charged balance based on the IBE analysis within predetermined uncertainty limits, without which this adjustment the models will fail to converge. Results of the model are not unique, and hence they need to be ground-truth with field observations on degree of evaporation (relative to source waters) and existing mineralogy phases. Only a handful of conceptual models will be simulated to quantify gypsum precipitation observed in the proximal, upper and middle sabkha.

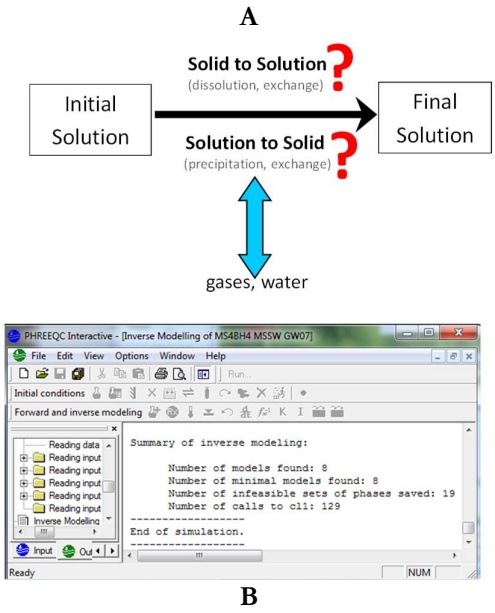

Figure 4-20. (**A**) Schematic of inverse modelling to understand water-rock interactions (highlighted by red question marks) whereby initial solution, final solution and reacting phases are known. (**B**) highlights the screenshot of the inverse modelling results on the program PHREEQC.

Calculations of mass balance processes were determined in geochemical modelling software PHREEQC (mixing with evaporation), which are constrained by ionic concentrations of Na, Cl, Mg, K, Ca, SO_4, HCO_3 along with pH and temperature in the initial and final solution. Parameters for the reaction of mineral phases were set to match those observed in the field and in the solution along the known flow path, which includes gypsum, calcite, dolomite, H_2O and CO_2. Results are shown in Figure 4-21.s

As shown in model 1 (Figure 4-21), the marine flooding event was simulated by mixing seawater with the present sabkha brine in the middle sabkha zone. The solution specifications for the initial solution is the local Mesaieed seawater. The mixing is simulated with brine hosted in middle sabkha (site J13), and the final solution is the brine underlying the Dammam (G7). The model shows that the brine in the middle of the sabkha can be stoichiometrically explained by precipitation of 0.01 mole of gypsum per kg of brine provided the solution has evaporated by nearly 4-fold (removing 40 mols of H_2O per kg of solution). The mass transfers also show a minor degassing of CO_2 and minor calcite precipitation, both with 0.001 mole per kg of seawater. The simulation of the resulting brine refluxed into the Dammam, shows that gypsum is again precipitated by 0.01 mole of gypsum per kg of brine with further evaporation of the mixed brine.

Inverse Modeling Results

S + 1 → 2

Solution	Solution Fraction	Phase mole transfers per kg	
S	0.78	Calcite	-0.001
1	5.22	Gypsum	-0.009
		CO2(g)	-0.001
		H2O(g)	-39.571

Model 1: SW -> Middle Sabkha

- Gypsum and minor calcite precipitation

Solution	Solution Fraction	Phase mole transfers per kg	
S	0.775	Dolomite	-0.001
1	5.37	Gypsum	-0.009
2	1.00	CO2(g)	-0.001
		H2O(g)	-39.860

Model 1.2: S + 1 -> Eocene under Middle S.

- Gypsum and minor dolomite precipitation

E → 3 → 4

Solution	Solution Fraction	Phase mole transfers per kg	
E	18.00	Dolomite	-0.001
4	1.00	Gypsum	-0.004
5	1.45	CO2(g)	-0.002
		H2O(g)	-49.526

Model 2: Proximal Sabkha

- Gypsum and minor dolomite precipitation

5 → 6

Solution	Solution Fraction	Phase mole transfers per kg	
4	6.30	Dolomite	-0.003
2	1.00	Gypsum	-0.004
		CO2(g)	-0.002
		H2O(g)	-40.572

Model 3: Middle sabkha at salt flat

- Gypsum and dolomite precipitation

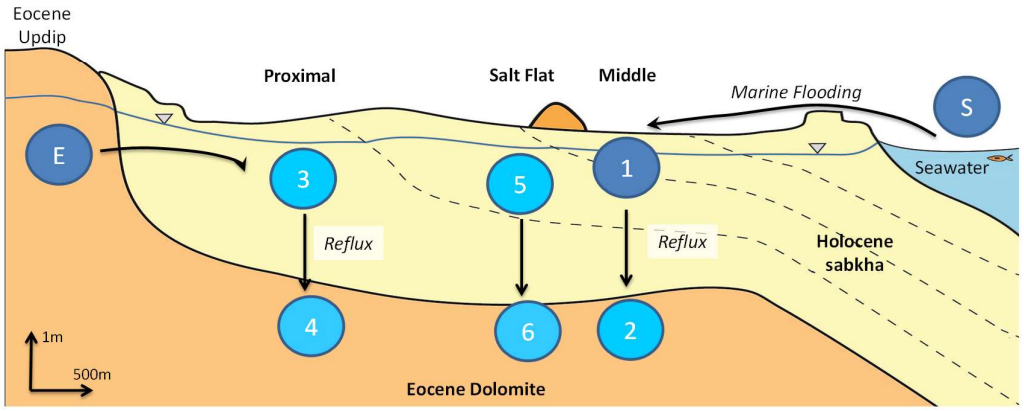

Figure 4-21. Results from four inverse geochemical models using PHREEQC. Phase mole transfer indicates the mole needed to transfer for the mass balance model, with negative indicating loss from brine to precipitation. In the case of H_2O it means how much water needs to be evaporated. Solution fraction indicates the relative proportion each solution needs to be for the batch reaction.

The second simulation (Model 2 in Figure 4-221) involves the continental waters updip (W4) and the proximal sabkha brine (M2p) as the initial solution while the Dammam underlying the sabkha (M2E) is the final solution. The model converged shows that the mass balance can be stoichiometrically explained by gypsum (0.01 mole), minor dolomite precipitation (0.001 mole), and degassing of CO_2 (0.002 mole). This also includes a condition that there is evaporation of 9-fold (removal of 49.5 mols of H_2O per kg of solution).

The reflux is simulated (Model 3 in Figure 4-21) using the sabkha brine that was sampled underlying the salt flat during the winter (JM4) as the initial solution and within the Dammam underlying the sabkha (G7) as the final solution. The model that converged shows that the brine in underlying the sabkha can be stoichiometrically explained by the precipitation of gypsum and dolomite in nearly equal

ratios, 0.004 and 0.003 mole per kg of brine, degassing of CO_2 (0.002 mole) provided there is a brine evaporation of 3.75 (removal of 40.6 mols of H_2O per kg of solution). This confirms the field observations of the gypsum in the core both in the sabkha and the Dammam aquifers.

All models show that the mass balance of water geochemistry today can be explained as gypsum precipitation is dominant, with minor precipitation of dolomite. Removal of CO_2 seems to be associated with the precipitation of dolomite. Release of CO_2 is likely occurring within the thin vadose zone for the (1) waters from the outcropping Dammam Formation updip that discharges into the sabkha and (2) residual marine waters at and above the water table.

4.6 Conclusion

This study attempts to understand the aqueous geochemistry in Mesaieed, a mixed siliciclastic-carbonate coastal sabkha that is located on the leeward side relative to the s*hamal*. This was done by quantifying the fluid chemistry in different sabkha zones in detail and model the water-rock interaction (WRI) using multiple proxy chemistry (XS and SI) within the sabkha aquifer. For a more holistic comparison of the system, comparison with the underlying Dammam Formation aquifer and using field observation of diagenetic evaporites (from Chapter 2) and the hydrogeological study (from Chapter 3) as ground truths were studied. Multitude of aqueous conservative and non-conservative geochemical processes that were quantified have exemplified the sabkha dynamics in mobilising solutes and precipitate minerals either as primary replacement minerals and secondary replacement minerals.

Br and Cl relationship not only highlights that Cl can be confidently used as a conservative tracer, but that evaporation is a dominant conservative process for the sabkha system. Evaporation process in Mesaieed has led to a cascade of other conservative processes including: (1) vertical mixing of the brines from the underlying Dammam aquifer into the sabkha porewaters, (2) brine reflux of the evaporated porewaters into the underlying Dammam aquifer, and (3) lateral mixing within the Dammam aquifer underlying different sabkha zones. The closeness in chemical composition of brines in both the sabkha and Dammam aquifer beneath each sabkha zone support a dominant vertical component allowing mixing of solutes, which confirms our equivalent freshwater head data in the hydrogeological study (Chapter 2). Additionally, the relationship of the aqueous ions to Cl have shown us that evaporation is likely to have led "domino effect" of non-conservative WRI processes such as gypsum precipitation, secondary dolomitisation with minor Mg-rich clay and celestine precipitation.

At present, the solutes in the proximal and upper sabkha are sourced from meteoric groundwaters hosted within the outcropping Dammam Formation updip aquifer, whilst seawater is the dominant source in the middle and the lower sabkha. This is supported by the principal component analysis which

shows a geochemical divide between the proximal-upper sabkha zones and the middle-lower sabkha zones. This means that the dominant solutes for the sabkha are different. Although both groundwater end-members are predominantly Na-Cl type, a significant molar proportion of secondary solutes for the outcropping Dammam Formation updip waters is SO_4>Mg>Ca whilst for the local seawater it is Mg>SO_4>Ca. Br confirmed only an insignificant exchange of fluid with halite so Cl can be confidently used as a conservative tracer to understand geochemical processes relative to conservative aqueous ions. Groundwaters within the outcropping Dammam Formation aquifer, located updip of the sabkha, have enriched concentrations of both Ca and SO_4 relative to rainfall and local seawater, reflecting dissolution of the gypsiferous beds within the dolomite bedrock, likely from Rus formation as hypothesized by Llyod et al (1987).

XS models provide a direct indication of water-rock interaction processes that has already occurred while saturation indices (SI) models inform us on the potential of the present-day waters for precipitation using geochemical mass balance equations. XS models are useful in normalizing evaporation effects using conservative ion from source waters as a proxy.

Sabkha waters, especially in the middle sabkha, are highly depleted in SO_4, Ca and Ca. The former two indicate the loss of solutes to gypsum precipitation (after ruling out sulphate reduction). Ca_{XS} and SO_{4XS} relationship has shown that modern sabkha waters have been actively precipitating gypsum especially in the middle of the sabkha, which ties with the highest gypsum distribution observed on the field in Chapter 2. While saturation indices indicate that the potential for gypsum precipitation within the proximal and upper sabkha is high, as evident from calcium and sulphate depletion, the massive gypsum cementation observed is partly a product of a relict process. This conclusion is supported by the SI models of the brines relative to gypsum about equilibrium (especially in the winter) and by the presence of surface crusts occurring as erosional remnants elevated relative to the modern Stokes surface.

Precipitation of gypsum within the sabkha results in groundwater which is significantly depleted in both calcium and sulphate. The degree of Ca depletion is markedly less than that of sulphate depletion, indicating an additional source of Ca within the brine. After accounting for gypsum precipitation, the associated Mg depletion in a 1:1 molar trend with delta Ca_{XS} indicates reflux-driven replacement of calcite by secondary dolomites, particularly within the Dammam Formation. Gypsum precipitation actively removes Ca from the system and the increase in aMg/aCa may facilitate dolomitization depending on kinetic constraints. While it may be difficult constrain the kinetics of the aqueous system, the 1:1 relationship of the XS calculations for the waters chemistry have shown us that secondary dolomitization process is very likely, as confirmed by SEM observations by Jameson and Puls (in press).

Dolomitization may be important in Mesaieed in releasing Ca, as suggested by reactive transport models of reflux dolomitization (Lu and Cantrell, 2016; Ehrenberg, 2006; Ehrenberg et al., 2006;

Rahimpour-Bonab, 2010), and thus providing additional source for further gypsum precipitation (Machel, 1986; Leary and Vogt, 1987). Existence of high percentage of dolomite may also facilitate dolomitization, as suggested by reactive transport modelling studies (Gabellone and Whitaker, 2016 and references therein) and laboratory experiments (Lumsden et al., 1995; Kaczmarek and Sibley, 2011) where the acceleration of the rate dolomitization is proportional to percentage dolomite.

Reactive transport modelling using mass balance geochemical constraints with PHREEQC helps to confirm and quantify our geochemical observations of gypsum and dolomite precipitation. The limitation to using PHREEQC as the chemical database for saline aqueous system does not currently have clay minerals.

Minor clay precipitation is evident from depletion in K, Mg, Al and Si which complements observations of authigenic Mg-clay on the field. However, current sabkha brine conditions of pH <8 are not conducive to precipitate clay in the lower sabkha, suggesting that marine inundation is important in providing the alkaline conditions for precipitation. Minor depletion of about Sr occurs only in the summer indicating very minor amounts of celestine precipitation, not aragonite precipitation as one would expect.

Evaporation of brines results in reflux downwards into the Dammam aquifer. Within the middle sabkha, these reflux brines remain supersaturated with respect to gypsum, providing a mechanism for forming evaporites in sequences that were not evaporitic during deposition, such as the Dammam. Saturation indices of brines relative to gypsum support this model especially within the middle sabkha.

Holistic understanding of the water-rock interaction and the controls of diagenetic distribution spatially can provide a fresh insights into the cumulative effect of these processes for a leeward coastal system that has a mixed siliciclastic-carbonate matrix. This study can reduce uncertainty in subsurface characterization workflows of analogous hydrocarbon reservoirs. 3-D geologic model and its facies distribution between wells can be confidently modelled in regions where well controls are limited. Additionally, an integrated understanding of the sabkha geochemistry allows us to build a robust 3-D reactive transport model of the petroleum systems to quantify the dissolution and precipitation of evaporitic minerals. This can substantially help with pre-drill understanding of the value of information before a well pad placement program. This study can provide insights to a more customized drilling and completion designs in order to avoid well paths with suspected heavy gypsum and dolomite cements.

5 Conclusions and Outlook

6,345 words

"If you are not part of the solution,

you are part of the precipitate"

5.1 Introduction

Evaporites and the associated carbonate minerals encapsulate a wide-range of water-rock interactions that can occur within arid mixed siliciclastic-carbonate systems, resulting in modification of rock properties such as porosity, permeability, and mineralogical composition. These alteration processes can happen by the supply and flow of reactive fluids to pore spaces where geochemical reactions are thermodynamically favoured. Whilst evaporites, clays and calcite react relatively quickly, kinetic constraints are important when considering dolomite diagenesis. As such, understanding the diagenetic provenance requires a combination of both hydrogeology and geochemistry.

Modern sabkhas are important as analogues for hydrocarbon reservoirs in arid zone sedimentary sequences and can even inform our understanding of paleoenvironments on Mars. Previous studies of modern sabkhas have largely focused on dolomitization in arid carbonate systems, due to "the dolomite problem" for hydrocarbon exploration. Despite the importance of understanding origin of evaporites in determining on the quality of hydrocarbon reservoir, little attention has been given to this. However, in the recent years this has changed when most of the reservoirs in the Middle East has reached production maturity, and thus require secondary and tertiary enhanced recovery. In addition, abundance of hydrocarbons is hosted in mixed arid clastic-carbonate systems and most studies on sabkhas are hosted in carbonate rock. Quantitative prediction of the source of solutes requires an understanding of the fundamental processes that provide sufficient fluid volumes of the appropriate chemical composition to produce the observed evaporitic overprint. The sabkha system is highly dynamic, and thus, understanding the overall behaviour of the system requires analysis of fluid sources, flow pathways, progressive evolution of intra-sedimentary brine, and resulting sequences of water-rock interactions.

Extensive fieldwork on sedimentological characterization, hydrogeologic testing, and geochemical sampling were undertaken for both Mesaieed and Dukhan sabkhas between February 2013 and March 2014 (a total of 16 weeks). However, construction of New Doha Port Authorities (NDP) in the south-east half of Mesaieed significantly affected the dataset collected from the middle-lower sabkha portion-from June 2013 onwards. As a result, fieldwork efforts and subsequent laboratory analysis for the Dukhan sabkha were intensified, with generous assistance from research supervisors, colleagues and Master's students. The effort generated nearly 1 GB of raw and structured data and approximately 10,000 data points.

However, a high volume of data in both structured and raw data formats was made available for use in this study by NDP Authority. Additionally, the NDP Authority provided generous permissions for site access which enabled data collection at an unprecedented high-resolution from (aquifer testing of over 50 wells with as little as 100 m laterally spacing). The 3-dimensional breadth of data for a relatively small sabkha area (6 x 10 km) is unprecedented. Such an opportunity of acquiring high-density

data within a single sabkha area or a modern setting is rare by both academic and industry standards. Hence, the focus of this thesis is to solely on maximizing useful information from Mesaieed's vast dataset.

Previous studies on sabkhas have often study them as a single system. The dominance of vertical flow compared to lateral flow for Mesaieed for only a small part of the sabkha, as was previously reported in Abu Dhabi (Sanford and Wood, 2001), necessitates a detailed study of how each part of sabkhas may differ. Our high-resolution dataset allowed the subdivision of the sabkha into different zones: the proximal and upper sabkha (which have contact with the continental bedrock updip), and the middle and lower sabkha (which are closer to the coast and make up the back-barrier sediment of the spits).

The purpose of this thesis is to document and understand:

1) Geomorphology and surface processes, to understand dynamic events such as drainage from updip, marine flooding, aeolian deposition and ephemeral salt formation, which helps to identify potential fluid and solute sources and sinks.
2) Quantitative primary sedimentology and secondary evaporites for both the Holocene sabkha and the Dammam, with a focus on the evaporite mineral gypsum.
3) Permeability variations to understand how to understand the aquifer properties of the Holocene sabkha and Dammam are affected by diagenesis.
4) Local climate, to provide context ural information on influences on the sabkha hydrology budget and conditions driving precipitation and dissolution of evaporites.
5) Hydrogeology, to reconcile potential sources of fluid and determine lateral and vertical fluid flow direction and rate.
6) Aqueous geochemistry of the sabkha, to determine water-rock interactions and processes that have already happened and thermodynamic potential of the brine to precipitate gypsum and associated minerals.

The following sections attempt to conclude and answer several overarching questions posed in Chapter 1 relating to early diagenesis of sabkha.

- What is the geomorphology and distribution of primary sediments and secondary evaporites in a leeward coastal sabkha in Mesaieed?
- What are the sources of fluids and flow pathways by which fluids are exchanged between marine waters, the updip aquifers, and the sabkha and the underlying aquifer?
- What are the sources of solutes for diagenetic evaporite mineralisation, and the subsequent evolution of the brine?

- In what way are hydrogeology and aqueous geochemistry able to provide insights into evaporite diagenesis, and what are its limitations?

5.2 Impact in the Petroleum Systems Characterization

"The present is the key to the past"

The uniformitarian principle is the basic assumption of using modern day sabkhas an analogue to understand hydrocarbon reservoirs in the subsurface. Using this study, the direct benefits will be the ability to build a more robust geologic models in in ancient reservoirs that were formed under similar arid environments, are mixed siliciclastic-carbonate systems or in a carbonate reservoir underlying a mixed siliciclastic-carbonate, and is positioned on the leeward coastal setting. With the technical opportunity to go from a classic sabkha model that has been dominated by Abu Dhabi sabkhas, this study highlights the heterogeneity presented in sabkha systems. Using Mesaieed as the other end member of sabkha models from the current Abu Dhabi sabkha model, we can now quantify and predict evaporite cements in mixed siliciclastic-carbonate leeward systems on an inter-well interpolation scale (Figure 5-2) in our static geologic and dynamic reservoir simulation models.

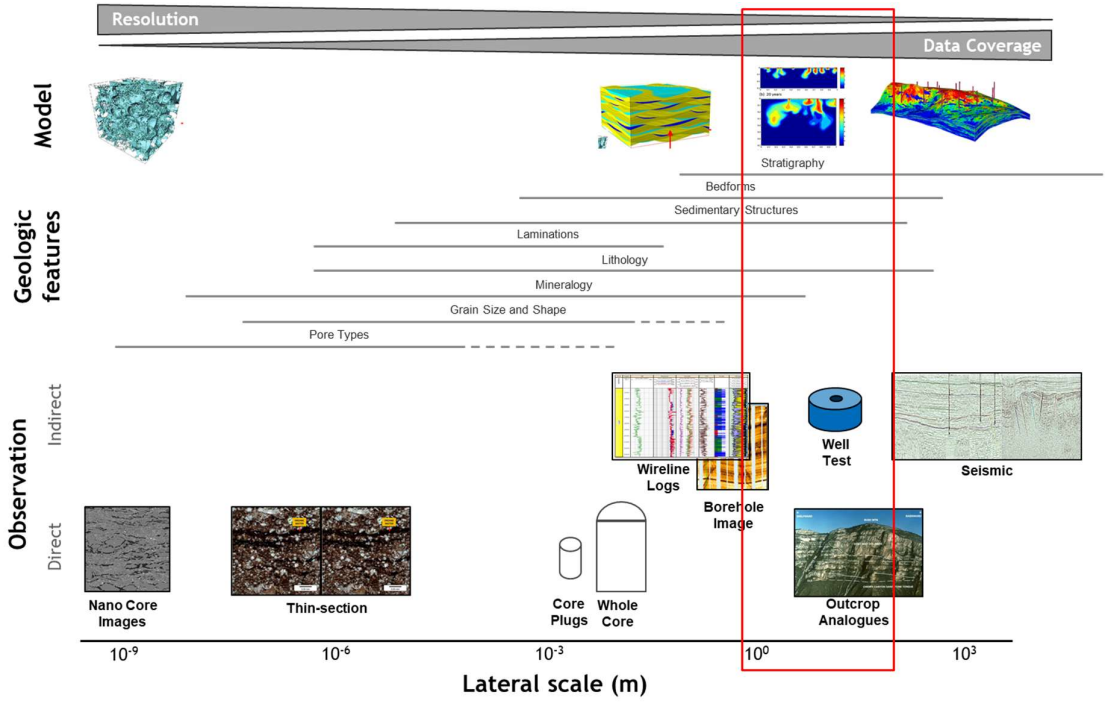

Figure 5-1. A plot of different geoscience models, geologic features and observational data by different lateral dimensional scale in meters. The red box highlights the inter-well scale that this thesis provides significant.

The capabilities from a higher density and higher quality data set provided for this thesis allows us to predict the sedimentation of a coastal sabkha and the corresponding evaporite diagenesis quantitatively using an integrated process-based method. This holistic study thus allows us to significantly reduce our model uncertainty in characterizing the lateral and vertical heterogeneity of the target reservoir .

This research impacts subsurface characterization efforts of petroleum systems, especially at higher mature stages for secondary and tertiary enhanced oil recovery. A simple example that can illustrate the value of this thesis is in aiding geoscientists in characterizing the lateral and vertical heterogeneity of the target reservoir that has experienced arid conditions, are mixed siliciclastic-carbonate systems or in a carbonate reservoir underlying a mixed siliciclastic-carbonate, and is positioned on the leeward coastal setting. Insights from this can impact the petroleum systems characterization application in a number of ways such as:

1. In the recovery of the whole core or cuttings during exploration or appraisal stage, sedimentologists are able to use distinguish different stages of sabkha evolution, the sabkha zones the wells are positioned and predict pre-drill locations with certainty where diagenetic evaporites may plug the reservoirs leading to a reduced reservoir quality.
2. Being able to plan well pad placements to maximise deliverability (high permeability) and storage (net pay, water saturation and porosity). For example, we will have the necessary data for drilling and completions to avoid zones of diagenetic evaporite cementation within the sabkha pores and the underlying formations, as observed in the upper and middle sabkha in Mesaieed where the reservoir quality is likely reduced substantially.
3. Refine lateral well placement during drilling (geosteering), to account for hazards posed by evaporitic cements.
4. Horizontal well completions by multi-stage hydraulic fracturing: selective plug and perforation positioning to favour zones that are non-evaporitic, and likely more productive. This will use significantly less natural resources such as sand and water.
5. Avoiding water disposal hazards in low-solubility zones, like halite. A good example of this is in the Delaware Basin where the Castille Formation consists of largely evaporites and water disposal is currently an expensive endeavour considering water disposal often occurs in the shallowest successions. This impacts the production of oil whereby water to oil ratio can reach up to 100:1. Therefore, understanding the sabkha system and how it impacts the surrounding formations can help to navigate around safety and environmental hazards that are posed by low solubility evaporitic zones.

However, evaporites are moderate to high solubility hence they easily remobilise in the subsurface. This method assumes the evolution and feedback of processes and environments through time are known,

such as fluctuation in seawater composition, global eustatic levels, regional tectonic movements, and climate change

5.3 Mesaieed vs Abu Dhabi Sabkha

The only significant prior studies of coastal sabkhas are in Abu Dhabi, United Arab Emirates. Studies of 3000 km^2 coastal sabkhas in Abu Dhabi have given the impression that sabkhas are comprised of carbonate host matrix, even when most of the sabkhas in the northeast parts of the Arabian Gulf are siliciclastic (Warren, 2016). The dominant primary sedimentology in Mesaieed is detrital aeolian siliciclastic, with increasing carbonate coastward up to 35% in the lower sabkha. While the interplay between carbonate and silicicic lastic will typically produce a mixed system of high lateral and vertical facies heterogeneity (Zeller et al., 2015), the less reactivity of siliciclastics will have implications on the water-rock processes.

For an apple and apple comparison, it would be more accurate to compare Mesaieed sabkha to Barr Al Hikman western sabkhas as it is both leeward and mixed siliciclastic-carbonate. Previous work done on Barr al Hikman sabkhas are very limited (see Mettraux, 2011). It is sedimentology-focused and looks at four sabkha areas with the western sabkha being closest to Mesaieed sabkha setting. The study is also only limited to the surface-water table stratigraphy, and therefore leaving us with no choice but to focus on comparing Mesaieed with Abu Dhabi instead to differentiate Mesaieed sabkha from the classic sabkha model that is currently being used extensively today.

Abu Dhabi's coastline is a windward facing, relative to prevailing northwestern shamal winds, barrier island-protected coastline, whilst Mesaieed is on the leeward side with no protection on the southeast. This difference in setting observed in Mesaieed, along with the formation of spit systems has resulted in both the progradation of Mesaieed coastward, and the aeolian erosion of the landward parts of the sabkha. Aeolian erosion of the Mesaieed sabkha creates a Stokes Surface, especially in the upper sabkha where nebkhas are not available for physical support. This process helps in keeping the water table close to the surface which is then more susceptible to greater pore evaporation. In contrast to published typical geologic sections from Abu Dhabi, the most common facies in Mesaieed sabkhas are cross-bedded siliciclastic deposited in depressions along the Pleistocene/Eocene-aged drainage (Jameson and Puls, in press).

In the summer months, Abu Dhabi sabkha is 25% less arid than Mesaieed. The Mesaieed sabkha region also receives approximately 30% less annual rainfall than in Abu Dhabi. Pore evaporation within Mesaieed is nearly twice greater than in the Abu Dhabi sabkha. The greater evaporation to rainfall ratio implies that evaporation will play a greater effect in driving the water table to saturation with respect to evaporites seen in Abu Dhabi.

The hydrological setting of Abu Dhabi has shown that in either continental or marine settings, rainfall makes up the overwhelming majority (99% in continental, ~90% in coastal) of water input into the Abu Dhabi sabkha system. Hydrogeochemical studies of Abu Dhabi to-date are dominated by ascending continental brine model, possibly driven by large hydraulic gradient from the Oman mountains to the east (Sanford and Wood, 2001; Wood et al., 2005; van Dam et al., 2009; Kraemer et al., 2014). These deep brines provide solutes into the sabkha which are then evapoconcentrated in coastal sabkhas (Wood et al., 2002;). The limitation to this study is that they did not consider hydrological input from the updip bedrock and assumed the lateral inflow from the updip will match the lateral outflow of sabkha brines. However, the problem with this mass balance assumption is that it is only true if there is no vertical flow component.

Hydrology in the Qatar peninsula, in contrast, resembles an island with a local meteoric lens (Eccleston and Harshash, 1981; Llyod et al., 1987). Consequently, there is a local hydraulic gradient driven by the outcropping Dammam Formation updip of Mesaieed, it is brackish and this has different implications for Mesaieed hydrogeochemistry. The southern half of Qatar's bedrock updip aquifers comprise both carboniferous and gypsiferous units and this may provide excess solutes when discharging into lower elevated coastal plains like Mesaieed (Eccleston and Harshash, 1981).

Hydrology studies in Abu Dhabi have similarly indicated that vertical flow is one order of magnitude larger than lateral flow. The well-rounded medium-grain siliciclastic nature in Mesaieed will mean that hydraulic conductivity is greater than the fine-grained carbonate sands in Abu Dhabi. This will have different implications to fluid flow in terms of lateral input from outcropping Dammam Formation, which itself is highly karstified.

5.4 Thesis Summary

5.4.1 Sedimentology Summary

A Holocene-age leeward coastal sabkha with siliciclastic-dominant host sediment was studied in unprecedented detail using time-lapse satellite imagery, multi-scale permeability and lost circulation data, carbon-14 derived age dates, mineralogy, and geomorphology data. Over 150 boreholes at both the sabkha and Dammam Formation, combined with 40 sabkha shallow pits, and historic satellite imagery provided a unique opportunity to characterize the dynamic processes and the sabkha system in-detail. This is the first detailed study ever done on an arid leeward coastal system, which provides an insight of a new sabkha end-member as compared to the classic sabkha model in Abu Dhabi. Mesaieed, the 75 km^2 area of interest, consists of Dammam carbonate bedrock overlain by variably lithified Holocene sediments. The flat sabkha, with about 1:1000-1:5000 of relief, is a result of Stoke's type deflation that allows flooding of marine waters to reach up to 8 km inland on the sabkha, with residual flood waters often observed in the middle sabkha.

The formation of Mesaieed sabkha is a complex relationship between a spit system, aeolian sedimentation, sea-level fall arid environment with little rainfall, and subsequent evaporite cementation. Observations of the height of the exposed Dammam Formation updip of the sabkha, erosional remnants of both Holocene-aged deposits and ^{14}C-based younging direction of sabkha sediments towards the coastline hints at the sea-level fall in the recent history. The drop in sea-level, circa 6,000 years BP, and aeolian supply from shamal winds, combined with the interplay of wind-dominated environment of deposition and tide-dominated low energy environment, were crucial components to the forced progradation of the coastal sabkha in Mesaieed. During the middle of the Holocene highstand (~4,000 yr BP), the sabkha experienced rapid seaward progradation of aeolian siliciclastics. In recent years (<3000 yr BP), carbonate accretion in the form of spits drive the remaining back barrier deposits in the middle and lower sabkha, comprising of mixed carbonate and siliciclastic. Preservation of the sabkha is driven by a combination of extensive gypsum cementation driven by meteoric discharge, shallow water table and beach ridges.

The internal stratigraphic and diagenetic architecture of Mesaieed is clearly reflected in the dynamics of primary sedimentation and secondary evaporite formation episodes. The sabkha is characterized by a predominantly siliclastic host sediment and gypsum as the syn-depositional diagenetic evaporite, and in that their distribution is controlled by a unique combination of a leeward coastal location, an evolving spit system, and an irregular surface topography, shallow water table and a falling sea-level history. The sabkha is divided into four zones based on the combination of geomorphology, primary mineralogy and diagenetic overprint observations, which are likely the result of its proximity to the coast and the updip continental sabkha (Figure 2-44). The sabkha zones were: (1) proximal sabkha, which is a semi-continental sabkha within upper part of valley in the Dammam Formation headland updip; (2) upper sabkha, which has extensive gypsum cementation, visible from the satellite imagery, and appears to act as a terminus between continental discharge and maximum and rare tidal flooding; (3) middle sabkha, a supratidal flat that is partially cemented by gypsum and within which ephemeral salt flat occurs, and (4) lower sabkha, which is supratidal to intertidal, with insignificant gypsum as crust and partially unprotected by beach ridges formed from a prograding spit system.

Previous study is limited to the Holocene sediments while this study attempts to understand the outcropping Dammam Formation updip and the Dammam underlying the sabkha. This study highlights the diagenetic features such as karsts and joints that will likely influence fluid flow while also highlight flow-inhibition features such as evaporite cementation, clay precipitation and possibly dolomite cements.

A similar relative to Mesaieed, the western sabkhas of Barr al Hikman would be another good modern analogue to further understand arid leeward coastal sabkha setting with mixed siliciclastic-carbonate host sediment (Mettraux et al., 2011). Bar al Hikman appears to represent the next geomorphology evolution for Mesaieed from a more open lagoonal setting to a more restricted evaporative

environment. This new study has implications for facies and diagenetic overprint trends for similar ancient arid siliciclastic-carbonate reservoirs in terms of understanding reservoir quality in the upstream oil and gas industry. Additionally this study provides a foundation for the study of hydrology, hydrogeology and aqueous geochemistry, with focus on the provenance of diagenetic gypsum within Holocene sediments, which will be discussed in subsequent chapters in the thesis.

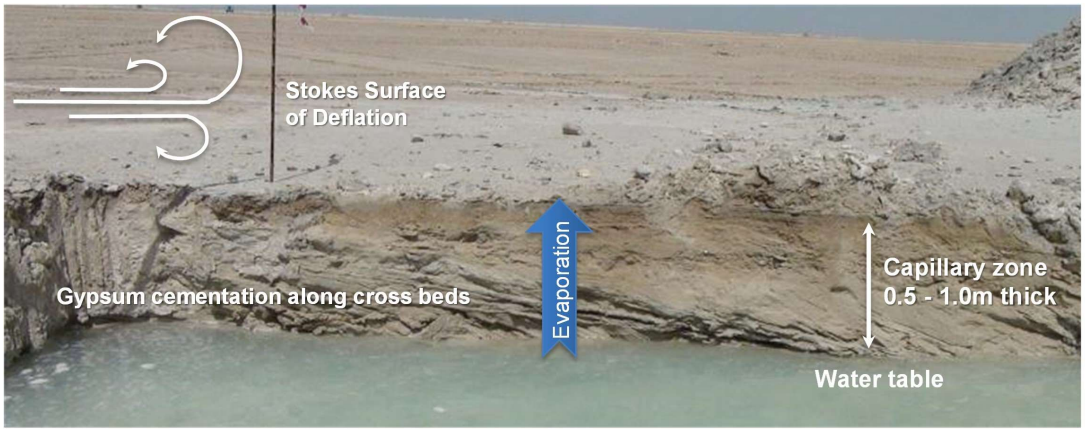

Figure 5-2. Processes observed within the sabkha at the near surface, with evaporation drawing porewaters up through the capillary zone.

5.4.2 Hydrogeology Summary

Quantifying groundwater flow systems is important to understanding fluid movement in the subsurface. The key importance of this study is the attempt to capture the sabkha groundwater flow components from a broader perspective. This includes understanding the climate and considering interactions between the waters hosted within deeper underlying aquifers and the updip meteoric aquifers.

Mesaieed is about 25% lower humidity than Abu Dhabi in the summer months, has about 30% lesser rainfall and is located on the leeward side of the prevailing wind. This aridity, combined with the siliciclastic nature of sabkhas and greater hydraulic conductivity, allows for the sabkha to be highly responsive to hydrologic events, such as rainfall, and also evaporation, compared to sabkhas in Abu Dhabi. Evaporation of pore waters is twice as high as that of Abu Dhabi evidence from time series water level data.

The drivers of flow within the sabkha system include evaporation, rainfall, lateral flow within the Dammam Formation, marine flooding, density-driven refluxes, ascending brine, and minor runoff. Empirical evidence using equivalent freshwater head and SEC as tracer confirms that the groundwater within both sabkha and Dammam formations is flowing from two different sources; outcropping Dammam Formation groundwaters and seawater via marine flooding and likely from the Dammam (in the lower sabkha). Brackish meteoric waters from the outcropping Dammam Formation updip discharges laterally into the proximal and upper sabkha, either as surface runoff or through the permeable

aquifers. Seawater appears to enter laterally from the coast through the more permeable Dammam underlying the lower sabkha and equivocally through percolation from the surface through seasonal marine flooding events.

The hydrogeology model derived from field data shows vertical flow of approximately one order of magnitude greater than lateral flow and that Rayleigh number shows that there is brine refluxing as a result of evapoconcentration of waters from the shallow sabkha. Lateral groundwater input from the outcropping Dammam Formation is important in sourcing the proximal and upper sabkha, while vertical flow dominates the sabkha and Dammam aquifers. For the proximal, upper, and middle sabkha it appears that downward flow is the dominant vertical component whereas upward flow into the lower sabkha from the Dammam is the main vertical component.

While barometric effects and tidal effects tell us the nature of the aquifer, their magnitudes are very small relative to the spatial differences in groundwater head (less or equal than 3 % of change in head Δh) Recharge, although rare, can give greater effects on two timescales, instantly and over several weeks. This demonstrates the necessity of correcting water levels before calculation of $h_{f,r}$.

In summary, the unsaturated zone of a sabkha is highly dynamic and responds to rainfall events quickly, which allows infiltration through the unsaturated zone. Salts on the surface or within the unsaturated zone are subject to undergo minor dissolution during rainfall. This inference may be important for calculation of solute budget especially in areas with high solubility evaporite minerals such as halite, but for Mesaieed this is insignificant.

In response to lateral hydraulic gradient by evaporation in sabkha, the solute budget indicates precipitation of minerals is likely driven by evaporation at the water table. This results in lowering of equivalent freshwater head and increasing brine salinity. The evapoconcentrated brines result in density instability and followed by reflux in most parts of the sabkha. In the lower sabkha this is not the case. Ascending brines dominate the vertical flow which allows the sabkha to increase in solutes over time. However, as gypsum precipitation is insignificant in the lower sabkha and is only limited to surface crusts, this means that the brines in the lower sabkha are increasing in concentration over time.

The importance of any groundwater head correction are often overlooked in major textbooks and papers (Simmons, 2005). This is the first study to attempt to understand groundwater flow in a sabkha system within a theoretical framework with necessary corrections of density referenced to well screen depth, using methods adapted from Post et al (2007). Groundwater level in a well varies over time and can be affected by barometric pressure, recharge, seasonal affects, local or regional pumping, earth and ocean tidal fluctuations, evaporation effects, and surface water fluctuations. Being a coastal sabkha with relatively permeable units, it is expected that some tidal influences would be felt landward. The extent of the tidal influence, requiring simultaneous monitoring of groundwater level wells in a sabkha system and the adjacent sea, has not previously been investigated.

Given the distribution of equivalent freshwater head $h_{f,r}$, the flow in the lower sabkha of Mesaieed agrees with the 'ascending brine model' theory proposed by Sanford and Wood (2001), in which upward leakage provides the source of solute. However, the evidence of evaporation-driven descending brine is observed in most parts of Mesaieed, which does not fit this model. The model based on the Abu Dhabi sabkha rests upon the assumption that the flow components within the updip of the sabkha (landward) would be the same with the lateral outflow (Sanford and Wood, 2001). These conclusions are not consistent with the budget fluxes for Mesaieed hydrology. This new model is based on hydrogeology data that are accessible in the outcropping Dammam Formation updip. The Mesaieed sabkha, although smaller than Abu Dhabi sabkhas by about one order of magnitude, highlights the heterogeneity in fluid and solute flow within a sabkha system.

As there is a mixture of evaporation-driven reflux flow within the proximal-upper-middle sabkha and an ascending brine recharge in the lower sabkha, I propose an empirical model of the hydrology of Mesaieed sabkha that is based on '**mixed evaporative-driven**' model. Upon examination of the hydrology models of Mesaieed, as well as comparison to the well-studied Abu Dhabi sabkha, there is no single flow system in any one sabkha or within the sabkha system. Different sites within the same sabkha may be subject to different flow systems, depending on the distance to the coast and the outcropping Dammam Formation. At any one time, one flow mechanism may dominate but the dominance of different flow systems is also likely to change through time, subject to shifting conditions such as sea level and climate, as well as diagenetic changes in porosity and permeability. The new hydrological framework will provide a proxy to understanding geochemical evolution of the brines in Chapter 4.

5.4.3 Geochemistry Summary

This study attempts to understand the aqueous geochemistry in Mesaieed, a mixed siliciclastic-carbonate coastal sabkha that is located on the leeward side relative to the s*hamal*. This was done by quantifying the fluid chemistry in different sabkha zones in detail and model the water-rock interaction (WRI) using multiple proxy chemistry (XS and SI) within the sabkha aquifer. For a more holistic comparison of the system, comparison with the underlying Dammam Formation aquifer and using field observation of diagenetic evaporites (from Chapter 2) and the hydrogeological study (from Chapter 3) as ground truths were studied. Multitude of aqueous conservative and non-conservative geochemical processes that were quantified have exemplified the sabkha dynamics in mobilising solutes and precipitate minerals either as primary replacement minerals and secondary replacement minerals.

Br and Cl relationship not only highlights that Cl can be confidently used as a conservative tracer, but that evaporation is a dominant conservative process for the sabkha system. Evaporation process in Mesaieed has led to a cascade of other conservative processes including: (1) vertical mixing of the brines from the underlying Dammam aquifer into the sabkha porewaters, (2) brine reflux of the evaporated porewaters into the underlying Dammam aquifer, and (3) lateral mixing within the Dammam

aquifer underlying different sabkha zones. The closeness in chemical composition of brines in both the sabkha and Dammam aquifer beneath each sabkha zone support a dominant vertical component allowing mixing of solutes, which confirms our equivalent freshwater head data in the hydrogeological study (Chapter 2). Additionally, the relationship of the aqueous ions to Cl have shown us that evaporation is likely to have led "domino effect" of non-conservative WRI processes such as gypsum precipitation, secondary dolomitisation with minor Mg-rich clay and celestine precipitation.

At present, the solutes in the proximal and upper sabkha are sourced from meteoric groundwaters hosted within the outcropping Dammam Formation updip aquifer, whilst seawater is the dominant source in the middle and the lower sabkha. This is supported by the principal component analysis which shows a geochemical divide between the proximal-upper sabkha zones and the middle-lower sabkha zones. This means that the dominant solutes for the sabkha are different. Although both groundwater end-members are predominantly Na-Cl type, a significant molar proportion of secondary solutes for the outcropping Dammam Formation updip waters is SO_4>Mg>Ca whilst for the local seawater it is Mg>SO_4>Ca. Br confirmed only an insignificant exchange of fluid with halite so Cl can be confidently used as a conservative tracer to understand geochemical processes relative to conservative aqueous ions. Groundwaters within the outcropping Dammam Formation aquifer, located updip of the sabkha, have enriched concentrations of both Ca and SO_4 relative to rainfall and local seawater, reflecting dissolution of the gypsiferous beds within the dolomite bedrock, likely from Rus formation as hypothesized by Llyod et al (1987).

XS models provide a direct indication of water-rock interaction processes that has already occurred while saturation indices (SI) models inform us on the potential of the present-day waters for precipitation using geochemical mass balance equations. XS models are useful in normalizing evaporation effects using conservative ion from source waters as a proxy.

Sabkha waters, especially in the middle sabkha, are highly depleted in SO_4, Ca and Ca. The former two indicate the loss of solutes to gypsum precipitation (after ruling out sulphate reduction). Ca_{XS} and SO_{4XS} relationship has shown that modern sabkha waters have been actively precipitating gypsum especially in the middle of the sabkha, which ties with the highest gypsum distribution observed on the field in Chapter 2. While saturation indices indicate that the potential for gypsum precipitation within the proximal and upper sabkha is high, as evident from calcium and sulphate depletion, the massive gypsum cementation observed is partly a product of a relict process. This conclusion is supported by the SI models of the brines relative to gypsum about equilibrium (especially in the winter) and by the presence of surface crusts occurring as erosional remnants elevated relative to the modern Stokes surface.

Precipitation of gypsum within the sabkha results in groundwater which is significantly depleted in both calcium and sulphate. The degree of Ca depletion is markedly less than that of sulphate depletion, indicating an additional source of Ca within the brine. After accounting for gypsum precipitation, the associated Mg depletion in a 1:1 molar trend with delta Ca_{XS} indicates reflux-driven replacement of calcite by secondary dolomites, particularly within the Dammam Formation. Gypsum precipitation actively removes Ca from the system and the increase in aMg/aCa may facilitate dolomitization depending on kinetic constraints. While it may be difficult constrain the kinetics of the aqueous system, the 1:1 relationship of the XS calculations for the waters chemistry have shown us that secondary dolomitization process is very likely, as confirmed by SEM observations by Jameson and Puls (in press).

Dolomitization may be important in Mesaieed in releasing Ca, as suggested by reactive transport models of reflux dolomitization (Lu and Cantrell, 2016; Ehrenberg, 2006; Ehrenberg et al., 2006; Rahimpour-Bonab, 2010), and thus providing additional source for further gypsum precipitation (Machel, 1986; Leary and Vogt, 1987). Existence of high percentage of dolomite may also facilitate dolomitization, as suggested by reactive transport modelling studies (Gabellone and Whitaker, 2016 and references therein) and laboratory experiments (Lumsden et al., 1995; Kaczmarek and Sibley, 2011) where the acceleration of the rate dolomitization is proportional to percentage dolomite.

Reactive transport modelling using mass balance geochemical constraints with PHREEQC helps to confirm and quantify our geochemical observations of gypsum and dolomite precipitation. The limitation to using PHREEQC as the chemical database for saline aqueous system does not currently have clay minerals.

Minor clay precipitation is evident from depletion in K, Mg, Al and Si which complements observations of authigenic Mg-clay on the field. However, current sabkha brine conditions of pH <8 are not conducive to precipitate clay in the lower sabkha, suggesting that marine inundation is important in providing the alkaline conditions for precipitation. Minor depletion of about Sr occurs only in the summer indicating very minor amounts of celestine precipitation, not aragonite precipitation as one would expect.

Evaporation of brines results in reflux downwards into the Dammam aquifer. Within the middle sabkha, these reflux brines remain supersaturated with respect to gypsum, providing a mechanism for forming evaporites in sequences that were not evaporitic during deposition, such as the Dammam. Saturation indices of brines relative to gypsum support this model especially within the middle sabkha.

Holistic understanding of the water-rock interaction and the controls of diagenetic distribution spatially can provide a fresh insights into the cumulative effect of these processes for a leeward coastal system. This study can reduce uncertainty in subsurface characterization workflows of analogous hydrocarbon reservoirs. For example, 3-D geologic model and its facies distribution between wells can be confidently modelled in regions where well controls are limited. This can substantially help with well

pad placement and drilling designs to avoid well paths with suspected heavy gypsum and dolomite cements.

5.5 Advanced Analytics Methodology

With the advent of 'Big Data', there is an increasing need for the use of multiple tools to extract meaningful information from data-rich systems. Given the volume of the Mesaieed geochemical dataset and the varying processes involved, multi-dimensional statistical treatment was used. This was done using principal component analysis (PCA) which is highly capable of producing unique solutions, independent of hypothesis on data distribution. The goals of this analysis were to extract important information, compress the size of the data and to simplify and analyse the structure of the variables and measurements as observed. PCA does not replace the need to investigate the regression between variables, but it allows a higher resolution observation in the variation, thereby delineating additional information and important variables that influence the system.

Using Chapter 4 as an axample, several visualization and modelling tools were used to understand the geochemical of the Mesaieed sabkha system: (1) principal component analysis to deconstruct a large, comprehensive dataset consisting of both laterally (sabkha zones) and vertically (stratigraphy) varied groundwater and highlight geochemical divides; (2) statistical analysis of variances (ANOVA) to tell us if the differences of each elemental ion within the lateral and vertical are statistically significantly different or not (3) solutes molality against chloride plots provide clues to solute behaviour with increasing evaporation which also identifies the seasonal effects that are not as obvious using other data visualizations methods ; (4) box plots to show the statistical variation and significance between waters of different sabkha zones and stratigraphy; (5) elemental molar ratio plots to normalize known conservative ion to compare solutes behaviour relative to other parameters; (6) XS plots to highlight whether there is a loss or gain of absolute concentration of a given solute relative to the source waters to give us insight on which processes may be dominant; (7) saturation indices (SI) provide theoretical evidence as to whether the waters can thermodynamically dissolve or precipitate the minerals (this, however, needs to be above critical saturation to actually separate significant precipitation or dissolution); (8) phase diagram to highlight the stability of minerals relative to activity molar ratios in six degrees of freedom; and (9) inverse modelling to provide thermodynamic accountability of the mass-balance of waters along known fluid flow pathways.

5.6 Outlook and Future Work

The study presented in this thesis focused on a broad (including the up-dip bedrock and the Dammam bedrock) and fine-scale (four sabkha zones) study to understand the origin of gypsum in a

coastal sabkha system. The width and breadth of data has provided a unique opportunity to understand the spatial differences in water-rock interaction processes within a sabkha system from source to sink. The research presented here provides insights into the first-order study of products and processes that furnishes a foundation from which further research can build upon. The final section outlines potential paths for future work to address important knowledge gaps revealed by this study.

5.6.1 Expansion of Sedimentology Research

The current progradation geocellular model can clearly be expanded to include facies modelling of the modern siliciclastic-carbonate ramp to highlight sabkha heterogeneity: The 3D model presents a framework to integrate existing geologic data and sedimentology reviews into capturing sub-metre-scale spatial facies heterogeneity. This data was obtained from NDP

5.6.2 Reactive Transport Modelling

A process-based approach has its own limitations. Hydrogeochemical characterization of the field represents merely a "diagenetic snapshot" at the time of study, and is usually mitigated with temporal study of seasonal influences. Although flow and diagenetic rates can be quantified, it provides no indication of the impact of extrinsic factors such as climate and sea-level, and temporal mechanisms that influence the rate and remobilization of the diagenetic products. Both the conditions that control fluid migration and the distribution of thermodynamic conditions will evolve through time in response to external factors within the geologic systems. Hydrogeology and geochemistry are often coupled, whereby rock alterations exercise control on fluid flow by altering the connected pore spaces.

Resolution can be obtained by using numerical methods such as reactive transport modelling (RTM) (Jones and Xiao, 2005, Whitaker and Xiao, 2010, Al-Helal et al., 2012). Several studies modelling outcrops (Gabellone et al., 2016; Budd and Park, 2018) and subsurface reservoir (Lu and Cantrell, 2016) focusing on ancient reflux dolomitization, but RTM has not been utilized on modern sabkha systems. Focus of the RTM studies have been on dolomitization despite poor understanding of the kinetics, and no studies were done on gypsum precipitation/dissolution. Such a technologically advanced method will allow us to explore the coupled fluid flow and geochemical reactions holistically and advance our understanding of diagenetic processes.

Using our understanding of processes controlling the formation of diagenetic evaporites in this study, we can use results of this study to model the evolution of evaporites over the Holocene with boundary and initial conditions constrained by field observations. The rock/sediment composition, fluid flow, geochemistry and boundary conditions are much easier to define in modern and recent than in ancient systems. Thus, RTM will allow understanding of all the key processes in a sabkha system from a holistic point of view, along with their temporal and spatial variation.

A preliminary flow model done using TOUGH2 code was done by author and Teoh in 2017. The reasonable next step would be using RTM to predict and quantify the remobilisation of the solutes into the Dammam host rock.

5.6.3 Comparison with Continental Sabkha

Using a similar methodology employed in this thesis, it will be useful to establish a broader understanding on sabkha models with a continental sabkha such as Dukhan, located west of Qatar. Data has been collected, analysed and investigated (Ooi et al., 2015). Preliminary results show substantial differences in the hydrology and geochemistry within Mesaieed, possibly due to the sabkha (1) having surface elevation below sea level and (2) being surrounded by outcropping Dammam Formation updip dolomite on all sides. Comparing the continental sabkha with Mesaieed will be key in enhancing our understanding of the dynamic systems.

5.6.4 Interactions with deep Eocene aquifer (Rus and Umm Er Rhaduma)

Interesting observations from field studies and analyses reveal anomalous hydrological and geochemical patterns within the deep Eocene (<20 m) especially in the middle and lower sabkha of Mesaieed. Whether or not the deep Eocene aquifers provide ascending brine into the Eocene and possibly in the lower sabkha (like in Abu Dhabi) remains a question. Although the Midra shale (in the Rus formation) is known to be a limitation in understanding the impact, it is due to limited samples (n=3).

5.6.5 Finer Scale: Vadose Zone

The knowledge gap that has been identified is the lack of understanding of water-rock interaction in the vadose zone of a sabkha system. Data has been collected and analysed in Mesaieed (n=2) and in a continental sabkha on the west of Qatar, Dukhan (n=10). Datasets include sedimentology, porosity, core-scale permeability, soil moisture, and associated water chemistry (major ions). Further insights gained from comprehensive analysis of vadose zone data will elucidate the nature of geologic and hydrogeochemistry components of an active vadose zone, with implications for understanding sabkha diagenesis.

References

Al-Amoudi, O. S. B., Abduljauwad, S. N., & El-Naggar, Z. R. (1992). Response of sabkha to laboratory tests: a case study. Engineering Geology, 33(2), 111-125.

"A Lexicon of Cave and Karst Terminology with Special to Environmental Karst Hydrology" EPA/600/R-02/003, 2002, EPA: Washington, DC., Speleogenesis Glossary

Abdi, H., & Williams, L. J. (2010). Principal component analysis. Wiley interdisciplinary reviews: computational statistics, 2(4), 433-459.

Abed, A. M. (2002) An Overview of an Inland Sabkha in Jordan: The Taba Sabkha, Southern Wadi Araba. Sabkha Ecosystem: Volume 1: The Arabian Peninsula and Adjacent Countries, p95.

Al-Amoudi, O. S. (1994). A state-of-the-art report on the geotechnical problems associated with sabkha soils and methods of treatment. In Proceedings of ASCE-SAS first regional conference and exhibition, Manama, Bahrain, American Society of Civil Engineers-Saudi Arabia Section (ASCE-SAS), Dhahran, Saudi Arabia (pp. 53-77).

Al-Amoudi, O. S. B., Abduljauwad, S. N., & El-Naggar, Z. R. (1992). Response of sabkha to laboratory tests: a case study. Engineering Geology, 33(2), 111-125.

Al-Amoudi, O. S. B. (1995). A review of the geotechnical and construction problems in sabkha environments and methods of treatment. Arabian Journal for Science and Engineering, 20(3), 405-432.

Al-Awadi, E., Mukhopadhyay, A., & Al-Senafy, M. N. (1998). Geology and hydrogeology of the Dammam Formation in Kuwait. Hydrogeology Journal, 6(2), 302-314.

Al-Awadi, E., Mukhopadhyay, A., Al-Senafy, M.N. (1998) Geology and Hydrogeology of the Dammam Formation in Kuwait. Hydrogeology Journal, 6 p302 -314.

Al-Hajari, S. A. (1991). Geology of the Tertiary and its influence on the Aquifer system of Qatar and eastern Arabia.

Al-Homidy, A. A., Dahim, M. H., & El Aal, A. K. A. (2017). Improvement of geotechnical properties of sabkha soil utilizing cement kiln dust. Journal of Rock Mechanics and Geotechnical Engineering, 9(4), 749-760.

Al-Hurban, A., & Gharib, I. (2004). Geomorphological and sedimentological characteristics of coastal and inland sabkhas, Southern Kuwait. Journal of arid environments, 58(1), 59-85.

Al-Raei, A. M., Al-Najjar, M., & Al-Thani, R. (2012). Pore water gradients below microbial mat surface of Umm Alhool sabkha in Qatar. In *Qatar Foundation Annual Research Forum* (No. 2012, p. EEP14).

Al-Saad, H. (2005). Lithostratigraphy of the Middle Eocene Dammam Formation in Qatar, Arabian Gulf: effects of sea-level fluctuations along a tidal environment. Journal of Asian Earth Sciences, 25(5), 781-789.

Alsharhan, A. S., & Kendall, C. S. C. (2003). Holocene coastal carbonates and evaporites of the southern Arabian Gulf and their ancient analogues. Earth-Science Reviews, 61(3), 94.

Alsharhan, A. S., Rizk, Z. A., Nairn, A. E. M., Bakhit, D. W., & Al Hajari, S. A. (Eds.). (2001). Hydrogeology of an arid region: the Arabian Gulf and adjoining areas. Elsevier.

Al-Youssef, M. (2003). Mineralogy, geochemistry and origin of Quaternary Sabkhas in the Qatar Peninsula, Arabian Gulf, Doctoral dissertation, University of Southampton.

Al-Youssef, M. (2014). Gypsum Crystals Formation and Habits, Umm Said Sabkha, Qatar. In Sabkha Ecosystems (pp. 23-54). Springer Netherlands.

American Public Health Association. (1995). Water Environment Federation. Standard methods for the examination of water and wastewater, 22nd edition.

Ashour, M. M., Mogheeth, S. A., Metwali, A. A., Al-Ghazali, G. A., Ghafour, S. A., Shaksipi, R., & Ali, A. A. (1991). Sabkhas in Qatar peninsula. In Geomorphological, geological and biological study (p. 514). Qatar University.

Appelo, C. A. J., & Postma, D. (1993). Groundwater, geochemistry and pollution. Balkema, Rotterdam.

Arnold, S. F. (1981). The theory of linear models and multivariate analysis (No. 04; QA278, A7.).

Atekwana, E. A., Atekwana, E. A., Rowe, R. S., Werkema, D. D., & Legall, F. D. (2004). The relationship of total dissolved solids measurements to bulk electrical conductivity in an aquifer contaminated with hydrocarbon. Journal of Applied Geophysics, 56(4), 281-294.

Babel, M., & Schreiber, B. C. (2014). 9.17-Geochemistry of evaporites and evolution of seawater. Treatise on geochemistry, 483-560.

Barnett, B., Townley, L. R., Post, V., Evans, R. E., Hunt, R. J., Peeters, L., ... & Boronkay, A. (2012). Australian groundwater modelling guidelines. National Water Commission, Canberra.

Basyoni, M. H., & Aref, M. A. (2016). Composition and origin of the sabkha brines, and their environmental impact on infrastructure in Jizan area, Red Sea Coast, Saudi Arabia. Environmental Earth Sciences, 75(2), 105.

Bazaraa, A. S., & Ahmed, S. (1991). Rainfall characterization in an arid area.

Bickle, M. J., & Powell, R. (1977). Calcite-dolomite geothermometry for iron-bearing carbonates. Contributions to Mineralogy and Petrology, 59(3), 281-292.

Billeaud, I., Caline, B., Livas, B., Tessier, B., Davaud, E., Frebourg, G., and Pabian-Goyheneche, C. (2014). The carbonate-evaporite lagoon of Al Dakhirah (Qatar): an example of a modern depositional model controlled by longshore transport. Geological Society, London, Special Publications, 388(1), 561-587.

Bischoff, J. L., Juliá, R., Shanks III, W. C., & Rosenbauer, R. J. (1994). Karstification without carbonic acid: Bedrock dissolution by gypsum-driven dedolomitization. Geology, 22(11), 995-998.

Bjørlykke, K. (2015). Mudrocks, Shales, Silica Deposits and Evaporites. In Petroleum Geoscience (pp. 217-229). Springer, Berlin, Heidelberg.

Blaauw, M. (2010). Methods and code for 'classical'age-modelling of radiocarbon sequences. quaternary geochronology, 5(5), 512-518.

Boggs, J. M., & Adams, E. E. (1992). Field study of dispersion in a heterogeneous aquifer: 4. Investigation of adsorption and sampling bias. Water Resources Research, 28(12), 3325-3336.

Boggs, S.J. (2009) Petrology of Sedimentary Rocks. Cambridge University Press: p 285.

Bontognali, T. R., Vasconcelos, C., Warthmann, R. J., Lundberg, R., & McKenzie, J. A. (2012). Dolomite-mediating bacterium isolated from the sabkha of Abu Dhabi (UAE). Terra Nova, 24(3), 248-254.

Bouwer, H. (1989). The Bouwer and Rice slug test—an update. Groundwater, 27(3), 304-309.

Bouwer, H., & Rice, R. C. (1976). A slug test for determining hydraulic conductivity of unconfined aquifers with completely or partially penetrating wells. Water resources research, 12(3), 423-428.

Braitsch, O. (1971). Natural Salt Sequences and Physico-chemical Models. In Salt Deposits Their Origin and Composition (pp. 153-214). Springer Berlin Heidelberg.

Bredehoeft, J.S, Papadopulos, I.S. (1965) Rates of Vertical Groundwater Movement Estimated from the Earth's Thermal Profile. Water Resources Research, Vol. 1, No. 2.

Budd, D. A. (1988). Aragonite-to-calcite transformation during fresh-water diagenesis of carbonates: insights from pore-water chemistry. Geological Society of America Bulletin, 100(8), 1260-1270.

Bush, P. R. (1970). Chloride-rich brines from sabkha sediments and their possible role in ore formation. Institution of Mining & Mutallurgy.

Butler, G. P. (1969). Modern evaporite deposition and geochemistry of coexisting brines, the sabkha, Trucial Coast, Arabian Gulf. Journal of Sedimentary Research, 39(1).

Butler Jr, J. J., Jin, W., Mohammed, G. A., & Reboulet, E. C. (2011). New insights from well responses to fluctuations in barometric pressure. Groundwater, 49(4), 525-533.

Canfield, D. E., & Des Marais, D. J. (1991). Aerobic sulfate reduction in microbial mats. Science, 251(5000), 1471.

Carr, P. A., & Van Der Kamp, G. S. (1969). Determining aquifer characteristics by the tidal method. Water Resources Research, 5(5), 1023-1031.

Cattell, R. B., & Jaspers, J. (1967). A general plasmode (No. 30-10-5-2) for factor analytic exercises and research. Multivariate Behavioral Research Monographs.

Chandler, F. W. (1988). Diagenesis of sabkha-related, sulphate nodules in the early Proterozoic Gordon Lake Formation, Ontario, Canada. Carbonates and Evaporites, 3(1), 75-94.

Chapuis, R. P. (2004). Predicting the saturated hydraulic conductivity of sand and gravel using effective diameter and void ratio. Canadian Geotechnical Journal, 41(5), 787-795.

Chapuis, R. P. (2012). Predicting the saturated hydraulic conductivity of soils: a review. Bulletin of Engineering Geology and the Environment, 71(3), 401-434.

Chen, K., Jiao, J.J., Huang, J., Huang, R., 2007. Multivariate statistical evaluation of trace elements in groundwater in a coastal area in Shenzhen, China. Environmental Pollution 147 (3), 771–780.

Chen, S.X., Shuchuan, P., Chuanhui, H., Huifang, X., 2004a. Mechanism of interaction between

Cheng, S. (1988), Trilinear Diagram Revisited: Application, Limitation, And an Electronic Spreadsheet Program. Ground Water, 26: 505–510. doi:10.1111/j.1745-6584.1988.tb00417.x

Church, P.E., and Granato, G.E., 1996, Bias in groundwater data caused by well-bore flow in long-screen wells: Groundwater, Vol. 34, No. 2, p. 262-273.

Clark, W. E. (1967). Computing the barometric efficiency of a well. Journal of the Hydraulics Division, 93(4), 93-98.

Clark, P. U., Dyke, A. S., Shakun, J. D., Carlson, A. E., Clark, J., Wohlfarth, B., ... & McCabe, A. M. (2009). The last glacial maximum. Science, 325 (5941), 710-714.

Cooper, H. H., & Jacob, C. E. (1946). A generalized graphical method for evaluating formation constants and summarizing well-field history. Eos, Transactions American Geophysical Union, 27(4), 526-534.

Cooper, H. H., Bredehoeft, J. D., Papadopulos, I. S., & Bennett, R. R. (1965). The response of well-aquifer systems to seismic waves. Journal of Geophysical Research, 70(16), 3915-3926.

Cooper, K.J. (2015) Biogeochemistry of an eogenetic karst island: implications for diagenesis. PhD Dissertation. University of Bristol.

Cunningham, W. L., & Schalk, C. W. (2011). Groundwater technical procedures of the US Geological Survey (No. 1-A1). US Geological Survey.

Curtis, R., Evans, G., Kinsman, D. J. J., & Shearman, D. J. (1963). Association of dolomite and anhydrite in the recent sediments of the Persian Gulf. Nature, 197(4868), 679-680.

Dam, R. L., Eustice, B. P., Hyndman, D. W., Wood, W. W., & Simmons, C. T. (2014). Electrical imaging and fluid modeling of convective fingering in a shallow water-table aquifer. Water Resources Research, 50(2), 954-968.

Davidson, E., Richardson, L., & Zoller, S. (2000, January). Control of lost circulation in fractured limestone reservoirs. In IADC/SPE Asia Pacific Drilling Technology. Society of Petroleum Engineers.

Davidson, E., Richardson, L., Zoller, S. Control of Lost Circulation in Fractured Limestone Reservoir. OADC/SPE Asia Pacific Drilling Technology, Document ID: SPE-62734-MS

De Groot, K. (1973). Geochemistry of tidal flat brines at Umm Said, SE Qatar, Persian Gulf.

Denison, R. E., Kirkland, D. W., & Evans, R. (1998). Using strontium isotopes to determine the age and origin of gypsum and anhydrite beds. *The journal of Geology*, *106*(1), 1-18.

Dhowian, A. W., Erol, A. O., & Sultan, S. (1987). Settlement predictions in complex sabkha soil profiles. Bulletin of the International Association of Engineering Geology-Bulletin de l'Association Internationale de Géologie de l'Ingénieur, 36(1), 11-21.

Didi-Ooi, S.M., Jameson, J., Whitaker, F., Strohmenger, C. (2015) Evaporite Diagenesis Model of a Continental Sabkha System: Insights from the Holocene at Dukhan, Qatar. AAPG Annual Convention and Exhibition Technical Talk.

Dohm, J. M., Anderson, R. C., Barlow, N. G., Miyamoto, H., Davies, A. G., Taylor, G. J., ... & Janes, D. (2008). Recent geological and hydrological activity on Mars: the Tharsis/Elysium corridor. Planetary and Space Science, 56(7), 985-1013.

Domenico, P. A., & Schwartz, F. W. 1990, Physical and chemical hydrogeology.

Drever, J. I. (1992). Chemical Weathering Rates of silicate rocks as a function of elevation in the southern Swiss Alps. Geochim. Cosmochim. Acta, 56, 3209-3216.

Drever, J. I. (1994), Murphy, K. M., Clow, D. W. (1994). Field weathering rates versus laboratory dissolution rates: an update. Mineralogical Magazine, 58A, 239-240.

Drever, J. I. (2002). The geochemistry of natural waters (Vol. 437). Englewood Cliffs: Prentice Hall.

Duggan, D.J (2014) Karst Prediction – Testing Predictions Against Data, State of Qatar. Masters of Science Thesis. University of Leeds, UK.

Eccleston BL, Pike JG, Harhash I (1981) The water resources in Qatar and their development. Food and Agricultural Organization of the United Nations

Eccleston, B. L., Pike, J. G., & Harhash, I. (1981). The Water Resources of Qatar and Their Development. Food and Agricultural Organization of the United Nations.

Edwards, H. G., Sadooni, F., Vítek, P., & Jehlička, J. (2010). Raman spectroscopy of the Dukhan sabkha: identification of geological and biogeological molecules in an extreme environment. Philosophical Transactions of the Royal Society of London A: Mathematical, Physical and Engineering Sciences, 368(1922), 3099-3107.

Ehrenberg, S.N. (2006) Porosity destruction in carbonate platforms. J. Petrol. Geol., 29, 41–52.

Ehrenberg, S.N., Eberli, G.P., Keramati, M. and Moallemi, S.A. (2006) Porosity-permeability relationships in interlayered limestone-dolostone reservoirs. AAPG Bull., 90, 91–114.

Embabi, N. S., & Ashour, M. M. (1985). Sand Dunes in Qatar Peninsula. University of Qatar.

Eugster, H. P., & Hardie, L. A. (1978). Saline lakes. In Lakes (pp. 237-293). Springer New York.

Evans, G., & Kirkham, A. (2002). Distribution of Sabkhat within the Arabian Peninsula and the adjacent countries. Sabkha Ecosystems. Kluwer Academic Publishers, 7-20.

Evans, G., Kendall, C. S. C., & Skipwith, P. (1964). Origin of the coastal flats, the sabkha, of the Trucial Coast, Persian Gulf. Nature, 202(4934), 759-761.

Evans, G., Schmidt, V., Bush, P., & Nelson, H. (1969). Stratigraphy and geologic history of the sabkha, Abu Dhabi, Persian Gulf. Sedimentology, 12(1-2), 145-159.

Fabuel-Pe´rez, I. (2008) 3D Reservoir Modeling of Upper Triassic Continental Mixed Systems: Integration of Digital Outcrop Models (DOMs) and High-Resolution Sedimentology. The Oukaimeden Sandstone Formation, Central High Atlas. Morocco.

Fairbridge, R. W. (1972). Climatology of a glacial cycle. Quaternary Research, 2(3), 283-302.

Fairchild, I. J., Borsato, A., Tooth, A. F., Frisia, S., Hawkesworth, C. J., Huang, Y., ... & Spiro, B. (2000). Controls on trace element (Sr–Mg) compositions of carbonate cave waters: implications for speleothem climatic records. Chemical Geology, 166(3-4), 255-269.

Ferris, J. G., & Knowles, D. B. (1954). The" slug test" for estimating transmissibility (No. 54-80).

Finn, T. (2017) Qatar New Port http://reut.rs/2AhRaY2

Fleet, M. E. L. (1965). Preliminary investigations into the sorption of boron by clay minerals. Clay Miner, 6(3), 3-16.

Flügel, E. (2013). Microfacies of carbonate rocks: analysis, interpretation and application. Springer Science & Business Media.

Freeze, R. A., & Cherry, J. A. (1979). Groundwater, 604 pp.

Finn (2017) Qatar says new port will help circumvent Arab sanctions, Reuters. https://www.reuters.com/article/us-gulf-qatar-port/qatar-says-new-port-will-help-circumvent-arab-sanctions-idUSKCN1BG1RP (Accessed on March 12th 2016)

Fryberger, S. G., Schenk, C. J., & Krystinik, L. F. (1988). Stokes surfaces and the effects of near-surface groundwater-table on Aeolian deposition. Sedimentology, 35(1), 21-41.

Galan, E., Singer, A. (2011). Developments in Palygorskite-Sepiolite Research. Developments in Clay Science.

Ganor, J., & Katz, A. (1989). The geochemical evolution of halite structures in hypersaline lakes: The Dead Sea, Israel. Limnology and Oceanography, 34(7), 1214-1223.

Ganor, J., Katz, A. (1989) The Geochemical Evolution of Halite Structures in Hypersaline Lakes: The Dead Sea, Israel.

Garcia-Romero, E., Sua´rez, M., 2010. On the chemical composition of sepiolite and palygorskite. Clays Clay Miner. 58, 1–20.

Garske, E. E., & Schock, M. R. (1986). An Inexpensive Flow-Through Cell and Measurement System for Monitoring Selected Chemical Parameters in Ground Water. Groundwater Monitoring & Remediation, 6(3), 79-84.

Geske, A., Lokier, S., Dietzel, M., Richter, D. K., Buhl, D., & Immenhauser, A. (2015). Magnesium isotope composition of sabkha porewater and related (Sub-) Recent stoichiometric dolomites, Abu Dhabi (UAE). *Chemical geology*, *393*, 112-124.

Gerdes, G., Krumbein, W.E., Holtkamp, E. (1985) Salinity and Water Activity Related Zonation of Microbial Communities and Potential Stromatolites of the Gavish Sabkha. Ecological Studies 53: Hypersaline Ecosystems pp 238-266.

Goldstein, R. H. (1986). Reequilibration of fluid inclusions in low-temperature calcium-carbonate cement. *Geology*, *14*(9), 792-795.

Goldstein, R. H., Franseen, E. K., & Mills, M. S. (1990). Diagenesis associated with subaerial exposure of Miocene strata, southeastern Spain: implications for sea-level change and preservation of low-temperature fluid inclusions in calcite cement. Geochimica et Cosmochimica Acta, 54(3), 699-704.

Gomis-Yagües, V., Boluda-Botella, N., & Ruiz-Beviá, F. (2000). Gypsum precipitation/dissolution as an explanation of the decrease of sulphate concentration during seawater intrusion. Journal of Hydrology, 228(1), 48-55.

Gonthier, G. J. (2007). Estimating Barometric Efficiency Using a Graphical Method on Nearly Continuous Data. Georgia Institute of Technology.

Goodall, T. M. (1995). *The geology and geomorphology of the Sabkhat Matti region (United Arab Emirates): a modern analogue for ancient desert sediments from north-west Europe*(Doctoral dissertation, University of Aberdeen).

Grötsch, J., Suwaina, O., Ajlani, G., Taher, A., El-Khassawneh, R., Lokier, S., ... & Dorp, J. V. (2003). The Arab Formation in central Abu Dhabi: 3-D reservoir architecture and static and dynamic modeling. *GeoArabia*, *8*(1), 47-86.

Groot, K.D. (1973). Geochemistry of tidal flat brines at Umm Said, SE Qatar, Persian Gulf.

Gulley, J. D., Martin, J. B., Moore, P. J., Brown, A., Spellman, P., & Ezell, J. E. (2014, December). Dissolution and Cave Formation in Eogenetic Limestone Aquifers by Spatial Heterogeneity in PCO2 at Water Tables. In AGU Fall Meeting Abstracts.

Gunatilaka, A., & Mwango, S. (1987). Continental sabkha pans and associated nebkhas in southern Kuwait, Arabian Gulf. Geological Society, London, Special Publications, 35(1), 187-203.

Gunatilaka, A. (1990). Anhydrite diagenesis in a vegetated sabkha, Al-Khiran, Kuwait, Arabian Gulf. Sedimentary Geology, 69(1-2), 95-116.

Gunatilaka, A. (1991). Dolomite formation in coastal Al-Khiran, Kuwait Arabian Gulf—a re-examination of the sabkha model. Sedimentary Geology, 72(1-2), 35-53.

Guo, W., & Langevin, C. D. (2002). User's guide to SEAWAT; a computer program for simulation of three-dimensional variable-density ground-water flow (No. 06-A7).

Gupta, U. C. (1993). Boron and its role in crop production. CRC press.

Halford, K.J., Kuniansky, E.L. (2002) Documentation of Spreadsheets for the Analysis of Aquifer-Test and Slug-Test Data. U.S Geological Survey Report 02-197.

Handford, C. R. (1981). Genetic characterization of recent and ancient sabkha systems. AAPG Bulletin, 65(9), 1685-1685.

Handford, C. R. (1982). Sedimentology and evaporite genesis in a Holocene continental-sabkha playa basin—Bristol Dry Lake, California. Sedimentology, 29(2), 239-253.

Hantush, M. S., & Jacob, C. E. (1955). Non-steady green's functions for an infinite strip of leaky aquifer. Eos, Transactions American Geophysical Union, 36(1), 101-112.

Harder, H. A. (1970). Boron content of sediments as a tool in facies analysis. Sedimentary Geology, 4(1-2), 153-175.

Hardie, L. A. (1967). The gypsum-anhydrite equilibrium at one atmosphere pressure. The American Mineralogist, 52, 171-200.

Hardie, L. A. (1984). Evaporites; marine or non-marine?. American Journal of Science, 284(3), 193-240.

Hardie, L. A. (1987). Dolomitization: A critical view of some current views: PERSPECTIVES. Journal of Sedimentary Research, 57(1).

Hem, J. D. (1985). Study and interpretation of the chemical characteristics of natural water (Vol. 2254). Department of the Interior, US Geological Survey.

Hillier, S. (1993). Origin, diagenesis, and mineralogy of chlorite minerals in Devonian lacustrine mudrocks, Orcadian Basin, Scotland. Clays and Clay Minerals, 41, 240-240.

Hiscock, K. M. (2009). Hydrogeology: principles and practice. John Wiley & Sons.

Holland, H. D., Horita, J., & Seyfried Jr, W. E. (1996). On the secular variations in the composition of Phanerozoic marine potash evaporites. Geology, 24(11), 993-996.

Holzbecher, E. O. (1998). Modeling density-driven flow in porous media: principles, numerics, software. Springer Science & Business Media.

Horton, Robert E. (1933) "The role of infiltration in the hydrologic cycle" Transactions of the American Geophysics Union, 14th Annual Meeting, pp. 446–460.

Hsü, K. J., & Schneider, J. (1973). Progress report on dolomitization—hydrology of Abu Dhabi sabkhas, Arabian Gulf. In The Persian Gulf (pp. 409-422). Springer, Berlin, Heidelberg.

Hsü, K. J., & Siegenthaler, C. (1969). Preliminary experiments on hydrodynamic movement induced by evaporation and their bearing on the dolomite problem. Sedimentology, 12(1-2), 11-25.

Hvorslev, M. J. (1951). Time lag and soil permeability in ground-water observations.

Illing, L. V., & Taylor, J. C. (1993). Penecontemporaneous dolomitization in Sabkha Faishakh, Qatar; evidence from changes in the chemistry of the interstitial brines. Journal of Sedimentary Research, 63(6), 1042-1048.

Illing, L. V., Wells, A. J., & Taylor, J. C. M. (1965). Penecontemporary dolomite in the Persian Gulp.

Jacob, C. E. (1940). On the flow of water in an elastic artesian aquifer. Eos, Transactions American Geophysical Union, 21(2), 574-586.

James, N. P., & Choquette, P. W. (1984). Diagenesis 9. Limestones-the meteoric diagenetic environment. Geoscience Canada, 11(4).

Jameson, J., Puls, D., & Kozar, M. G. (2009, January). Holocene Sabkha and Coastal Systems of Qatar: Process Models for the Interpretation of Ancient Arabian Plate Carbonate-Evaporite Reservoirs. In International petroleum technology conference. International Petroleum Technology Conference.

Jameson, J., & Strohmenger, C. J. (2013). Back-Barrier Sediment Dynamics: A Major Control on Modeling Sediment Properties, Cyclicity and Depositional Profiles-Examples from the Arid Coastline of Qatar. AAPG Search and Discovery Article, 90163.

Jameson, J. and Puls, D., (in press), Holocene Sediments of Qatar as Analogues to Arid Climate Carbonate Reservoirs, AAPG Memoir publication.

John, V. C., Coles, S. L., & Abozed, A. I. (1990). Seasonal cycles of temperature, salinity and water masses of the western Arabian Gulf. Oceanologica Acta, 13(3), 273-281.

Jolliffe, I. T. (2002). Principal component analysis and factor analysis. Principal component analysis, 150-166.

Jones, G.D. and Xiao, Y.T. (2005) Dolomitization, anhydrite cementation, and porosity evolution in a reflux system: insights from reactive transport models. AAPG Bull., 89, 577–601.

Kaczmarek, S.E. and Sibley, D.F. (2011) On the evolution of dolomite stoichiometry and cation order during hightemperature synthesis experiments: an alternative model for the geochemical evolution of natural dolomites. Sed. Geol., 240, 30–40

Kamp, G. (1976). Determining aquifer transmissivity by means of well response tests: The underdamped case. Water Resources Research, 12(1), 71-77.

Karakas, Z., Kadir, S., 1998. Mineralogical and genetic relationships between carbonate and sepiolite–palygorskite formations in the Neogene lacustrine Konya Basin, Turkey. Carbonate Evaporite 13, 198–206.

Kassler, P. (1973). The structural and geomorphic evolution of the Persian Gulf. In The Persian Gulf (pp. 11-32). Springer, Berlin, Heidelberg.

Kastner, M. (1984). Sedimentology: control of dolomite formation. *Nature*, *311*(5985), 410.

Kendall, A. C., & Walters, K. L. (1978). The age of metasomatic anhydrite in Mississippian reservoir carbonates, southeastern Saskatchewan. Canadian Journal of Earth Sciences, 15(3), 424-430.Schlumberger (2017) Petrel User Manual 2017.

Kendall, C. G. S. C., & Alsharhan, A. S. (Eds.). (2011). Quaternary Carbonate and Evaporite Sedimentary Facies and Their Ancient Analogues: A Tribute to Douglas James Shearman (Special Publication 43 of the IAS). John Wiley & Sons.

Kendall, C. G. S. C., & Skipwith, S. P. A. E. (1969). Geomorphology of a recent shallow-water carbonate province: Khor al Bazam, Trucial Coast, Southwest Persian Gulf. Geological Society of America Bulletin, 80(5), 865-892.

Kendall, C. S. C., & Skipwith, P. (1968). Recent algal stromatolites of the Khor al Bazam, Abu Dhabi, the southwest Persian Gulf. Geol. Soc. Am. Spec. Pap, 101, 108.

Keys, W. S. (1990). Borehole geophysics applied to ground-water investigations (No. 02-E2). USGPO; For sale by the Books and Open-File Reports Section, U.S. Geological Survey.

Kimrey, J. O. (1985). *Proposed artificial recharge studies in northern Qatar* (No. 85-343). US Geological Survey,.

Kinsman, D. J. (1969). Modes of formation, sedimentary associations, and diagnostic features of shallow-water and supratidal evaporites. AAPG Bulletin, 53(4), 830-840.

Kinsman, D. J., & Park, R. K. (1976). .4 Algal Belt and Coastal Sabkha Evolution, Trucial Coast, Persian Gulf. Developments in Sedimentology, 20, 421-433.

Kipp, K. L. (1985). Type curve analysis of inertial effects in the response of a well to a slug test. Water Resources Research, 21(9), 1397-1408.

Kirkham, A. (2011). Halite, sulphates, sabkhat and salinas of the coastal regions and Sabkha Matti of Abu Dhabi, United Arab Emirates. Quaternary carbonate and evaporite sedimentary facies and their ancient analogues: A Tribute to Douglas James Shearman, 265-276.

Komatsu, G., Ori, G. G., Di Lorenzo, S., Rossi, A. P., & Neukum, G. (2007). Combinations of processes responsible for Martian impact crater "layered ejecta structures" emplacement. Journal of Geophysical Research: Planets, 112(E6).

Kraemer, T. F., Wood, W. W., & Sanford, W. E. (2014). Distinguishing seawater from geologic brine in saline coastal groundwater using radium-226; an example from the Sabkha of the UAE. Chemical Geology, 371, 1-8.

Krauskopf, K., & Bird, D. (1995). Surface chemistry: the solution-mineral interface. Introduction to geochemistry (Ed MG-HI Editions) Mc Graw-Hill International Editions edn. Earth Sciences and Geology Series, 135-163.

Kreuter, H. (2012) Goethermal Application: Geothermal Cooling. Renewable Energy TP. Accessed via http://www.esmap.org/sites/esmap.org/files/Kreuter_Cooling_Day2_Optimized.pdf

Lambeck, K. (1996). Sea-level change and shore-line evolution in Aegean Greece since Upper Palaeolithic time. Antiquity, 70(269), 588-611.

Lambeck, K., Antonioli, F., Purcell, A., & Silenzi, S. (2004). Sea-level change along the Italian coast for the past 10,000 yr. Quaternary Science Reviews, 23(14-15), 1567-1598.

Lambeck, K., Purcell, A., & Dutton, A. (2012). The anatomy of interglacial sea levels: the relationship between sea levels and ice volumes during the Last Interglacial. Earth and Planetary Science Letters, 315, 4-11.

Lambeck, K., Yokoyama, Y., & Purcell, T. (2002). Into and out of the Last Glacial Maximum: sea-level change during Oxygen Isotope Stages 3 and 2. Quaternary Science Reviews, 21(1), 343-360.

Leary, D. A., & Vogt, J. N. (1987). Diagenesis of permian (guadalupian) San Andres formation, central basin platform, west Texas. *AAPG (Am. Assoc. Pet. Geol.) Bull.;(United States)*, *71*(CONF-870606-).

Lehmann, E. L., & D'abrera, H. J. (1975). Nonparametrics: statistical methods based on ranks. Holden-Day.

Leyshon, J.A. and W.Y. James. 1993. Boron toxicity and irrigation management. Pp. 207-226, In Boron And Its Role In Crop Production, (Umesh C. Gupta, ed.) CRC Press, Inc.; Boca Raton, FL.

Lippmann, F. (1973). Crystal chemistry of sedimentary carbonate minerals. In *Sedimentary Carbonate Minerals* (pp. 5-96). Springer, Berlin, Heidelberg.

Lloyd, J.W., Heathcoat, J.A. (1985) Natural Inorganic Chemistry in Relation to Groundwater. Clarendon Press, Oxford.

Lloyd, J. W., Pike, J. G., Eccleston, B. L., & Chidley, T. R. E. (1987). The hydrogeology of complex lens conditions in Qatar. Journal of hydrology, 89(3-4), 239-258.

Lokier, S., & Steuber, T. (2008). Quantification of carbonate-ramp sedimentation and progradation rates for the late Holocene Abu Dhabi shoreline. Journal of Sedimentary Research, 78(7), 423-431.

Lokier, S., & Steuber, T. (2009). Large-scale intertidal polygonal features of the Abu Dhabi coastline. *Sedimentology*, *56*(3), 609-621.

Lokier, S. W. (2012). Development and evolution of subaerial halite crust morphologies in a coastal sabkha setting. *Journal of arid environments*, *79*, 32-47.

Lokier, S. W. (2013). Coastal sabkha preservation in the Arabian Gulf. Geoheritage, 5(1), 11-22.

Lokier, S. W., Bateman, M. D., Larkin, N. R., Rye, P., & Stewart, J. R. (2015). Late Quaternary sea-level changes of the Persian Gulf. *Quaternary research*, *84*(1), 69-81.

Lokier, S. W., Andrade, L. L., Court, W. M., Dutton, K. E., Head, I. M., van der Land, C., ... & Sherry, A. (2017). A new model for the formation of microbial polygons in a coastal sabkha setting. The Depositional Record.

Lumsden, D.N., Morrison, J.W. and Lloyd, R.V. (1995) The role of iron and Mg/Ca ratio in dolomite synthesis at 192°C. J. Geol., 103, 51–61

Lu, P., & Cantrell, D. (2016). Reactive transport modelling of reflux dolomitization in the Arab-D reservoir, Ghawar field, Saudi Arabia. *Sedimentology*, *63*(4), 865-892.

Lucia, F. J. (1995). Rock-fabric/petrophysical classification of carbonate pore space for reservoir characterization. AAPG bulletin, 79(9), 1275-1300.

Lusczynski, N. J. (1961). Head and flow of ground water of variable density. Journal of Geophysical Research, 66(12), 4247-4256.

Machel, H.G. (1986) Early lithification, dolomitization, and anhydritization of Upper Devonian Nisku buildups, subsurface of Alberta, Canada. In: Reef Diagenesis (Eds J. Schroeder and B. Purser), pp. 336–356. Springer, Berlin, Heidelberg

Machel, H. G. (2004). Concepts and models of dolomitization: a critical reappraisal. Geological Society, London, Special Publications, 235(1), 7-63.

Machel, H. G. (2013). Secondary anhydrites in deeply buried Devonian carbonates of the Alberta Basin, Canada. Carbonates and evaporites, 28(3), 267-280.

Malek, E., Bingham, G.E., McCurdy, G.D., 1990. Evapotranspiration from the margin and moist playa of a closed desert valley. J. Hydrol. 120, 15–34.

Martin, J. B., & Moore, P. J. (2008). Sr concentrations and isotope ratios as tracers of ground-water circulation in carbonate platforms: Examples from San Salvador Island and Long Island, Bahamas. Chemical Geology, 249(1-2), 52-65.

Matzarakis, A., & Fröhlich, D. (2015). Sport events and climate for visitors—the case of FIFA World Cup in Qatar 2022. *International journal of biometeorology*, *59*(4), 481-486.

Masch, F. D., & Denny, K. J. (1966). Grain size distribution and its effect on the permeability of unconsolidated sands. Water Resources Research, 2(4), 665-677.

McClain, M. E., Swart, P. K., & Vacher, H. L. (1992). The hydrogeochemistry of early meteoric diagenesis in a Holocene deposit of biogenic carbonates. Journal of Sedimentary Research, 62(6).

McKay, C. P., Rask, J. C., Detweiler, A. M., Bebout, B. M., Everroad, R. C., Chanton, J. P., ... & Kapili, B. (2016). An Unusual Inverted Saline Microbial Mat Community in an Interdune Sabkha in the Rub'Alkhali (the Empty Quarter), UAE: an Analog for Habitats on Present Mars.

McKay, C.P. (2016) Titan as the abode of life. Life, 6, 8; doi:10.3390/life6010008.

McKay, C.P., Rask, J., Detweiler, A.M., et al. (2016) An unusual inverted saline microbial mat community in an interdune sabkha in the Rub' al Khali (the Empty Quarter), United Arab Emirates. PLoS ONE 11(3): e0150342. doi:10.1371/journal.pone.0150342.

McKenzie, J. A. (1981). Holocene dolomitization of calcium carbonate sediments from the coastal sabkhas of Abu Dhabi, UAE: a stable isotope study. The Journal of Geology, 89(2), 185-198.

McKenzie, J. A., Hsü, K. J., & Schneider, J. F. (1980). Movement of subsurface waters under the sabkha Abu Dhabi, UAE, and its relation to evaporative dolomite genesis.

McKenzie, J. A., Hsü, K. J., & Schneider, J. F. (1980). Movement of subsurface waters under the sabkha Abu Dhabi, UAE, and its relation to evaporative dolomite genesis.

Mehemmed Shahin, M. (2009). Road Construction on Sabkha Soils.

Merritt, M. L. (2004). Estimating hydraulic properties of the Floridan aquifer system by analysis of earth-tide, ocean-tide, and barometric effects, Collier and Hendry Counties, Florida (pp. 1803-1817). US Department of the Interior, US Geological Survey.

Mettraux, M., Homewood, P. W., Kwarteng, A. Y., & Mattner, J. (2011). Coastal and continental sabkhas of Barr Al Hikman, Sultanate of Oman. Int. Assoc. Sedimentol. Spec. Publ, 43, 183-204.

Ministry of Environment (2009) Studying and developing the natural and artificial recharge of the groundwater aquifer in the state of Qatar, Project Final Report. State of Qatar, 2009..

Möller, D. (1990). The Na/Cl ratio in rainwater and the seasalt chloride cycle. Tellus B, 42(3), 254-262.

Morrow, D. W., & Ricketts, B. D. (1988). Experimental investigation of sulfate inhibition of dolomite and its mineral analogues.

Müller, D. W., McKenzie, J. A., & Mueller, P. A. (1990). Abu Dhabi sabkha, Persian Gulf, revisited: application of strontium isotopes to test an early dolomitization model. Geology, 18(7), 618-621.

Montes-Hernandez, G., Findling, N., Renard, F., & Auzende, A. L. (2014). Precipitation of ordered dolomite via simultaneous dissolution of calcite and magnesite: New experimental insights into an old precipitation enigma. Crystal Growth & Design, 14(2), 671-677.

Moore, C. H. (1989). Carbonate diagenesis and porosity (Vol. 46). Elsevier.

Moore, C. H., & Wade, W. J. (2013). Carbonate reservoirs: Porosity and diagenesis in a sequence stratigraphic framework (Vol. 67). Newnes.

Moore, P. J., Martin, J. B., & Screaton, E. J. (2009). Geochemical and statistical evidence of recharge, mixing, and controls on spring discharge in an eogenetic karst aquifer. Journal of Hydrology, 376(3), 443-455.

Moore, P. J., Martin, J. B., Screaton, E. J., & Neuhoff, P. S. (2010). Conduit enlargement in an eogenetic karst aquifer. Journal of hydrology, 3

Mor, Z., Assouline, S., Tanny, J., Lensky, I. M., & Lensky, N. G. (2018). Effect of water surface salinity on evaporation: The case of a diluted buoyant plume over the Dead Sea. Water Resources Research, 54(3), 1460-1475.

Müller, D. W., McKenzie, J. A., & Mueller, P. A. (1990). Abu Dhabi sabkha, Persian Gulf, revisited: application of strontium isotopes to test an early dolomitization model. Geology, 18(7), 618-621.

Najafi, H. S., & Noye, B. J. (1997). Modelling tides in the Persian Gulf using dynamic nesting (Doctoral dissertation).

Neal, M., Neal, C., & Brahmer, G. (1997). Stable oxygen isotope variations in rain, snow and streamwaters at the Schluchsee and Villingen sites in the Black Forest, SW Germany. Journal of hydrology, 190(1-2), 102-110.

New Doha Port Project Steering Committee (2008) Volume 2 Geotechnical Report, Land and Marine Site Investigation. GME07004-GEO-001.

New Doha Port Project (2010) Environmental Soil and Hydrogeological Site Investigations. Report No G-698-2 (Rev 2) and G-698-1 (Rev. 1).

New Doha Port (2011) Soil and Groundwater Investigations, New Doha Port Steering Committee. Data report P-070876-NDP-PR-14.3, March 2011.

Nield, D. A., Simmons, C. T., Kuznetsov, A. V., & Ward, J. D. (2008). On the evolution of salt lakes: Episodic convection beneath an evaporating salt lake. Water resources research, 44(2).

Nield, D. A., Kuznetsov, A. V., & Simmons, C. T. (2013). Deep Saline Fluids in Geologic Basins: The Possible Role of the Soret Effect. Transport in porous media, 99(2), 297-305.

Nielsen, D.M. and Nielsen, G.L. 2006. Ground-Water Sampling In: D. M. Nielsen (editor), Practical Handbook of Environmental Site Characterization and Ground-Water Monitoring. Taylor & Francis Group, CRC Press. Boca Raton. pp. 959-1112.

Nordstrom, D. K., Plummer, L. N., Wigley, T. M. L., Wolery, T. J., BALL, J. W., Jenne, E. A., ... & Hoffman, M. (1979). A comparison of computerized chemical models for equilibrium calculations in aqueous systems.

Oki, D.S., Presley, T.K. (2008) Causes of Borehole Flow and Effects on Vertical Salinity Profiles in Coastal Aquifers. U.S. Geological Survey, Pacific Islands Water Science Center report, 20th Salt Water Intrusion Meeting.

Ori, G. G., Marinangeli, L., Di Lorenzo, S., Ogliani, F., Seu, R., & Biccari, D. (2002). The Martian subsurface from the orbiting GPR MARSIS and SHARAD: Detection and analysis of possible flood basalts. In Lunar and Planetary Science Conference (Vol. 33).

Ori, G.G. (2010) The sedimentary record of modern and ancient dry lakes, In: Cabrol, N.A., Grin, E.A., eds, Lakes on Mars. Elsevier

Paine, J. G. (2003), Determining salinization extent, identifying salinity sources, and estimating chloride mass using surface, borehole, and airborne electromagnetic induction methods, Water Resour. Res., 39, 1059, doi:10.1029/2001WR000710, 3.

Paquette, J., & Reeder, R. J. (1995). Relationship between surface structure, growth mechanism, and trace element incorporation in calcite. Geochimica et Cosmochimica Acta, 59(4), 735-749.

Parkhurst, D. L., & Appelo, C. A. J. (2013). Description of input and examples for PHREEQC version 3: a computer program for speciation, batch-reaction, one-dimensional transport, and inverse geochemical calculations (No. 6-A43). US Geological Survey.

Parsons, M.L. (1970) Groundwater thermal regime in a glacial complex. Water Resources Res., 6 (6), 1701-1729.

Patterson, R. J., & Kinsman, D. J. (1977). Marine and continental groundwater sources in a Persian Gulf coastal sabkha. Studies in Geology, 4, 381-397.

Patterson, R. J., & Kinsman, D. J. J. (1982). Formation of diagenetic dolomite in coastal sabkha along Arabian (Persian) Gulf. AAPG Bulletin, 66(1), 28-43.

Pedregosa, F., Varoquaux, G., Gramfort, A., Michel, V., Thirion, B., Grisel, O., ... & Vanderplas, J. (2011). Scikit-learn: Machine learning in Python. *Journal of machine learning research*, *12*(Oct), 2825-2830.

Perthuisot, J. P. (1977). La Sebkha de Doukhane (Qatar) et la transformation gypse--> anhydrite+ eau. Bulletin de la Societe geologique de France, 7(5), 1145-1149.

Picha, F. (1978). Depositional and diagenetic history of Pleistocene and Holocene oolitic sediments and sabkhas in Kuwait, Persian Gulf. Sedimentology, 25(3), 427-450.

Pierson, B. J. (1981). The control of cathodoluminescence in dolomite by iron and manganese. Sedimentology, 28(5), 601-610.

Plummer, L. N., & Busenberg, E. (1982). The solubilities of calcite, aragonite and vaterite in CO2-H2O solutions between 0 and 90 C, and an evaluation of the aqueous model for the system CaCO3-CO2-H2O. Geochimica et cosmochimica acta, 46(6), 1011-1040.

Plummer, L. N., Parkhurst, D. L., Fleming, G. W., & Dunkle, S. A. (1988). A computer program incorporating Pitzer's equations for calculation of geochemical reactions in brines. US Geological Survey Water-Resources Investigations Report, 88(4153), 310.

Post, V., Kooi, H., & Simmons, C. (2007). Using hydraulic head measurements in variable-density ground water flow analyses. Groundwater, 45(6), 664-671.

Post, V., & Abarca, E. (2010). Preface: Saltwater and freshwater interactions in coastal aquifers. *Hydrogeology Journal*, *18*(1), 1-4.

Post, V. E., & von Asmuth, J. R. (2013). Hydraulic head measurements—new technologies, classic pitfalls. Hydrogeology Journal, 21(4), 737-750.

Purkis, S., Rivers, J., Strohmenger, C. J., Warren, C., Yousif, R., Ramirez, L., & Riegl, B. (2017). Complex interplay between depositional and petrophysical environments in Holocene tidal carbonates (Al Ruwais, Qatar). Sedimentology, 64(6), 1646-1675.

Purser, B. H. (1973). Sedimentation around bathymetric highs in the southern Persian Gulf. In *The Persian Gulf* (pp. 157-177). Springer, Berlin, Heidelberg.

Purser, B. H., & Evans, G. (1973). Regional sedimentation along the Trucial coast, SE Persian Gulf. In The Persian Gulf (pp. 211-231). Springer, Berlin, Heidelberg.

Purser, B. H., & Seibold, E. (1973). The principal environmental factors influencing Holocene sedimentation and diagenesis in the Persian Gulf. In the Persian Gulf (pp. 1-9). Springer, Berlin, Heidelberg.

Purser, B.H. (1985) Coastal Evaporite Systems, in Hypersaline Ecosystems: The Gavish Sabkha, Friedman, G.M., Krumbein, W.E. (Eds.)

Ragab, A. I., Hilmy, M. E., & Al-Hitmy, H. H. (1991). Sediment distribution, mineralogy and geochemistry of the sabkha sequence of Umm Said, Qatar. Earth Sci Ser, 5, 1-15.

Rahimpour-Bonab, H., Esrafili-Dizaji, B., & Tavakoli, V. (2010). Dolomitization and anhydrite precipitation in Permo-Triassic carbonates at the South Pars gasfield, offshore Iran: controls on reservoir quality. *Journal of Petroleum Geology*, *33*(1), 43-66.

Rao, P. G., Al-Sulaiti, M., & Al-Mulla, A. H. (2001). Winter Shamals in Qatar, Arabian Gulf. Weather, 56(12), 444-451.

Ravenscroft, P., & McArthur, J. M. (2004). Mechanism of regional enrichment of groundwater by boron: the examples of Bangladesh and Michigan, USA. Applied Geochemistry, 19(9), 1413-1430.

Ravikumar, P., Somashekar, R. K., & Prakash, K. L. (2015). A comparative study on usage of Durov and Piper diagrams to interpret hydrochemical processes in groundwater from SRLIS river basin, Karnataka, India. *Elixir International Journal*, *80*, 31073-31077.

Reeder, R. J., & Nakajima, Y. (1982). The nature of ordering and ordering defects in dolomite. Physics and Chemistry of Minerals, 8(1), 29-35.

Reynolds, R. M. (1993). Physical oceanography of the Gulf, Strait of Hormuz, and the Gulf of Oman—Results from the Mt Mitchell expedition. Marine Pollution Bulletin, 27, 35-59.

Riegl, B., Poiriez, A., Janson, X., & Bergman, K. L. (2010). The gulf: facies belts, physical, chemical, and biological parameters of sedimentation on a carbonate ramp. In Carbonate Depositional Systems: Assessing Dimensions and Controlling Parameters (pp. 145-213). Springer, Dordrecht.

Roach, L. H., Mustard, J. F., Murchie, S., Langevin, Y., Bibring, J. P., Bishop, J., ... & Herkenhoff, K. (2007, March). CRISM spectral signatures of the north polar gypsum dunes. In *Lunar and Planetary Science Conference* (Vol. 38, p. 1970).

Roberts, J. A., Kenward, P. A., Fowle, D. A., Goldstein, R. H., González, L. A., & Moore, D. S. (2013). Surface chemistry allows for abiotic precipitation of dolomite at low temperature. *Proceedings of the National Academy of Sciences*, *110*(36), 14540-14545.

Robinson, B. W., & Gunatilaka, A. (1991). Stable isotope studies and the hydrological regime of sabkhas in southern Kuwait, Arabian Gulf. Sedimentary geology, 73(1-2), 141-159.

Rose, S., & Long, A. (1988). Monitoring dissolved oxygen in ground water: some basic considerations. Groundwater Monitoring & Remediation, 8(1), 93-97.

Ross, R. (2009) Applications of A Modern GIS (Geographic Information System) Geodatabase In Geotechnical, Geophysical And Geological Analyses. In International Petroleum Technology Conference. International Petroleum Technology Conference.

Rossel, N. C. (1982). Clay mineral diagenesis in Rotliegend aeolian sandstones of the southern North Sea. *Clay minerals*, *17*(1), 69-77.

Rosenberg, T. M., Preusser, F., Blechschmidt, I., Fleitmann, D., Jagher, R., & Matter, A. (2012). Late Pleistocene palaeolake in the interior of Oman: a potential key area for the dispersal of anatomically modern humans out-of-Africa?. *Journal of Quaternary Science*, *27*(1), 13-16.

Rosenberg, T. M., Preusser, F., Risberg, J., Plikk, A., Kadi, K. A., Matter, A., & Fleitmann, D. (2013). Middle and Late Pleistocene humid periods recorded in palaeolake deposits of the Nafud desert, Saudi Arabia. *Quaternary Science Reviews*, *70*, 109-123.

Rounds, S.A., Wilde, F.D., Ritz, G.F. (2013) Dissolved oxygen (ver. 3.0): U.S. Geological Survey Techniques of Water-Resources Investigations, book 9, chap. A6, sec. 6.2, http://water.usgs.gov/owq/FieldManual/Chapter6/6.2_v3.0.pdf.

Sabtan, A. A., & Shehata, W. M. (2003). Hydrogeology of Al-Lith Sabkha, Saudi Arabia. Journal of Asian Earth Sciences, 21(4), 423-429.

Sanford, W. E., & Wood, W. W. (2001). Hydrology of the coastal sabkhas of Abu Dhabi, United Arab Emirates. Hydrogeology Journal, 9(4), 358-366.

Shahin, M. (2009) Road Construction on Sabkha Soils. http://dspace.univ-tlemcen.dz/bitstream/112/688/1/Road-Construction-on-Sabkha-Soils.pdf (Accessed on April 1st 2016)

Shearman, D. J. (1966). Origin of marine evaporites by diagenesis. Trans. Inst. Min. Metall, 75, 208-215.

Shearman, D. J. (1985). Syndepositional and late diagenetic alteration of primary gypsum to anhydrite. In Sixth international symposium on salt (Vol. 1, pp. 41-50). Salt Institute.

Shehata, W. M., & Amin, A. A. (1997). Geotechnical hazards associated with desert environment. Natural hazards, 16(1), 81-95.

Shepherd, R. G. (1989). Correlations of permeability and grain size. Groundwater, 27(5), 633-638.

Sherwood, J. E., Stagnitti, F., Kokkinn, M. J., & Williams, W. D. (1991). Dissolved oxygen concentrations in hypersaline waters. Limnology and Oceanography, 36(2), 235-250.

Sherwood, J. E., Stagnitti, F., Kokkinn, M. J., & Williams, W. D. (1992). A standard table for predicting equilibrium dissolved oxygen concentrations in salt lakes dominated by sodium chloride. International Journal of Salt Lake Research, 1(1), 1-6.

Shinn, E. A. (1973). Sedimentary accretion along the leeward, SE coast of Qatar Peninsula, Persian Gulf. In The Persian Gulf (pp. 199-209). Springer, Berlin, Heidelberg.

Shinn, E. A. (2010). Interplay between Holocene sedimentation and diagenesis, and implications for hydrocarbon exploitation: return to the sabkha of Ras Umm Said, Qatar. Quaternary carbonate and evaporite sedimentary facies and their ancient analogues: A Tribute to Douglas James Shearman, 133-148.

Shinn, E. A. (2011). Interplay between Holocene sedimentation and diagenesis, and implications for hydrocarbon exploitation: return to the sabkha of Ras Umm Said, Qatar. Quaternary carbonate and evaporite sedimentary facies and their ancient analogues: A Tribute to Douglas James Shearman, 133-148.

Shinn, E. A. (2011). Interplay between Holocene sedimentation and diagenesis, and implications for hydrocarbon exploitation: return to the sabkha of Ras Umm Said, Qatar. Quaternary carbonate and evaporite sedimentary facies and their ancient analogues: A Tribute to Douglas James Shearman, 133-148.

Simmons, C. T., Fenstemaker, T. R., & Sharp Jr, J. M. (2001). Variable-density groundwater flow and solute transport in heterogeneous porous media: approaches, resolutions and future challenges. Journal of Contaminant Hydrology, 52(1-4), 245-275.

Simmons, C. T. (2005). Variable density groundwater flow: From current challenges to future possibilities. Hydrogeology Journal, 13(1), 116-119.

Simms, M. A., Garven, G. (2004). Thermal convection in faulted extensional sedimentary basins: theoretical results from finite-element modeling. Geofluids, 4(2), 109-130.

Slater, L., & Lesmes, D. P. (2002). Electrical-hydraulic relationships observed for unconsolidated sediments. Water Resources Research, 38(10).

Slowakiewicz, M., Pancost, R. D., Thomas, L., Tucker, M. E., Didi-Ooi, S. M., & Whitaker, F. (2014, January). Holocene intertidal microbial mats of Qatar and their implications for petroleum source rock formation in carbonate-siliciclastic-evaporite systems. In IPTC 2014: International Petroleum Technology Conference.

Smart, P. L., Dawans, J. M., & Whitaker, F. (1988). Carbonate dissolution in a modern mixing zone. Nature, 335(6193), 811-813.

Smart, P.L., Dawans, J.M., Whitaker, F.F. (1988) Carbonate Dissolution in a Modern Mixing Zone. Nature Vol. 335 p311-813.

Spane, F. A. (2002). Considering barometric pressure in groundwater flow investigations. Water resources research, 38(6), 14-1.

Stannard, D. I., & Weltz, M. A. (2006). Partitioning evapotranspiration in sparsely vegetated rangeland using a portable chamber. Water Resources Research, 42(2).

Streetly, M. J., & Kotoub, S. (1998). Determination of aquifer properties in northern Qatar for application to artificial recharge. *Quarterly Journal of Engineering Geology and Hydrogeology*, *31*(3), 199-209.

Stringfield, V. T., & LeGrand, H. E. (1971). Effects of karst features on circulation of water in carbonate rocks in coastal areas. Journal of Hydrology, 14(2), 139-157.

Strohmenger, C. J., Al-Mansoori, A., Al-Jeelani, O., Al-Shamry, A., Al-Hosani, I., Al-Mehsin, K., & Shebl, H. (2010). The sabkha sequence at Mussafah Channel (Abu Dhabi, United Arab Emirates): facies stacking patterns, microbial-mediated dolomite and evaporite overprint. GeoArabia, 15(1), 49-90.

Strohmenger, C. J., Steuber, T., Ghani, A., Barwick, D. G., Al-Mazrooei, S. H., & Al-Zaabi, N. O. (2010). Sedimentology and chemostratigraphy of the Hawar and Shu'aiba depositional sequences, Abu Dhabi, United Arab Emirates. Barremian-Aptian stratigraphy and hydrocarbon habitat of the eastern Arabian Plate. GeoArabia Special Publication, 4, 341-365.

Strohmenger, C. J., & Jameson, J. (2015). Modern coastal systems of Qatar as analogues for arid climate carbonate reservoirs: improving geological and reservoir modelling. First Break, 33(5), 41-50.

Stumm, F., Chu, A., Lange, A.D., Paillet, F.L., Williams, J.H, Lane, Jr. J.W. (2001) Use of Advanced Borehole Geophysical Techniques to Delineate Fractured-Rock Ground-Water Flow and Fractures Along Water-Tunnel Facilities in Northern Queens County, New York. USGS, WRIR 00-4276. Accessed via http://ny.water.usgs.gov/pubs/wri/wri004276/wrir00-4276.pdf

Sullivan, M. D., Haszeldine, R. S., Boyce, A. J., Rogers, G., & Fallick, A. E. (1994). Late anhydrite cements mark basin inversion: isotopic and formation water evidence, Rotliegend Sandstone, North Sea. Marine and Petroleum Geology, 11(1), 46-54.

Sun, S. Q., & Esteban, M. (1994). Paleoclimatic controls on sedimentation, diagenesis, and reservoir quality: lessons from Miocene carbonates. AAPG bulletin, 78(4), 519-543.

Taghavi, F., Asadi, A. (2008) The Persian Gulf 12th April 2007 dust storm: Observation and model analysis. EUMETSAT Meteorological Satellite Conference, Darmstadt, Germany.

Taylor, J. C. M., & Illing, L. V. (1969). Holocene intertidal calcium carbonate cementation, Qatar, Persian Gulf. Sedimentology, 12(1-2), 69-107.

Tyler, S. W., Muñoz, J. F., & Wood, W. W. (2006). The response of playa and sabkha hydraulics and mineralogy to climate forcing. Groundwater, 44(3), 329-338.

U.S. Geological Survey (2015). National field manual for the collection of water-quality data: U.S. Geological Survey Techniques of Water-Resources Investigations, book 9, chaps. A1-A10, available online at http://pubs.water.usgs.gov/twri9A.

Uhlman, K. (1991). The geochemistry of boron in a landfill monitoring program. Groundwater Monitoring & Remediation, 11(4), 139-143.

UNESCO (2008) Khor Al-Adaid Natural Reserve. Accessed on 01/05/2017 via http://whc.unesco.org/en/tentativelists/5317/

Unpublished PhD thesis, University of Manchester, 275 pp.

Usiglio, M. J. (1849). Etudes sur la composition de l'eau de la Mediterranee et sur l'exploitation des sels qu'elle contient. Annales Chim. Phys., ser 3, 27, 172-191.

Van Dam, R. L., Simmons, C. T., Hyndman, D. W., & Wood, W. W. (2009). Natural free convection in porous media: First field documentation in groundwater. Geophysical Research Letters, 36(11).

Van Dam, R. L., Eustice, B. P., Hyndman, D. W., Wood, W. W., & Simmons, C. T. (2014). Electrical imaging and fluid modeling of convective fingering in a shallow water-table aquifer. *Water Resources Research*, *50*(2), 954-968.

Van Driessche, A. E. S., Benning, L. G., Rodriguez-Blanco, J. D., Ossorio, M., Bots, P., & García-Ruiz, J. M. (2012). The role and implications of bassanite as a stable precursor phase to gypsum precipitation. science, 336(6077), 69-72.

Velde, B. (1995). Composition and mineralogy of clay minerals. In Origin and mineralogy of clays (pp. 8-42). Springer Berlin Heidelberg.

Velde, B. B., & Meunier, A. (2008). The origin of clay minerals in soils and weathered rocks. Springer Science & Business Media.

Vuillemin, A., Ndiaye, M., Martini, R., & Davaud, E. (2011). Cement stratigraphy: image probes of cathodoluminescent facies. *Swiss Journal of Geosciences*, *104*(1), 55-66.

Walton, W. C. (1970). Groundwater resource evaluation. McGraw-Hill series in water resources and environmental engineering (USA) eng.

Wang, K., Hu, X., Zhao, P., & Yin, Z. (2016). Natural dolomite modified with carbon coating for cyclic high-temperature CO2 capture. *Applied energy*, *165*, 14-21.

Warren, J. K. (2010). Evaporites through time: Tectonic, climatic and eustatic controls in marine and nonmarine deposits. Earth-Science Reviews, 98(3), 217-268.

Warren, J. K. (2006). Evaporites. Springer.

Warren, J. K. (2016). Evaporites: A geological compendium. Springer.

Warren, J. K., & Kendall, C. G. S. C. (1985). Comparison of sequences formed in marine sabkha (subaerial) and salina (subaqueous) settings--modern and ancient. AAPG Bulletin, 69(6), 1013-1023.

Watson, A. (1985). Structure, chemistry and origins of gypsum crusts in southern Tunisia and the central Namib Desert. Sedimentology, 32(6), 855-875.

Weijermars, R. (1999). Quaternary evolution of Dawhat Zulum (half moon bay) region eastern province, Saudi Arabia. GeoArabia, 4(1), 71-90.

Wells, A. J. (1962). Recent dolomite in the Persian Gulf. Nature, 194(4825), 274-275.

Wetzel, R. G. (2001). Limnology: lake and river ecosystems. Gulf Professional Publishing, p151-153.

Whitaker, F. F., & Smart, P. L. (1997). Hydrogeology of the Bahamian archipelago. Geology and hydrogeology of carbonate islands: Amsterdam, Elsevier, 183-216.

Whitaker, F. F., Smart, P. L., & Jones, G. D. (2004). Dolomitization: from conceptual to numerical models. Geological Society, London, Special Publications, 235(1), 99-139.Whitaker, F. F., & Smart, P. L. (2007). Geochemistry of meteoric diagenesis in carbonate islands of the northern Bahamas: 1. Evidence from field studies. Hydrological Processes, 21(7), 949-966.

Whitaker, F. F., & Smart, P. L. (2007). Geochemistry of meteoric diagenesis in carbonate islands of the northern Bahamas: 1. Evidence from field studies. Hydrological Processes, 21(7), 949-966.

Whitaker, F.F., Didi-Ooi, S.M., Jameson, J. and Strohmenger, C. (2014) Origins of evaporites in a Holocene mixed clastic and carbonate coastal sabkha: Preliminary hydrological and geochemical data from Mesaieed sabkha, Qatar. IPTC 17567.

Williams, A. H., Walkden, G. M. (2002). Late Quaternary highstand deposits of the southern Arabian Gulf: a record of sea-level and climate change. Geological Society, London, Special Publications, 195(1), 371-386.

Wilson, M. J., Deer, W. A., Howie, R. A., & Zussman, J. (2013). Rock-Forming Minerals, Volume 3C, Sheet Silicates: Clay Minerals. In *Geological Society, London*.

Wood, W. W., & Böhlke, J. K. (2017). Density-Driven Free-Convection Model for Isotopically Fractionated Geogenic Nitrate in Sabkha Brine. *Groundwater*, *55*(2), 199-207.

Wood, W. W., Sanford, W. E., & Al Habshi, A. R. S. (2002). Source of solutes to the coastal sabkha of Abu Dhabi. Geological Society of America Bulletin, 114(3), 259-268.

Wood, W. W., Rizk, Z. S., Alsharhan, A. S. (2003). Timing of recharge, and the origin, evolution and distribution of solutes in a hyperarid aquifer system. Developments in water science, 50, 295-312.

Wood, W. W., Sanford, W. E., Al Habshi, A. R. S. (2002). Source of solutes to the coastal sabkha of Abu Dhabi. Geological Society of America Bulletin, 114(3), 259-268.

Wood, W. W., Sanford, W. E., Frape, S. K. (2005). Chemical openness and potential for misinterpretation of the solute environment of coastal sabkhat. Chemical Geology, 215(1-4), 361-372.

Wood, W. W. (2011). Source of paleo-groundwater in the Emirate of Abu Dhabi, United Arab Emirates: evidence from unusual oxygen and deuterium isotope data. Hydrogeology journal, 19(1), 155-161.

Wray, J. J., Noe Dobrea, E. Z., Arvidson, R. E., Wiseman, S. M., Squyres, S. W., McEwen, A. S., ... & Murchie, S. L. (2009). Phyllosilicates and sulfates at Endeavour Crater, Meridiani Planum, Mars. Geophysical Research Letters, 36(21).

Wray, J.J., Murchie, S.L., Squyres, S.W., Seelos, F.P., Tornabene, L.L. (2009) Diverse aqueous environments on ancient Mars revealed in the Southern Highlands. Geology, Nov 2009, v. 37

Xie, Q., Chen, T., Zhou, H., Xu, X., Xu, H., Ji, J., ... & Balsam, W. (2013). Mechanism of palygorskite formation in the Red Clay Formation on the Chinese Loess Plateau, northwest China. Geoderma, 192, 39-49.

Xie, Y., Simmons, C. T., & Werner, A. D. (2011). Speed of free convective fingering in porous media. Water Resources Research, 47(11).

Yechieli, Y., & Wood, W. W. (2002). Hydrogeologic processes in saline systems: playas, sabkhas, and saline lakes. Earth-Science Reviews, 58(3-4), 343-365.

Zhang, F., Xu, H., Konishi, H., Kemp, J. M., Roden, E. E., & Shen, Z. (2012). Dissolved sulfide-catalyzed precipitation of disordered dolomite: Implications for the formation mechanism of sedimentary dolomite. *Geochimica et Cosmochimica Acta*, *97*, 148-165.

Zeller, M., Verwer, K., Eberli, G. P., Massaferro, J. L., Schwarz, E., & Spalletti, L. (2015). Depositional controls on mixed carbonate–siliciclastic cycles and sequences on gently inclined shelf profiles. *Sedimentology*, *62*(7), 2009-2037.

6 Appendixes

6.1 Fundamentals

6.1.1 Diagenesis

Diagenesis is the syndepositional and postdepositional alteration of a rock by any processes, whether mechanical, chemical, physical, and/or biological. This includes processes such as precipitation (which may, or may not lead to cementation), and dissolution, both of which alter the pore network and the subsequent elemental composition. Common diagenetic environments in which porosity can form or be destroyed are meteoric, marine, and subsurface (Moore and Wade, 2013). The meteoric diagenetic environment is characterized by subaerial events and the exposure to fresh to brackish continental groundwaters or surface waters. These waters will have a range of mineral saturation states relative to carbonate or evaporite minerals. The marine diagenetic environment is characterized by marine pore fluids commonly saturated as a function of evaporite and carbonate species.

Timing of diagenesis is related with the environments at where it occurs, and we can attempt to divide them into early diagenesis and late diagenesis. Early diagenesis refers to alteration of sediment in the near-surface environment with subaerial exposure at a time of early burial up to hundreds of meters whereby temperatures are not high and connate fluids are continuously present. This thesis will place emphasis on early diagenesis of evaporites and associated carbonates with regards to both meteoric and marine environments in Mesaieed, Qatar.

Deciphering a diagenetic framework typically involves two frameworks: a hydrogeological framework and a geochemical framework. The hydrogeological framework applies to a regional scale of transport of fluids, to and from the area of interest, and thus the chemical reactants and products (in the form of solutes). The geochemical framework incorporates the chemical interactions of the solute-bearing fluid and the host rock. Water-rock interactions should satisfy two conditions, (1) whether the geochemical reactions are thermodynamically or kinetically favoured, and (2) whether there is a supply of solute reactants and subsequent removal of solute product. Having just one or the other condition will mean that diagenetic modification of the geologic body will not occur.

6.1.2 Hydrology and Hydrogeology

Hydrology is the study of the water resources and water cycle, while hydrogeology is the study of the distribution and movement of groundwater within the aquifer or rock. The hydrogeological framework, especially in the near surface, is often influenced by the hydrological system. Combining these two "hydro-facets" enables us to understand the flux of waters both on the surface and in the subsurface, which controls the geochemical distribution of solutes and, subsequently, influences the diagenetic processes. The focus of this thesis is on the meteoric systems developed in the peninsula setting of Qatar.

Within the area of study, four arid hydrological zones have been recognized: vadose, saline phreatic, mixing and saline zones. The vadose zone is an unsaturated zone in the form of capillary fringe and air phase within its pore network. As tidal flooding and/or continental waters flow downwards into this zone, via gravity-driven flow, the waters will travel to the water table. The upper contact of saline phreatic zone is thus the water table, whereby the pore bodies are completely fluid-saturated.

When two water bodies of different density (such as a brine plume and a brackish water body) are adjacent, the interface between them is a transitional layer called a 'mixing zone'. In an arid peninsula setting, a freshwater to brackish water body typically forms a lens above the denser saline body (Eccleston et al., 1981). However, at the coastal edges of a peninsula like the sabkhas forming a rim around Qatar, where there is low relief and discharge plains, a thin saline plume (saline zones) often forms vertically from the surface. The differences in salinity can contaminate fresh groundwater updip.

6.1.3 Geochemistry

As this thesis emphasizes water-rock interaction, this section includes both aqueous geochemistry and rock geochemistry.

6.1.3.1 Evaporite Geochemistry

Evaporite is a rock typically found in arid environment that is precipitated from brine solution, often due to evaporation on the surface or the near subsurface (Warren, 2016). Warren (2016) restricts the use of the terminology to near-surface to surface hydrologic systems that are driven by solar evaporation, but the term is loosely used in the mining and oil and gas industries to also include subsurface mineral salts that precipitate in response to remobilization, burial, hydrothermal and cryogenic processes. Evaporites, which include both *primary evaporites* in basin-fill sequence and *secondary (diagenetic) evaporites*, formed diagenetically in sabkha-type facies, account for less than 2% of sedimentary rocks (Kirkland and Evans, 1981; Warren, 2006).

Within hydrocarbon systems, the evaporites play several roles: (1) as thick-bedded primary (subaqueous) evaporites forming seals, for example the Jurassic Arab Formation in the Ghawar oil field, or (2) as intra-formational cementation that reduces reservoir quality which are typically observed in the Permo-Triassic Khuff Formation in the North Field. This study focuses on the latter. Elsewhere in the world, economically important evaporitic carbonate reservoirs include the Permian Basin of West Texas and New Mexico and Zechstein formation.

Evaporite geochemistry has been well-studied, with extensive reviews by workers Usiglio (1849), Hardie (1984), Logan (1987), Bąbel and Schreiber (2014), and Warren (2016). Evaporites such as gypsum, $CaSO_4.2H_2O$ and anhydrite, $CaSO_4$, comprise of ~90% of both the ancient and modern evaporites precipitated (Warren, 2016). Gypsum is more common at the Earth's surface and in the near-surface while anhydrite is commonly observed in the subsurface. Much of the anhydrite appears to be

secondary and is derived from gypsum dewatering (Gunatilaka, 1990; Hardie, 1967, Warren, 2016). The crystallization field starts from approximately 150‰ for gypsum, up to the beginning of halite crystallization field at 290-320‰ (Bąbel and Schreiber, 2014).

In brines saturated with calcium Ca and SO_4 ions, Ca^{2+} in solutes combine with sulphate ions, gypsum or anhydrite may precipitate, and thus lowering the sulphate and Ca^{2+} content in the brine:

$$Ca^{2+}_{(aq)} + SO_4^{2-}{}_{(aq)} + 2H_2O \rightleftharpoons CaSO_4.2H_2O_{(s)} \text{ (gypsum)} \quad (1.1)$$

$$Ca^{2+}_{(aq)} + SO_4^{2-}{}_{(aq)} \rightleftharpoons CaSO_{4(s)} \text{ (anhydrite)} \quad (1.2)$$

(where g = gas phase, aq = aqueous or soluble in water, s = solid phase)

When seawater, where Na and Cl are dominant ions, is evaporating, halite (NaCl) can precipitate:

$$Na^{+}_{(aq)} + Cl^{-}_{(aq)} \rightleftharpoons NaCl_{(s)} \text{ (halite)} \quad (1.3)$$

6.1.3.2 Carbonate Geochemistry

Carbonate, an anionic form of the $(CO_3)^{2-}$ with common divalent metallic cations such as Ca and Mg, hosts about 25% of the world's freshwater that is available for human consumption (Moore et al., 2009). It also hosts most of the unconventional oil reserves, including the Grosmont reservoir (Machel et al., 2012), and about 50% of the world's oil and gas reserves (Figure 1-1) (World Energy Outlook, 2006).

Carbonate equilibria is controlled by four main equations. Carbon dioxide (CO_2) is a soluble atmospheric gas that easily dissolves in waters:

$$CO_{2(g)} \rightleftharpoons CO_{2(aq)} \quad (1.4)$$

While the hydration of this aqueous CO_2 forms carbonic acid,

$$CO_{2(aq)} + H_2O \rightleftharpoons H_2CO_{3(aq)} \quad (1.5)$$

it can rapidly dissociate into H^+ and bicarbonate (HCO_3^-) into solution and subsequently dissociation of the bicarbonate into H^+ and CO_3^- (Appelo and Postma, 1993).

$$H_2CO_{3(aq)} \rightleftharpoons HCO^{-}_{3(aq)} + H^{+}_{(aq)} \quad (1.6)$$

$$HCO_{3(aq)} \rightleftharpoons CO_3^{2-}{}_{(aq)} + H^+{}_{(aq)} \quad (1.7)$$

Carbonic acid is a common source of acidity in water resources, it increases the solubility of calcite, $CaCO_3$, a calcium carbonate mineral. This, in turn will increase the concentration of carbonic acid in the solution, leading to a negative feedback, dissolving more $CaCO_3$.

$$CaCO_{3(s)}\,(calcite) + CO_{2(g)} + H_2O_{(l)} \rightleftharpoons Ca_2^{2+}{}_{(aq)} + 2HCO_3^{3-}{}_{(aq)} \quad (1.8)$$

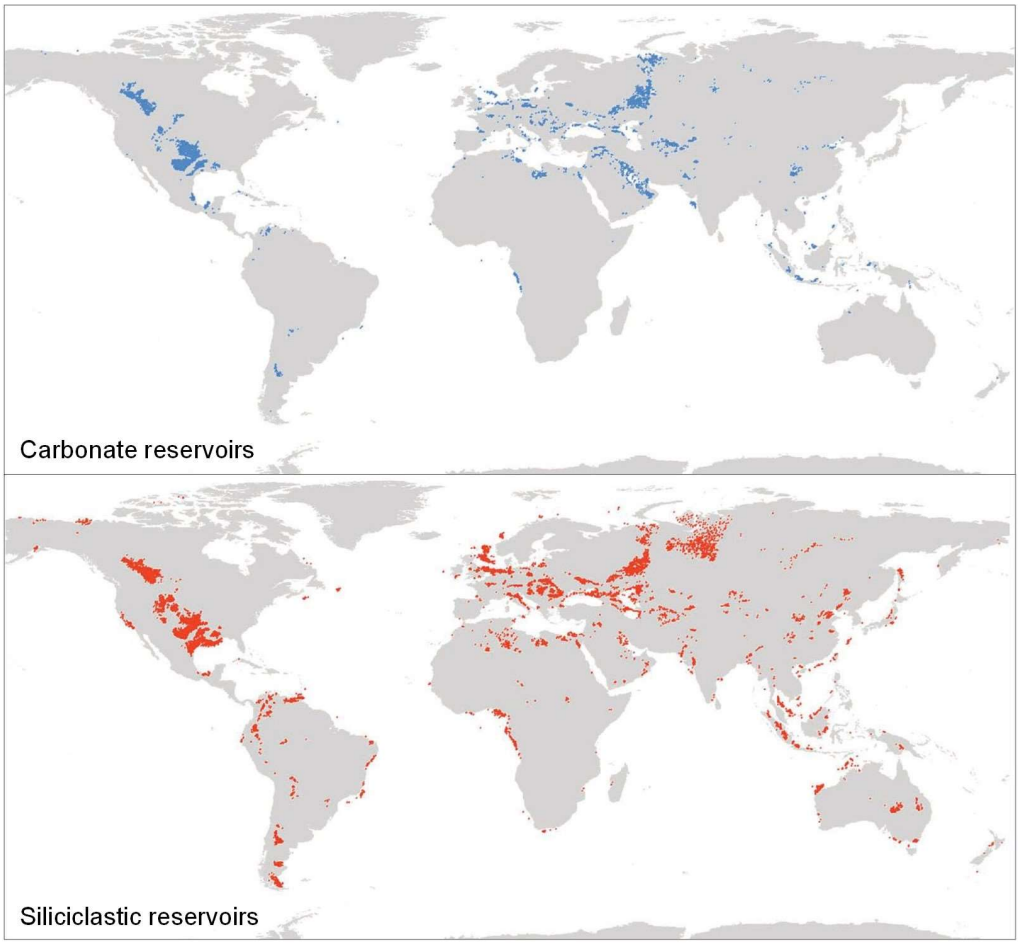

Figure 6-1. Geographic distribution of oil and gas reservoirs sorted by lithology (modified from Ehrenberg and Nadeau, 2004)

The loss of CO_2, often due to degassing, will reverse the process and cause precipitation of $CaCO_3$. Calcite precipitation can be driven by evaporation of seawater which degasses the bicarbonate HCO_3^- ions (Holland et al., 1996).

6.2 Major dust and sand source regions of Qatar

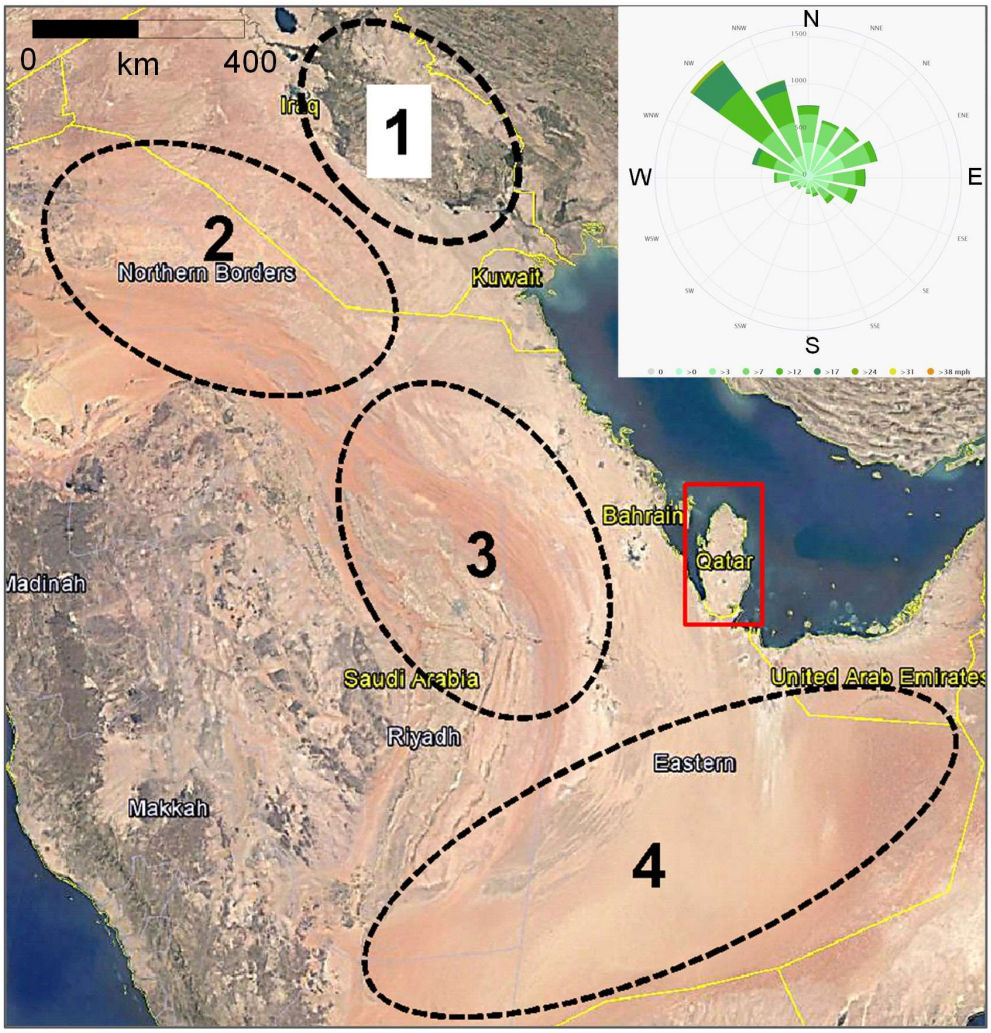

Figure 6-2 Major dust and sand sources regions for Qatar (in red box) for any wind direction plotted on Google Earth Pro satellite image. Inset on the top right is wind rose diagram for Doha showing prevailing wind. Aeolian sediment in Qatar is sourced from three main regions, highlighted in Figure 1-6. Region 1 is known as the Mesopotamian Plain or fertile crescent encompassing Tigris and Euphrates River delta and flow plains (Wilkerson, 1991). Region 2 is northwest Saudi Arabia within the extension of Syrian Desert, known as Great Nafuq Desert (Pye, 1987; Bukhari, 1993) with abundance in sand dunes, alluvial fans, lake beds and dry washes. Ad Dahma Desert (Region 3) provides a continuous supply and most of the Arabian Peninsula dust storms as it is oriented northwest – southeast. Minor source appears to come from the southeastern segment Rub al-Khali Desert (Region 4) which is the most arid and hottest desert in the region (Pye, 1987).

6.3 Core-Scale Permeability

6.3.1 Method

1. Grain Size Analysis (GSA)

Particle grain size has long been used to estimate permeability (Masch and Denny, 1966; Freeze and Cherry, 1979; Shepherd, 1989; Slater and Lesmes, 2002; Chapuis and Driver, 2012). The Chapuis method relates d_{10} and e to predict K_{sat} via the equation:

$$K_{sat} = 2.462^2 \left(\frac{d_{10}^2 e^3}{1+e} \right)^{0.7825}$$

Where d_{10} is the grainsize at which 10% of the sediment is finer than d and e is the void ratio ($e = \frac{\phi}{1-\phi}$).

Sabkha pits were sampled at 10-20 cm depth intervals depending on visible changes in colour and size of sediment grains, from the surface down to about 30cm below the water table in various places in Mesaieed. Analysis of grain size used Dynamic Imaging Analysis (DIA) technology, which is more efficient than traditional sieving methods. It uses a camera to capture high-resolution digital pictures of particles which are then analyzed by software which calculates the dimensions of every single particle (both the shape and size) in the photographs. Sediments were dried in an oven at 50 °C for 36 hours before being analysed using Retsch CAMSIZER® P4 to quantify the samples' particle size distribution and particle shape of granules to within n ±1% in the range of 20 μm to 30 mm (Figure 2-6A). The sediments were examined under a binocular microscope to estimate the compositional mineralogy of the samples to deduce the sediment's porosity and void ratio which is further used to estimate sediments' permeability. The limitations to approximation of laboratory-scale permeability from grainsize analysis include the lack of accounting for diagenetic alteration of sands and the lack of quantifying intraparticle porosity. This may then slightly underestimate the permeability calculations. Vertical variation in permeability may be anticipated to reflect on the texture and types of evaporites precipitated.

2. Falling Head Test (FHT)

The falling head test (FHT), or permeameter method is typically used on fine and medium grained soil. It is likely also applicable for cemented soils where GSA cannot be used as sediments in the FHT are sampled as a whole unit rather than disintegrated, as in GSA. Cylindrical high-pressure PVC casing was cut into push cores with a height of 3 cm and internal diameter of 3 cm. These cones were used to collect 21 cm^3 of sabkha sediment at incremental depth intervals of 3-5 cm from the ground surface depending on the heterogeneity of the sabkha, i.e. grain size variation and degree of cementation (Figure 2-6B). Push cores with minimum wall thickness were chosen (1.58 mm) and sharpened at their tips

to facilitate driving of push cores into sabkha sediments with minimal sediment disturbances. Compaction at the side of the core during collection was insignificant < 1 mm. A laboratory was set up on the field for this test. Using a stop watch, graduated pipette and retort stand, this test measures the flow of water through a saturated 6 cm PVC soil sample connected to the graduated pipette which provides the measurement of the fall of the water head (Figure 2-6C). Sabkha brine was used instead of distilled water in order to avoid salt dissolution and resulting overestimation of permeability. A hydrodynamic head was simulated using pipettes and sabkha water, which thus allow hydraulic conductivity to be calculated via (Head, 1982):

$$K = \frac{2.3aL}{At} \log\left(\frac{h_1}{h_2}\right)$$

Where a and L makes up the volume of the pipette volume, A is the area of the sample, t is the time taken for brines to drain through the push core, and $\frac{h_1}{h_2}$ is the ratio of height of brine in the column to the height of the pipette.

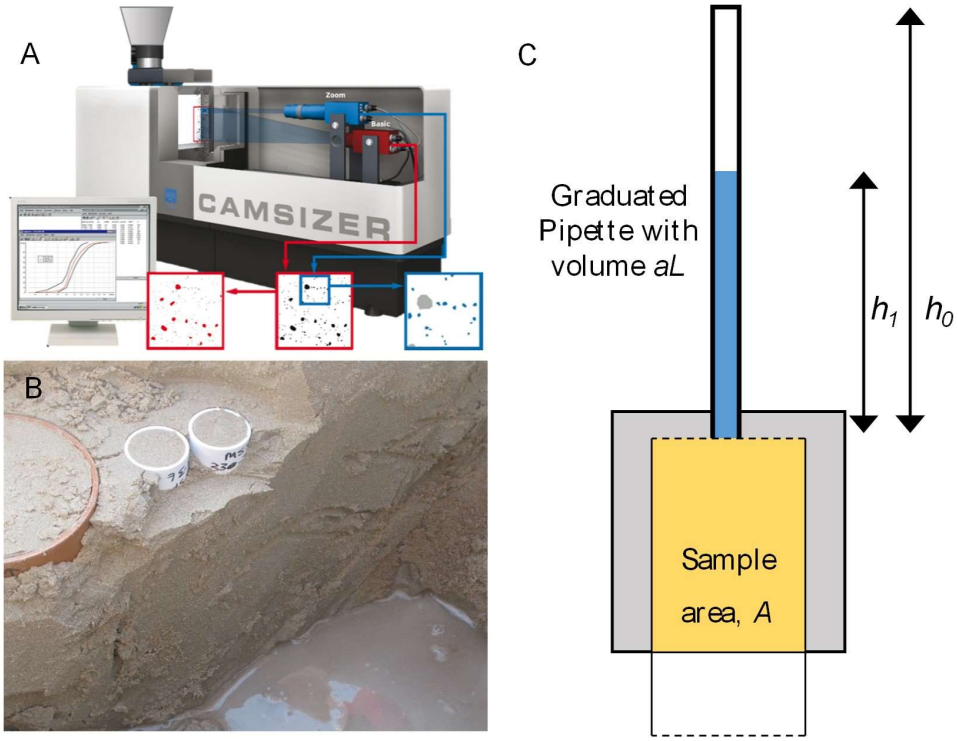

Figure 6-3. (**A**) Camsizer (**B**) Core plugs used to collect unsaturated samples in the sabkha pit for falling head test (FHT) for permeability (**C**) Schematic diagram of FHT with dashed lines representing gauze mesh that was used to prevent remobilisation of sample sediments.

6.3.2 Method Comparison

Comparison of methods for permeability analysis revealed differences due to testing methods, over a different permeability range. Both testing method and absolute permeability values influence the data and hence it will be discussed here.

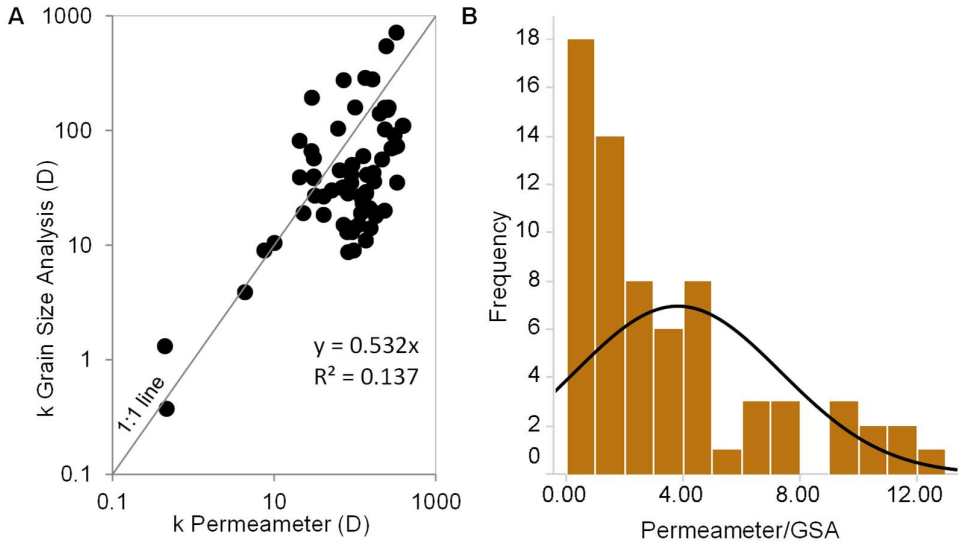

Figure 6-4. (**A**) Log plot highlights comparison of Holocene permeability *k* (in Darcies) from two laboratory-scale tests (GSA vs FHT permeameter). Data includes permeability tested in similar sabkha environment in Dukhan (n = 69). The extreme values are not from normal sabkha environment but rather from subaqueous lake. (**B**) Histogram plot with Gaussian distribution curve of permeameter to GSA ratio to highlight the skewness of the dataset towards permeameter measurements. FHT:GSA plot shows that most are within 1 to 2, with some results up to 12.

The relationship between different laboratory-scale permeability tests, FHT (falling head test) and grain-size-analysis-derived permeability (GSA) (Figure 2-33A) highlights a good 1:1 relationship that is limited to below 20 D. The 1:1 relationship becomes less consistent above 20 D. Figure 2-35B uses the ratio of permeabilities measured by permeameter to the one derived from GSA to illustrates the skewness of the methods. 71% of samples analysed using FHT exhibit higher permeability, with 30% of FHT being almost magnitude higher than permeability derived from GSA. The higher permeability in FHT measurements may be explained by a combination of the smooth PVC surface used for coring and the non-plastic nature of the sabkha sand which resulted in the creation of higher permeability pathways around the edges of the sample during FHT tests. This may have allowed water to bypass during the falling head experiments, leading to an over-estimation of the permeability. Hence for discussion of the Holocene sabkha, we will use GSA dataset for laboratory-scale.

The outcome of this study is that measuring permeability with falling head test (FHT) method is generally useful. However, using grain size analysis for sabkha sediments may be more efficient to measure permeabilities greater than 20 D.

6.4 Time-lapse Satellite Imagery of Mesaieed Sabkha

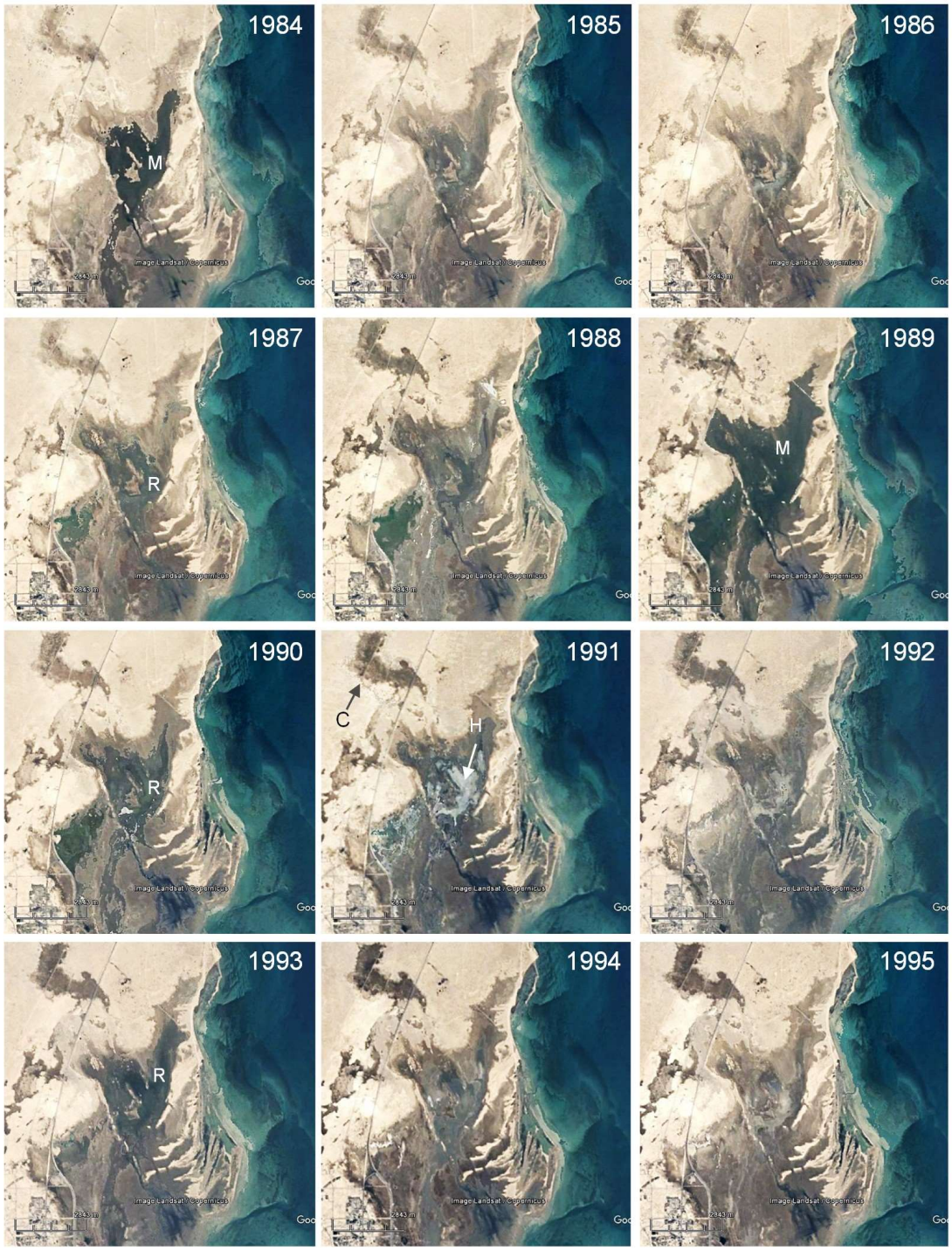

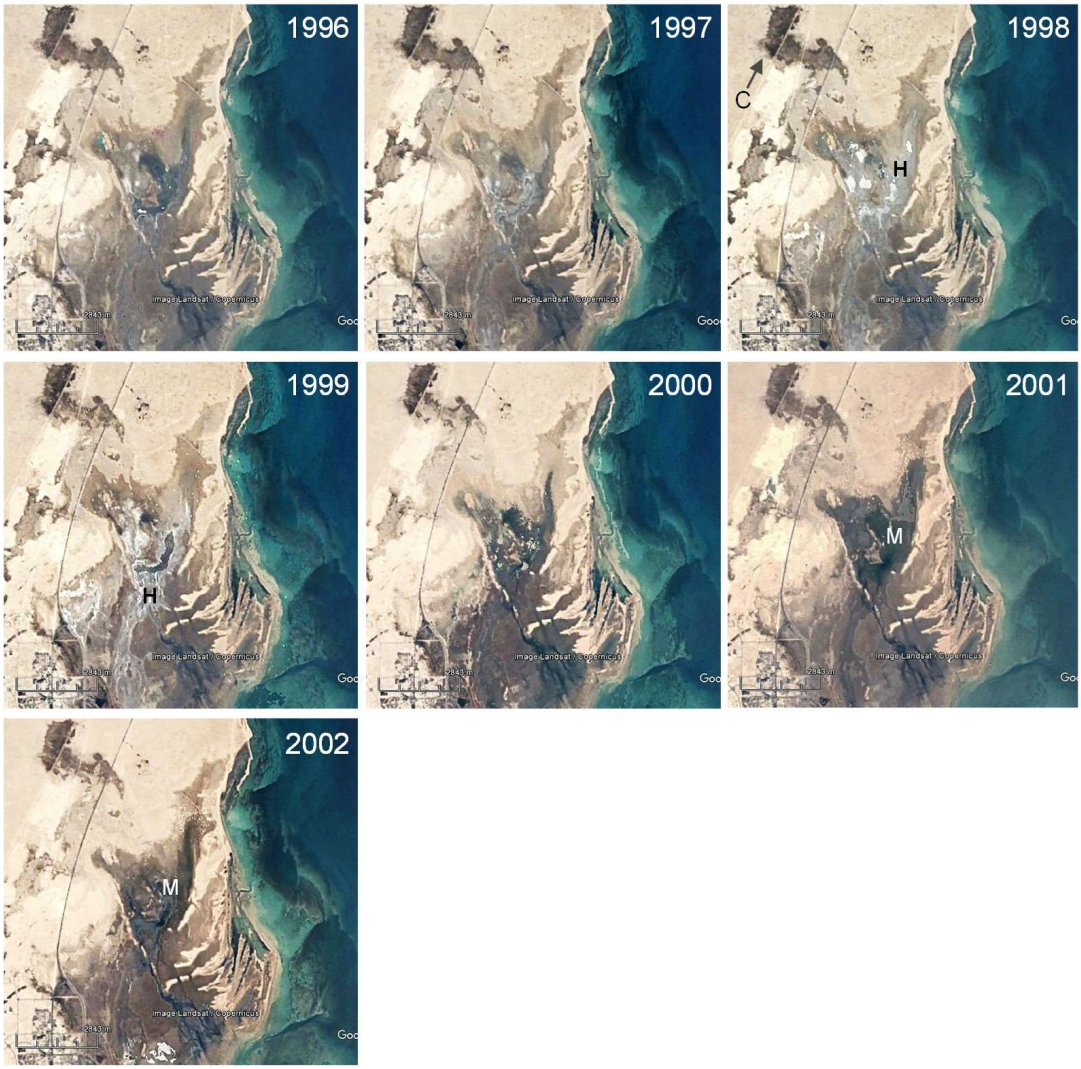

M: Marine flooding; S: Stabilised sheet sand; C: Continental Meteoric discharge; H: Salt flat

Figure 6-5 Time lapse of satellite imagery (taken in December month) showing sequence of seasonal tidal flooding (labelled M) in Mesaieed with the formation of ephemeral halite crust (labelled H). **1984**: Marine flooding with limits up to middle sabkha. **1985**: Mesaieed on normal days with minor pooling of seawater in the middle sabkha. **1988:** Continental meteoric waters (labelled C) are seen pooling the proximal sabkha. **1989**: Maximum tidal flooding on days with low pressure system, high neap tides and storm. **1990**: Retreat of tide leaving local individual pools of marine waters in low elevation in the upper and middle sabkha. **1991**: When no marine flooding occurs, evaporite salts form in the middle sabkha where abandoned pools of water were. (Satellite imagery source: Google Earth Pro 2017). Intense rainfall of 245 mm in December 1983 contributed to the residual flood in the middle sabkha, which is extrapolated from flood in the lower sabkha that is observed to has retreated as seen in the following year's image, whereas effects and extent of flooding from a 24 mm rainfall in December 1989 is shown in the satellite image captured on the same month.

6.5 Climate data

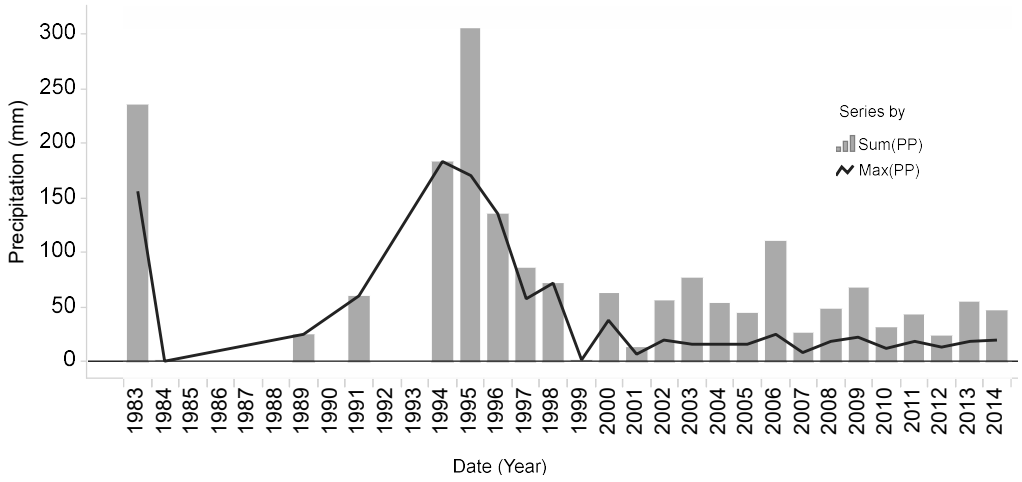

Figure 6-6 Graph highlighting annual sum of precipitation (PP) (bar chart) and maximum rainfall (solid line) in 24-hour period. For many months the average monthly rainfall is very low (<10mm), with the exception for January and December which are generally the wettest (average 13 and 15 mm, respectively). The same pattern is seen in the annual data whereby drought persisted (between 1985 and 1993, 1998 to 2000) with rare but intense thunderstorms in between (up to 182 mm over a few hours) until late 2000. 2001 onwards marks period of more consistent rainfall.

6.6 PCA of Mesaeeid Sabkha Geochemistry

The dataset was further analyzed separately for a) the both lower and middle sabkha (MS-LS), which data suggests are seawater-sourced, and b) proximal and lower sabkha (PS-US), which are updip continental waters sourced.

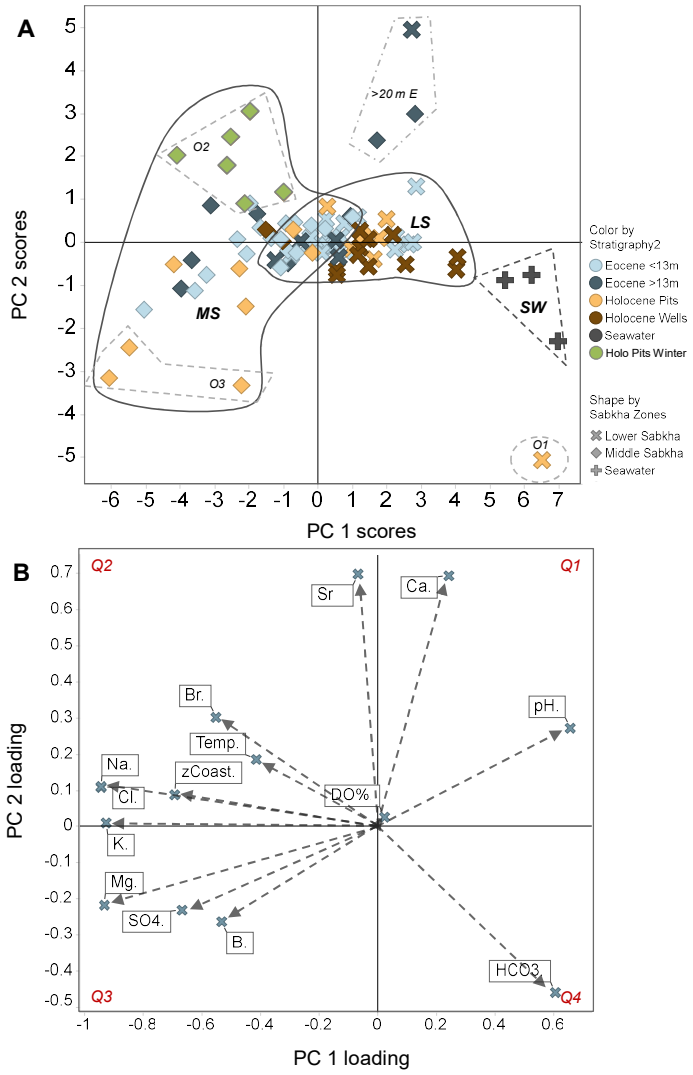

Figure 6-7. Principal component loading and scores for seawater, **middle** and **lower sabkha** groundwater chemistry with horizontal and vertical lines intersecting zero and grouping representing the sabkha zone the waters are in. (**A**) Plot of PC scores for different zones (vary by colour) and formations the waters are hosted in (vary with colour). Outliers are identified as group O1 (JJ08), O2 (Holocene pit waters sampled in the winter) and O3 (Holocene pits sampled directly on the ephemeral salt flat). (**B**) Plot of PC loadings within different quadrants. PC scores plot (Figure 4-5A) show three major clusters for the waters' host formation – seawater (fourth quadrant), the lower sabkha (second and third quadrant) and the middle sabkha (first and fourth quadrant), with the Holocene pits in the middle sabkha showing a higher variability. For Holocene-hosted waters, there is a significant divide between the lower and middle sabkha clusters, possibly indicating very little lateral mixing of groundwater. For Eocene-hosted waters, there is an overlap which likely indicate a lateral mixing of groundwater. The indistinguishable proximity of both Eocene and Holocene clusters within each sabkha zone suggests that vertical groundwater flow occurs. All these supports the hydrogeological observations from Chapter 3. The lower sabkha cluster and ~50% of the Eocene beneath the middle sabkha lie close to the origin, indicating they do not significantly contribute to the major variances seen in the system, and their variability lies parallel along PC 1. Seawater samples have a strong positive loading on PC 1, but an only slightly negative loading on PC 2. The lower sabkha cluster is

distributed along the PC 1 axis. Samples closest to the coast are more similar to seawater, suggesting an evolution or mixing of waters. The groundwater with the highest variance (i.e. furthest away from the origin) are within the middle sabkha. Waters from the Holocene wells and the shallow Eocene have low variance in PC2, but the three deep Eocene outliers are evident in the first quadrant. The single Holocene pit outlier (marked on Figure 4.5A as O1) in the fourth quadrant is located very close (<10 m) to the coast. Outlier groups marked as O2 are subset of Holocene samples that were taken during the winter. In the third quadrant marked as O3 (M10, Q3, Q4) are all waters sampled on the ephemeral salt flat in the middle of the sabkha. When considering both PC loadings and scores plot for only the middle and lower sabkha, there is an evidence of mixing of two groundwater end-members in this system. PCA loadings plot (Figure 4-5B) show that within PC 1, which accounts for 43.9 % of the variance, strong positive loadings are seen for pH and HCO_3 and strong negative loadings correspond to Na, Cl, SO_4, Mg, K, Br, B, and distance from the coast. This indicates that seawater (strong positive PC 1 scores) that enters this part of the sabkha has lower concentration of these ions but relatively high pH and HCO_3. The high negative PC 1 scores seen within the middle sabkha, especially the Holocene pits, indicate that evaporation and water-rock interaction are major processes. The high positive PC 2 scores that correlate with deep Eocene aquifer have a statistical association with high Ca, Sr and pH, which indicates that deep brine contains relatively high concentration of Ca, Sr and a high pH, 2, and a low concentration of HCO3 and H^+. The three Holocene pit outliers, being a product of evaporation as highlighted by their location on the ephemeral salt flat, the maximum evaporation increases most major ions in the groundwater, but appears to be associated with a decrease in Ca and Sr. This may indicate a loss of Ca and Sr to evaporites such as $CaSO_4$ and $SrSO_4$, but a strong positive SO_4 on PC1 with Na and Cl makes it difficult to differentiate between SO_4 concentrated by evaporation of seawater and SO_4 from precipitation and dissolution of evaporites, which can be done by XS calculation.

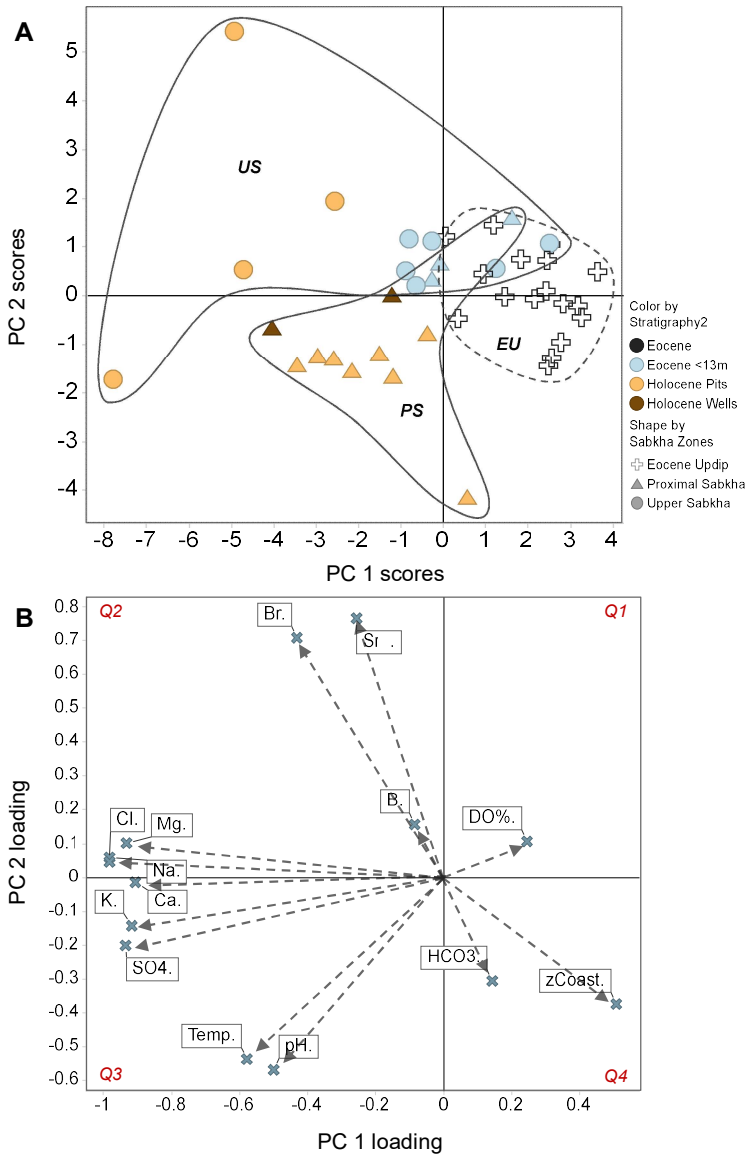

Figure 6-8. Principal component loading and scores for **proximal** and **upper sabkha** groundwater chemistry with horizontal and vertical lines intersecting zero and grouping representing the sabkha zone the waters are in. (**A**) Plot of PC scores for different zones (vary by colour) and formations the waters are hosted in (vary with colour). (**B**) Plot of PC loadings within different quadrants. PC scores plot (Figure 4-6A) show 3 major clusters for the waters – the outcropping Dammam Formation updip, proximal sabkha and upper sabkha – indicating that geography (i.e. sabkha zones) is an important significant. Waters within the Eocene underlying both the proximal and upper sabkha show an almost indistinguishable proximity and overlap with the outcropping Dammam Formation aquifer. However, Holocene pit waters are quite different in proximity from upper sabkha. Proximal sabkha samples are mostly on the second quadrant (negative PC1 and PC2 scores). Upper sabkha Holocene aquifer are variable which coincide with strong negative PC1 scores. The waters from the Holocene wells, which are deeper than pits, and the Eocene wells are clustered closer to the origin. PC loadings plot (Figure 4-6B) highlight that within PC 1, which accounts for 46 % of the variance, there are strong negative loadings for Na, Cl, SO_4, Mg, Ca, and K while a strong positive loading for distance from the coast (and minor positive loading for DO %), indicating an inverse relationship. This can be inferred that the further it is from the coast – the higher these ionic concentrations are (and to an extent a minor lowering DO %). For PC 2, which accounts for 14.6 % of the variance, there are strong negative loadings for pH and temperature while strong positive loadings for Br and Sr. Within PC 3 (not shown), accounting for only 9.1 % of the variance, there are strong positive loadings for HCO_3 and B, while a strong negative loading for DO %.

6.7 Flowthrough Pond

An example of a salina is illustrated by a flowthrough pond filled with gypsum precipitates located in the upper sabkha (Chapter 2, Figure 2-18, 2-19). A vertical hydrochemical profile of the pond to the depth of 5.0 m below the water surface (Figure 4-15) and as of February of 2013, the pond has an average SEC of 183±29 mS/cm which is three times the salinity of local seawater (66 mS/cm) and water temperature of 31.1±1.5, pH of 8.12±0.02 which is expected of water that flows through carbonate rock and DO of 8.39±0.77 mg l^{-1} (114.2±14.9 %) which indicates an oxidized or well aerated pond. The source of aeration can be through the karstified system of the Dammam bedrock, the extent of it is unknown due to its low visibility. It is unlikely that sulphate reduction is mobilizing masses of sulphate to alter the Ca/SO_4 ratio. SEC increases with depth from the surface to 5 m below by 78.7 mS/cm which shows that evaporation on the surface the denser waters then flow downwards in this open system. The pond gets cooler with depth by 3.7°C from 32.8°C at the surface. pH increases only slightly by 0.03 with depth, which reflects a long residency of the water especially when closer to bottom the Eocene bedrock. Water sitting and circulating relatively well within the Dammam bedrock is bound to be more alkaline.

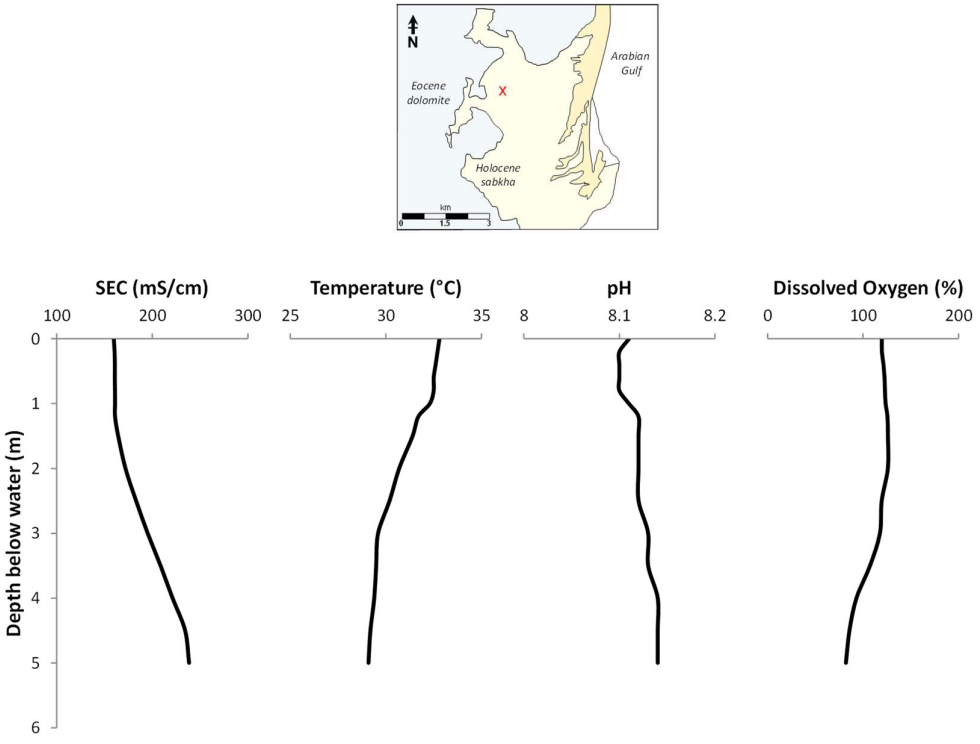

Figure 6-9 .Geochemical characteristics of flowthrough pond showing salinity as SEC, temperature, pH and dissolved oxygen.

Dissolved oxygen has an overall reduction of 1.86 mg l^{-1} (37.5%). Such reduction with increased salinity is common in modern day surface hypersaline settings due to the lack of biotal diversity at higher salinity which improves in preservation potential (Warren, 2003). However, our surface brine does not correspond with present day surface brines from Warren (1986) whereby the general dissolved oxygen with the associated salinity in present-day surface brines from Warren (1986) is about 4-5 mg/l for salinity of about range 20-180 ‰ (SEC range of about 50-350 mS/cm). This can be due to the very effective vertical circulation of groundwater allowing exchange of gas between atmosphere and the flowthrough pond.

Biographical Sketch

Didi Ooi was born in Hospital Adventist, Penang state of Malaysia. Her parents moved to Borneo when she was two and celebrated the move by ascending a 4,030m granitic dormant volcano Mt. Kinabalu (on her daddy's back, of course!). She started at Yuk Yu Kindergarten in Kota Kinabalu before she continued her elementary education in SRK St. Francis Convent for another six years and high school in SM St Francis Convent for another five years.

Upon graduation in 2005, she continued her pre-university GCE Cambridge A-Levels studies in Sinaran Institute for 18 months. This was followed by the national examination STPM just 6 months after as an independent candidate. Following the mass examinations, she worked at Honda for two years while taking up accounting part-time and Marine Science in a local university while waiting for medical school to (financially) materialise.

When she was got into International Medical University – she received an undergraduate scholarship by Shell to further her studies abroad in 2009 to alleviate her parents' financial burden. She then graduated from University of Bristol with a Bachelor of Science in Geology (Honours) in 2012, along with some accolades such as Best Final Year Research, Highest in Sedimentology and Structural Geology and Dean's Commendation for First Class Achievers. After being part of a research crew assisting Dr. Cooper in Andros, Bahamas – she got an offer by ExxonMobil to do her PhD in Geology at the University of Bristol under the tutelage of Fiona Whitaker, Jeremy Jameson, and Christian Strohmenger.

Having lived/worked in Malaysia, Singapore, Middle East and United Kingdom – she is now settled in Houston, Texas where the future of the technology hub is. This complements with her present interest in utilizing advanced analytics and emerging technologies to elevate our understanding in geoscience, with special interest in Artificial Intelligence (such as Machine Learning and Deep Learning). Her recent collaborations include:

Didi-Ooi, S.M., Zhang, L.C, Zhan, C. (2018) Ensemble Learning for Lithofacies Classification with Well Logs. Janet Watson: The Impact of Big Data in Geoscience. *Technical Presentation.*

Zhan, C., Zhang, L.C., Zhong, Z., **Didi-Ooi, S.M.**, Lin, Y. (2018) Deep Learning Approach in Automatic Iceberg-Ship Detection with Remote Sensing Data. SEG International Geophysical Conference and Exposition 2018. *Technical Presentation.*

Didi-Ooi, S.M. (in press, 2018) Simple Machine Learning: A Mini Tutorial. In 52 Things You Should Know About Geocomputing. Agile Libre Publications. Link: https://github.com/didiooi/ProjectHutton

Didi-Ooi, S.M., Whitaker, F. (2018) A Cure for the Curse of Dimensionality: A Case Study of Using Principal Component Analysis. Janet Watson: The Impact of Big Data in Geoscience. *Poster.*

Didi-Ooi, S.M. (2018) How to Get Started in Data Science. Published LinkedIn Article. Link: https://www.linkedin.com/pulse/how-get-started-data-science-sher-didi-ooi/

Jobe, D., **Didi-Ooi, S.M.**, Hami-Eddine, K., Lowell, J., Sen, V. (2017) Hutton: A Cognitive Geoscience Assistance. Subsurface Hackathon 2017 *(won first place and Popular Choice Award*).

Pettitt, E., **Didi-Ooi, S.M.**, Welte, G. (2017) Utilizing Home Sharing Data to Address Civic Issues Through Applied Visualizations. City of Houston Hackathon 2017. Link: https://github.com/didiooi/CivicAirBnB

PhD-related technical presentations and extended abstracts include:

Didi-Ooi, S.M., Whitaker, F., Jameson, J, Strohmenger, C.J. (2015) Deciphering Diagenesis in a Holocene Coastal Sabkha System. International Petroleum Technology Conference (IPTC)

Didi-Ooi, S.M., Whitaker, F., Jameson, J, Strohmenger, C.J. (2015) Evaporite Diagenesis Models of a Continental Sabkha System: Insights from the Holocene at Dukhan, Qatar. AAPG Annual Convention and Exhibition.

Didi-Ooi, S.M., Whitaker, F., Jameson, J, Strohmenger, C.J. (2014) Origin of Diagenetic Evaporites. AAPG Annual Convention and Exhibition.

Slowakiewicz, M., Pancost, R., Thomas, L., Tucker, T.E., **Didi-Ooi, S.M.** (2014) Holocene intertidal microbial mats of Qatar and their implications for petroleum source rock formation in carbonate-siliciclastic-evaporite systems. IPTC 2014: International Petroleum Technology Conference. #

Whitaker, F., **Didi-Ooi, S.M.**, Jameson, J, Strohmenger, C.J. (2014) Origins of evaporites in a Holocene mixed clastic and carbonate coastal sabkha: Preliminary hydrological and geochemical data from Mesaieed sabkha, Qatar. IPTC 2014: International Petroleum Technology Conference. #

Didi-Ooi, S.M., Whitaker, F., Jameson, J, Strohmenger, C.J. (2013) Comparative Sedimentology, Geomorphology and Hydrochemistry of Continental and Coastal Sabkha Systems, Qatar. Qatar Foundation Annual Research Conference, EESP 02

Electronic Appendix

Due to the word and page limit with printing this dissertation, appendixes are located on a Microsoft OneDrive cloud which can be accessed via the following link:

https://1drv.ms/f/s!Ag4a_4HPc8GJgc54MgNcGl4Ux-EhwA

If there are any questions regarding accessing the files, please contact the author at

didiooi@hotmail.com